Springer Theses
Recognizing Outstanding Ph.D. Research

Hui Zhou

Combustible Solid Waste Thermochemical Conversion

A Study of Interactions and Influence Factors

Springer

Springer Theses

Recognizing Outstanding Ph.D. Research

Aims and Scope

The series "Springer Theses" brings together a selection of the very best Ph.D. theses from around the world and across the physical sciences. Nominated and endorsed by two recognized specialists, each published volume has been selected for its scientific excellence and the high impact of its contents for the pertinent field of research. For greater accessibility to non-specialists, the published versions include an extended introduction, as well as a foreword by the student's supervisor explaining the special relevance of the work for the field. As a whole, the series will provide a valuable resource both for newcomers to the research fields described, and for other scientists seeking detailed background information on special questions. Finally, it provides an accredited documentation of the valuable contributions made by today's younger generation of scientists.

Theses are accepted into the series by invited nomination only and must fulfill all of the following criteria

- They must be written in good English.
- The topic should fall within the confines of Chemistry, Physics, Earth Sciences, Engineering and related interdisciplinary fields such as Materials, Nanoscience, Chemical Engineering, Complex Systems and Biophysics.
- The work reported in the thesis must represent a significant scientific advance.
- If the thesis includes previously published material, permission to reproduce this must be gained from the respective copyright holder.
- They must have been examined and passed during the 12 months prior to nomination.
- Each thesis should include a foreword by the supervisor outlining the significance of its content.
- The theses should have a clearly defined structure including an introduction accessible to scientists not expert in that particular field.

More information about this series at http://www.springer.com/series/8790

Hui Zhou

Combustible Solid Waste Thermochemical Conversion

A Study of Interactions and Influence Factors

Doctoral Thesis accepted by
Tsinghua University, Beijing, China

Springer

Author
Dr. Hui Zhou
Department of Earth and Environmental Engineering
Columbia University
New York, NY
USA

Supervisor
Prof. Yanguo Zhang
Department of Thermal Engineering
Tsinghua University
Beijing
China

ISSN 2190-5053 ISSN 2190-5061 (electronic)
Springer Theses
ISBN 978-981-10-3826-6 ISBN 978-981-10-3827-3 (eBook)
DOI 10.1007/978-981-10-3827-3

Library of Congress Control Number: 2017930654

Printed on acid-free paper

This Springer imprint is published by Springer Nature
The registered company is Springer Nature Singapore Pte Ltd.
The registered company address is: 152 Beach Road, #22-06/08 Gateway East, Singapore 189721, Singapore

This thesis is dedicated to my grandmother, who passed away a few weeks after my graduation

Supervisor's Foreword

The organization and design of the clean and efficient utilization of combustible solid waste (CSW) require the accurate understanding of thermochemical characteristics of the fuels. Since the components of CSW have a great variety with different properties, this issue is very difficult to solve. This study built a widely applicable novel method, i.e., the theory and system of basic components, to accurately describe the thermochemical reaction characteristics of CSW with various components. The description of the thermochemical characteristics of real CSW by a limited number of basic components provides the scientific basis of the mathematical simulation and technological design.

This thesis focuses on the thermochemical conversion characteristics of CSW in China and selects nine kinds of basic components (hemicellulose, cellulose, lignin, pectin, starch, PE, PS, PVC, and PET) based on the classification of CSW components in China. The main results include the following: The pyrolysis of CSW basic components were investigated both in thermogravimetric analyzer (TGA) and self-designed Macro-TGA. The peak analysis-least square method (PA-LSM) was developed for the kinetic calculation. The fast pyrolysis was carried out in a fixed bed reactor at 800 °C, and the product distribution, gas production, and polycyclic aromatic hydrocarbons (PAHs) formation characteristics were investigated. During the pyrolysis of lignin and PVC, with the increase in temperature, the molecular weight of tar increased, and the amount of PAHs increased. The generation of HCl decreased with the increase in temperature during PVC pyrolysis. In both TGA and fixed bed reactor, the co-pyrolysis of cellulose and lignin presented the strongest interaction, which increased the amount of tar.

Based on the selection of nine kinds of CSW basic components, this thesis investigated the thermochemical conversion characteristics of basic components and obtained the influence of different factors and component interactions on the

thermochemical conversion characteristics. These conclusions provided the possibility of systematic description of the thermochemical conversion characteristics of CSW with breakthrough methodology and had significant values for the further study and industrial application.

The thesis was well written with clear logic and concept, which contributed it to be an excellent doctoral thesis.

Beijing, China
January, 2017

Prof. Yanguo Zhang

Abstract

The treatment of combustible solid waste (CSW) is a severe problem around the world. Thermochemical conversion is an effective waste-to-energy (WTE) technology. Based on the cluster analysis of CSW in China, this dissertation selects nine types of basic components (hemicellulose, cellulose, lignin, pectin, starch, polyethylene (PE), polystyrene (PS), polyvinyl chloride (PVC), and polyethylene terephthalate (PET)) to study.

The pyrolysis experiments of CSW basic components were carried out in thermogravimetric analyzer (TGA) and self-designed Macro-TGA. Peak analysis-least square method (PA-LSM) was developed to perform kinetic calculations. Complicated pyrolysis reactions could be described by a series of parallel reactions, and the kinetic characteristics of pyrolysis could be reproduced from kinetic parameters accurately.

The fast pyrolysis of basic components was carried out in a fixed bed reactor at 800 °C. The product distribution, gas products, and polycyclic aromatic hydrocarbons (PAHs) generation were analyzed. PS and PVC produced the most PAHs. Naphthalene was the most abundant PAH, and phenanthrene and fluorene were the most abundant 3-ring PAHs. PAHs might be generated directly from the aromatic structure for PS, PET, and lignin. PAHs generated from PE might be via Diels–Alder type of reactions. For polysaccharide compounds, PAHs might be generated with benzenes and cyclopentadiene (CPD) as intermediates.

Regarding the pyrolysis of lignin and PVC, with the increase in temperature, the molecular mass of tar increased, so did the PAH yields. For the pyrolysis of PVC, HCl yield decreased with the increase in temperature. Slow pyrolysis generated more tar and less PAHs than fast pyrolysis. Gasification in air or CO_2 generated less total PAHs than that in N_2. NaCl, NaOH, and $CuCl_2$ all had inhibition effect on the production of PAHs. The pyrolysis of lignin started from depolymerization, and then, the secondary reactions (demethoxylation, dehydroxylation, and demethylation) were promoted with the increase in temperature. For the slow pyrolysis of lignin, secondary reactions were unlikely to happen. The pyrolysis of PVC could be divided into two processes: dechlorination and chain scission. In the process of fast

pyrolysis, chlorination and chain scission happened almost simultaneously; thus, the dechlorination process was incomplete.

In TGA and fixed bed reactor, the co-pyrolysis of cellulose and lignin showed strong interactive effect, and the tar yield increased. The interaction between PVC and cellulose was strong, and the interaction promoted pyrolysis at low temperatures and inhibited pyrolysis at higher temperatures. The interactions of PVC and lignocellulosic basic components decreased the HCl yield and increased the tar yield significantly, and most PAH components were decreased. Lignocellulosic components could act as a catalyst which promoted the chain scission of PVC.

Based on the selection of nine types of basic components of CSW, this dissertation investigates the thermochemical characteristics of basic compounds and delineates the influence of different factors on the thermochemical characteristics and the influence of interactions between basic components on the thermochemical characteristics. The works in this paper provide a theoretical basis for the clean and high-efficiency utilization of CSW as well as the basic knowledge for further understanding the thermochemical conversion mechanisms of complex fuels.

Keywords Combustible solid waste (CSW) · Thermochemical conversion · Interaction · Kinetic · Polycyclic aromatic hydrocarbon (PAH)

Parts of this thesis have been published in the following journal articles:

[1] Zhou H, Long Y, Meng A, Li Q, Zhang Y. The pyrolysis simulation of five biomass species by hemi-cellulose, cellulose and lignin based on thermo-gravimetric curves. Thermochimica Acta, 2013, 566:36–43.

[2] Zhou H, Meng A, Long Y, Li Q, Zhang Y. An overview of characteristics of municipal solid waste fuel in China: Physical, chemical composition and heating value. Renewable & Sustainable Energy Reviews, 2014, 36:107–122.

[3] Zhou H, Meng A, Long Y, Li Q, Zhang Y. Classification and comparison of municipal solid waste based on thermochemical characteristics. Journal of the Air & Waste Management Association, 2014, 64(5):597–616.

[4] Zhou H, Meng A, Long Y, Li Q, Zhang Y. Interactions of municipal solid waste components during pyrolysis: A TG-FTIR study. Journal of Analytical and Applied Pyrolysis, 2014, 108:19–25.

[5] Zhou H, Wu C, Onwudili J A, Meng A, Zhang Y, Williams P T. Polycyclic aromatic hydrocarbon formation from the pyrolysis/gasification of lignin at different reaction conditions. Energy & Fuels, 2014, 28:6371–6379.

[6] Zhou H, Wu C, Meng A, Zhang Y, Williams P T. Effect of interactions of biomass constituents on polycyclic aromatic hydrocarbons (PAH) formation during fast pyrolysis. Journal of Analytical and Applied Pyrolysis, 2014, 110:264–269.

[7] Zhou H, Meng A, Long Y, Li Q, Zhang Y. A review of dioxin-related substances during municipal solid waste incineration. Waste Management, 2015, 36:106–118.

[8] Zhou H, Wu C, Onwudili J A, Meng A, Zhang Y, Williams P T. Polycyclic aromatic hydrocarbons (PAH) formation from the pyrolysis of different municipal solid waste fractions. Waste Management, 2015, 36:136–146.

[9] Zhou H, Wu C, Onwudili J A, Meng A, Zhang Y, Williams P T. Effect of interactions of PVC and biomass components on the formation of polycyclic aromatic hydrocarbons (PAH) during fast co-pyrolysis. RSC Advances, 2015, 5(15):11371–11377.

[10] Zhou H, Long Y, Meng A, Li Q, Zhang Y. Interactions of three municipal solid waste components during co-pyrolysis. Journal of Analytical and Applied Pyrolysis, 2015, 111:265–271.

[11] Zhou H, Long Y, Meng A, Li Q, Zhang Y. Classification of municipal solid waste components for thermal conversion in waste-to-energy research. Fuel, 2015, 145:151–157.

[12] Zhou H, Long Y, Meng A, Li Q, Zhang Y. Thermogravimetric characteristics of typical municipal solid waste fractions during co-pyrolysis. Waste Management, 2015, 38:194–200.

[13] Zhou H, Long Y, Meng A, Chen S, Li Q, Zhang Y. A novel method for kinetics analysis of pyrolysis of hemicellulose, cellulose, and lignin in TGA and macro-TGA. RSC Advances, 2015, 5(34):26509–26516.

[14] Long Y, Zhou H, Meng A, Li Q, Zhang Y. Interactions among biomass components during co-pyrolysis in (macro)thermogravimetric analyzers. Korean Journal of Chemical Engineering, 2016, 33:2638–2643.

[15] Zhou H, Wu C, Onwudili J A, Meng A, Zhang Y, Williams P T. Influence of process conditions on the formation of 2–4 ring polycyclic aromatic hydrocarbons from the pyrolysis of polyvinyl chloride. Fuel Processing Technology, 2016, 144:299–304.

Acknowledgements

This thesis is finished under the supervision of Prof. Yanguo Zhang, who is also my undergraduate class teacher. We have known each other for more than nine years. After many communications with Prof. Zhang, I decided to apply a Ph.D. During my most difficult and confused time, the guide from Prof. Zhang could usually make me retake the direction and confidence. His profound thoughts, tolerant personality, broad knowledge, and rigorous academic attitude benefited me greatly.

Aihong Meng and Qinghai Li provided many guidance, assistance, and support during my doctoral study. The conduct of my doctoral project and writing of academic articles cannot go smoothly without the advice and suggestions from Aihong Meng. The help in five years cannot be expressed in just a few words.

Ruiming Yang provided a lot of help on analyses of TGA-FTIR, ICP-AES, and GC-MS. I really appreciated his patience and professional dedication. Dongwu Chang provided a lot of support on GC analyses, proximate analyses, and heating value measurement. Yingli Gong provided a lot of help on ultimate analyses.

From November 2013 to April 2014, I conducted part of my doctoral research under the supervision of Prof. Paul Williams at Leeds University, who is very approachable and helpful. Dr. Chunfei Wu contributed many opinions and suggestions on my research, and Dr. Jude Onwudili provided a lot of help and support for PAH analysis.

The communications with colleagues in our group on research and life are really unforgettable. Especially, Yanqiu Long and Shen Chen provided considerable help on my research. During my visit to Leeds, friendship with Juniza Md Saad and Amal Al-Rahbi made that time very impressive.

DTE 62 is my undergraduate class. We are keeping the cohesion like before until now. No matter the Ph.D. students studying in Tsinghua, or good friends working outside, I feel warm inside every time I think about them. Hope that we can keep this relationship after many years.

It has been around fourteen years since I study or work outside home. My parents are my strongest support, providing endless love and selfless giving. Wish healthy and happiness are always around you.

From September 2010, Ran Wei accompanied my whole doctoral life and made the originally dull study days more colorful. We had to separate for many days and reunite for only a few days, which made me treasure this relationship more. She gives me not only care in life, but also encouragement when I am depressed. She also gives me the motivation to become a better person!

Contents

List of Figures

List of Tables

Chapter 1
Introduction

Abstract The amount of combustible solid waste (CSW) is increasing with the development of economics and people's living standards. The increasing CSW causes many environmental problems, such as land occupation, air pollution, and water pollution. In this chapter, the composition and trend of CSW in China are statistically analyzed. There are three main CSW disposal methods, i.e., landfill, compost, and waste-to-energy. Thermochemical conversion of CSW is one method of waste-to-energy (WTE), which is also the theme of this research. However, two special pollutions, polychlorinated dibenzo-*p*-dioxin/dibenzofurans (PCDD/Fs) and polycyclic aromatic hydrocarbons (PAHs), are unwanted from this process. In the second part of this chapter, the current research situations are then intensively reviewed from the perspective of single components and multiple components. After that, the common experimental apparatuses, fixed bed, fluidized bed, and rotary kiln are reviewed. With the summary of the previous research, the aim and main content of this thesis are then illustrated.

Keywords Combustible solid waste (CSW) · Waste-to-energy (WTE) · Thermochemical conversion

1.1 Research Background

1.1.1 Current Situation and Crisis of CSW in China

Combustion solid waste, also called municipal solid waste, is the solid waste produced from the daily life of urban residents. Its main components include food residue, wood waste, paper, plastics, metal, glass, ceramics, and ash.

With the rapid development of the economy, acceleration of urbanization process, and improvement of people's living standards, the amount of CSW increases year by year. China Statistical Yearbook (NBSC 2014) reported that the amount of municipal CSW in China reached 172 million tons in 2013. Figure 1.1 summarizes

H. Zhou, *Combustible Solid Waste Thermochemical Conversion*, Springer Theses,
DOI 10.1007/978-981-10-3827-3_1

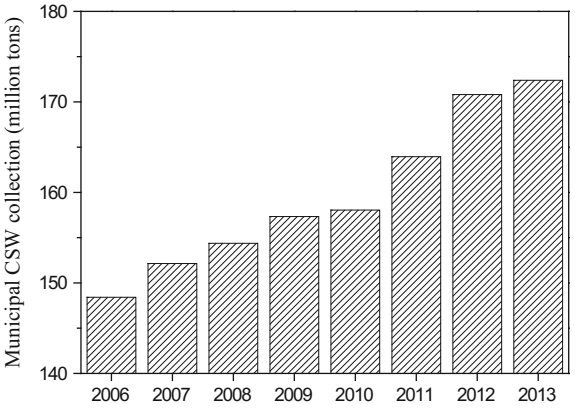

Fig. 1.1 Municipal CSW collection amount in China

the amount of municipal CSW in different years (NBSC 2007, 2008, 2009, 2010, 2011, 2012, 2013, 2014).

Continuous production of CSW causes a series of problems, such as land occupation, air pollution, and water pollution. Therefore, how to disposal municipal CSW is an urgent and significant issue for the sustainable development of cities (Huai et al. 2008).

1.1.2 Components and Trend of CSW in China

CSW is a complicated mixture, whose chemical characteristics are related to the properties of its components. The physical components of CSW are related to the local climate, lifestyle, and economic level (Liu and Wu 2011; Yi et al. 2011; Kathirvale et al. 2004; Gidarakos et al. 2006; Boer et al. 2010). In developed and high living standard cities, the fractions of plastics, paper, and fibers in CSW are high; in coal-based cities, the fractions of coal cinder and sand are higher (Boer et al. 2010). In recent years, with the increase in municipal CSW amount, the components of municipal CSW change at the same time. The inorganic fraction decreases, organic fraction increases, combustible fraction increases, and utilizable value increases (Li et al. 2009; Xiao et al. 2007; Liu et al. 2006).

The sampling and analysis methods for domestic waste (MHURDC 2009) stipulate that CSW includes organics and inorganics, as shown in Table 1.1. Organics include food residue, wood waste, paper, textiles, plastics, and rubber; inorganics include metal, glass, ceramics, and ash.

According to statistical analysis of public information, the average components of CSW in China are shown in Fig. 1.2. The average fractions of combustibles and incombustibles are 81.26 and 18.74%, respectively. The fraction order of combustible components from high to low is food residue, plastics, paper, textiles, wood waste, and rubber (Zhou et al. 2014).

Table 1.1 Classification of CSW

Classification	Component	Specific source
Organics	Food residue	Rice, flour, animal carcass, meat, vegetables, fruit peel
	Wood waste	Waste wood, disposable chopsticks, flowers, grass, fallen leaves, tree branches
	Paper	Wrapping paper, paperboard, office paper, tissue paper, newspapers, magazine
	Textiles	Old clothes, cloth shoes
	Plastics	Film, bottles, tube, bags, toys
	Rubber	Rubber shoes, belt, bags
Inorganics	Metal	Iron sheets, iron wire, cans, metal parts, toys, furniture, pan
	Glass	Glass fragments, bottles, tubes, mirror, instruments, balls
	Ceramics	Stone, tile, cement block, pot, ceramics, lime
	Ash	Furnace slag, soil
	Other	Batteries, gypsum, etc.

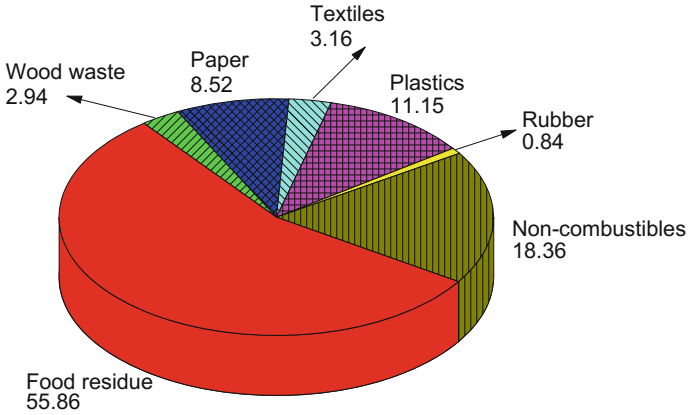

Fig. 1.2 Average fractions of physical components in CSW. Reprinted from Zhou et al. 2014, Copyright 2014, with permission from Elsevier

1.1.3 The Disposal Methods of CSW

Currently, there are three main CSW disposal methods: landfill, compost, and waste-to-energy.

1. Landfill is the oldest CSW disposal method and still popular in many countries all over the world. The most significant advantage of landfill is low cost and availability to various kinds of CSW. In addition, other disposal methods also need landfill finally, such as the combustion slag and fly ash (Williams 2005).

The main disadvantage of landfill is the occupation of a large amount of land resource, which is even severe in the eastern coastal areas with high population density in China. Many cities are facing the issue of no land to fill. Meanwhile, landfill gas is a hazardous secondary pollution source. Methane is a strong greenhouse gas, whose direct emission will exacerbate global warming. Large amounts of methane may also reach the explosion concentration. Furthermore, the landfill leachate is a toxic pollutant, which may contaminate soil and underground water.

2. Compost is the aerobic biodegradation process of organics such as yard waste and food residue. The degradation products of compost are relatively stable, which may improve the soil structure, provide nutrition as fertilizer, and help to maintain the soil moisture. However, compost may generate greenhouse gas such as carbon dioxide and methane. Moreover, since the improper classification of CSW, the fertilizer may contain pollutants such as heavy metals (Williams 2005). Therefore, the compost percentage of CSW in China is decreasing year by year. From 2011, the amount of compost is not counted in NBSC any more, as shown in Fig. 1.3.
3. Waste-to-energy is the process using CSW as a fuel directly or indirectly and converting it to energy. In recent years, WTE technology has been widely applied around the world (Cheng and Hu 2010). The thermochemical conversion of CSW (combustion, pyrolysis, and gasification) is a typical WTE technology. CSW is disposed at a fast rate at high temperatures. Thermochemical conversion can handle different kinds of CSW effectively, especially municipal CSW without classification. Its main advantages include the following: (1) The mass of CSW can be reduced by 70–80%, and the volume can be reduced by 80–90%, which can save landfill area (Consonni et al. 2005); (2) organic pollutants such as halogenated hydrocarbons can be destroyed (McKay 2002; Buekens and Cen 2011); (3) the inorganic pollutants can be aggregated, which can help the further effective disposal; (4) metals can be recycled from bottom

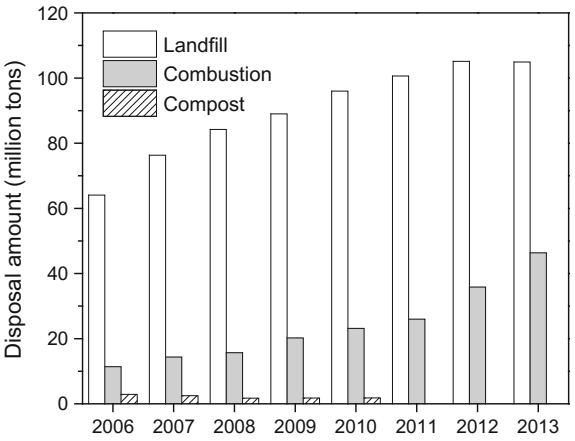

Fig. 1.3 CSW disposal methods in China in recent years

slag; (5) greenhouse gases from anaerobic decomposition of organics can be reduced; and (6) different kinds of energy can be obtained, such as electricity and thermal energy (Arena 2012).

Combustion is regarded as the CSW disposal method that can replace landfill (Eriksson et al. 2007). From the 1970s, with the development of flue gas treatment technologies and combustion facility manufacture technologies, combustion of CSW is adopted by more and more countries (Yi et al. 2011). From the 1980s, advanced incineration technologies and facilities are introduced into China from abroad, and independent development is realized gradually. As shown in Fig. 1.3, the amount of combustion of CSW increases from 3.7 to 46.3 million tons from 2003 to 2013, and the number of incineration plant increases from 47 to 166 from 2003 to 2013 (NBSC 2004. 2014).

In recent years, the pyrolysis and gasification of CSW have attracted extensive attentions (Liu and Liu 2005). Pyrolysis and gasification represent new WTE methods, which can convert CSW into gas, liquid, and solid that can be further utilized with better economic performance (Luo et al. 2010).

1.1.4 Pollutants from CSW Thermochemical Conversion

With the increase in industrial applications of CSW thermochemical conversion, some environmental issues stand out gradually. The secondary pollution is the bottleneck problem limiting the application of CSW thermochemical conversion technology worldwide.

Besides common pollutants such as CO, SO_x, and NO_x, the secondary pollutants of CSW thermochemical conversion mainly include heavy metals (such as Hg, Cd, Pb, and Cu), acid gases (such as HCl), PCDD/Fs, and PAHs. PCDD/Fs and PAHs are two significant organic pollutants.

1.1.4.1 PCDD/Fs

PCDD/Fs are the summaries of a class of compounds, including polychlorinated dibenzo-*p*-dioxins (PCDDs) and polychlorinated dibenzofurans (PCDFs), which are composed of 75 and 135 homologues, respectively, as shown in Fig. 1.4.

PCDD/Fs are solid at ambient temperatures, with high melting and boiling points, low vapor pressures, and low water solubility. They are among the most toxic chemicals and confirmed by US Environmental Protection Agency (USEPA) as severe cancerogens. PCDD/Fs are very stable in the environment. Because of their high lipotropism, PCDD/Fs are easy to accumulate in living bodies, damage human immune system, and disturb hormonal regulation (Mckay 2002).

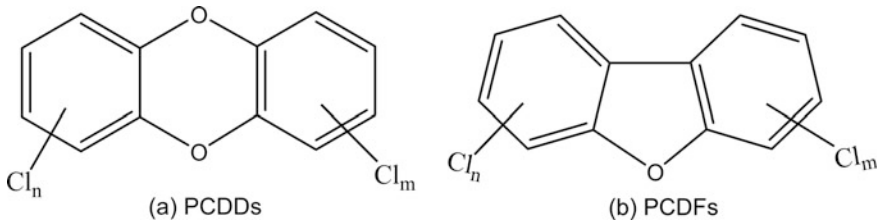

Fig. 1.4 Structure of PCDD/Fs. Reprinted from Zhou et al. (2015), Copyright 2015, with permission from Elsevier

1.1.4.2 PAHs

Another group of significant pollutants from CSW thermochemical conversion process is PAHs. PAHs have very strong carcinogenic, teratogenic, and mutagenic effects, as well as bioaccumulative effect (Samanta et al. 2002; Moeckel et al. 2014; Ionescu et al. 2012). PAHs from CSW thermochemical conversion may form the core of PM 2.5 and then be absorbed by the human body from breath (Miller et al. 1979; Ragazzi et al. 2013; Buonanno et al. 2011; Richter and Howard 2000). In addition, one of the significant formation pathways of PCDD/Fs is the de novo process of soot and PAHs in fly ash at 200–400 °C (Iino et al. 1999; Fullana and Sidhu 2005; Chin et al. 2012).

Though there are various kinds of PAHs in the environment, USEPA has listed 16 kinds of PAHs as priority pollutants, including naphthalene, acenaphthylene, acenaphthene, fluorene, phenanthrene, anthracene, fluoranthene, pyrene, benzo[*a*] anthracene, chrysene, benzo[*b*]fluoranthene, benzo[*k*]fluoranthene, benzo[*a*]pyrene, dibenzo[*a*, *h*]anthracene, benzo[*g*, *h*, *i*]perylene, and indeno[1, 2, 3-*cd*]pyrene (OFR 2000). In 2007, the global emission of 16 PAHs is approximately 504 Gg (Shen et al. 2013).

1.2 The Research Status of Thermochemical Conversion of CSW

1.2.1 Overview of CSW Thermochemical Conversion Processes

The thermochemical conversion of CSW includes pyrolysis, gasification, and combustion. The characteristics of them are shown in Table 1.2 (Arena 2012).

As shown in Fig. 1.5, pyrolysis could produce gas, tar, and char that can be further utilized. In addition, pyrolysis is the fundamental process of gasification and combustion (Di Blasi 2009; Skreiberg et al. 2011). Therefore, the research of CSW pyrolysis is the basic research of CSW thermochemical conversions.

Table 1.2 Characteristics of pyrolysis, gasification, and combustion of CSW

Thermochemical conversion	Pyrolysis	Gasification	Combustion
Purpose	Converting CSW to gas and condensed phase	Converting CSW to high HHV gas, including CO, H_2, and CH_4	Converting CSW to high-temperature flue gas, mainly CO_2 and H_2O
Atmosphere	No oxidant	Partial oxidizing atmosphere (oxidant amount lower than the stoichiometric value)	Oxidizing atmosphere (oxidant amount usually higher than the stoichiometric value)
Reaction medium	None	Air, pure oxygen, steam, or CO_2	Air
Temperature	500–800 °C	550–1600 °C	850–1200 °C
Pressure	Micro-positive pressure	Normal pressure	Normal pressure
Gas products	CO, H_2, CH_4, and other hydrocarbons	CO, H_2, CO_2, H_2O, and CH_4	CO_2 and H_2O
Pollutants	H_2S, HCl, NH_3, HCN, tar, and dust	H_2S, HCl, NH_3, HCN, tar, and dust	SO_2, NO_x, HCl, PAHs, PCDD/Fs, and dust

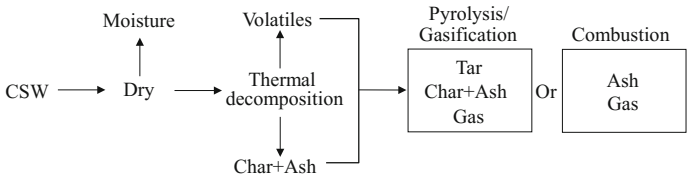

Fig. 1.5 Processes of CSW thermochemical conversions

1.2.2 The Research Status of Thermochemical Conversion of CSW Single Components

The components of CSW are complicated and vary from place to place. The physical components of CSW from different regions are different. Even for CSW from the same region and the same year, the physical components of CSW reported by different researchers may be quite different (Xi et al. 2010). In addition, the lab-scale research of CSW usually takes samples of gram level (Zhang et al. 2008b; Velghe et al. 2011), which means great randomness during the sampling process of real CSW. Therefore, more and more studies choose CSW single components for study.

As shown in Table 1.3, many researchers have used thermogravimetric analyzer (TGA) (Singh et al. 2012; Chang et al. 1996), fixed bed reactor (An et al. 2006;

Table 1.3 Summary of research of CSW thermochemical conversion

Author, year	Sample	Apparatus	Research content	Influential factor
Li et al. (1999a)	Paper, paperboard, cotton cloth, plastics, rubber, vegetables, orange peel, wood	Rotary kiln	Gas amount and heating value	Heating type, moisture, particle size
Jiang et al. (2002)	Wood chopsticks, rubber	TGA, fluidized bed reactor	Mass loss kinetics	
Guo et al. (2000)	Grass and trees, food residue, plastics, white foam, cloth, paper	TGA	Kinetics	Heating rate
		Fixed bed reactor	Gas products	
Dai et al. (2001)	Waste tire	Circulating fluidized bed (CFB) reactor	Tar amount and composition, gas composition	Temperature, particle size, feeding position
Li et al. (1999c)	Wood, PE, waste tire	Rotary kiln	Gas amount and heating value, tar composition, char amount and composition	Temperature
Liu et al. (2000)	PS	Bubbling fluidized bed (BFB) reactor	Conversion rate	
Jimenez et al. (1999)	PVC	TGA	Kinetics	Heating rate
Luo et al. (2010)	Plastics, food residue, wood	Fixed bed reactor		Particle size
Sorum et al. (2001)	Newspaper, cardboard, recycled paper, glossy paper, spruce, LDPE, HDPE, PP, PS, PVC, juice carton	TGA	Kinetics	
Mo et al. (2013)	Virgin PS, expanded PS, PS container	TGA	Products	
Miranda M et al. (2013)	Rubber tire wastes	High-pressure reactor	Kinetics, tar	Temperature, residence time, kinetic model
Chen et al. (2014)	Hemicellulose, cellulose, lignin	TGA	Kinetics	
Stefanidis et al. (2014)	Hemicellulose, cellulose, lignin	TGA, fixed bed reactor	Kinetics, product distribution	Catalyst
Li et al. (2013)	Cellulose, LDPE	TGA, fixed bed reactor	Kinetics, tar composition, gas composition	Catalyst
Gui et al. (2013)	PVC	Fixed bed reactor	Nascent tar	Residence time, heating rate

Shen et al. 2007; Luo et al. 2010), fluidized bed reactor (Liu et al. 2000; Dai et al. 2001), pyrolyzer (Garcia et al. 1992), or rotary kiln (Li et al. 1999b, c) for the study of CSW thermochemical conversion. The research content includes mass loss kinetics, gas products, and tar characteristics. The influential factors cover atmosphere, heating rate, and catalyst. However, in general, the research of influential factors is not systematic enough.

Some studies choose typical components in CSW for research. However, for a specific component in CSW, such as plastics, different researchers have reported different proximate and ultimate analyses' results and thermochemical conversion kinetic parameters (Qing et al. 2005; Zhang et al. 2008a; Guo et al. 2001). Actually, plastics are not a single component, which include low-density polyethylene (LDPE), high-density polyethylene (HDPE), polypropylene (PP), polystyrene (PS), polyvinyl chloride (PVC), and polyethylene terephthalate (PET).

Therefore, some studies focus on relative standard components for investigation, such as cellulose, lignin, and PVC (Chen et al. 2014; Gui et al. 2013). These components have relatively determinate, universal, and repeatable characteristics. In addition, they can be used to simulate complex real components. For example, biomass is mainly composed of hemicellulose, cellulose, and lignin (Zhou et al. 2013), and then, the research of biomass can be transferred to the research of these three components.

1.2.2.1 Kinetics

Basic kinetic research can help to predict the behavior of CSW during thermochemical conversion processes and design better industrial reactors (Cho et al. 2012; Zhang et al. 2014a). In the research of kinetics, several models have been developed, including single reaction model, segmented reaction model, distributed activation energy model (DAEM), and paralleled reaction model (PRM).

Single reaction model is the simplest model, which is suitable to describe single-step reactions. The pyrolysis of cellulose can be described by a first-order reaction, with the activation energy (AE) 33.4 kcal mol^{-1} and frequency factor 6.79×10^9 s^{-1}. However, single reaction model usually has difficulties in simulating complex multi-step reactions (Bigger et al. 1998).

The segmented reaction model is widely used to describe the linear programmed temperature TGA tests, which divides a complex reaction into several segments according to the temperature range (Lu et al. 2009). Guo et al. (2000) investigated the pyrolysis kinetics of typical CSW components in TGA and reported that the pyrolysis of combustibles in CSW followed the basic pyrolytic kinetic equations and could be described by one or multiple first-order reactions. Chang et al. (1996) carried out the pyrolysis of printing paper and writing paper in TGA at 400–850 K with the heating rates of 1, 2, and 5 K min^{-1}. The pyrolysis of these two papers had two segments, which could be described by a two-reaction model. Lopez-Velazquez et al. (2013) studied the pyrolysis of orange waste in N_2 atmosphere in TGA. The pyrolytic process could be regarded as multistage reaction, i.e.,

(i) dehydration below 120 °C; (ii) pyrolysis at 125–450 °C when degradation of lignocellulose reached the maximum with the release of gas and energy; and (iii) pyrolysis of lignin above 450 °C. However, kinetic parameters from segmented reaction model are very sensitive to the selection of start temperature and end temperature, which are usually very subjective. In addition, the assumption of segmented reaction model that only one reaction happens at a temperature range is not correct sometimes, such as for the pyrolysis of complex biomass.

Distributed activation energy model is a relatively advanced kinetic model (Várhegyi et al. 2009; Wu et al. 2014b), which assumes a series of irreversible first-order reactions happen simultaneously to form the distribution of activation energy (Zhang et al. 2014a). Zhang et al. (2014a) found that Gaussian-DAEM could reproduce the derivative thermogravimetric (DTG) curve of cellulose pyrolysis accurately. However, the error was considerable for the prediction of the pyrolytic kinetics of hemicellulose and lignin. Therefore, the authors developed Double-Gaussian-DAEM, which used two Gaussian distributed AE series to depict the pyrolysis of hemicellulose and lignin. Nevertheless, since AE is described as a series of values and even a distribution diagram, this model is difficult to be applied and compared (Sonobe and Worasuwannarak 2008).

Paralleled reaction model is an emerging reaction model in recent years, which regards complicated reactions as several paralleled reactions. Sorum et al. (2001) studied the pyrolysis of 11 typical CSW components and reported that biomass pyrolysis could be described by three paralleled pyrolytic reactions of hemicellulose, cellulose, and lignin. PVC pyrolysis could also be described by three paralleled reactions. However, during the actual operation, how to separate the paralleled reactions is an intractable problem.

TGA is the most common used experimental method for the research of kinetic characteristics (Zhang et al. 2014b; Chen and Kuo 2010). However, in TGA experiments, the temperature is elevated only after the samples are put in the TGA, and thus, the heating rate is limited to tens of degrees per minute (Seo et al. 2011), while heating rate is proved to have a significant effect on kinetics (Biagini et al. 2008). Meanwhile, the sample mass in TGA is microgram level, with negligible heat and mass transfer effects, which is quite different from industrial reactions. Therefore, Zheng et al. (2009) employed a self-designed TGA with the maximal heating rate of 864.8 °C min^{-1} to investigate the pyrolysis of six typical CSW components. The results have shown that the pyrolytic characteristics of high heating rate and low heating rate are significantly different, especially for biomass. With the increase in heating rate, some reaction processes occurred at the same time and the mass loss peaks of these reactions were merged.

1.2.2.2 Gas, Liquid, and Solid Distribution

The main products of CSW combustion are gas and ash, while the products of pyrolysis and gasification include gas, tar, and char. The gases contain not only CO_2 but also combustible components H_2, CO, CH_4, and other light hydrocarbons. The

tar contains both water and organic components; the char contains carbon and ash. Therefore, in order to obtain aimed products, such as syngas or tar, the research of product distribution of CSW thermochemical conversion is very meaningful.

Heating rate has a significant influence on product distribution of pyrolytic process. The experiments in rotary kiln have shown that gas amount of pyrolysis mainly depended on the residence time at high temperatures. The gas production rate from fast pyrolysis was much higher than that from slow pyrolysis (Li et al. 1999a).

Temperature also has a significant influence on the distribution of pyrolytic products. He et al. (2010) investigated the syngas from CSW catalytic pyrolysis using lab-scale downstream fixed bed reactor at 750–900 °C. The results showed that with the increase in temperature, the syngas production increased and the concentration of H_2 and CO increased.

Some studies have explored the influence of particle size on mass distribution of pyrolytic products. For example, Luo et al. (2010) pyrolyzed typical CSW components such as plastics, food residue, and wood in fixed bed at 800 °C. The results showed that sample particle size had a significant influence on pyrolytic product distribution and composition. With the decrease in sample particle size, gas amount increased, tar and char decreased, H_2 and CO increased, and ash and solid carbon increased. For food residue with high amounts of fixed carbon and ash, the influence was more significant.

1.2.2.3 Gas Production

The combustion of CSW produces mainly CO_2 and H_2O, while gas products from pyrolysis and gasification are more complicated. In addition to inorganic gases H_2, CO, and CO_2, pyrolysis and gasification generate CH_4, C_2H_4, and other light hydrocarbons.

Temperature has a significant influence on gas products. Garcia et al. (1992) investigated the relationship of 13 kinds of pyrolytic products and temperature (500–900 °C) using Pyroprobe 1000. The results showed that the amount of methane, ethylene + acetylene, ethane, propane, propene, butene, and butane increased with temperature from 500 to 900 °C, and the amount of methanol + formaldehyde, acetaldehyde, ethanol, and water did not change significantly with temperature. The pyrolytic experiments by Li et al. (1999a) in rotary kiln showed that with the increase in pyrolytic temperature, more C–H bonds broke, which made the amount of H_2 increase, and the amount of C_2H_4 and C_2H_6 decrease. The heating value of pyrolytic gas increased first and then decreased. Agarwal et al. (2013) pyrolyzed vegetable waste using a self-designed packed bed reactor and studied the influence of process parameters such as temperature on pyrolytic gas and its composition. When the temperature was 1073 K, the amount of pyrolytic gas was the highest (260 ml g^{-1}), and the concentration of H_2 reached the maximum (32.68%).

1.2.2.4 Tar and PAH Formation

Many studies involve the formation of tar, especially PAHs during CSW pyrolysis.

Production of bio-oil from biomass is the technology with increasing concerns in both academia and industry. The pyrolytic experiments in fixed bed by Dieguez-Alonso et al. (2013) have shown that 2-ring aromatics were the main PAHs from the pyrolysis of pine and beech. With the increase in residence time, 3-ring and 4-ring aromatics increased.

Hemicellulose, cellulose, and lignin are the three main components of biomass, which also have high percentages of CSW. McGrath et al. (2003) investigated the PAH formation during cellulose pyrolysis at 300–650 °C and found that 2–4-ring PAHs could be detected above 400 °C. The authors hold the point that the formation of PAHs experienced carbonization process, and the solid materials experienced chemical transformation and rearrangement.

Compared to hemicellulose and cellulose, the pyrolysis of lignin generated the most PAHs. Wu et al. (2013) studied the pyrolytic characteristics of hemicellulose, cellulose, and lignin in a two-stage reactor. Naphthalene was detected in the tar of all the pyrolytic experiments, while the most was found in lignin tar. In addition, various kinds of PAHs were detected in lignin tar. Font et al. (2003) investigated the decomposition of Kraft lignin in a horizontal furnace at 800–1100 °C under air atmosphere. Naphthalene, acenaphthylene, phenanthrene, fluoranthene, and pyrene were detected. In addition, with the increase in temperature, the generation of PAHs increased. The research of Asmadi et al. (2011a, b) has shown that the lignin pyrolysis happened from the crack of weak α ether bonds and β ether bonds, with the release of guaiacyl and syringyl aromatic compounds. These aromatics further reacted to form catechols and pyrogallols, and then, PAHs were generated. Dorrestijn et al. (2000) have reported that at 200–400 °C, the linkages between lignin units broke, and α–O–4 ether bond was the weakest. With the further increase in temperature, secondary reactions happened to form catechols from guaiacols. Strong C–C bonds were formed from the structure of C-center radicals, and thus, tar was formed. Thomas et al. (2007) performed the pyrolysis and gasification experiments of lignin model compound such as catechol in a laminar flow reactor. Catechol was completely converted above 850 °C, and the increase in oxygen concentration reduced the hydrocarbons.

Some research involved the tar formation of plastics pyrolysis. When LDPE was pyrolyzed in a closed batch reactor, aliphatic hydrocarbons were the main components, while aromatics including naphthalene increased with the increase in temperature and residence time (Onwudili et al 2009). Liu et al. (2000) pyrolyzed PS in a fluidized bed reactor at 450–700 °C, and the main products were styrene monomer, bipolymer, and trimer. The pyrolytic liquid accounted for more than 90%, and the amount of gas and char was low. Secondary reactions reduced the amount of styrene monomer, but increased the monocyclic compounds with the boiling point below 200 °C. Wang et al. (2003) investigated the PAHs released from PVC combustion and found that with the increase in temperature from 500 to

1000 °C, the amount of PAHs decreased from 4000 to 2000 $\mu g\ g^{-1}$ and fluorene, phenanthrene, and anthracene all decreased.

Overall, since CSW is a complex mixture including plastics and biomass (Zhou et al. 2014; Burnley 2007), increasing amounts of studies begin to focus on CSW model compounds, such as cellulose, lignin, PE, and PS. (Luo et al. 2010; Yang et al. 2007). However, comparison of pyrolytic processes of different model components in different reactors and conditions is very difficult. To compare the pyrolytic characteristics of different components, experiments under the same conditions are necessary.

1.2.3 The Research Status of Thermochemical Conversion of CSW Multiple Components

During CSW thermochemical conversion processes, interactions may happen among components. The reaction characteristics are very complicated, which are not the simple linear superposition of single components (Wen 2006).

In the research of interactions of CSW multiple components, the interactions between two components are the basic knowledge. The common method is testing the mixture with the ratio 1:1 and then comparing it with linear superposition results of single components (Giudicianni et al. 2013; Wang et al. 2011; Hosoya et al. 2007).

1.2.3.1 Kinetics

Most of the experimental studies of CSW pyrolytic kinetics use single components, and only a few studies focus on the interactions of multiple components. It has been reported that the interactions among components were usually non-negligible (Wang et al. 2011; Wu et al. 2014a).

Jiang et al. (2002) investigated the co-combustion properties of wood chopsticks and rubber in TGA and fluidized bed. In the fluidized bed, the mass of reacted carbon was calculated from the real-time CO_2 concentration in the flue gas, and further, the real-time mass loss of combustion could be obtained. The results showed that the combustion characteristics of the mixture in TGA could be indicated from single-component superposition, while the combustion characteristics in fluidized bed could not be indicated from single-component superposition. The authors believed that the combustion could be separated into stages in TGA with a low heating rate and, thus, the interactions were insignificant, while the combustion stages happened simultaneously in the fluidized bed reactor, so the interactions were significant. In this study, the effects of H, S, Cl, and N were ignored in the mass loss calculation of fluidized bed reaction, which might bring some errors.

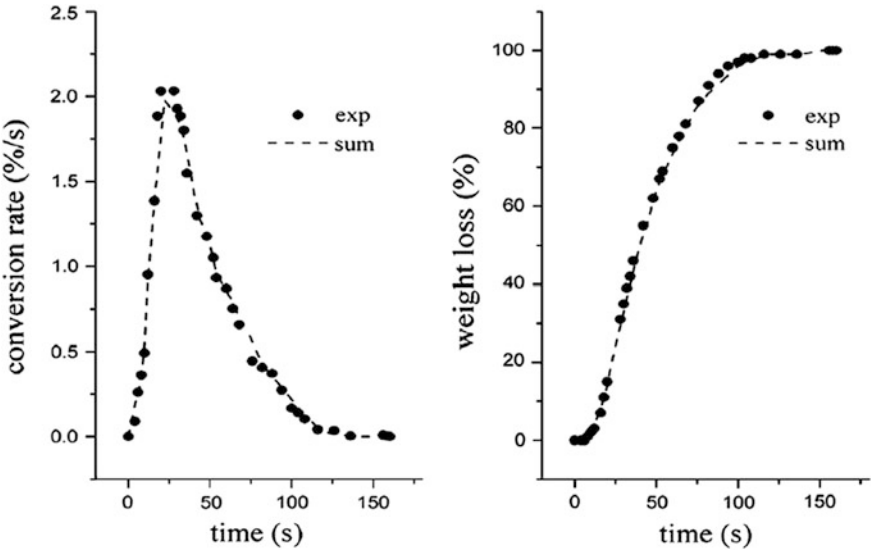

Fig. 1.6 Conversion rate and weight loss for pyrolysis of biomass mixture. Reprinted from Zheng et al. (2009), Copyright 2009, with permission from Elsevier

Biomass and plastics are the most important categories in CSW, and thus, many studies focus on the interactions of them. Zheng et al. (2009) investigated the pyrolysis of 6 CSW components and their mixtures in a self-designed TGA. As shown in Figs. 1.6 and 1.7, the interaction between two biomass components was weak, while the interaction between polyethylene (PE) and wastepaper was stronger. The reason was deemed that the absorbed heat by PE pyrolysis decreased the heating rate of wastepaper pyrolysis, and that was also why the interactions were much stronger at high heating rate reactions.

Many studies have shown that the interactions between PVC and biomass were very strong during co-pyrolysis. Matsuzawa et al. (2001) investigated the interactions between cellulose and PE, PP, PS, as well as PVC, and found that only PVC could interact with cellulose. The Fourier transform infrared spectroscopy (FTIR) analysis has shown that the char from cellulose/PVC co-pyrolysis had fewer hydroxyls and more C=O and C=C bonds than that from cellulose pyrolysis alone. The authors believed that Cl from PVC pyrolysis promoted dehydration, scission of glucose ring, and char formation. Sorum et al. (2001) investigated the co-pyrolysis of newspaper and plastics in TGA, as shown in Fig. 1.8. No significant interaction was observed between newspaper and LDPE, while the addition of PVC increased the reactivity of newspaper. The possible reason was the released HCl interacted with cellulose, catalyzed acid hydrolysis reactions, and decreased the stability of cellulose. The detailed reason needed further research.

The research of interactions usually uses the mixture of two components, because the mixture of more than three components is very complicated, and thus,

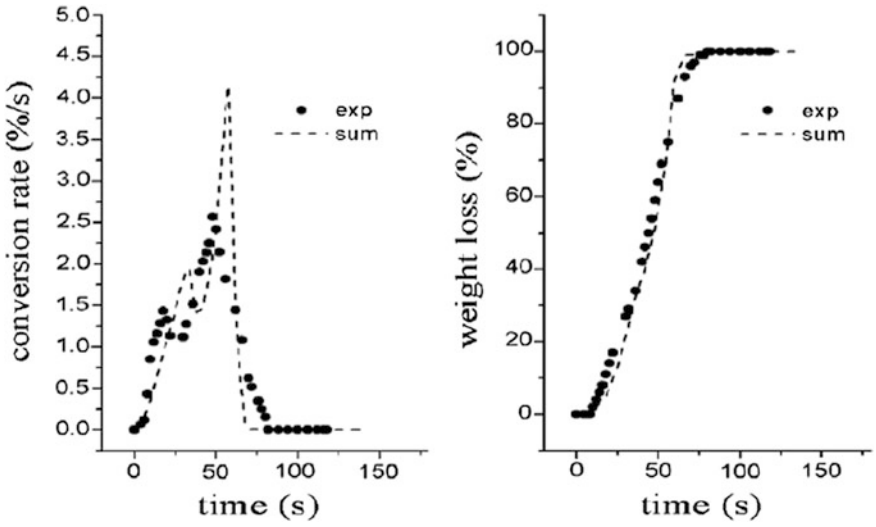

Fig. 1.7 Conversion rate and weight loss for pyrolysis of the mixture of PE and wastepaper. Reprinted from Zheng et al. (2009), Copyright 2009, with permission from Elsevier

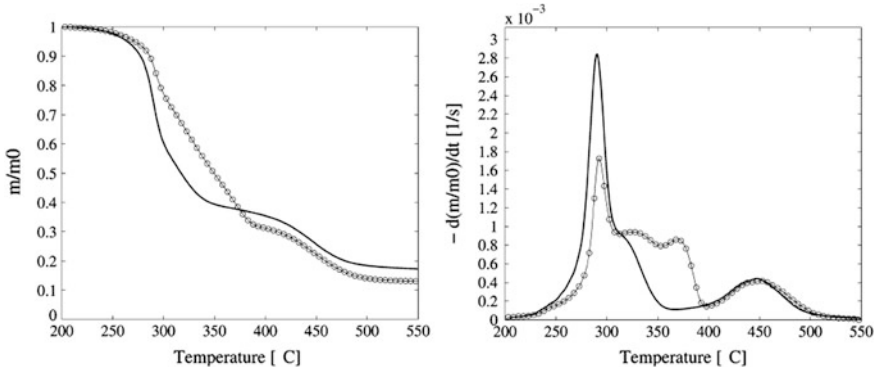

Fig. 1.8 TG and DTG curves of pyrolysis of the mixture of PVC and newspaper [mixture experiments (——), superposition of single components (-o-o-o-)]. Reprinted from Sorum et al. (2001), Copyright 2001, with permission from Elsevier

the mechanisms are even harder to explore. Therefore, these studies are mainly qualitative research to explore whether there are significant interactions. Guo et al. (2001) investigated the combustion characteristics of CSW mixtures using TGA. As shown in Fig. 1.9, the experimental results of co-combustion are different from the linear superposition of kinetic model results.

Up till now, the kinetic studies of interactions of CSW mainly focus on experiments of slow pyrolysis (Matsuzawa et al. 2001; McGhee et al. 1995).

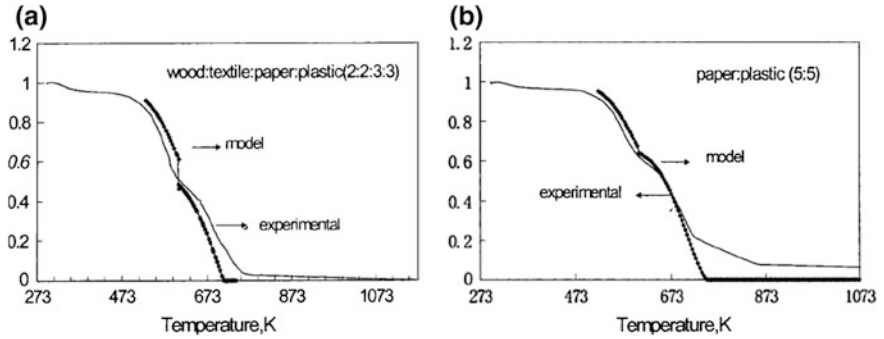

Fig. 1.9 Comparison of the kinetic model and experimental results. Reprinted with the permission from Guo et al. (2001). Copyright 2001 American Chemical Society

Meanwhile, most of them are in TGA reactor, and the interaction studies of fast pyrolysis in lab-scale reactors are rare. As is well-known, the heat and mass transfer effects of fast pyrolysis in lab-scale reactors are strong, which means that the interactions in fast pyrolysis are quite different from those in slow pyrolysis. For slow pyrolysis, if the pyrolysis of one component is finished when the pyrolysis of the other begins, the interaction between these two components will be very limited. For fast pyrolysis, since all the components pyrolyze almost at the same time, the interactions may be significant. In addition, compared to slow pyrolysis, fast pyrolysis is regarded as the promising technology to produce tar and char (Tsai et al. 2006).

1.2.3.2 Gas, Liquid, and Solid Distribution

These three biomass components (hemicellulose, cellulose, and lignin) usually present at the same time. Therefore, the interactions among these three components are worth studying. Giudicianni et al. (2013) studied the gasification of biomass components and the interactions of pairwise mixtures in a steam atmosphere. The results showed that the main interactions happened between cellulose and lignin, and the interactions had influences on both amount and composition of solid and gas. Hosoya et al. (2007) also investigated the interactions between cellulose and lignin during co-pyrolysis and reported that the generation of gas, tar, and char was all affected by interactions at 800 °C. Lignin promoted the formation of levoglucose and small molecules from cellulose pyrolysis, and inhibited the formation of char. Cellulose inhibited the char of secondary reactions of lignin pyrolysis and promoted the formation of compounds such as guaiacol, 4-methylguaiacol, and 4-vinylguaiacol.

The product distribution of co-pyrolysis of biomass and plastics is widely studied. When pine cone was pyrolyzed together with synthetic polymers (PE, PP,

and PS) at 500 °C, mixture experiments generated more liquid products than linear superposition results. The co-pyrolysis of cellulose and synthetic polymers generated more gas products and less char (Brebu et al. 2010). Caglar and Aydinli (2009) studied the co-pyrolysis of hazelnut shell and ultra-high molecular weight PE (UHMWPE). The results showed that co-pyrolysis generated less liquid and more gas, which was inverse to the results of Brebe et al.

From 1.2.3.1, the co-pyrolysis of PVC and biomass has significant influences on kinetics. The experiments of McGhee et al. (1995) showed that during the co-pyrolysis of PVC and straw, the amount of char was higher than the superposition of single-component pyrolysis. Meanwhile, the reactivity of char decreased. The authors deemed that HCl interacted with cellulose below 600 K.

1.2.3.3 Gas Production

The interactions of biomass have a complex influence on gas products. The steam gasification of Giudicianni et al. (2013) showed that due to the interactions between hemicellulose and cellulose, the generation of CO_2 and CO increased, while other fractions (H_2 and hydrocarbons) increased slightly, and the gas heating value did not change significantly. The interactions between cellulose and lignin also had insignificant influence on gas heating value. The generation of CO was inhibited at high temperatures. The reason might be lignin inhibited the thermopolymerization of levoglucose and promoted the generation of small molecules from cellulose pyrolysis. The mixture of hemicellulose and lignin promoted the generation of CO_2 below 800 K and promoted the generation of CO_2 and H_2 above 800 K.

The co-gasification of biomass and plastics has a significant influence on gas products. Alvarez et al. (2014) investigated the co-gasification of biomass and PP in a steam atmosphere and found that the mixture of PP and biomass increased the production of H_2. Wilk and Hofbauer (2013) investigated the co-gasification in the steam of four kinds of plastics and biomass in a dual CFB reactor. The results indicated that co-gasification had a significant effect on gas composition, and the effect was nonlinear. Due to interactions, the generation of CO and CO_2 increased, while the generation of CH_4 and C_2H_4 decreased. Li et al. (2013) investigated the co-pyrolysis of cellulose and LDPE and found that interactions increased the generation of CO and CO_2 and decreased the generation of C_1–C_3 hydrocarbons, which was consistent with the results of Wilk et al. The authors deemed that oxygenates from cellulose could react with small hydrocarbons from LDPE and increased the generation of CO and CO_2 with the formation of aromatics.

1.2.3.4 Tar Formation

A few studies involved the effect of interactions of three biomass components on the composition of tar. The pyrolysis test of Wang et al. (2011) has shown that the

interactions between hemicellulose and cellulose strongly promoted the generation of 2, 5-diethoxytetrahydrofuran and inhibited the generation of altrose and levoglucose. The presence of cellulose increased the generation of acetic acid and 2-furaldehyde from hemicellulose pyrolysis. Stefanidis et al. (2014) carried out two kinds of mixture experiments: the mixture of hemicellulose and cellulose (1:1) (Mix 1) and the mixture of hemicellulose, cellulose, and lignin (1:1:1) (Mix 2). The results have shown that the experimental results had significant differences from calculated results. Both of these two mixture experiments observed the decrease in sugar (mainly levoglucose), while ketones increased for Mix 1 and phenols increased for Mix 2. Hosoya et al. (2007) investigated the co-gasification of cellulose and lignin and found that the presence of cellulose promoted the generation of guaiacol, 4-methylguaiacol, and 4-vinylguaiacol from lignin.

Since agricultural waste is usually mixed with plastic film, Dorado et al. (2014) studied the catalytic pyrolysis of the mixture of biomass and plastics (PET, PP, HDPE, LDPE, and PS) using pyrolysis–gas chromatography/mass spectrometry (Py-GC/MS). The results showed that the mixture of biomass and PE, PP, or PET increased the generation of aromatic compounds (toluene, xylene, and ethylbenzene). The reason might be that the oxygenates (such as furans) from biomass pyrolysis could react with alkenes from plastic pyrolysis to form aromatics.

The research of interactions of CSW thermochemical conversion can be summarized as follows:

(1) The research of interactions focused on TGA reactor, while the research on gram-scale reactor was rare;
(2) The research of interactions focused on kinetics, while the research on gas and tar generation was rare, and the research on PAH formation was rarer;
(3) The research of interactions focused on slow pyrolysis, while the research of fast pyrolysis was rare, and the interactions of fast pyrolysis might be quite different from that of slow pyrolysis. For example, during slow pyrolysis, if the decomposition of one component is finished when the other begins to decompose, the interactions may be weak. During fast pyrolysis, two components pyrolyze almost at the same time, and the interactions may be strong.

1.3 The Research Status of CSW Thermochemical Conversion Reactor

Besides commonly used TGA and pyrolyzer, the research apparatus of CSW thermochemical conversion includes fixed bed, fluidized bed, and rotary kiln, each of which has a corresponding industrial reactor.

1.3.1 Fix Bed Reactor

An et al. (2006) pyrolyzed the CSW mixture using a fixed bed reactor under N_2 atmosphere, as shown in Fig. 1.10. The heating power was 7.5 kW, and the furnace had inner diameter 200 mm and height 300 mm. The particle size was less than 1 cm, and the sample mass for each run was 600 g. Before the test, the air was purged out. The test was performed between 300 and 700 °C. The effect of reaction temperature on solid products was investigated in this reactor. Compared to other studies, the sample mass of this batch reaction was relatively high, and the particle size was large, which might enhance the heat and mass transfer during the reaction. This reactor was similar to the industrial reactor, which might also increase the random errors of the experimental results.

He et al. (2010) investigated CSW catalytic pyrolysis to produce syngas using a lab-scale downstream fixed bed reactor at 750–900 °C, as shown in Fig. 1.11. The core part of catalytic pyrolysis system was a steel tube with inner diameter 81 mm and height 1400 mm. The gas purification part included fiber wool filter, cooling system (10, 11, and 12) to separate water and condensable organic vapor (tar), and gas measurement apparatus (13). The produced gas was measured by a flowmeter and sampled by gas bags at fixed time intervals. The gas composition (H_2, CO, CO_2, CH_4, C_2H_4, and C_2H_6) was measured by off-line micro-GC. Since the gas analysis by GC needed some time, it was difficult to measure online. Therefore, the intermittent measurement was an eclectic method to obtain semi-online results. However, the intermittent measurement increased the difficulty of operation.

In order to obtain the pyrolytic kinetics of CSW in lab-scale reactors, Zheng et al. (2009) used a specially designed thermogravimetric analysis apparatus, as shown in Fig. 1.12. The apparatus included reaction system, carrier gas system,

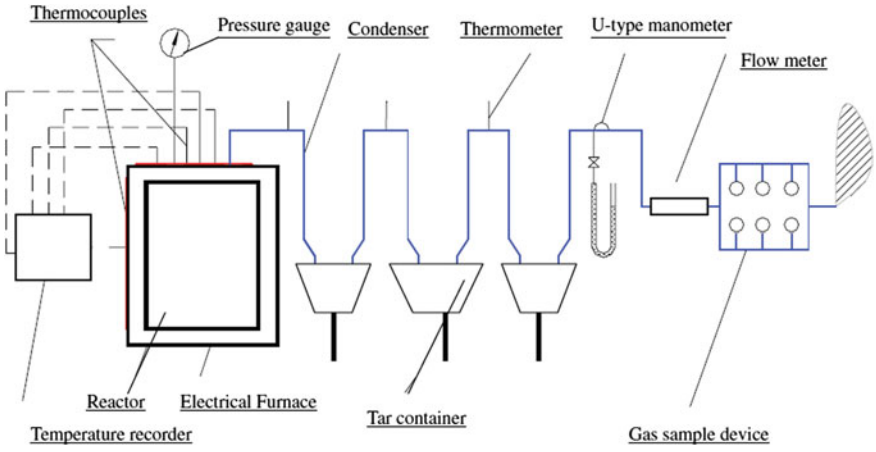

Fig. 1.10 Schematic diagram of CSW pyrolysis. Reproduced from An et al. (2006) by permission of John Wiley & Sons Ltd

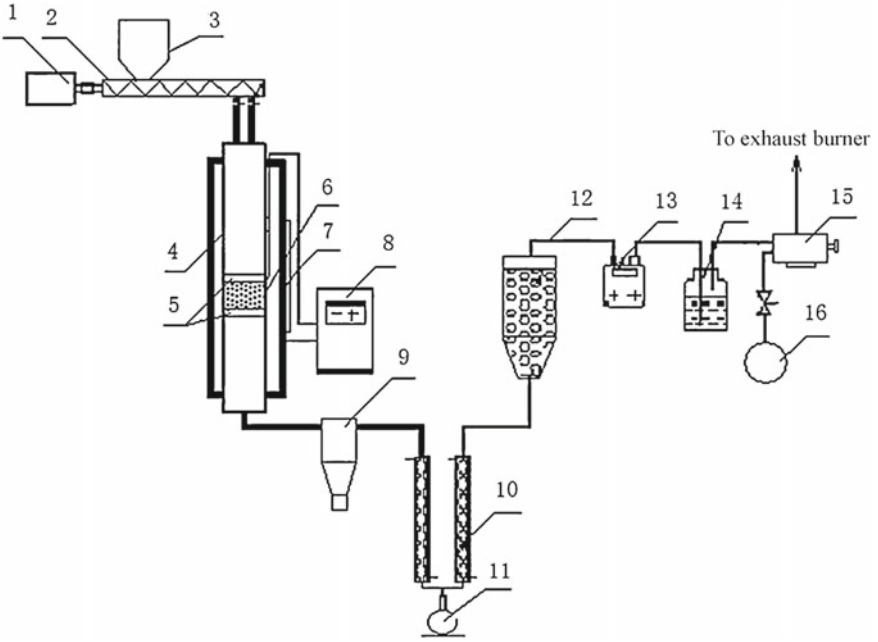

1-Motor; 2-screw feed; 3-hopper; 4-fixed bed reactor; 5-porous ceramic; 6-catalyst; 7-furnace; 8-temperature controller; 9-cyclone separator; 10-condenser; 11-flask; 12-filter; 13-gas flowmeter; 14-silica gel; 15-air pump; 16-gas bag

Fig. 1.11 Diagram of downstream fixed bed reactor. Reprinted from He et al. (2010), Copyright 2010, with permission from Elsevier

data collection system, temperature control system, and lift system. The core part of the reactor was an alundum tube with the diameter 60 mm and length 1.2 m. The precision of the electronic scale was 0.1 mg, with a crucible hung below. The mass data were collected by computer every 2 s. Before the test, the system was blown by 2 L min^{-1} N_2 for 30 min to make sure the inert atmosphere. When the temperature reached setting temperature (750, 850, or 950 °C), the N_2 flow rate was adjusted to 1 L min^{-1} and the furnace was moved to the reaction zone. Each test lasted for 30 min to make sure that the mass loss was completed. The sample mass of each test was 2 g. This reactor was a trial of the online mass measurement of gram-level sample pyrolysis, while the movement of furnace impeded the operation of the experiments.

1.3.2 Fluidized Bed Reactor

Liu et al. (2000) investigated PS pyrolysis using fluidized bed reactor at 400–800 °C under N_2 atmosphere, as shown in Fig. 1.13. The bed material particle size of quartz

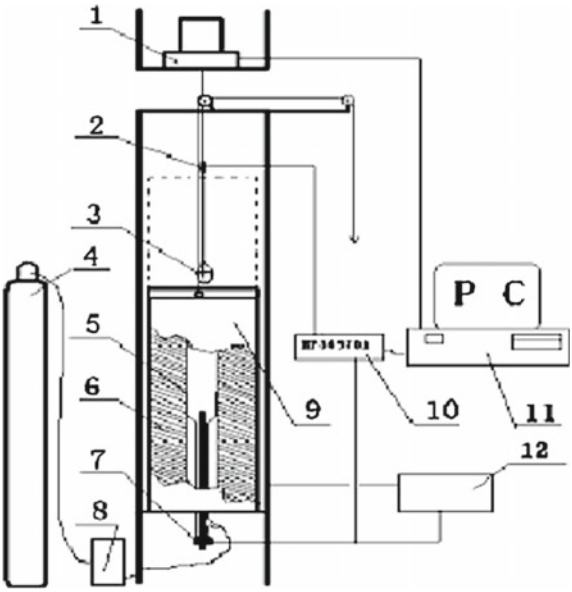

1-Electronic scale; 2-thermocouple; 3-crucible; 4-N_2 cylinder; 5-quartz tube; 6-electrical heating; 7-thermocouple; 8-flowmeter; 9-furnace; 10-data collection; 11-computer; 12-temperature-controller

Fig. 1.12 Constant temperature thermogravimetric analysis reactor. Reprinted from Zheng et al. (2009), Copyright 2009, with permission from Elsevier

bed was 20–40 mesh. The fluidized zone height was 150–200 mm, and the diameter was 60 mm. The gas flow speed was 0.6–0.7 m s^{-1}, with the residence time approximately 0.3 s. The sample mass of each test was 10 g. There was a two-step valve at the top of the feeding tube to prevent the fluidizing gas from getting out and the external air from getting into the reactor. Pyrolyzed gas was cooled by water in a one-stage vertical shell and tube heat exchanger, where liquid products and a part of solid could be collected. After that, gas was cooled to −10 °C by dry ice in a steel coil, where most large molecular compounds could be condensed. The liquid products were analyzed by GC. The non-condensable small molecular gases were absorbed by a two-stage *N*-methyl-2-pyrrolidone and taken from a bypass. The accuracy of each test was evaluated according to the total mass balance calculation.

Dai et al. (2001) pyrolyzed waste tire in a CFB, as shown in Fig. 1.14. The reactor included five parts such as combustion chamber, screw feeder, reactor, cooling system, and gas circulation pump, with the capacity of 5 kg h^{-1}. The vertical tube part of CFB was composed of heat-resistant steel tube with 100 mm diameter and steel air distributor with 88 φ3 mm holes. The reactor height from air distributor to gas outlet was 2.9 m, and the gas residence time was approximately 1.5 s. The gas was analyzed by GC; the pyrolysis oil was dissolved in chloroform, and dried and weighed. Aromatics and non-hydrocarbons were dissolved in benzene and methanol, respectively, and analyzed by GC-MS. This large-scale continuous reactor was similar to the industrial reactor.

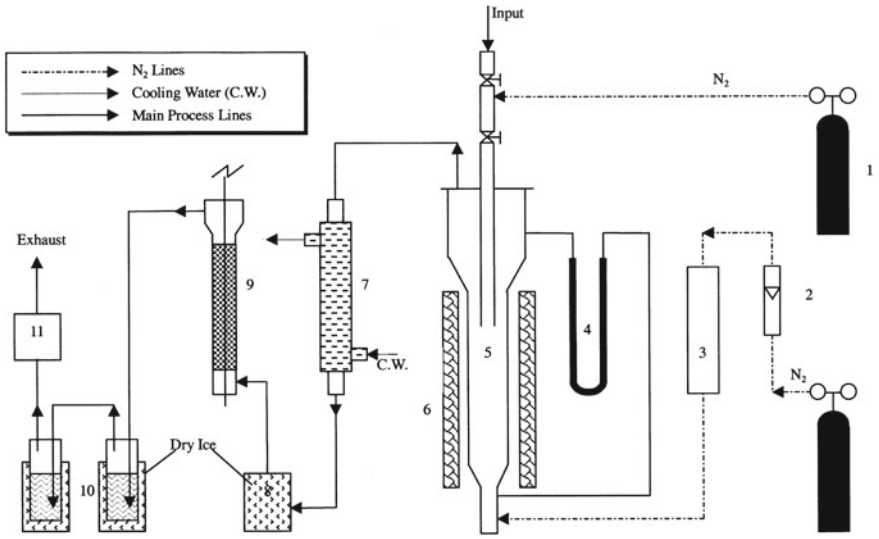

1-N_2 cylinder; 2-flowmeter; 3-gas preheater; 4-U-shape pressure gauge; 5-fluidized bed reactor; 6-clamshell furnace; 7-primary condenser; 8-dry ice condenser; 9-electrostatic demister; 10-bubble sorption unit; 11-gas bag

Fig. 1.13 Fluidized bed reactor for PS pyrolysis. Reprinted from Liu et al. (2000), Copyright 2000, with permission from Elsevier

Megaritis et al. (1998) built a high-pressure fluidized bed reactor (up to 1000 °C, 40 bar) for pyrolysis, gasification, and combustion experiments, as shown in Fig. 1.15. The main body of the reactor was 504 mm long, with the inner diameter 34 mm. The reactor was heated by heating wire. A quartz tube was placed in the furnace loosely to prevent the corrosion and catalytic effect. Sample (up to 2000 mg) was fed in batches from a two-stage gas valve. The tar and char amount would be measured, and the gas was analyzed after drying.

1.3.3 Rotary Kiln Reactor

Li et al. (1999c) investigated waste pyrolysis in a rotary kiln reactor, as shown in Fig. 1.16. The length of the rotary kiln was 0.450 m, and the inner diameter was 0.205 m. Pyrolysis gas went through the spiral condenser, where most of tar and water could be condensed. The left tar and water would be captured by a filter filled with quartz fiber. The weight of condenser and filter was measured to get the tar and water amount. The gas flow was measured by an accumulated flowmeter. A gas sampler at the end of the system controlled the magnetic valve of the sampling ball automatically. Finally, gas composition (H_2, CO, CH_4, CO_2, O_2, N_2, C_2H_4, and

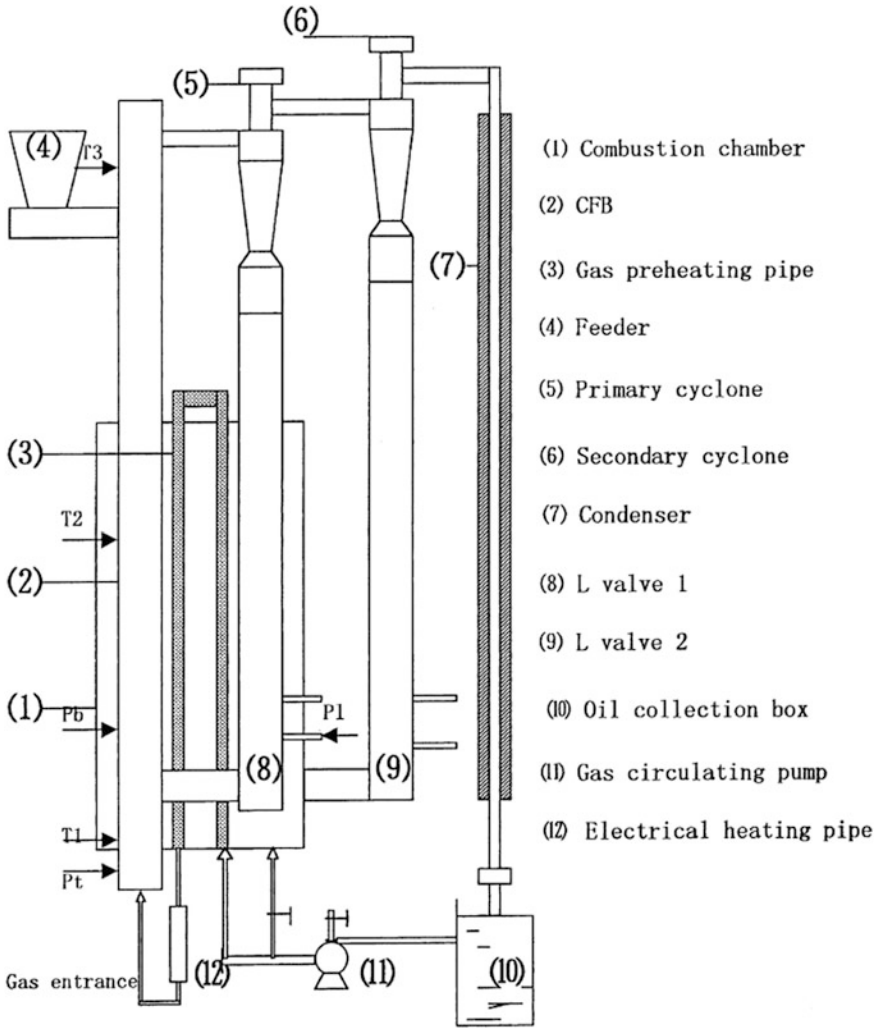

Fig. 1.14 CFB reactor for waste tire pyrolysis. Reprinted from Dai et al. (2001), Copyright 2001, with permission from Elsevier

C_2H_6) was analyzed by GC, and tar was analyzed according to the SY5119-86 Standard.

Overall, in lab-scale research, gram-level sample was usually tested in batches. A few studies realized continuous experiments, closer to the industrial device, while the complexity of experimental apparatus and operation was increased, which increased the difficulty of repeatability. In addition, most studies utilized only one reactor, and the comparison of different reactors was rare.

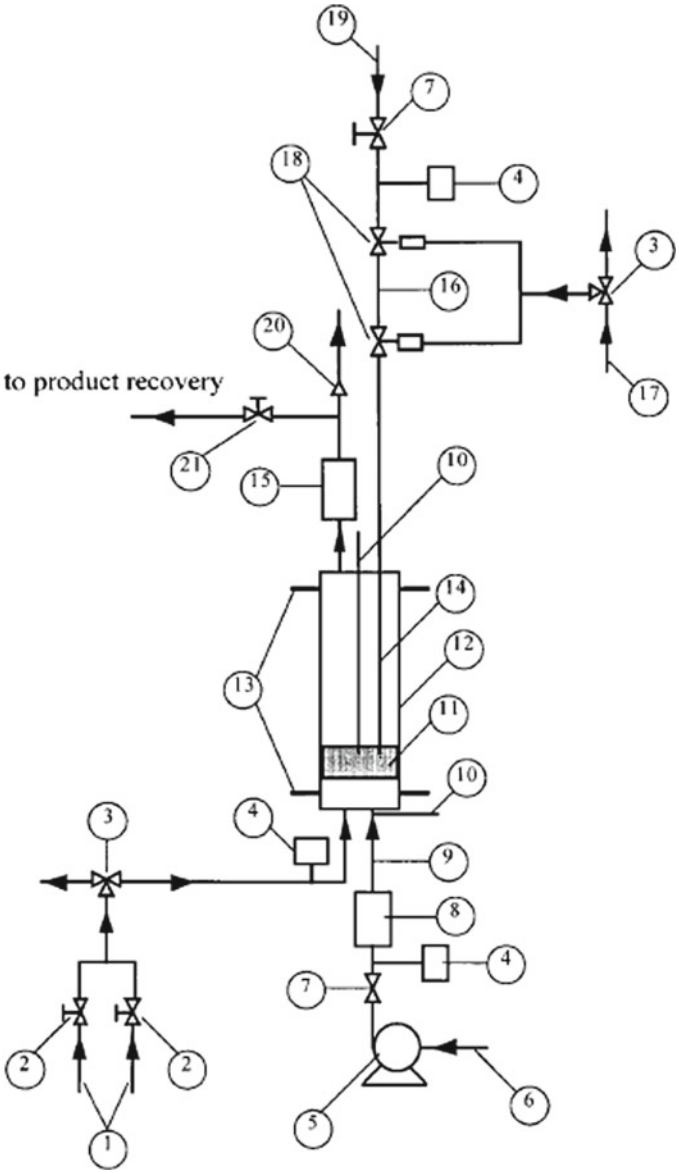

1-Gas supply; 2-flowmeter; 3-three-way valve; 4-pressure sensor; 5-flow pump; 6-water supply; 7-valve; 8-steam generator; 9-heating wire; 10-thermocouple; 11-material bed; 12-reactor; 13-electrode; 14-sample injection tube; 15-tar collection; 16-sample; 17-air supply; 18-pneumatic valve; 19-gas injection tube; 20-safety valve; 21-flow control valve

Fig. 1.15 Schematic diagram of high-pressure fluidized bed reactor. Reprinted with the permission from Megaritis et al. (1998). Copyright 1998 American Chemical Society

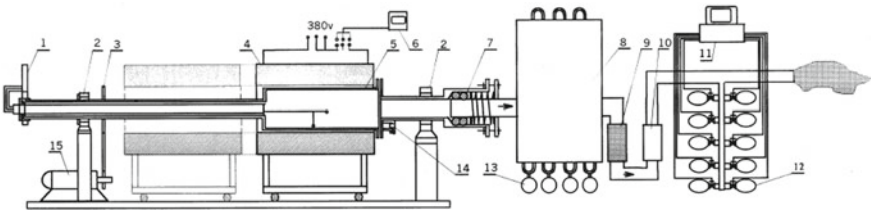

1-Thermocouple; 2-support; 3-gear drive; 4-furnace; 5-rotary kiln; 6-temperature control; 7-seel; 8-tubular condenser; 9-filter; 10-accumulated flowmeter; 11-computer; 12-gas sample device; 13-tar collection; 14-feeder; 15-adjustable-speed motor

Fig. 1.16 Systematic diagram of the rotary kiln. Reprinted from Li et al. (1999c), Copyright 1999, with permission from Elsevier

1.4 Summary of Current Research

From the above, there is some outcome from the research of CSW thermochemical conversion, and some general conclusions were obtained. However, there are still some problems needed to be further study.

(1) CSW is a complex mixture, and the composition of CSW varies from time to time and place to place. Therefore, limited by the randomness of sampling, the studies of real CSW mixture are not easy to be repeated by others. Some studies choose typical components of CSW, while the definitions of some components are vague. For example, food residue and plastics contain many subcomponents themselves. Therefore, more and more studies choose model compounds, such as cellulose and PVC for thermochemical conversion research.

(2) Previous studies on PAHs focused on only several materials, and there was a lack of comparison of PAH generation from different CSW components.

(3) During CSW thermochemical conversion processes, the interactions among different components make the reaction characteristics very complicated, which may be not the simple linear superposition of those of single components. Currently, the studies on CSW components interactions are rare and not systematical. The research of interactions was mainly on TGA reactor, and the research on gram-level reactor was rare; the research of interactions was mainly on kinetics, and the research on gas and tar generation was rare; the research of interactions was mainly slow pyrolysis, and the research of fast pyrolysis was rare, while the interactions for fast pyrolysis might be quite different from those of slow pyrolysis.

(4) TGA, fixed bed reactor, fluidized bed reactor, and rotary kiln are common reactors for CSW thermochemical conversion research, while the comparison of different reactors was rare. The kinetic research was mainly on TGA reactor, with milligram sample and low heating rate, while there is a lack of kinetic research on gram-level reactor with high heating rates.

1.5 Research Objectives and Main Content

1.5.1 Research Objectives

In this thesis, the model compounds with determinate and simple characteristics, good universality and repeatability, and ability to describe complicated real CSW are defined as basic components (BC). This thesis investigated the thermal reaction kinetics, product mass distribution, gas product characteristics, and PAH formation characteristics of CSW basic components (CSWBCs) in different platforms based on the selection of basic components of CSW. Meanwhile, this thesis explores the influence of temperature, heating rate, atmosphere, and inorganics on CSWBC thermochemical conversions. Finally, the interactions and mechanisms of different components during thermochemical conversions will be investigated.

1.5.2 Main Research Content

This study focuses on four aspects of CSW thermochemical conversion processes: kinetics, product distribution characteristics, gas release characteristics, and PAH generation characteristics, as shown in Fig. 1.17. Kinetics are basic characteristics of CSW thermochemical conversion reaction. This thesis compared the kinetics on both TGA and Macro-TGA and built the connection between these two platforms. Product distribution characteristics mean the mass percentage of gas, tar (including water), and char (carbon and ash) from CSW thermochemical conversion. Similar to coal, CSW thermochemical conversion process generates not only CO_2 and H_2O, but also NO_x, HCl, and SO_2. Pyrolysis and gasification also generate H_2, CO, and

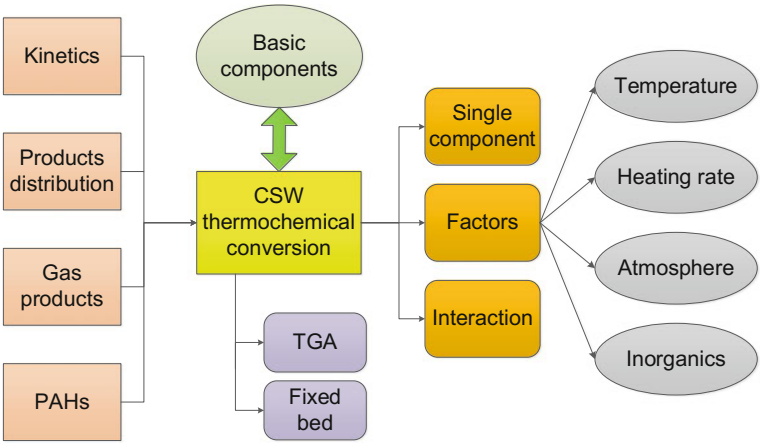

Fig. 1.17 Overall research ideas of this thesis

C_xH_y. These gases analyzed in this thesis include not only common H_2, CO, CO_2, CH_4, and C_2–C_4, but also aldehyde ketones, carboxylic acids, and HCl. Another important pollutant from CSW thermochemical conversion is PAHs. This thesis investigated PAH generation from CSW thermochemical conversion processes in a fixed bed reactor and discussed the formation mechanisms of PAHs. The platforms of this thesis included TGA that can express intrinsic reactions and lab-scale fixed bed reactor that can simulate industrial furnace. The product analysis methods included FTIR, GC, MS, size-exclusion chromatography (SEC), and scanning electron microscopy–energy-dispersive X-ray spectroscopy (SEM-EDX).

1.5.2.1 Basic Component Selection

CSW is a complex mixture that varies from time to time and place to place. To systematically investigate thermochemical characteristics of CSW, based on statistical analysis of CSW, basic components were selected, which will be shown in Chap. 2.

1.5.2.2 Pyrolytic Characteristic of Basic Components

The pyrolytic characteristics of nine basic components were investigated in TGA and fixed bed reactor under an inert atmosphere. The reaction kinetics were studied and compared in TGA and Macro-TGA; the product distribution characteristics were studied in fixed bed reactor; the gas production characteristics were studied in TG-FTIR and fixed bed; the PAH generation characteristics were investigated in fixed bed. Finally, based on the above experimental results, the basic component thermochemical conversion mechanisms and PAH formation mechanisms were proposed. This part will be introduced mainly in Chap. 3.

1.5.2.3 Influential Factors of Thermochemical Conversion of Basic Components

The influential factors of CSW thermochemical conversion include temperature, heating rate, atmosphere, and inorganics. Two basic components were chosen: Lignin was chosen as the representative of biomass basic components, and PVC was chosen as the representative of plastic basic components. The influences of different temperatures (500–900 °C), different heating rates (fast heating and slow heating), different atmospheres (N_2, air, and CO_2), and inorganics (NaCl, NaOH, and $CuCl_2$) on thermochemical conversion characteristics of these two basic components were investigated. Based on this, the thermochemical conversion mechanisms of these two components were analyzed. This part will be discussed in Chap. 4.

1.5.2.4 Influence of Interactions on Pyrolytic Characteristics of Basic Components

Based on the research of single-component pyrolytic characteristics and influential factors, two kinds of interactions were chosen for study: the interactions among lignocellulosic basic components and the interactions between PVC and lignocellulosic basic components. The kinetics, product distribution, gas products, and PAH formation characteristics of interactions were studied in both TGA and fixed bed reactor. This part will be discussed in Chap. 5.

References

Agarwal M, Tardio J, Mohan SV (2013) Biohydrogen production from kitchen based vegetable waste: Effect of pyrolysis temperature and time on catalysed and non-catalysed operation. Bioresou Technol 130:502–509

Alvarez J, Kumagai S, Wu C et al (2014) Hydrogen production from biomass and plastic mixtures by pyrolysis-gasification. Int J Hydrogen Energ 39:10883–10891

An DW, Wang ZM, Zhang ST et al (2006) Low-temperature pyrolysis of municipal solid waste: influence of pyrolysis temperature on the characteristics of solid fuel. Int J Energ Res 30:349–357

Arena U (2012) Process and technological aspects of municipal solid waste gasification. A rev Waste Manage 32:625–639

Asmadi M, Kawamoto H, Saka S (2011a) Thermal reactions of guaiacol and syringol as lignin model aromatic nuclei. J Anal Appl Pyrol 92:88–98

Asmadi M, Kawamoto H, Saka S (2011b) Gas- and solid/liquid-phase reactions during pyrolysis of softwood and hardwood lignins. J Anal Appl Pyrol 92:417–425

Biagini E, Fantei A, Tognotti L (2008) Effect of the heating rate on the devolatilization of biomass residues. Thermochim Acta 472:55–63

Bigger SW, Scheirs J, Camino G (1998) An investigation of the kinetics of cellulose degradation under non-isothermal conditions. Polym Degrad Stabil 62:33–40

Boer DE, Jedrczak A, Kowalski Z et al (2010) A review of municipal solid waste composition and quantities in Poland. Waste Manage 30:369–377

Brebu M, Ucar S, Vasile C et al (2010) Co-pyrolysis of pine cone with synthetic polymers. Fuel 89:1911–1918

Buekens A, Cen K (2011) Waste incineration, PVC, and dioxins. J Mater Cycles Waste 13:190–197

Buonanno G, Stabile L, Avino P et al (2011) Chemical, dimensional and morphological ultrafine particle characterization from a waste-to-energy plant. Waste Manage 31:2253–2262

Burnley SJ (2007) A review of municipal solid waste composition in the United Kingdom. Waste Manage 27:1274–1285

Caglar A, Aydinli B (2009) Isothermal co-pyrolysis of hazelnut shell and ultra-high molecular weight polyethylene: The effect of temperature and composition on the amount of pyrolysis products. J Anal Appl Pyrol 86:304–309

Chang CY, Wu CH, Hwang JY et al (1996) Pyrolysis kinetics of uncoated printing and writing paper of MSW. J Environ Eng 122:299–305

Chen W, Kuo P (2010) A study on torrefaction of various biomass materials and its impact on lignocellulosic structure simulated by a thermogravimetry. Energy 35:2580–2586

Chen T, Wu J, Zhang J et al (2014) Gasification kinetic analysis of the three pseudocomponents of biomass-cellulose, semicellulose and lignin. Bioresour. Technol 153:223–229

Cheng HF, Hu YN (2010) Municipal solid waste (MSW) as a renewable source of energy: Current and future practices in China. Bioresour Technol 101:3816–3824
Chin Y, Lin C, Guo-Ping C et al (2012) PCDD/F Formation Catalyzed by the Metal Chlorides and Chlorinated Aromatic Compounds in Fly Ash. Aerosol Air Qual Res 12:228–236
Cho JM, Chu S, Dauenhauer PJ et al (2012) Kinetics and reaction chemistry for slow pyrolysis of enzymatic hydrolysis lignin and organosolv extracted lignin derived from maplewood. Green Chem 14:428–439
Consonni S, Giugliano M, Grosso M (2005) Alternative strategies for energy recovery from municipal solid waste. Waste Manage 25:123–135
Dai XW, Yin XL, Wu CZ et al (2001) Pyrolysis of waste tires in a circulating fluidized-bed reactor. Energy 26:385–399
Di Blasi C (2009) Combustion and gasification rates of lignocellulosic chars. Prog Energ Combust 35:121–140
Dieguez-Alonso A, Anca-Couce A, Zobel N (2013) On-line tar characterization from pyrolysis of wood particles in a technical-scale fixed-bed reactor by applying Laser-Induced Fluorescence (LIF). J Anal Appl Pyrol 102:33–46
Dorado C, Mullen CA, Boateng AA (2014) H-ZSM5 Catalyzed Co-Pyrolysis of Biomass and Plastics. ACS Sustain Chem Eng 2:301–311
Dorrestijn E, Laarhoven LJJ, Arends IWCE et al (2000) The occurrence and reactivity of phenoxyl linkages in lignin and low rank coal. J Anal Appl Pyrol 54:153–192
Eriksson O, Finnveden G, Ekvall T et al (2007) Life cycle assessment of fuels for district heating: A comparison of waste incineration, biomass- and natural gas combustion. Energ Policy 35:1346–1362
Font R, Esperanza M, García AN (2003) Toxic by-products from the combustion of Kraft lignin. Chemosphere 52:1047–1058
Fullana A, Sidhu SS (2005) Fate of PAHs in the post-combustion zone: Partial oxidation of PAHs to dibenzofuran over CuO. J Anal Appl Pyrol 74:479–485
Garcia AN, Font R, Marcilla A (1992) Kinetic-studies of the primary pyrolysis of municipal solid-waste in a Pyroprobe-1000. J Anal Appl Pyrol 23:99–119
Gidarakos E, Havas G, Ntzamilis P (2006) Municipal solid waste composition determination supporting the integrated solid waste management system in the island of Crete. Waste Manage 26:668–679
Giudicianni P, Cardone G, Ragucci R (2013) Cellulose, hemicellulose and lignin slow steam pyrolysis: Thermal decomposition of biomass components mixtures. J Anal Appl Pyrol 100:213–222
Gui B, Qiao Y, Wan D et al (2013) Nascent tar formation during polyvinylchloride (PVC) pyrolysis. P Combust Inst 34:2321–2329
Guo X, Yang X, Chen Y et al (2000) 可燃固体废弃物的热解动力学 (Pyrolytic kinetics of combustion of MSW). J Chem Ind Eng (China) 51:615–619
Guo XF, Wang ZQ, Li HB et al (2001) A study on combustion characteristics and kinetic model of municipal solid wastes. Energ Fuel 15:1441–1446
He MY, Xiao B, Liu SM et al (2010) Syngas production from pyrolysis of municipal solid waste (MSW) with dolomite as downstream catalysts. J Anal Appl Pyrol 87:181–187
Hosoya T, Kawamoto H, Saka S (2007) Cellulose–hemicellulose and cellulose–lignin interactions in wood pyrolysis at gasification temperature. J Anal Appl Pyrol 80:118–125
Huai XL, Xu WL, Qu ZY et al (2008) Numerical simulation of municipal solid waste combustion in a novel two-stage reciprocating incinerator. Waste Manage 28:15–29
Iino F, Imagawa T, Takeuchi M et al (1999) De novo synthesis mechanism of polychlorinated dibenzofurans from polycyclic aromatic hydrocarbons and the characteristic isomers of polychlorinated naphthalenes. Environ Sci Technol 33:1038–1043
Ionescu G, Zardi D, Tirler W et al (2012) A critical analysis of emissions and atmospheric dispersion of pollutants from plants for the treatment of residual municipal solid waste. U Politeh Buch Ser 74:227–240

Jiang F, Pan Z, Liu S et al (2002) 混合垃圾在热重分析仪和流化床中的燃烧特性 (Combustion characteristics of mixed municipal solid waste in thermogravimetric analysis and lab scale fluidized bed). Environ Sci 23:114–118
Jimenez A, Lopez J, Torre L et al (1999) Kinetic analysis of the thermal degradation of PVC plastisols. J Appl Polym Sci 73:1069–1079
Kathirvale S, Yunus N, Sopian K et al (2004) Energy potential from municipal solid waste in Malaysia. Renew Energ 29:559–567
Li A, Li X, Li S et al (1999a) 回转窑热解城市垃圾制造中热值燃气的试验 (Experiment on manufacture medium-heating value fuel gas by pyrolyzing municipal refuse in a rotary kiln). J Chem Ind Eng (China) 50:101–107
Li AM, Li XD, Li SQ et al (1999b) Experimental studies on municipal solid waste pyrolysis in a laboratory-scale rotary kiln. Energy 24:209–218
Li AM, Li XD, Li SQ et al (1999c) Pyrolysis of solid waste in a rotary kiln: influence of final pyrolysis temperature on the pyrolysis products. J Anal Appl Pyrol 50:149–162
Li Z, Yang L, Qu X et al (2009) Municipal solid waste management in Beijing City. Waste Manage 29:2596–2599
Li X, Zhang H, Li J et al (2013) Improving the aromatic production in catalytic fast pyrolysis of cellulose by co-feeding low-density polyethylene. Appl Catal A-Gen 455:114–121
Liu YS, Liu YS (2005) Novel incineration technology integrated with drying, pyrolysis, gasification, and combustion of MSW and ashes vitrification. Environ Sci Technol 39:3855–3863
Liu C, Wu XW (2011) Factors influencing municipal solid waste generation in China: A multiple statistical analysis study. Waste Manage Res 29:371–378
Liu Y, Qian J, Wang J (2000) Pyrolysis of polystyrene waste in a fluidized-bed reactor to obtain styrene monomer and gasoline fraction. Fuel Process Technol 63:45–55
Liu ZQ, Liu ZH, Li XL (2006) Status and prospect of the application of municipal solid waste incineration in China. Appl Therm Eng 26:1193–1197
Lopez-Velazquez MA, Santes V, Balmaseda J et al (2013) Pyrolysis of orange waste: A thermo-kinetic study. J Anal Appl Pyrol 99:170–177
Lu C, Song W, Lin W (2009) Kinetics of biomass catalytic pyrolysis. Biotechnol Adv 27:583–587
Luo SY, Xiao B, Hu ZQ et al (2010) Effect of particle size on pyrolysis of single-component municipal solid waste in fixed bed reactor. Int J Hydrogen Energ 35:93–97
Matsuzawa Y, Ayabe M, Nishino J (2001) Acceleration of cellulose co-pyrolysis with polymer. Polym Degrad Stabil 71:435–444
McGhee B, Norton F, Snape CE et al (1995) The copyrolysis of poly(vinylchloride) with cellulose derived materials as a model for municipal waste derived chars. Fuel 74:28–31
McGrath TE, Chan WG, Hajaligol MR (2003) Low temperature mechanism for the formation of polycyclic aromatic hydrocarbons from the pyrolysis of cellulose. J Anal Appl Pyrol 66:51–70
McKay G (2002) Dioxin characterisation, formation and minimisation during municipal solid waste (MSW) incineration: review. Chem Eng J 86:343–368
Megaritis A, Zhuo Y, Messenbock R et al (1998) Pyrolysis and gasification in a bench-scale high-pressure fluidized-bed reactor. Energ Fuel 12:144–151
MHURDC (Ministry of Housing and Urban-Rural Development of China) (2009) 生活垃圾采样和分析方法 (Sampling and analysis methods for domestic waste). China Standards Press, Beijing
Miller FJ, Gardner DE, Graham JA et al (1979) Size Considerations for Establishing a Standard for Inhalable Particles. J Air Pollut Control Assoc 29:610–615
Miranda M, Pinto F, Gulyurtlu I et al (2013) Pyrolysis of rubber tyre wastes: A kinetic study. Fuel 103:542–552
Mo Y, Zhao L, Chen CL et al (2013) Comparative pyrolysis upcycling of polystyrene waste: thermodynamics, kinetics, and product evolution profile. J Therm Anal Calorim 111:781–788
Moeckel C, Monteith DT, Llewellyn NR et al (2014) Relationship between the concentrations of dissolved organic matter and polycyclic aromatic hydrocarbons in a typical U.K. Upland Stream. Environ Sci Technol 48:130–138

NBSC (National Bureau of Statistics of China) (2004) China statistical yearbook, 2004. China Statistics Press, Beijing
NBSC (National Bureau of Statistics of China) (2007) China statistical yearbook, 2007. China Statistics Press, Beijing
NBSC (National Bureau of Statistics of China) (2008) China statistical yearbook, 2008. China Statistics Press, Beijing
NBSC (National Bureau of Statistics of China) (2009) China statistical yearbook, 2009. China Statistics Press, Beijing
NBSC (National Bureau of Statistics of China) (2010) China statistical yearbook, 2010. China Statistics Press, Beijing
NBSC (National Bureau of Statistics of China) (2011) China statistical yearbook, 2011. China Statistics Press, Beijing
NBSC (National Bureau of Statistics of China) (2012) China statistical yearbook, 2012. China Statistics Press, Beijing
NBSC (National Bureau of Statistics of China) (2013) China statistical yearbook, 2013. China Statistics Press, Beijing
NBSC (National Bureau of Statistics of China) (2014) China statistical yearbook, 2014. China Statistics Press, Beijing
OFG (Office of the Federal Register) (2000) Code of federal regulations. Government Printing Office, Washington, U.S
Onwudili JA, Insura N, Williams PT (2009) Composition of products from the pyrolysis of polyethylene and polystyrene in a closed batch reactor: Effects of temperature and residence time. J Anal Appl Pyrol 86:293–303
Qing S, Wang H, Wu Z et al (2005) 城市垃圾中生物质在热分析仪中燃烧的动力学模型研究 (Study on characteristics of combustion of municipal solid waste with thermal analyzers). Environ Poll Control 27:24–28
Ragazzi M, Tirler W, Angelucci G et al (2013) Management of atmospheric pollutants from waste incineration processes: the case of Bozen. Waste Manage Res 31:235–240
Richter H, Howard J (2000) Formation of polycyclic aromatic hydrocarbons and their growth to soot—a review of chemical reaction pathways. Prog Energ Combust 26:565–608
Samanta SK, Singh OV, Jain RK (2002) Polycyclic aromatic hydrocarbons: environmental pollution and bioremediation. Trends Biotechnol 20:243–248
Seo DK, Park SS, Kim YT et al (2011) Study of coal pyrolysis by thermo-gravimetric analysis (TGA) and concentration measurements of the evolved species. J Anal Appl Pyrol 92:209–216
Shen BX, Wu CF, Guo BB et al (2007) Pyrolysis of waste tyres with zeolite USY and ZSM-5 catalysts. Appl Catal B-Environ 73:150–157
Shen H, Huang Y, Wang R et al (2013) Global atmospheric emissions of polycyclic aromatic hydrocarbons from 1960 to 2008 and future predictions. Environ Sci Technol 47:6415–6424
Singh S, Wu CF, Williams PT (2012) Pyrolysis of waste materials using TGA-MS and TGA-FTIR as complementary characterisation techniques. J Anal Appl Pyrol 94:99–107
Skreiberg A, Skreiberg Ø, Sandquist J et al (2011) TGA and macro-TGA characterisation of biomass fuels and fuel mixtures. Fuel 90:2182–2197
Sonobe T, Worasuwannarak N (2008) Kinetic analyses of biomass pyrolysis using the distributed activation energy model. Fuel 87:414–421
Sorum L, Gronli MG, Hustad JE (2001) Pyrolysis characteristics and kinetics of municipal solid wastes. Fuel 80:1217–1227
Stefanidis SD, Kalogiannis KG, Iliopoulou EF et al (2014) A study of lignocellulosic biomass pyrolysis via the pyrolysis of cellulose, hemicellulose and lignin. J Anal Appl Pyrol 105:143–150
Thomas S, Ledesma EB, Wornat MJ (2007) The effects of oxygen on the yields of the thermal decomposition products of catechol under pyrolysis and fuel-rich oxidation conditions. Fuel 86:2581–2595
Tsai WT, Lee MK, Chang YM (2006) Fast pyrolysis of rice straw, sugarcane bagasse and coconut shell in an induction-heating reactor. J Anal Appl Pyrol 76:230–237

Várhegyi G, Chen H, Godoy S (2009) Thermal decomposition of wheat, oat, barley, and Brassica carinata straws. A kinetic study. Energ Fuel 23:646–652
Velghe I, Carleer R, Yperman J et al (2011) Study of the pyrolysis of municipal solid waste for the production of valuable products. J Anal Appl Pyrol 92:366–375
Wang Z, Wang J, Richter H et al (2003) Comparative study on polycyclic aromatic hydrocarbons, light hydrocarbons, carbon monoxide, and particulate emissions from the combustion of polyethylene, polystyrene, and poly(vinyl chloride). Energ Fuel 17:999–1013
Wang SR, Guo XJ, Wang KG et al (2011) Influence of the interaction of components on the pyrolysis behavior of biomass. J Anal Appl Pyrol 91:183–189
Wen J. (2006) 城市生活垃圾热解特性试验研究及预测模型 (Experimental study on the pyrolysis characteristics of MSW and its prediction model). Dissertation, Zhejing University
Wilk V, Hofbauer H (2013) Co-gasification of plastics and biomass in a dual fluidized-bed steam gasifier: possible interactions of fuels. Energ Fuel 27:3261–3273
Williams PT (2005) Waste treatment and disposal. Wiley, Chichester
Wu CF, Wang ZC, Huang J et al (2013) Pyrolysis/gasification of cellulose, hemicellulose and lignin for hydrogen production in the presence of various nickel-based catalysts. Fuel 106:697–706
Wu J, Chen T, Luo X et al (2014a) TG/FTIR analysis on co-pyrolysis behavior of PE, PVC and PS. Waste Manage 34:676–682
Wu W, Mei Y, Zhang L et al (2014b) Effective activation energies of lignocellulosic biomass pyrolysis. Energ Fuel 28:3916–3923
Xi B, Xia X, Su J et al (2010) 城市固体废物系统分析及优化管理技术 (System analysis and optimal management technology of municipal solid waste). Science Press, Beijing
Xiao Y, Bai XM, Ouyang ZY et al (2007) The composition, trend and impact of urban solid waste in Beijing. Environ Monit Assess 135:21–30
Yang H, Yan R, Chen H et al (2007) Characteristics of hemicellulose, cellulose and lignin pyrolysis. Fuel 86:1781–1788
Yi S, Yoo KY, Hanaki K (2011) Characteristics of MSW and heat energy recovery between residential and commercial areas in Seoul. Waste Manage 31:595–602
Zhang C, Yu J, Fan D et al (2008a) 中国城市垃圾典型组分热解特性及动力学研究 (A study of pyrolysis characteristics and kinetics analysis of typical constituents of municipal solid waste in China). J Eng Therm Energy Power 23:561–566
Zhang Y, Chen Y, Meng A et al (2008b) Experimental and thermodynamic investigation on transfer of cadmium influenced by sulfur and chlorine during municipal solid waste (MSW) incineration. J Hazard Mater 153:309–319
Zhang J, Chen T, Wu J et al (2014a) A novel Gaussian-DAEM-reaction model for the pyrolysis of cellulose, hemicellulose and lignin. RSC Adv 4:17513–17520
Zhang J, Chen T, Wu J et al (2014b) Multi-Gaussian-DAEM-reaction model for thermal decompositions of cellulose, hemicellulose and lignin: Comparison of N2 and CO2 atmosphere. Bioresour Technol 166:87–95
Zheng J, Jin YQ, Chi Y et al (2009) Pyrolysis characteristics of organic components of municipal solid waste at high heating rates. Waste Manage 29:1089–1094
Zhou H, Long Y, Meng A et al (2013) The pyrolysis simulation of five biomass species by hemi-cellulose, cellulose and lignin based on thermogravimetric curves. Thermochim Acta 566:36–43
Zhou H, Meng A, Long Y et al (2014) An overview of characteristics of municipal solid waste fuel in China: Physical, chemical composition and heating value. Renew Sust Energ Rev 36:107–122
Zhou H, Meng A, Long Y et al (2015) A review of dioxin-related substances during municipal solid waste incineration. Waste Manage 36:106–118

Chapter 2
Research Method

Abstract We know that the combustible solid waste (CSW) is a very complicated mixture of different components. Therefore, is there a way to simplify the research of CSW? The answer is yes. In this chapter, the classification of CSW based on thermochemical characteristics was first proposed. Based on the classification, nine kinds of basic components (hemicellulose, cellulose, lignin, pectin, starch, polyethylene (PE), polystyrene (PS), polyvinyl chloride (PVC), and polyethylene terephthalate (PET)) were selected to simplify the study on thermochemical conversion of CSW. After that, the experimental systems in this study, including thermogravimetric analyzer (TGA), Macro-TGA, and horizontal fixed bed reactor, were introduced. TGA-Fourier transform infrared spectroscopy (FTIR) was used to obtain the intrinsic kinetics and gas products; Macro-TGA was used to obtain the gram level reaction kinetics with heat and mass transfer effect; and horizontal fixed bed reactor was used to obtain the product distribution, gas generation, and polycyclic aromatic hydrocarbons (PAHs) formation characteristics. Finally, the kinetic analysis method for slow pyrolysis and fast pyrolysis was introduced.

Keywords Combustible solid waste (CSW) · Basic component · Thermogravimetric analyzer (TGA) · Macro-TGA

2.1 Selection of Basic Components

2.1.1 Classification of CSW

According to physical composition, CSW can be classified into 6 categories, i.e., food residue, wood waste, paper, textiles, plastics, and rubber. However, there is a lack of CSW classification based on thermochemical characteristics. To further understand the thermochemical characteristics of CSW and explore the possibility of basic component selection, a series of CSW typical components were chosen for pre-experiments.

H. Zhou, *Combustible Solid Waste Thermochemical Conversion*, Springer Theses,
DOI 10.1007/978-981-10-3827-3_2

In pre-experiments, 26 kinds of CSW components were analyzed. The proximate analysis, ultimate analysis, and heating value measurement were tested in China Coal Research Institute (CCRI) and the Lab of Thermal Engineering, Tsinghua University. Proximate analyses were carried out based on GB/T 212 standard; C and N were analyzed based on GB/T 476 standard; N was analyzed based on GB/T 19,117; S was analyzed based on GB/T 214; and O was obtained from subtraction. Higher heating value (HHV) was measured based on GB/T 213. As shown in Table 2.1, the results of proximate analyses and heating values were based on the dry basis (drying at 105 °C) to eliminate the effect of moisture. The results of ultimate analyses were based on the dry ash-free basis.

The proximate and ultimate analyses of these components can be expressed in the ternary diagrams as shown in Fig. 2.1. As shown in Fig. 2.1a, 26 kinds of typical CSW could be classified into 5 groups according to proximate analyses. Group I includes PS, low-density polyethylene (LDPE), high-density polyethylene (HDPE), and polypropylene (PP), whose volatile matter content is nearly 100%, and the ash and fixed carbon content is close to zero, which has also been reported by other studies (Zheng et al. 2009; Li et al. 1999; Sorum et al. 2001). Group II includes PVC, absorbent cotton gauze, PET, tissue paper, terylene, cotton cloth, rice, and potato. Their ash content was low, and the volatile content was high. Newspaper and blank printing paper could be classified into one group, with the volatile content around 80% and the ash content close to 10%. Orange peel and tangerine peel could be classified into one group, with the ash amount lower than 3% and fixed carbon content approximately 20%. Other components, including some food residue components, wood waste, and rubber, could be classified into the last group, with the ash amount 7–19%, the volatile content 63–74%, and fixed carbon amount 15–26%. It could be concluded that the CSW component classification based on thermochemical characteristics was not the same with the physical classification.

The ternary figure of ultimate analyses is shown in Fig. 2.1b, where C and H are combined, and N, S, and Cl are combined (Vassilev et al. 2010). Twenty-six kinds of components could be classified into four groups. PVC itself was a group, with 56.96% chlorine content. LDPE, HDPE, PP, PS, and rubber could be classified into one group, with relatively high carbon content (>83%) and hydrogen content (>6%). PE and PP had similar elementary compositions, which has also been reported by others (Zheng et al. 2009; Li et al. 1999; Sorum et al. 2001). Terylene and PET could be classified into one group, with around 62% C, 4% H, 33% O, and a small amount of N and S (<0.3%). Actually, terylene and PET are different forms of the same chemical structure. Other components, including food residue, wood waste, paper, and textiles, could be classified into the last group, with 40–60% C + H, 40–60% O, less than 5% N + S + Cl. This group is biomass or natural polymers. The studies of Li et al. (1999) and Sorum et al. (2001) also showed that newspaper, paperboard, sawdust, and cotton cloth had similar elementary composition.

The classification of CSW components based on HHV is shown in Table 2.2. The HHVs of PP, HDPE, and LDPE were the highest (>40 MJ kg^{-1}); the HHVs of

Table 2.1 Proximate and ultimate analyses of CSW components

Group	Sample	Proximate analysis[d] (wt%)			Ultimate analysis[daf] (wt%)					HHV[d] (MJ kg^{-1})
		A	V	FC	C	H	O	N	S	
Food residue	Chinese cabbage	9.91	67.60	22.49	47.49	5.88	41.79	4.11	0.73	16.99
	Rice	0.40	84.42	15.18	45.97	6.35	45.74	1.69	0.25	18.14
	Potato	3.15	79.52	17.33	44.41	5.33	47.82	1.81	0.64	17.10
	Tangerine peel	2.91	76.49	20.60	48.74	5.92	43.83	1.43	0.08	18.47
	Banana peel	10.85	64.38	24.77	35.80	4.79	54.93	4.37	0.10	16.39
	Pakchoi	18.44	63.97	17.59	43.37	5.93	48.64	1.25	0.81	18.90
	Celery	14.58	65.36	20.06	38.46	6.16	54.52	0.21	0.65	13.57
	Orange peel	2.15	77.93	19.92	40.28	6.12	52.46	1.08	0.06	17.10
	Spinach	15.97	65.26	18.77	47.58	6.48	43.93	1.57	0.43	17.08
Wood waste	Poplar wood	7.54	73.85	18.61	51.36	5.89	41.00	1.52	0.22	18.50
	Poplar leaf	15.69	68.74	15.57	49.54	5.24	43.30	1.32	0.59	16.85
	Chinar leaf	9.23	69.74	21.03	52.95	4.88	40.51	1.01	0.65	19.12
	Gingko leaf	11.62	73.19	15.19	41.35	5.54	50.88	1.36	0.87	15.28
Paper	Blank printing paper	10.69	79.33	9.98	45.12	5.31	48.91	0.38	0.28	13.51
	Tissue paper	0.52	90.47	9.01	45.18	6.13	48.32	0.25	0.11	17.25
	Newspaper	8.07	79.54	12.39	48.01	5.71	45.86	0.33	0.09	17.16
Textiles	Cotton cloth	1.52	84.53	13.95	46.51	5.80	46.98	0.43	0.28	17.43
	Absorbent cotton gauze	0.14	94.85	5.01	46.74	5.69	47.23	0.27	0.08	16.82
	Terylene	0.49	88.60	10.91	62.16	4.14	33.12	0.29	0.28	20.86
Plastics	PS	0.04	99.57	0.39	86.06	6.27	1.93	5.73	0.00	38.93
	LDPE	0.00	99.98	0.02	85.98	11.20	2.61	0.21	0.00	46.48
	HDPE	0.18	99.57	0.25	85.35	12.70	1.90	0.05	0.14	46.36
	PVC	0.00	94.93	5.07	38.34	4.47	56.96[a]	0.23	0.00	20.83
	PP	0.02	99.98	0.00	83.51	10.64	5.63	0.22	0.00	45.20
	PET	0.09	90.44	9.47	63.01	4.27	32.69	0.04	0.00	23.09
Rubber	Rubber	10.24	62.83	26.93	89.53	6.70	1.07	0.69	2.02	35.74

Reprinted from Zhou et al. (2015b), Copyright 2015, with permission from Elsevier
Note: *A* ash; *V* volatile; *FC* fixed carbon; *d* dry basis; *daf* dry ash-free basis
[a]It is chlorine here

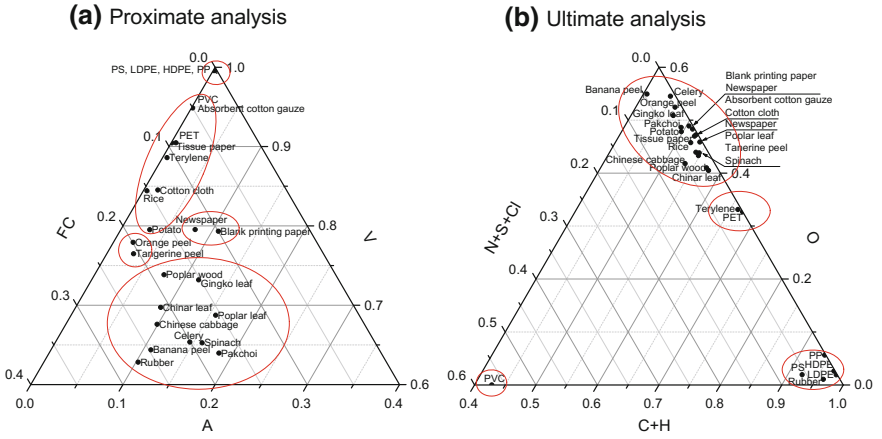

Fig. 2.1 Chemical composition of CSW components. Reprinted from Zhou et al. (2015b), Copyright 2015, with permission from Elsevier

Table 2.2 Classification of CSW components based on HHV

Heating value (MJ kg^{-1})	CSW components
>40	PP, HDPE, LDPE
30–40	Rubber, PS
20–30	PVC, terylene, PET
10–20	Blank printing paper, celery, banana peel, absorbent cotton gauze, poplar leaf, Chinese cabbage, spinach, potato, orange peel, newspaper, tissue paper, cotton cloth, rice, tangerine peel, poplar wood, pakchoi, chinar leaf, gingko leaf

rubber and PS were also very high (30–40 MJ kg^{-1}); the HHVs of PVC, terylene, and PET were between 20 and 25 MJ kg^{-1}; for other components, including food residue, wood waste, paper, and textiles, the heating values were 10–20 MJ kg^{-1}. It could be concluded that the classification based on HHV was similar to that based on ultimate analyses, as shown in Fig. 2.1b.

TGA experiments were carried out to understand the pyrolytic characteristics of CSW components. The heating zone was from room temperature to 1000 °C, with the heating rate 10 °C min^{-1} and carrier gas N_2. According to TG characteristics, cluster analysis could be applied to CSW components. *N* sets of data were exported from the TG curves of two components, denoted by vector *X* and *Y*. The mass was relative mass, with the unit %.

$$X = (x_1, x_2, x_3, \ldots, X_N), \quad Y = (y_1, y_2, y_3, \ldots, y_N) \tag{2.1}$$

The distance between two TG curves was calculated by Euclidean distance, which was the most common distance metric, with the definition that the absolute distance of two vectors in multi-dimensional space (Janowitz 2010).

$$\mathrm{dist}(X, Y) = \sqrt{\sum_{i=1}^{N} (x_i - y_i)^2} \tag{2.2}$$

During cluster analysis, data were selected every 10 °C between 100 and 1000 °C, which was large enough to reflect the TG characteristics. Group distance was utilized during the combination of groups. During the operation of cluster analysis step-by-step, the most similar components were clustered firstly, and the components with the most significant difference were clustered at last. Cluster analysis was carried out by SPSS. As shown in Fig. 2.2, 26 kinds of components could be classified into 11 groups.

As shown in Fig. 2.2, four kinds of wood waste components (chinar leaf, poplar leaf, poplar wood, and ginkgo leaf) could be classified into a group, whose derivative thermogravimetric (DTG) curves are shown in Fig. 2.3a. The main peaks of these four components are 320–350 °C, and there is a shoulder peak around 280 °C. Another peak is located around 700 °C, which is similar to the characteristics of spruce as reported by others (Sorum et al. 2001). The main compositions of wood waste are hemicellulose, cellulose, and lignin. The first peak (shoulder peak) was derived from the decomposition of hemicellulose (Yang et al. 2007); the main peak was derived from the decomposition of cellulose, which is also the main composition of wood waste (Skreiberg et al. 2011); the peak at 700 °C was derived from the decomposition of lignin (Zhou et al. 2013).

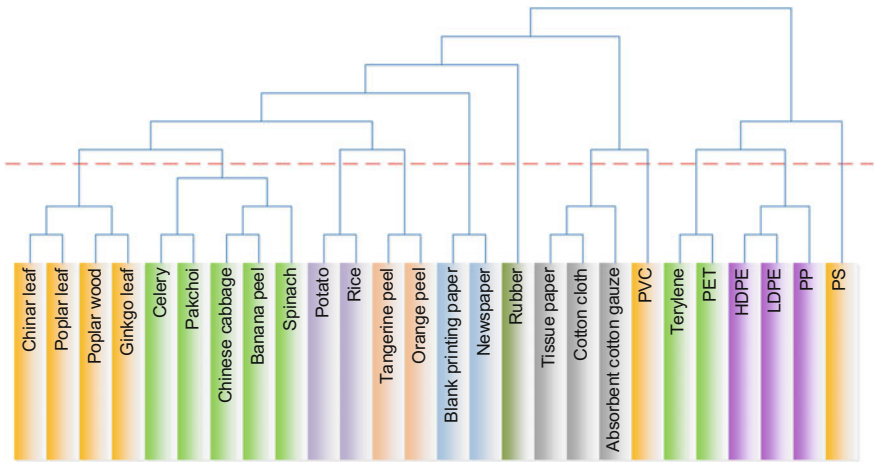

Fig. 2.2 Dendrogram of the cluster analysis of CSW components based on TG characteristics. Reprinted from Zhou et al. (2015b), Copyright 2015, with permission from Elsevier

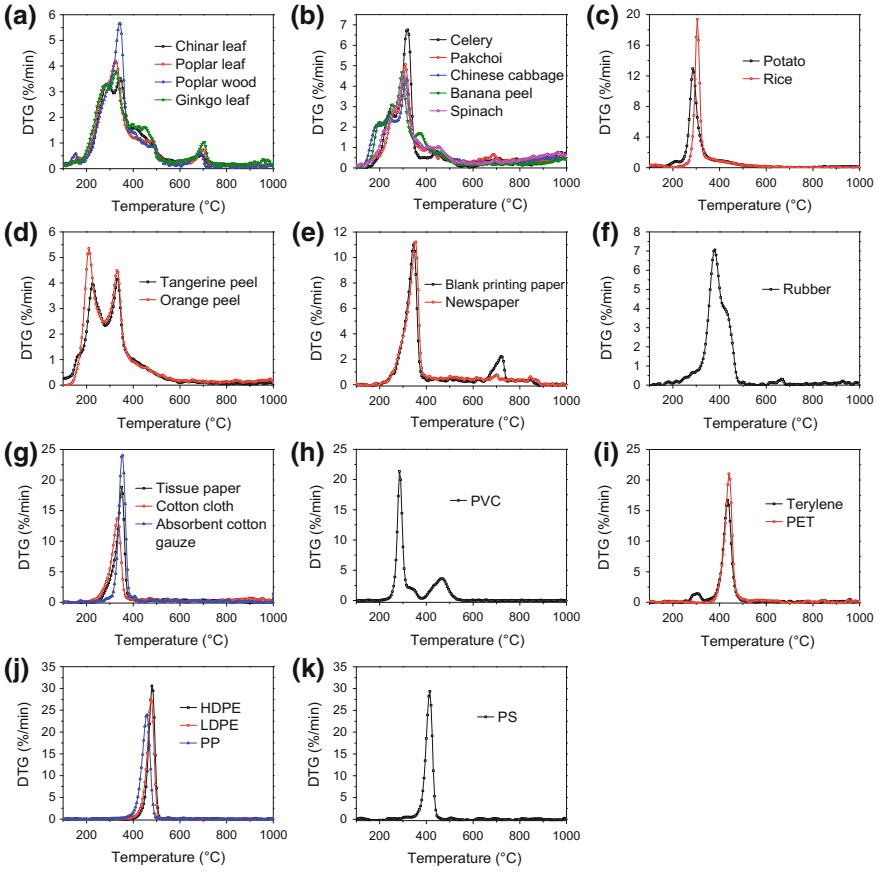

Fig. 2.3 DTG curves of different categories of CSW components based on thermogravimetric characteristics (Reprinted from Zhou et al. (2015a, b), Copyright 2015, with permission from Elsevier)

Five kinds of food residue components could be classified into a group, as shown in Fig. 2.2. The main peaks of this group were 290–320 °C, due to the decomposition of hemicellulose and cellulose; another one or two shoulder peaks at 200–260 °C were derived from the decomposition of hemicellulose (Zhou et al. 2013).

Potato and rice could be classified into a group, whose peaks were near 300 °C. Actually, the main composition of potato and rice is all starch (Dumitriu 2004). Two kinds of fruit peel, tangerine peel and orange peel, could be classified into a group, with two peaks, as shown in Fig. 2.3d. The first peak was at 210–230 °C, from the decomposition of pectin and hemicellulose (Fisher et al. 2002); the second peak was at 331–333 °C, from the decomposition of cellulose (Miranda et al. 2009; Lopez-Velazquez et al. 2013). Blank printing paper and newspaper could be classified into a group, with the main peak around 350 °C, from the decomposition

of cellulose, which is the main composition of paper (Soares et al. 1995; Wu et al. 2002, 2003). Chang et al. (1996) investigated the pyrolysis of uncoated printing paper and obtained similar results. However, blank printing paper had a mass loss peak at 721.7 °C, from the decomposition of additive $CaCO_3$ (Wu et al. 1997; Zhao et al. 2013). The pyrolysis of rubber was different from other components, with the main peak at 378.4 °C. Tissue paper, cotton cloth, and absorbent cotton gauze could be classified into a group, with a single peak at 333–353 °C, due to the decomposition of cellulose (Abidi et al. 2014; Yin et al. 2007).

PVC has a high content of chlorine, whose pyrolysis could be divided into two main stages. The first stage was dechlorination process, at 350–375 °C, with the peak at 286.3 °C. The second stage was the decomposition of C–H structure (Zhou et al. 2014), with the peak at 469.7 °C (Fig. 2.3h). Sorum et al. (2001) have reported similar results of PVC decomposition. Terylene and PET have the same structure, and thus, their TG characteristics were similar, with the main peak around 440 °C. It should be noted that terylene had a small peak at 304.9 °C, maybe due to impurity. The pyrolytic characteristics in TGA of HDPE, LDPE, and PP were similar, with only one peak at 455–485 °C. The pyrolytic characteristics of HDPE and LDPE were almost the same, which was consistent with the results of Sorum et al. (2001). The pyrolytic characteristics of PS were different from other plastics, with a single peak at 413.9 °C (Fig. 2.3k), lower than the peak temperatures of HDPE, LDPE, and PP.

According to the results in Fig. 2.1, Table 2.2, and Fig. 2.2, CSW can be classified according to proximate and ultimate analyses, heating value, and TG characteristics. Proximate analysis, ultimate analysis, and heating value provide a sketchy classification, while TG characteristics provide a detailed classification. Therefore, TG characteristics can be regarded as the "fingerprint" feature of CSW.

2.1.2 *Selection of Basic Components*

According to previous results, nine kinds of components are chosen as basic components, as shown in Fig. 2.4. Pectin, starch, hemicellulose, cellulose, and lignin are basic components for food residue category, and hemicellulose, cellulose, and lignin are basic components for wood waste and paper. Since PET and terylene are similar, and cotton cloth and biomass are similar, hemicellulose, cellulose, lignin, and PET are chosen as basic components for textiles. Since HDPE, LDPE, and PP have similar characteristics, PE, PS, PVC, and PET was chosen as basic components for plastic materials. Since the rubber content in CSW is very low (<1 wt%), as shown in Fig. 1.2, it was neglected when choosing basic components. These nine basic components could be divided into two groups. Hemicellulose, cellulose, lignin, starch, and pectin were biomass basic components. Therein, hemicellulose, cellulose, and lignin were the most important, which could be also called lignocellulosic basic component. PE, PS, PVC, and PET were plastic basic components.

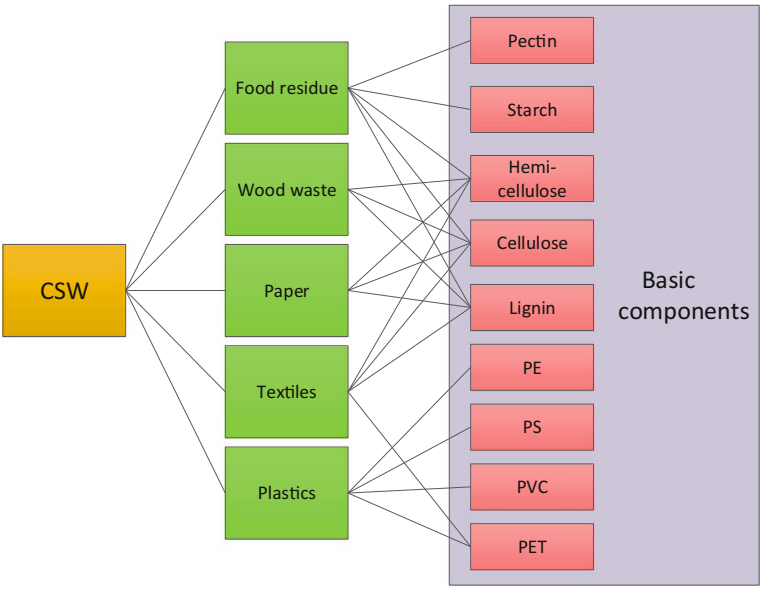

Fig. 2.4 Selection of basic components

During the selection of representatives of basic components, multiple samples were considered, as shown in Table 2.3. Considering sample stability, particle size, purity, availability, price, and authority, representatives were selected for each basic component, shown by bold and underline in Table 2.3. Since hemicellulose is a class of polysaccharides, xylan is usually selected as representative of hemicellulose for research (Couhert et al. 2009).

2.1.3 Basic Characteristics of Basic Components

The structural formulas of these nine basic components are shown in Fig. 2.5. Hemicellulose is a very complex polysaccharide, with various monomers. Cellulose and starch are natural polymers based on glucose monomer. Lignin has three main monomers, i.e., paracoumaryl alcohol, coniferyl alcohol, and sinapyl alcohol (Dorrestijn et al. 2000; Chatel and Rogers 2014). Pectin is a group of galacturonic acid, existing as the cell wall composition of the fruit, root, stem, and leaves of the plant. PE, PS, PVC, and PET are common plastics in CSW, whose structure is relatively simple.

The particle sizes of these nine basic components were less than 150 μm. Before the tests, samples were dried at 105 °C to remove the moisture. The proximate analyses, ultimate analyses, and heating values are shown in Table 2.4. In biomass components, lignin had the highest fixed carbon content (24.69%) and element

Table 2.3 Selection of representatives of basic components

Basic component	Real sample	Basic component	Real sample
Hemicellulose	Xylan (CSC)	Starch	Soluble starch (Jingqiu)
	Xylan (Sigma)		Starch from potato (Sigma)
Cellulose	Absorbent cotton		Starch from wheat (Sigma)
	Absorbent cotton gauze		**Starch from rice (Sigma)**
	Filter paper	PE	LDPE (Yangli)
	Microcrystalline cellulose (Jingqiu)		PE (Yanshan)
	Microcrystalline cellulose (RCL)		HDPE (Goodfellow)
	Microcrystalline cellulose (Sigma)		**HDPE (Yangli)**
Lignin	Sodium lignin sulfonate (Xingzhenghe)	PS	PS (Yanshan)
	Industrial lignin (Shanfeng)		PS (Goodfellow)
	Alkaline lignin (TCI)		**PS (Yangli)**
	Alkaline lignin (Kanto)	PVC	PVC (Yanshan)
	Sodium lignin sulfonate (TCI)		PVC (Yangli)
	Dealkaline lignin (TCI)		**PVC (Sigma)**
Pectin	**Pectin from citrus peel (Sigma)**	PET	**PET (Yangli)**

Note: *CSC* Corporation Service Company; *Sigma* Sigma-Aldrich Ltd.; *Jingqiu* Beijing Jingqiu Chemical Co., Ltd.; *RCL* Research Chemicals Ltd.; *Xingzhenghe* Shenyang Xingzhenghe Chemical Co., Ltd; *Shanfeng* Changzhou Shanfeng Chemical Industry Co., Ltd.; *TCI* Tokyo Chemical Industry Co., Ltd.; *Kanto* Kanto Chemical Co., Ltd.; *Yangli* Shanghai Yangli Mechanical and Electrical Technology Co., Ltd.; *Yanshan* SINOPEC Beijing Yanshan Company; *Goodfellow* Goodfellow Cambridge Ltd.

carbon content (63.86%), and the lowest volatile content (46.10%) and O content (25.83%). Meanwhile, the sulfur content of lignin was very high, maybe due to the separation process. Cellulose had the highest volatile content (92.07%), the lowest fixed carbon content (4.63%), and almost no ash. The high volatile content of cellulose and high sulfur content of lignin have also been reported by others (Couhert et al. 2009; Yoon et al. 2012). Plastic basic components had very high volatile content, and PVC and PET had a certain amount of fixed carbon. PE had the highest H content (11.20%), and PVC had the highest Cl content (56.96%), which was consistent with the report of Li et al. (1999). PET had the highest O content (32.69%), as shown in Table 2.4.

Except for PE and PS, the dry basis HHV of the basic components varied between 15.44 and 23.09 MJ kg^{-1}. The HHV of PS was 38.93 MJ kg^{-1}, and the

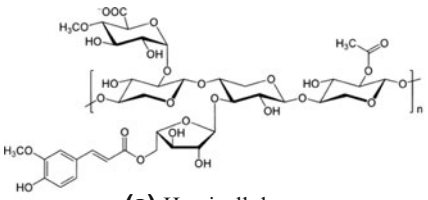

(a) Hemicellulose

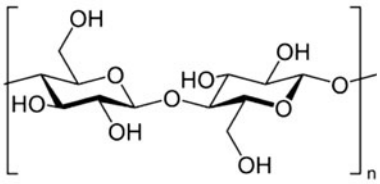

(b) Cellulose

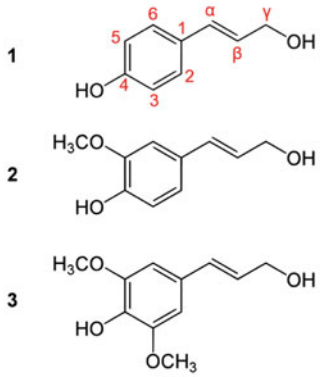

(c) Lignin monomer

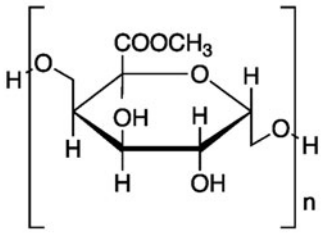

(d) Pectin

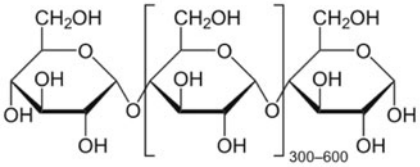

(e) Starch

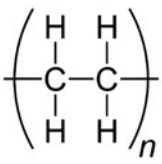

(f) PE

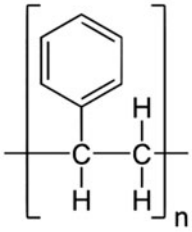

(g) PS

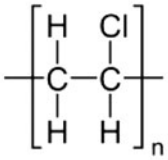

(h) PVC

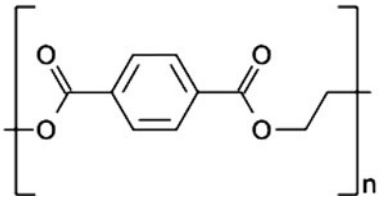

(i) PET

Fig. 2.5 Structural formula of basic components

Table 2.4 Proximate analyses, ultimate analyses, and heating values of basic components

Category	Basic component	Proximate analysis[d] (wt%)			Ultimate analysis[daf] (wt%)					HHV[d] (MJ kg^{-1})
		A	V	FC	C	H	O	N	S	
Biomass	Hemicellulose	2.11	78.57	19.33	39.18	6.32	54.50	0.00	0.01	17.47
	Cellulose	0.00	95.21	4.79	44.51	6.25	47.93	1.29	0.01	27.14
	Lignin	16.15	54.61	29.25	63.86	4.45	25.83	0.18	5.67	21.01
	Pectin	3.38	74.53	22.09	44.25	4.97	50.14	0.48	0.16	15.44
	Starch	0.14	95.20	4.66	43.83	5.21	50.56	0.20	0.19	17.31
Plastics	PE	0.00	99.98	0.02	85.98	11.20	2.61	0.21	0.00	46.48
	PS	0.04	99.57	0.39	86.06	6.27	1.93	5.73	0.00	38.93
	PVC	0.00	94.93	5.07	38.34	4.47	56.96[a]	0.23	0.00	20.83
	PET	0.09	90.44	9.47	63.01	4.27	32.69	0.04	0.00	23.09

Reprinted from Zhou et al. (2015c), Copyright 2015, with permission from Elsevier
Note: *A* Ash; *V* Volatile; *FC* fixed carbon; *d* dry basis; *daf* dry ash-free basis
[a]It is chlorine here

HHV of PE was as high as 46.48 MJ kg^{-1}, which was consistent with the report of Zheng et al. (2009).

To further understand the main functional groups of the basic components, solid FTIR was tested, as shown in Fig. 2.6. The main functional groups were shown in Table 2.5. The main functional groups of biomass were OH, CH_2, crystal water, CH_2 connected with oxygen or COOH, CH_3, alcohol, phenol, C–O in carboxylic

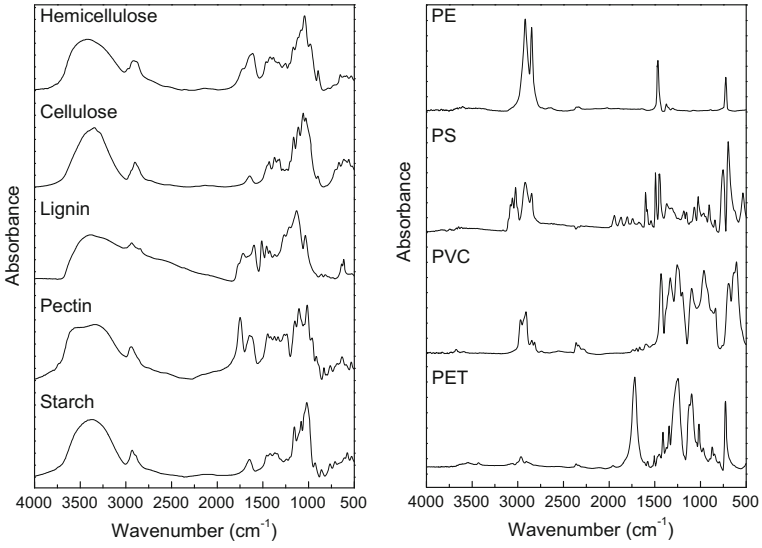

Fig. 2.6 Solid FTIR spectrums of nine basic components

Table 2.5 Main functional groups of basic components from FTIR

Functional group	Hemicellulose	Cellulose	Lignin	Pectin	Starch	PE	PS	PVC	PET
OH stretching	3435	3345	3393	3335	3374				
Symmetrical stretching of CH_2 bonded with O									2967
CH_2-connected halogen-bonded C								2970	
CH_2 asymmetrical stretching	2915	2900	2937	2939	2932	2919	2920	2910	2906
CH_2 symmetrical stretching						2848	2848	2847	
Benzene ring							1942		1960
C=O stretching				1750					1717
Aromatic ester carbonyl stretching			1716						
C=C							1748	1700	
C=C stretching								1667	
Inorganic crystal water deviational vibration	1613	1645	1597	1645	1647				
CH_2=CHCl								1597	
Benzene ring C=C stretching			1514				1541 1492		1505
CH_2 deviational vibration	1464	1458	1463	1447	1458	1467	1452		1455
CH_2 connected with O or COOH	1424	1431	1426	1418	1418				1410
Deformation of CH_2-connected halogen-bonded C								1431	
CH_3 symmetrical deviational vibration	1384	1372	1372	1375	1372	1374	1373		1372
C–OH plane bending	1326	1335 1318 1283		1334	1306				1343
Alkane CH_2 twisting							1312		
Aryl ether			1266						
C–O stretching	1251	1236		1266	1240				
Stretching of C–O in alcohol, phenol, or carboxylic acid	1167	1164	1210	1238 1150	1156				1244

(continued)

Table 2.5 (continued)

Functional group	Hemicellulose	Cellulose	Lignin	Pectin	Starch	PE	PS	PVC	PET
Stretching of C–O in secondary alcohol		1113	1130	1104	1080				1121
C–C stretching						1081	1111	1097	1097
CH in-plane bending in aromatic ring							1068		1045
C–O stretching in primary alcohol	1044	1059	1035	1015	1020				1017
CH_2=CHCl								962	
Polycyclic ether	982	1032		962	929				970
β bond in cellulose	896	899			861				
CH out-of-plane in aromatic ring			856 817				840 755		872 846 793
Methyl benzoate									725
C–Cl stretching								689 605	
Out-of-plane bending of C–OH in alcohol	654	666	636	635					
Inorganic salts	531	615 559	614 526	533	608 576 528				

acid, C–O in primary alcohol, and inorganic salts. The functional groups of lignin also included carbonyl in aromatic ester, benzene ring, and aryl ether. The functional groups of PE were simple, mainly CH_2; PS also had benzene ring, C=C, and CH in aromatic ring besides CH_2; PVC also had CH_2-connected halogen-bonded carbon, CH_2=CHCl, and C–Cl; PET had CH_2 connected to oxygen, benzene ring, C=O, CH_2 connected to oxygen or COOH, C–OH, C–O, CH in aromatic ring, polycyclic ether, and methyl benzoate.

2.2 Experimental System

This research first carried out thermochemical conversion experiments in TGA-FTIR to explore mass loss and gas release characteristics of intrinsic chemical reactions. Furthermore, the mass loss kinetics were investigated in a self-designed Marco-TGA, while product distribution, gas products, and PAHs formation were investigated in another self-designed horizontal fixed bed reactor.

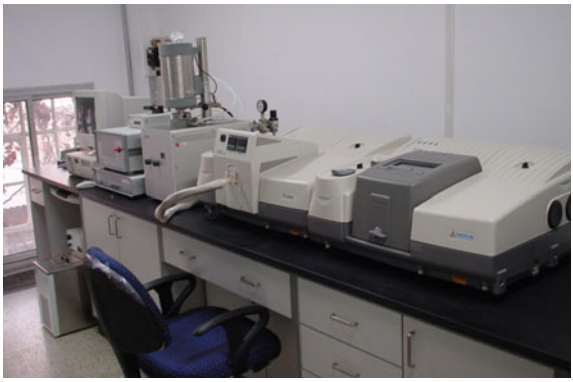

Fig. 2.7 Thermogravimetric analyzer-Fourier transform infrared spectroscopy

2.2.1 TGA-FTIR

The TGA-FTIR used in this study is shown in Fig. 2.7. The TGA is NETZSCH STA 409 C/3/F, with the carrier gas flow rate 100 ml min^{-1}, the heating rate 10 °C min^{-1}, and the temperature range from room temperature to 1000 °C. The particle sizes of these nine basic components were less than 150 μm. In TGA tests with these particle sizes, the influence of heat and mass transfer could be neglected (Bockhorn et al. 1999).

To verify the repeatability of TGA tests, lignin pyrolysis was chosen to run the repeated tests. As shown in Fig. 2.8, the repeatability of TG and DTG curves from three tests was quite good.

The gases from TGA will be blown into FTIR (Nicolet Nexus 670) by N_2. The transfer line and FTIR gas cell were kept at 150 °C. The range of FTIR spectrum was 4000–400 cm^{-1}, with the resolution 1 cm^{-1}. To obtain the gas amount per unit mass samples, the mass of samples in TGA was divided.

2.2.2 Macro-TGA

TGA is the most common method to investigate the kinetics of thermochemical reactions. In TGA experiments, the usual procedure is to load the sample first and then increase the furnace temperature. Therefore, the heating rate in TGA is usually less than 100 °C min^{-1} (Seo et al. 2011). Research has shown that heating rate had a significant influence on thermochemical kinetics (Biagini et al. 2008). In TGA, the heat and mass transfer is usually neglected, which is quite different from industrial reactors. In addition, the sample mass in TGA is usually milligram level, which is too low to investigate the interactions between samples. Based on the above reasons, a Macro-TGA which can realize gram level sample and online mass measurement of fast thermochemical reactions is designed to better investigate the component interactions of the thermochemical conversion process.

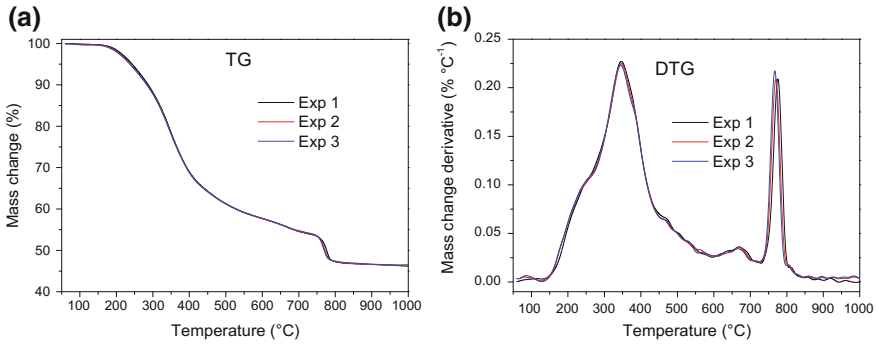

Fig. 2.8 Repeatability of TGA experiments

2.2.2.1 Experimental System

As shown in Figs. 2.9 and 2.10, the reaction system is composed of gas supply system, reaction system, and mass measurement system.

The gas was supplied into the reactor bottom from the high-pressure gas cylinder. The mass flow rate was controlled by a mass flow controller with the flow rate 1 L min^{-1}.

The reaction system was composed of furnace, quartz tube, and quartz crucible. The furnace was vertical, and the size is shown in Fig. 2.11. The heating element was HRE resistance wire, which was arranged annularly to obtain uniform temperature

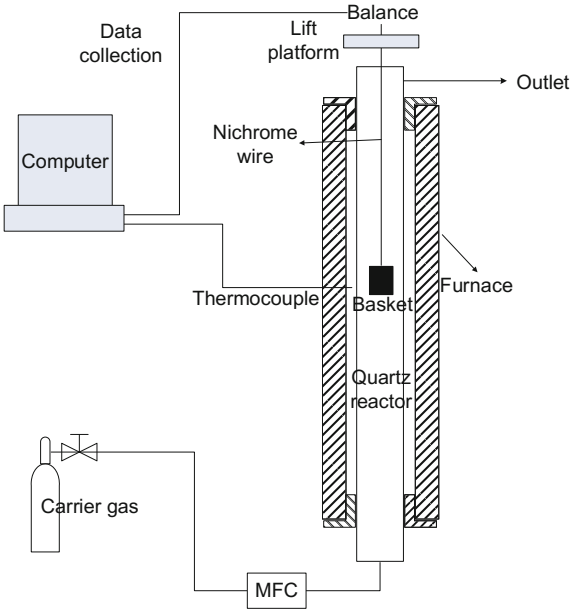

Fig. 2.9 Schematic diagram of Macro-TGA system (Zhou et al. 2015a)—Reproduced by permission of The Royal Society of Chemistry

Fig. 2.10 Photo of Macro-TGA

distribution. The highest temperature of the furnace could reach 1200 °C. The inner diameter of the furnace was 80 mm. The heating zone was 800 mm long. The constant temperature zone was 350 mm long, with the temperature fluctuation less than 1 °C. The furnace had three temperature zones, and the rated power was 5 kW. The highest heating rate could reach 40 °C min^{-1}.

The furnace could be split to load reactor. The temperature could be monitored and controlled by a computer.

The inner diameter of the fixed bed quartz tube reactor was 60 mm, and the length was 1500 mm, with upper and lower ends extending furnace 250 mm. The ends of the quartz tube were sealed by 304 stainless steel multi-stage sealing quick release flanges.

The quartz crucible is shown in Fig. 2.12. It was cylinder-shaped, with the inner diameter 30 mm, height 30 mm, and weight 18 g. In each test, the sample mass was 1.50 ± 0.01 g.

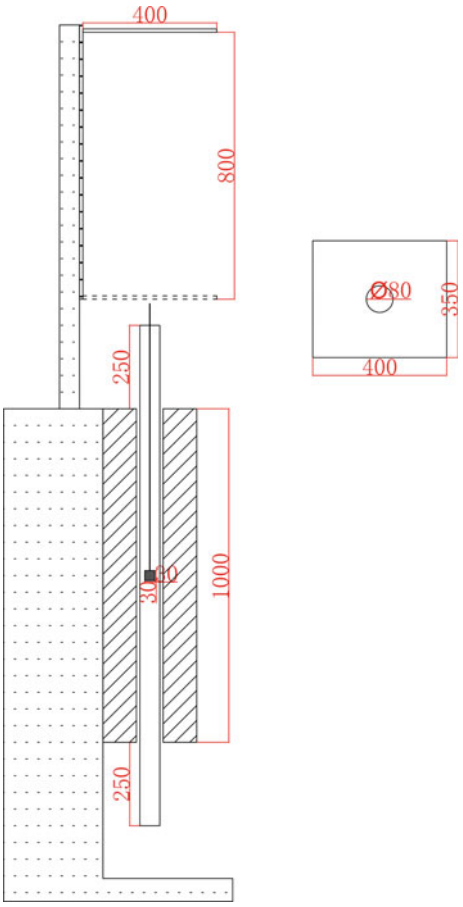

Fig. 2.11 Geometry of Macro-TGA

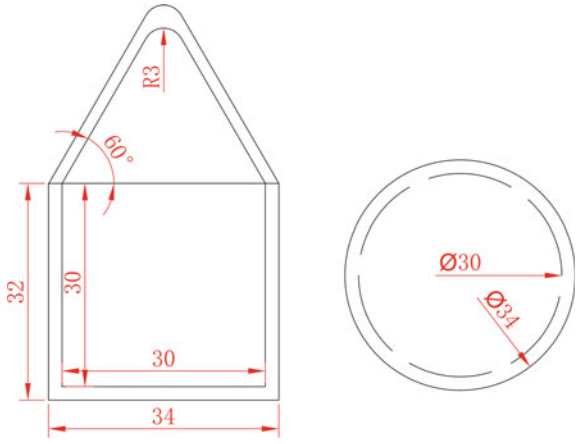

Fig. 2.12 Geometry of quartz crucible

As shown in Fig. 2.9, the online mass measurement was realized through a balance in the fixed bed reactor. The mass measurement system was composed of metal wire, balance, lift platform, and computer. As shown in Fig. 2.11, the crucible was hung below the balance by a metal wire. The top flange had a 5 mm hole in the center. The metal wire was 0.2 mm long, and made of Cr20Ni80 (20 wt% Cr and 80 wt% Ni). The metal wire was not brittle and not easy to break at high temperatures. The maximum permissible temperature was 1200 °C, with the linear expansion coefficient 1.8×10^{-5} °C^{-1} (Zou et al. 2009). From the definition of linear expansion coefficient $l_t = l_0(1 + a\Delta t)$, when the furnace temperature increased from 20 to 1000 °C, imagining that temperature was linearly distributed along metal wire, i.e., the upper end was 20 °C and the lower end was 1000 °C, the extension of 1-m metal wire was

$$\Delta l = \int_0^1 \alpha \Delta t(l) \mathrm{d}l = 8.82 \text{ mm} \tag{2.3}$$

As shown in Fig. 2.11, an electric lift platform was arranged above the furnace, with the track length 800 mm. The lift module was driven by motor and ball screw to reduce the vibration. The lowest position and highest position of the platform are shown in Fig. 2.11. The platform was 350 mm wide, 400 mm long, and dismountable. The maximum bearing capacity was more than 10 kg. Platform center had a φ 80 mm hole, homocentric with the furnace center.

The balance was Metter Toledo ME 204E, with the maximum capacity 220 g, readability 0.1 mg, repeatability 0.1 mg, setting time 2 s, and sensitivity temperature drift 2.0 ppm °C^{-1}. The balance base was 344 mm long and 210 mm wide. The height of the balance was 344 mm, and the net weight was 4.5 kg. During the experiments, the data of the balance could be collected by a computer at the sampling baud rate 9600 bps.

2.2.2.2 Experimental Procedure

Two kinds of experiments were carried out in Macro-TGA: slow pyrolysis and fast pyrolysis. The procedure of slow pyrolysis was as follows:

(1) Open gas cylinder, adjust mass flow controller, and purge the reactor for 1 h;
(2) Load the sample ($\sim$1.5 g) into the crucible and hang the crucible below the balance;
(3) Set furnace temperature program and start to ramp;
(4) When the furnace temperature was around 50 °C, start to collect data from balance and write down the furnace temperature;
(5) When the temperature was stable at 1000 °C, stop collecting data from balance and save balance and temperature data.

The procedure of fast pyrolysis was as follows:

(1) Open gas cylinder, adjust mass flow controller, and purge the reactor for 1 h;
(2) When the furnace temperature was stable at setting temperature, collect data from balance;
(3) Open the top flange, put crucible with sample in reactor and make sure it hung below the balance;
(4) When the change of balance reading was less than 0.01 g min^{-1}, the reaction was thought ended. Stop collecting data from balance and save balance data.

2.2.2.3 Experimental System Debugging

To calibrate the temperature of fixed bed reactor, define the top of the furnace as 0 cm and the bottom of the furnace as 100 cm. The temperature was then calibrated every 10 cm from 4 to 100 cm by a thermocouple (precalibrated). As shown in Fig. 2.13, the tubular furnace had a more than 20-cm-long constant temperature zone at the furnace center with the deviation less than 5 °C, which satisfied the demand of experiments.

To obtain the relationship of furnace display temperature and real temperature, the display temperature and real temperature at reactor center (50 cm) were fitted by a polynomial. The fitting function was $t_r = \sum_0^9 a_i t_f^i$, and the coefficients were shown in Table 2.6. The fitting results are shown in Fig. 2.14.

According to multiple tests, the sampling period of balance was 0.087365 s, and the sampling frequency was 11.45 Hz.

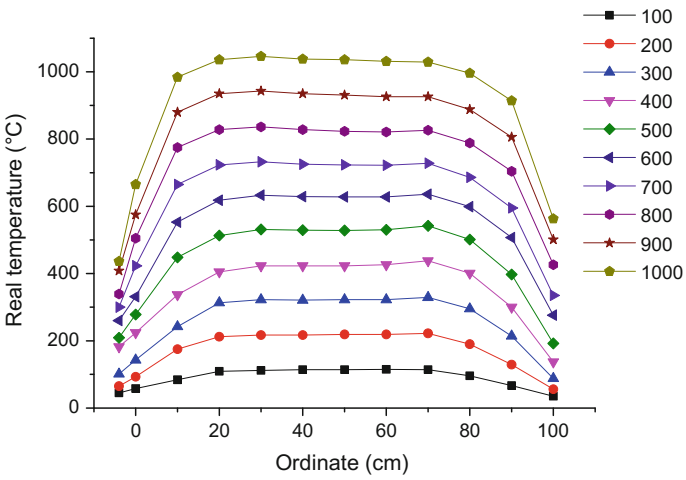

Fig. 2.13 Temperature calibration of Macro-TGA

Table 2.6 Fitting results of furnace display temperature and real temperature

Coefficient	a_0	a_1	a_2	a_3	a_4
Value	-1.30×10	1.80	-8.36×10^{-3}	4.68×10^{-5}	-1.59×10^{-7}
Coefficient	a_5	a_6	a_7	a_8	a_9
Value	3.51×10^{-10}	-5.14×10^{-13}	4.79×10^{-16}	-2.55×10^{-19}	5.87×10^{-23}

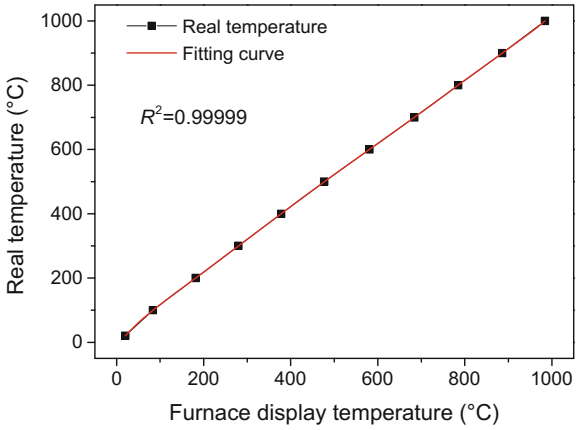

Fig. 2.14 Calibration curve of furnace display temperature and real temperature

The change of temperature might affect the results of balance. The effects might come from the expansion of metal wire, the mass change of quartz crucible, or the temperature drift of balance itself. To obtain the influence of temperature on balance measurement, a blank test was performed. The blank test was heating the empty crucible at the heating rate of 10 °C min^{-1} in N_2 (1 L min^{-1}). The result is shown in Fig. 2.15. The fluctuation of original signal could be filtered to obtain a smooth signal. According to many tests, the optimal cutoff frequency was 0.00689 Hz.

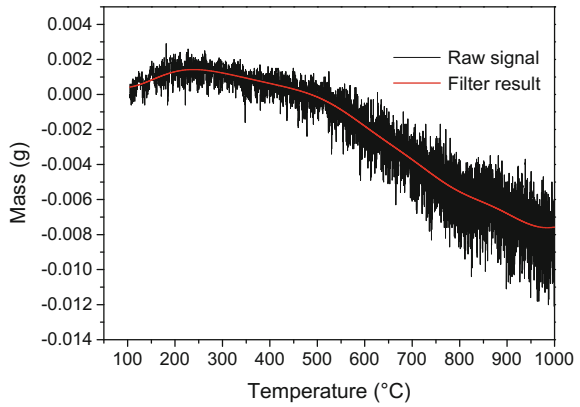

Fig. 2.15 Mass change of linear ramping blank experiment

When the start mass was zero at room temperature, the mass decreased to −0.008 g at 1000 °C. Considering the sample mass for each test was 1.5 g, the influence of temperature change was 0.53%. The blank result was subtracted for each test to obtain the real result.

To verify the repeatability of Macro-TGA, the repeated tests were performed for slow pyrolysis and fast pyrolysis of lignin. As shown in Fig. 2.16, the repeatability of Macro-TGA experiments was quite good.

2.2.2.4 Influence of Sample Mass and Particle Size

To investigate the influence of sample mass on pyrolysis, fast pyrolysis and slow pyrolysis of PVC were studied, as shown in Fig. 2.17. During the slow pyrolysis, the sample mass (0.5–4.5 g) did not affect mass loss process significantly. During the fast pyrolysis, the sample mass affected reaction process significantly. With the

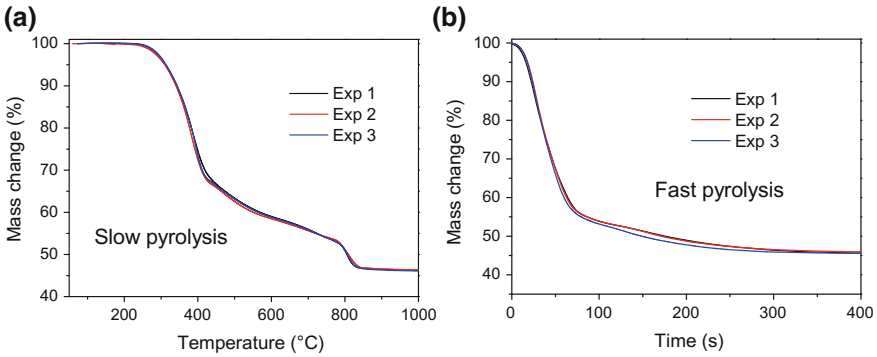

Fig. 2.16 Repeatability of Macro-TGA experiments (example of lignin)

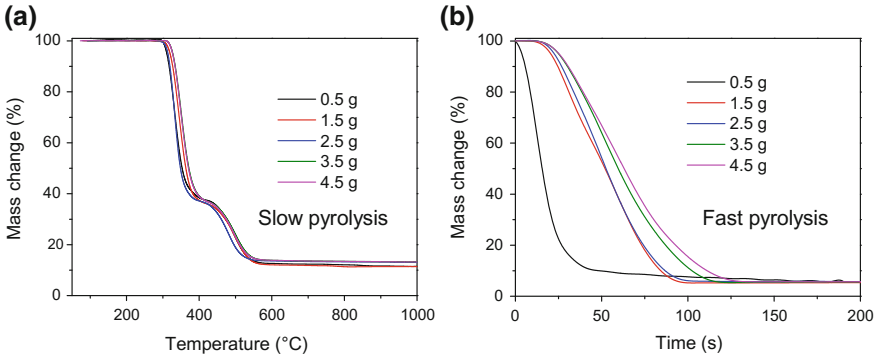

Fig. 2.17 Influence of sample mass on Macro-TGA experiments (example of PVC)

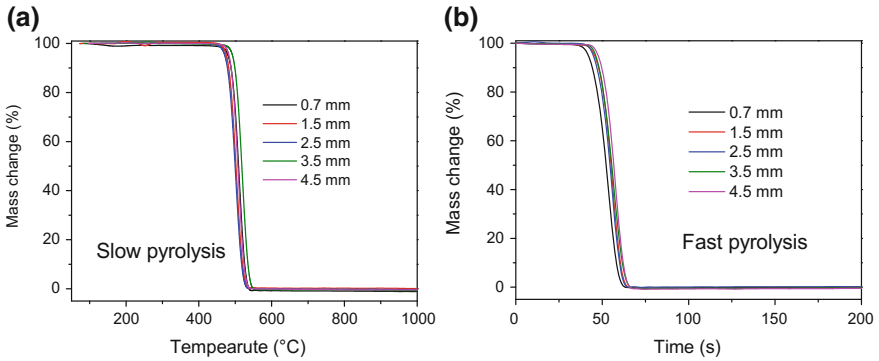

Fig. 2.18 Influence of sample particle size on Macro-TGA experiments (example of PE)

increase of sample mass, the mass loss process was slower and the reaction time was longer, due to the strong heat and mass transfer effect during fast pyrolysis. When the sample mass was 0.5 g, the curve smoothness was poor. Therefore, 1.5 g sample was adopted in the following experiments.

To investigate the influence of particle size on mass loss, the slow pyrolysis and fast pyrolysis of PE of different particle sizes (0.7–4.5 mm) were performed, as shown in Fig. 2.18. The influence of particle size on slow pyrolysis and fast pyrolysis was insignificant, which denoted that the heat and mass transfer effect caused by particle size was not obvious in Macro-TGA experiments.

2.2.3 Horizontal Fixed Bed Reactor (HFBR)

2.2.3.1 Experimental System

The horizontal fixed bed reaction system is shown in Figs. 2.19 and 2.20, including tubular furnace, tar collection system, and gas collection system. The steel reactor

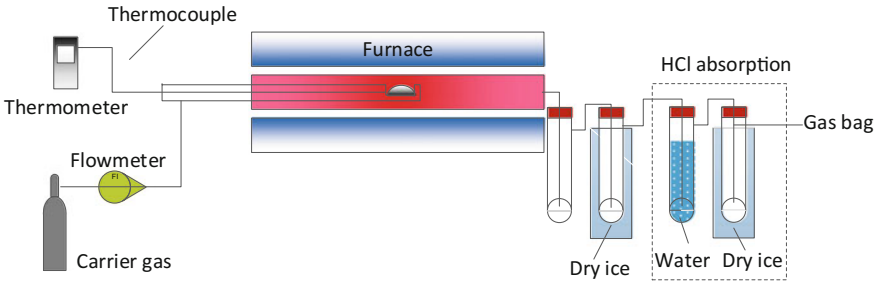

Fig. 2.19 Diagram of horizontal fixed bed reactor. Reprinted from Zhou et al. (2016), Copyright 2016, with permission from Elsevier

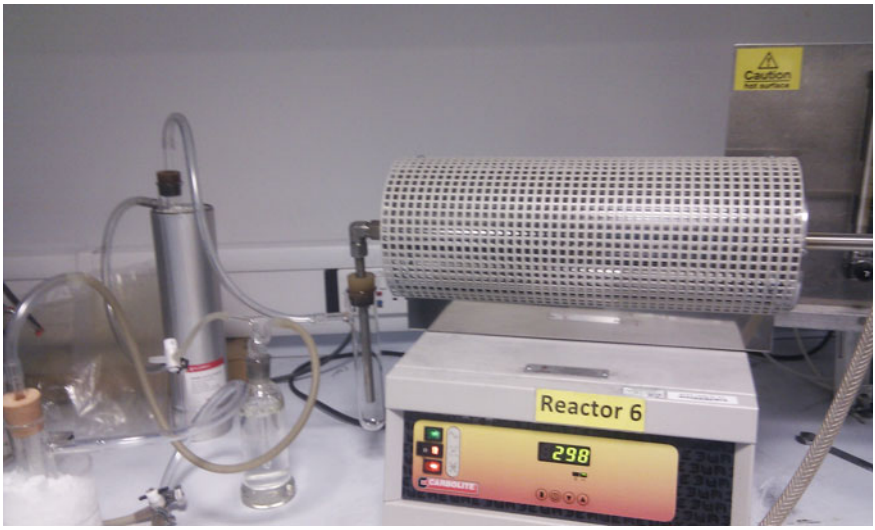

Fig. 2.20 Horizontal fixed bed reactor

was 40 cm long, with the diameter 1 cm. The carrier gas flow rate was 100 ml min^{-1}, and the residence time at 800 °C was approximately 2.6 s. For fast pyrolysis reaction, the reactor was preheated to setting temperature. When the temperature was stabilized, sample boat with around 1 g sample was inserted into the reactor very fast. The average heating rate of fast pyrolysis was around 350 °C min^{-1}, which was just a rough average evaluation of heating, since the heating rate for fast pyrolysis was not stable. For slow pyrolysis, the sample was put in the reactor first, and then the furnace was heated up to setting temperature at 10 °C min^{-1}. The reactor was kept at the final temperature for another 30 min to make sure the reaction was completed.

The products first went through two condensers to collect tar. The first condenser was cooled by air, and the second condenser was cooled by dry ice. Preliminary experiments have shown that these two condensers were good enough to collect the tar. If HCl was produced from the reaction, HCl absorption bottle filled with water and a water collection bottle cooled by dry ice were added between tar collection system and gas collection system. Preliminary experiments have shown the HCl collection effect by water was the same with that by NaOH solution. The non-condensable gases were collected by a Tedlar™ gas bag. Gas collection time was 20 min longer than reaction time to make sure the completed collection of gases. After the reaction, product mass balance (recovery rate) was calculated to verify the reliability of the experiment.

2.2.3.2 Gas Analysis

After the non-condensable gases were collected by a gas bag, they were analyzed by GC. H_2, CO, and N_2 were analyzed by a Varian 3380 GC, with 60–80 mesh molecular sieve column and carrier gas Ar. CO_2 was analyzed by another Varian 3380 GC, with 80–100 mesh molecular sieve column and carrier gas Ar. C_1–C_4 was analyzed by the third Varian 3380 GC, with flame ionization detector (FID), 80–100 mesh Hysep column, and carrier gas N_2. According to the concentration of N_2, together with the known N_2 flow rate and time, the amount of other gases could be calculated.

2.2.3.3 Analysis of PAHs

During each experiment, the mass of tar was calculated from the mass difference of condensers and connection tubes before and after the reaction. After that, different solvents were used to wash the condensers to get the aliphatics, aromatics, and oxygenates. Firstly, hexane was used to wash the condensers to collect all the aliphatics and part of aromatics and oxygenates. Secondly, ethyl acetate was used to wash the condensers to collect the rest of the aromatics and oxygenates. The collected tar samples are shown in Fig. 2.21. Thirdly, the water in the tar was removed by filtering through a column with anhydrous sodium sulfate. An EPH column packed with SiO_2 and Al_2O_3 was used to separate aliphatics, aromatics, and oxygenates in hexane. Firstly, the column was rinsed with pure hexane, and then, let tar solution go through the column and use more hexane to wash the column. Therefore, aliphatics would still be in hexane solution, and other compounds would

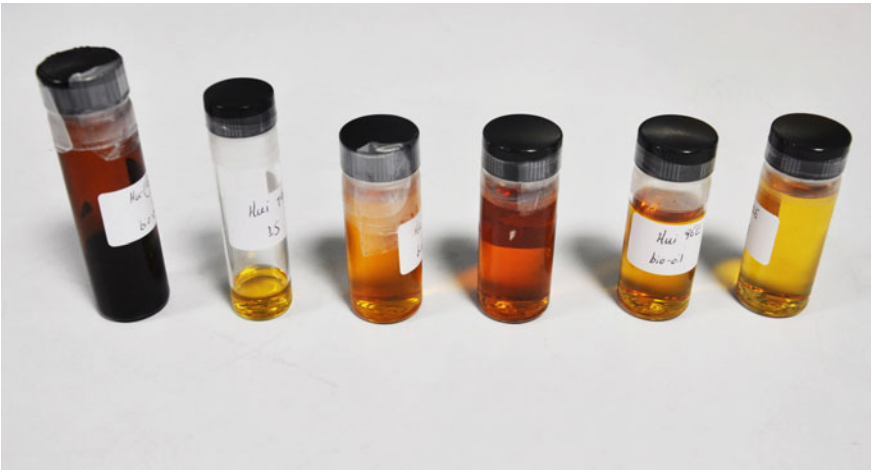

Fig. 2.21 Collected tar samples

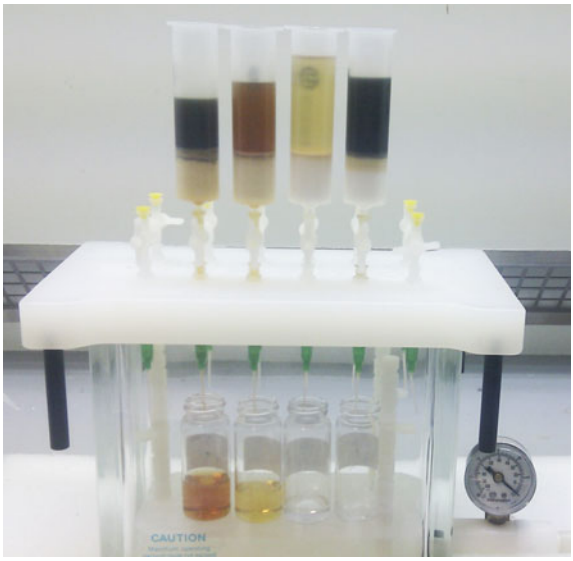

Fig. 2.22 Separation process in EPH column

be captured by EPH column. Other compounds could be washed out by ethyl acetate. The vacuum filtration process was shown in Fig. 2.22.

Finally, PAHs in aromatic fractions were analyzed by a Varian CP-3800 GC coupled with Varian Saturn 2200 MS. The GC column was 30 m × 0.25 μm. Every time, 2 μl sample was injected. The injection inlet temperature was 290 °C. The column temperature program was as follows: stay at 50 °C for 6 min; ramp to 210 °C at 5 °C min^{-1} and stay for 1 min; ramp to 300 °C at 8 °C min^{-1}. The total analysis time was 61 min. The transfer line temperature was 280 °C; the manifold temperature was 120 °C; and the ion trap temperature was 220 °C. The ion trap was initially switched off for 7 min to let the solvent flow in before data collection to protect the ion trap. During the measurement, 2-hydroxyacetophenone was used as internal standard (IS). GC/MS was calibrated by Sigma-Aldrich standard sample PAH Mix 3 to obtain quantitative results. During the measurement, ten kinds of 2–4 ring PAHs listed by USEPA with priority were detected, together with two naphthalene derivatives (1-methylnaphthalene and 2-methylnaphthalene). Since benzo [*a*]anthracene and chrysene could not be separated by GC, the concentrations of these two compounds were reported together.

Meanwhile, the molecular weight of tar was measured by size exclusion chromatography (SEC). In SEC test, compounds with high molecular weight came out first (Blanco et al. 2012). The instrument used in this study was Perkin Elmer Modular 225. Tar was first distilled to almost dry, then dissolved in tetrahydrofuran (THF), and kept the concentration around 0.2%. Polymer Laboratories 5 μm separation column was adopted in this study, and PS with molecular weight 800–860 000 g mol^{-1}, benzene, and PAHs were used for calibration. The detector was Perkin Elmer Series 200a refractive index detector.

2.3 Kinetic Analysis Method

The kinetics of pyrolysis means the mass loss properties for a pyrolytic reaction. Basic kinetic studies can help us to predict the pyrolytic behavior and then design better pyrolytic reactor (Cho et al. 2012; Zhang et al. 2014). Many studies have chosen DTG curves to investigate the kinetics, since DTG curves are more convenient for the kinetic calculation. In addition, DTG curves are more sensitive than TG curves, which means the tiny change in TG curves will be magnified in corresponding DTG curves (Caballero and Conesa 2005; Budrugeac 2002).

2.3.1 Kinetic Analysis Method of Slow Pyrolysis

The pyrolytic processes of many samples are complicated and cannot be denoted by a single kinetic reaction. In the paralleled reaction kinetic model, pyrolysis can be regarded as the superposition of a series of independent reactions (Manya et al. 2003).

$$\frac{\mathrm{d}m}{\mathrm{d}\tau} = \sum_{i=1}^{n} \frac{\mathrm{d}m_i}{\mathrm{d}\tau} \tag{2.4}$$

In Eq. (2.4), m denotes the sample conversion at time τ, with the unit %.

To obtain normalized results, α_i was used to denote the normalized conversion rate of Reaction i, i.e.,

$$\alpha_i = m_i / m_{i\infty} \tag{2.5}$$

In Eq. (2.5), $m_{i\infty}$ denotes the final conversion rate of Reaction i. Therefore, we know that $\alpha_{i\infty} = 100\%$.

Since DTG curves of slow pyrolysis may have multiple peaks, supposing that each peak (including shoulder peak) represents a reaction, peak analysis method could be used to divide the overall reaction into several single peak reactions. The reaction of each peak can be described by Gaussian peak, which is the most commonly used peak shape for peak analysis (Guo 2011).

The kinetics of each reaction can be expressed by (Coats and Redfern 1964)

$$\frac{\mathrm{d}\alpha_i}{\mathrm{d}\tau} = k_i (1 - \alpha_i)^{n_i} \tag{2.6}$$

$$k_i = A_i \exp\left(-\frac{E_i}{RT}\right) \tag{2.7}$$

Here, k_i denotes the reaction rate of Reaction i; E_i denotes the apparent activation energy (kJ mol^{-1}); A_i denotes pre-exponential factor (min^{-1}); n_i is reaction order; R is universal gas constant (kJ mol^{-1} K^{-1}); T is absolute temperature (K).

In slow pyrolytic experiments, heating rate β is constant,

$$\beta = \frac{\mathrm{d}T}{\mathrm{d}\tau} \tag{2.8}$$

Therefore,

$$\frac{\mathrm{d}\alpha_i}{\mathrm{d}T} = \frac{A_i}{\beta}\exp\left(-\frac{E_i}{RT}\right)(1-\alpha_i)^{n_i} \tag{2.9}$$

To calculate E_i, A_i, and n_i, least square method (LSM) was used.

$$S = \sum_{j=1}^{N}\left[\left(\frac{\mathrm{d}\alpha}{\mathrm{d}T}\right)_j^{\exp} - \left(\frac{\mathrm{d}\alpha}{\mathrm{d}T}\right)_j^{\mathrm{cal}}\right]^2 \tag{2.10}$$

In Eq. (2.10), N denotes points of data; $(\mathrm{d}\alpha/\mathrm{d}T)_{\exp}$ denotes experimental value; $(\mathrm{d}\alpha/\mathrm{d}T)_{\mathrm{cal}}$ denotes calculation value. Average deviation index (*ADI*) was used to evaluate the accuracy of the calculation results:

$$\mathrm{ADI} = \frac{\sqrt{S/N}}{(d\alpha_i/dT)_{\max}^{\exp}} \times 100\% \tag{2.11}$$

In Eq. (2.11), $(d\alpha_i/dT)_{\max}^{\exp}$ denotes the maximum of experimental value.

2.3.2 Kinetic Analysis Method of Fast Pyrolysis

Since fast pyrolysis usually ends in a short time, many peaks in slow pyrolysis may be combined for fast pyrolysis, but peak analysis method could still be applied. For fast pyrolysis, Avrami-Erofeev Equation was widely used (Hancock and Sharp 1972; Go et al. 2008). Each peak can be described as

$$1-\alpha_i = \exp(-k_i\tau^{n_i}) \tag{2.12}$$

In Eq. (2.12), k_i and n_i are determined by experiments, and τ denotes time.

Taking the natural logarithm of Eq. (2.12),

$$\ln(1-\alpha_i) = -k_i\tau^{n_i} \tag{2.13}$$

Therefore, LSM can still be used to obtain the optimal k_i and n_i.

The advantage of peak analysis-least square method (PA-LSM) is that DTG curves can be divided into paralleled reactions according to the peaks, which is more direct and has clear physical significance. LSM can help to find the optimal kinetic parameters more accurately, and avoid the errors from the assumption in integral method and differential method.

2.4 Summary

This chapter is the introduction of research methods, including three parts, selection of research objects, experimental apparatus, and kinetic analysis methods.

(1) Based on the statistical analysis of CSW in China, nine basic components (hemicellulose, cellulose, lignin, pectin, starch, PE, PS, PVC, and PET) were selected. The characteristics of basic components were analyzed, including proximate analyses, ultimate analyses, heating values, and functional groups in solid FTIR.
(2) Three experimental platforms were introduced: TGA, Macro-TGA, and horizontal fixed bed reactor. The latter two reactors were self-designed. Macro-TGA realized the online mass measurement of the thermochemical reaction of gram level sample, which could be applied to both fast reaction and slow reaction with good repeatability and reliability. PAHs from a horizontal fixed bed reactor were collected and analyzed. The PAHs in tar could be collected by a two-stage condenser system. In addition, aliphatics, aromatics, and oxygenates were separated for the better measurement of PAHs. The GC/MS was calibrated to obtain the quantitative results.
(3) Based on parallel reaction model, peak analysis method was used to separate the paralleled reactions. Complex thermochemical reactions could be divided into several paralleled reactions, and then the kinetic parameters were determined by least square method.

This chapter introduced the selection method of basic components and fundamental characteristics (proximate analyses, ultimate analyses, heating values, and functional groups), experimental platforms (TGA, Macro-TGA, and horizontal fixed bed reactor), and kinetic analysis method (PA-LSM). This chapter is the foundation of the following research.

References

Abidi N, Cabrales L, Haigler CH (2014) Changes in the cell wall and cellulose content of developing cotton fibers investigated by FTIR spectroscopy. Carbohyd Polym 100:9–16

Biagini E, Fantei A, Tognotti L (2008) Effect of the heating rate on the devolatilization of biomass residues. Thermochim Acta 472:55–63

Blanco PH, Wu C, Onwudili JA et al (2012) Characterization of tar from the pyrolysis/gasification of refuse derived fuel: influence of process parameters and catalysis. Energ Fuel 26:2107–2115
Bockhorn H, Hornung A, Hornung U et al (1999) Modelling of isothermal and dynamic pyrolysis of plastics considering non-homogeneous temperature distribution and detailed degradation mechanism. J Anal Appl Pyrol 49:53–74
Budrugeac P (2002) Differential non-linear isoconversional procedure for evaluating the activation energy of non-isothermal reactions. J Therm Anal Calorim 68:131–139
Caballero JA, Conesa JA (2005) Mathematical considerations for nonisothermal kinetics in thermal decomposition. J Anal Appl Pyrol 73:85–100
Chang CY, Wu CH, Hwang JY et al (1996) Pyrolysis kinetics of uncoated printing and writing paper of MSW. J Environ Eng 122:299–305
Chatel G, Rogers RD (2014) Review: oxidation of lignin using ionic liquids—an innovative strategy to produce renewable chemicals. ACS Sustain Chem Eng 2:322–339
Cho JM, Chu S, Dauenhauer PJ et al (2012) Kinetics and reaction chemistry for slow pyrolysis of enzymatic hydrolysis lignin and organosolv extracted lignin derived from maplewood. Green Chem 14:428–439
Coats AW, Redfern JP (1964) Kinetic parameters from thermogravimetric data. Nature 201:68–69
Couhert C, Commandre JM, Salvador S (2009) Is it possible to predict gas yields of any biomass after rapid pyrolysis at high temperature from its composition in cellulose, hemicellulose and lignin? Fuel 88:408–417
Dorrestijn E, Laarhoven LJJ, Arends IWCE et al (2000) The occurrence and reactivity of phenoxyl linkages in lignin and low rank coal. J Anal Appl Pyrol 54:153–192
Dumitriu S (2004) Polysaccharides: structural diversity and functional versatility. CRC Press, Boca Raton, Florida
Fisher T, Hajaligol M, Waymack B et al (2002) Pyrolysis behavior and kinetics of biomass derived materials. J Anal Appl Pyrol 62:331–349
Go K, Son S, Kim S (2008) Reaction kinetics of reduction and oxidation of metal oxides for hydrogen production. Int J Hydrogen Energ 33:5986–5995
Guo H (2011) A simple algorithm for fitting a Gaussian function. IEEE Signal Proc Mag 28:134–137
Hancock JD, Sharp JH (1972) Method of comparing solid-state kinetic data and its application to the decomposition of kaolinite, brucite, and $BaCO_3$. J Am Ceram Soc 55:74–77
Janowitz MF (2010) Ordinal and relational clustering. World Scientific Publishing Co. Pte. Ltd, Singapore
Li AM, Li XD, Li SQ et al (1999) Experimental studies on municipal solid waste pyrolysis in a laboratory-scale rotary kiln. Energy 24:209–218
Lopez-Velazquez MA, Santes V, Balmaseda J et al (2013) Pyrolysis of orange waste: a thermo-kinetic study. J Anal Appl Pyrol 99:170–177
Manya JJ, Velo E, Puigjaner L (2003) Kinetics of biomass pyrolysis: a reformulated three-parallel-reactions model. Ind Eng Chem Res 42:434–441
Miranda R, Bustos-Martinez D, Blanco CS et al (2009) Pyrolysis of sweet orange (Citrus sinensis) dry peel. J Anal Appl Pyrol 86:245–251
Seo DK, Park SS, Kim YT et al (2011) Study of coal pyrolysis by thermo-gravimetric analysis (TGA) and concentration measurements of the evolved species. J Anal Appl Pyrol 92:209–216
Skreiberg A, Skreiberg Ø, Sandquist J et al (2011) TGA and macro-TGA characterization of biomass fuels and fuel mixtures. Fuel 90:2182–2197
Soares S, Camino G, Levchik S (1995) Comparative study of the thermal decomposition of pure cellulose and pulp paper. Polym Degrad Stabil 49:275–283
Sorum L, Gronli MG, Hustad JE (2001) Pyrolysis characteristics and kinetics of municipal solid wastes. Fuel 80:1217–1227
Vassilev SV, Baxter D, Andersen LK et al (2010) An overview of the chemical composition of biomass. Fuel 89:913–933
Wu CH, Chang CY, Lin JP (1997) Pyrolysis kinetics of paper mixtures in municipal solid waste. J Chem Technol Biot 68:65–74

Wu CH, Chang CY, Tseng CH (2002) Pyrolysis products of uncoated printing and writing paper of MSW. Fuel 81:719–725

Wu CH, Chang CY, Tseng CH et al (2003) Pyrolysis product distribution of waste newspaper in MSW. J Anal Appl Pyrol 67:41–53

Yang H, Yan R, Chen H et al (2007) Characteristics of hemicellulose, cellulose and lignin pyrolysis. Fuel 86:1781–1788

Yin C, Li J, Xu Q et al (2007) Chemical modification of cotton cellulose in supercritical carbon dioxide: synthesis and characterization of cellulose carbamate. Carbohyd Polym 67:147–154

Yoon HC, Pozivil P, Steinfeld A (2012) Thermogravimetric pyrolysis and gasification of lignocellulosic biomass and kinetic summative law for parallel reactions with cellulose, xylan, and lignin. Energ Fuel 26:357–364

Zhang J, Chen T, Wu J et al (2014) A novel Gaussian-DAEM-reaction model for the pyrolysis of cellulose, hemicellulose and lignin. RSC Adv 4:17513–17520

Zhao D, Dai Y, Chen K et al (2013) Effect of potassium inorganic and organic salts on the pyrolysis kinetics of cigarette paper. J Anal Appl Pyrol 102:114–123

Zheng J, Jin YQ, Chi Y et al (2009) Pyrolysis characteristics of organic components of municipal solid waste at high heating rates. Waste Manage 29:1089–1094

Zhou H, Long Y, Meng A et al (2013) The pyrolysis simulation of five biomass species by hemi-cellulose, cellulose and lignin based on thermogravimetric curves. Thermochim Acta 566:36–43

Zhou H, Meng A, Long Y et al (2014) Interactions of municipal solid waste components during pyrolysis: a TG-FTIR study. J Anal Appl Pyrol 108:19–25

Zhou H, Long Y, Meng A et al (2015a) A novel method for kinetics analysis of pyrolysis of hemicellulose, cellulose, and lignin in TGA and macro-TGA. RSC Adv 5:26509–26516

Zhou H, Long Y, Meng A et al (2015b) Classification of municipal solid waste components for thermal conversion in waste-to-energy research. Fuel 145:151–157

Zhou H, Wu C, Onwudili JA et al (2015c) Polycyclic aromatic hydrocarbons (PAH) formation from the pyrolysis of different municipal solid waste fractions. Waste Manage 36:136–146

Zhou H, Wu C, Onwudili JA et al (2016) Influence of process conditions on the formation of 2–4 ring polycyclic aromatic hydrocarbons from the pyrolysis of polyvinyl chloride. Fuel Process Technol 144:299–304

Zou X, Nan H, Han L et al (2009) 电热合金的研究现状及发展趋势 (Research progress on electrothermal alloy). Foundry Technol 30:554–557

Chapter 3
Pyrolysis Characteristics of Basic Components

Abstract For the nine combustible solid waste (CSW) basic components proposed in Chap. 2, pyrolytic experiments in thermogravimetric analyzer (TGA), Macro-TGA, and horizontal fixed bed reactor (HFBR) were performed. Kinetics were fundamental characteristics of pyrolytic reactions. The slow pyrolytic kinetics of intrinsic chemical reactions were studied in TGA, and the fast and slow pyrolytic kinetics with heat and mass transfer effect were studied in Macro-TGA, which was more similar to industrial fixed bed reactor. Finally, the kinetics from different conditions were compared. In addition, the product (gas, liquid, and solid) distribution was studied in horizontal fixed bed reactor. The gas products from TGA pyrolysis were analyzed by Fourier transform infrared spectroscopy (FTIR), and the gas products from horizontal fixed bed reactor were analyzed by gas chromatography (GC). Polycyclic aromatic hydrocarbons (PAHs) are important pollutants during thermochemical conversions of CSW. Therefore, the PAHs formation characteristics were quantitatively studied in the horizontal fixed bed reactor. Based on the above results, the pyrolytic mechanisms and the PAHs formation mechanisms were further explored.

Keywords Combustible solid waste (CSW) · Basic component · Pyrolysis · Polycyclic aromatic hydrocarbons (PAHs)

3.1 Kinetics

In this section, the pyrolytic kinetic parameters of basic components were calculated by peak analysis-least square method (PA-LSM), and the pyrolytic mass loss curves were reproduced from the calculated parameters.

H. Zhou, *Combustible Solid Waste Thermochemical Conversion*, Springer Theses,
DOI 10.1007/978-981-10-3827-3_3

3.1.1 Kinetics of Pyrolysis in TGA

3.1.1.1 TG and Derivative Thermogravimetric (DTG) Characteristics

The pyrolytic TG and DTG curves of nine basic components in TGA are shown in Fig. 3.1. For five biomass basic components, the pyrolysis of hemicellulose, lignin, and pectin happened early (~200 °C). The research of Yang et al. (2007) has also shown that the hemicellulose pyrolysis began from 220–315 °C. As shown in Fig. 3.1a, c, the pyrolysis of cellulose and starch started at higher temperatures (~300 °C). The final residue of lignin at 1000 °C was the highest (46.2%),

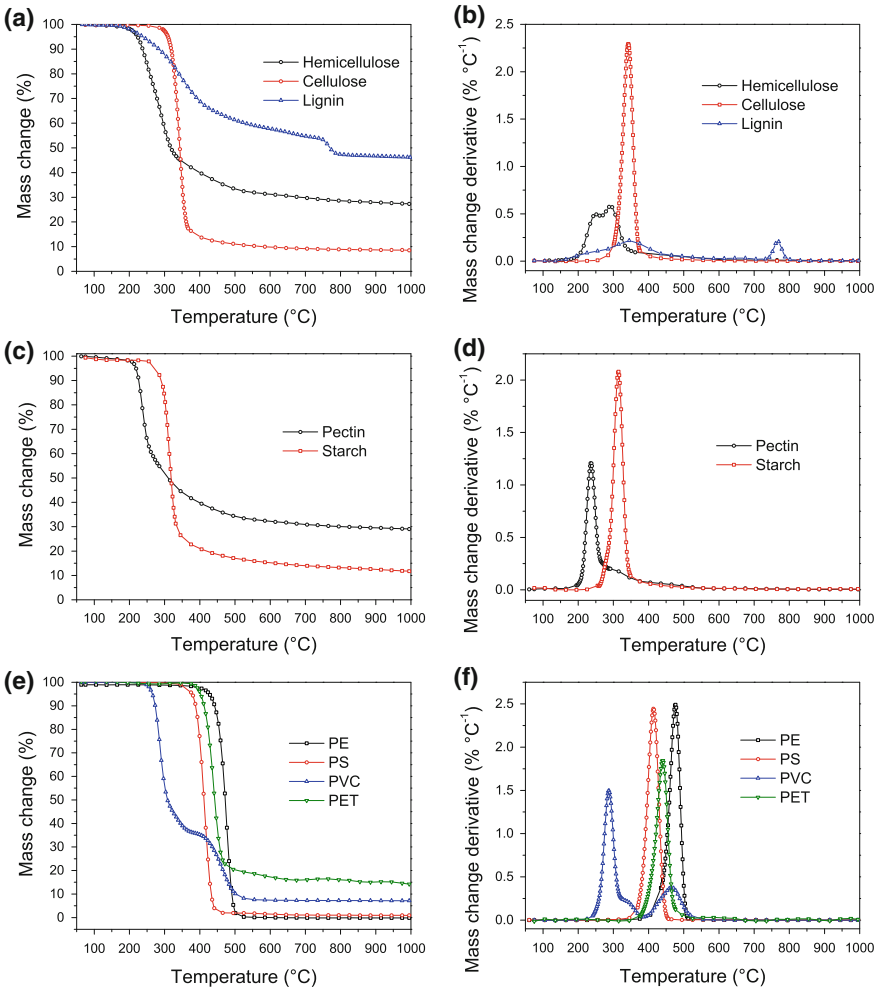

Fig. 3.1 Pyrolytic TG and DTG curves of basic components in TGA

followed by pectin (29.0%) and hemicellulose (27.3). As shown in Fig. 3.1b and d, hemicellulose pyrolysis had two obvious peaks, at 244.9 and 296.1 °C, respectively. Cellulose pyrolysis had only one peak, at 344.2 °C. The research of Zhang et al. (2014) has shown that cellulose pyrolysis occurred between 287 and 387 °C. Lignin pyrolysis was a very complicated and slow process, with two obvious peaks at 337.9 and 767.9 °C. Yang et al. (2007) studied lignin pyrolysis in TGA and found that lignin pyrolysis happened in a wide temperature range (100–900 °C). The pyrolysis of pectin and starch had a characteristic peak, as shown in Fig. 3.1d. The peak of pectin was at 236.5 °C, and the peak of starch was at 312.8 °C.

For four kinds of plastics, their pyrolytic curves were relatively simple. The order of thermal stability from low to high was polyvinyl chloride (PVC) < polystyrene (PS) < polyethylene terephthalate (PET) < polyethylene (PE). The residual mass of PE and PS was almost zero, while PET and PVC had some solid residue. The pyrolysis of PE, PS, and PET had only one DTG peak at 474.0, 412.5, and 437.7 °C, respectively. PVC pyrolysis had two obvious DTG peaks, at 286.5 and 461.3 °C.

3.1.1.2 Kinetics

PA-LSM was adopted to calculate the kinetic parameters of basic component pyrolysis. The calculated kinetic parameters of biomass were shown in Fig. 3.2. The DTG curve of hemicellulose could be fitted by three peaks, with the R^2 0.9977. Besides the above two peaks, there was a flat peak at 366.1 °C. Cellulose pyrolysis could be fitted by a single peak, with the R^2 0.9925, which proved that Gaussian peak was suitable to describe pyrolytic peaks. Since lignin pyrolysis was a slow and complex process, five Gaussian peaks were needed to denote the DTG curve (R^2 = 0.9918). Besides two obvious peaks at 337.9 and 767.9 °C, there were three peaks at 227.7, 478.4, and 649.3 °C. Pectin pyrolysis could be simulated by two peaks, with an obvious peak at 236.5 °C, and another flat peak at 297.6 °C, as shown in Fig. 3.2f. Starch pyrolysis could be fitted by a single peak at 312.8 °C.

The pyrolytic kinetic parameters of plastic basic components are shown in Fig. 3.3. Since the pyrolytic processes of PE, PS, and PET were simple, they could be simulated by a single peak. In comparison, the pyrolysis of PVC needed three peaks for simulation, with the R^2 0.9974.

The parameters of basic components pyrolysis calculated by PA-LSM are shown in Table 3.1, where the percentage means the relative percentage of each peak area, namely the relative mass loss percent of each part. As is well known, activation energy (AE) is a very important parameter for chemical reactions. As shown in Table 3.1, the AE of different reactions varied from 26 to 1090 kJ mol^{-1}. Meanwhile, the values of AE were related to the shape of the peaks. The sharper the peak was, the higher the AE was.

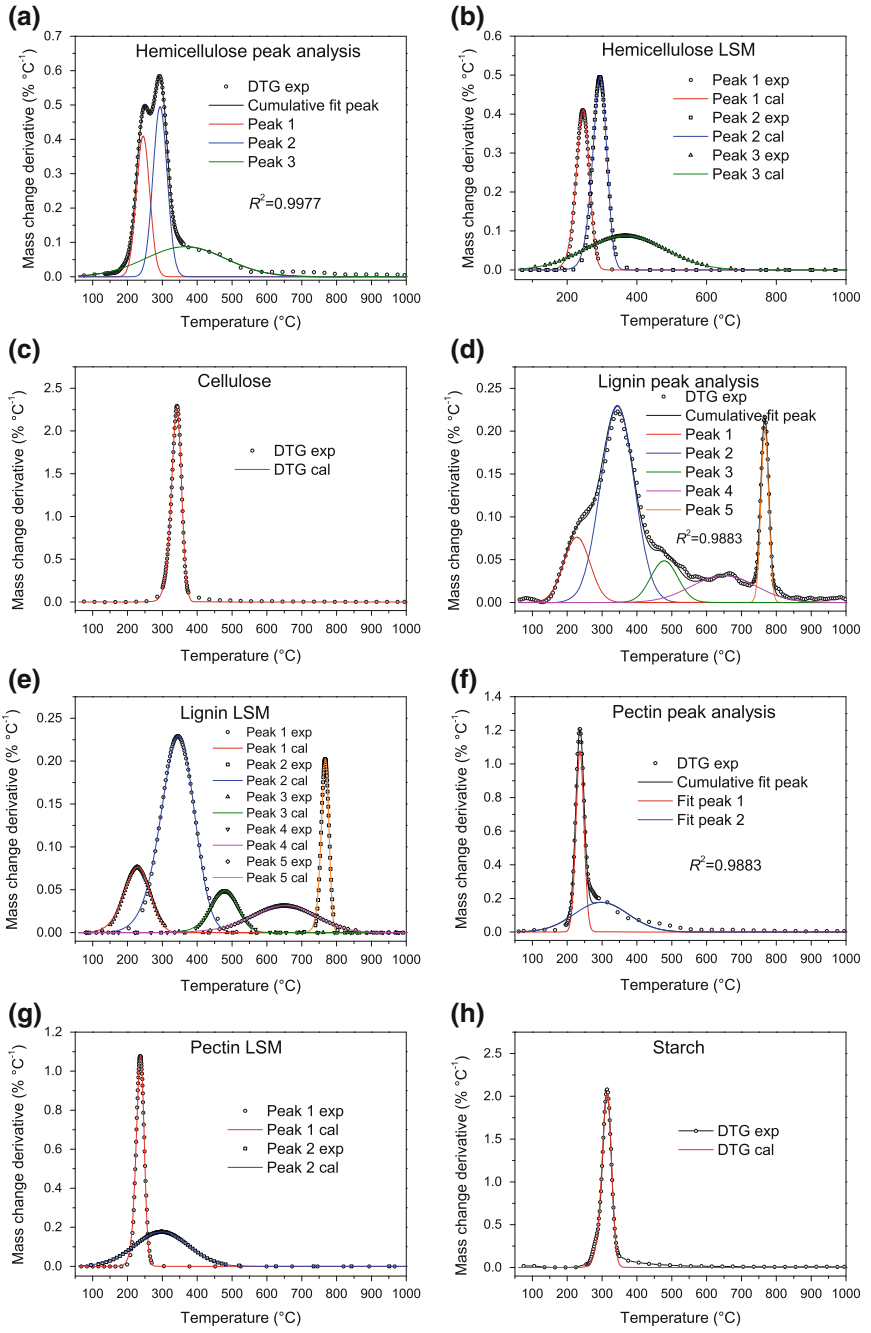

Fig. 3.2 Pyrolytic kinetic calculation of biomass basic components in TGA

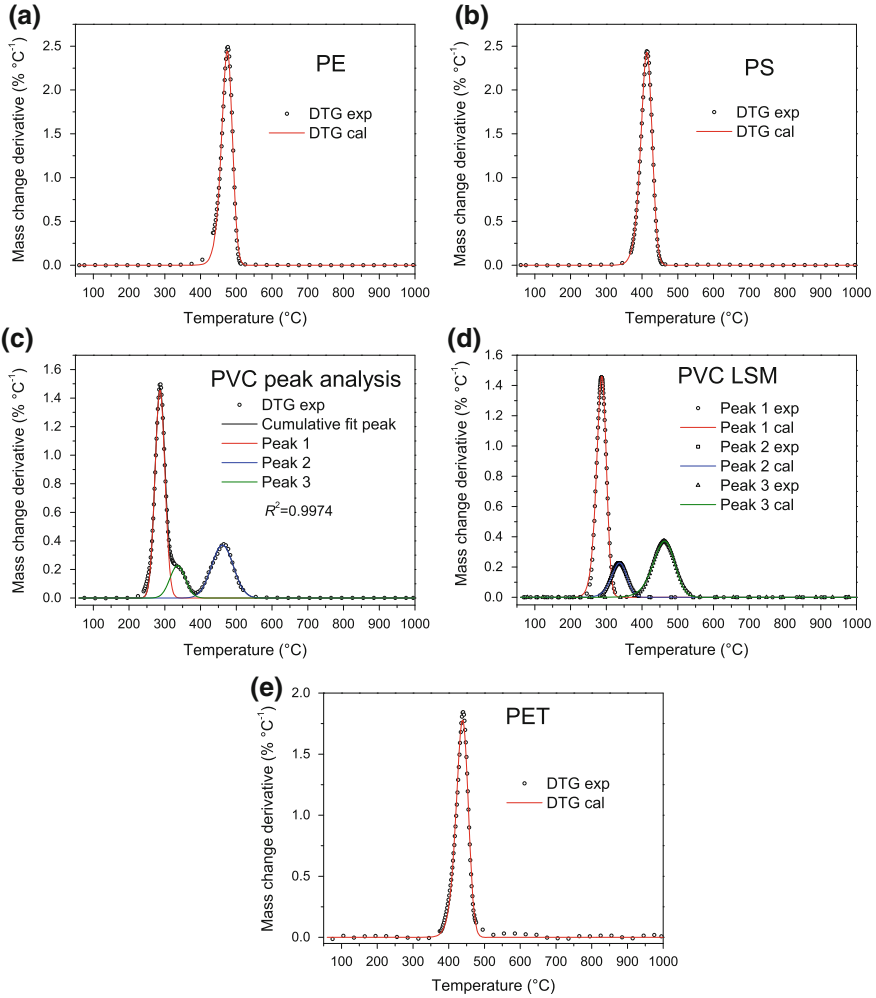

Fig. 3.3 Pyrolytic kinetic calculation of plastic basic components in TGA

Index n is reaction order, which is related to reaction mechanism (Wang et al. 2014). For different reactions, n varied from 1.08 to 1.60. *ADI* values were all smaller than 2, which proved the reproductivity of DTG curves was good. The results in Figs. 3.2 and 3.3 also showed that the differences between calculation results and experimental results were very small.

Encinar and González (2008) pyrolyzed plastics in TGA at the heating rate of 10 °C min^{-1} and obtained that the AE of PS pyrolysis was 231.9 kJ mol^{-1}; the AE of PE pyrolysis was 259.7 kJ mol^{-1}; and the AE of PET pyrolysis was

Table 3.1 Pyrolytic kinetic parameters of basic components in TGA

Sample	Reaction	Percentage (%)	Peak temperature (°C)	E (kJ mol^{-1})	A (min^{-1})	n	Average deviation index (ADI)
Hemicellulose	1	27.9	244.8	146	3.37×10^{14}	1.49	1.58
	2	36.1	293.5	164	6.58×10^{14}	1.49	1.58
	3	40.0	366.1	26	9.19	1.08	0.23
Cellulose	1	100.0	340.8	279	4.41×10^{23}	1.54	1.64
Lignin	1	13.6	227.7	62	8.61×10^{5}	1.35	1.32
	2	52.8	344.3	73	3.05×10^{5}	1.34	1.29
	3	9.0	478.4	144	3.04×10^{9}	1.43	1.48
	4	13.9	649.3	81	3.91×10^{3}	1.27	1.13
	5	10.7	767.1	1090	5.85×10^{54}	1.6	1.87
Pectin	1	47.6	236.5	245	1.18×10^{25}	1.55	1.78
	2	52.4	297.6	34	1.52×10^{2}	1.18	0.78
Starch	1	100.0	312.8	267	5.46×10^{23}	1.55	1.77
PE	1	100.0	474.0	397	4.68×10^{27}	1.56	1.81
PS	1	100.0	412.5	321	1.99×10^{24}	1.55	1.79
PVC	1	55.3	286.5	244	4.99×10^{22}	1.54	1.76
	2	13.5	335.9	179	1.13×10^{15}	1.50	1.72
	3	31.4	461.3	181	2.93×10^{12}	1.47	1.68
PET	1	100.0	437.7	317	1.4×10^{23}	1.54	1.78

235.7 kJ mol^{-1}. Overall, the AE values by Encinar et al. were lower than those in this study. The reason might be that Encinar et al. supposed the reaction order was constant 1, while in this study, the reaction orders obtained from LSM was approximately 1.5. Similarly, Varhegyi et al. (1989) pyrolyzed cellulose in TGA at the heating rate of 10 °C min^{-1}, supposing the reaction order was 1.2 and obtained the AE was 234 kJ mol^{-1}, which was also lower than that in this study.

3.1.2 Kinetics of Slow Pyrolysis in Macro-TGA

3.1.2.1 TG and DTG Characteristics

The slow pyrolysis curves of nine basic components in Macro-TGA are shown in Fig. 3.4. Similar to that in TGA, the heating rate was 10 °C min^{-1} and the temperature range was room temperature to 1000 °C. As shown in Fig. 3.4a, hemicellulose pyrolysis could be separated into two stages: the first stage had a high pyrolytic rate, and the second stage was relatively slow. Cellulose pyrolysis had only one peak at 385.1 °C, as shown in Fig. 3.4b. Lignin pyrolysis had two obvious peaks. The pyrolysis of pectin had an obvious turn at 295 °C: before this temperature, the pyrolysis was fast; after this temperature, the pyrolysis was slow. Meanwhile, it should be noted that pectin pyrolysis happened very early, around 250 °C. The pyrolysis of starch was similar to that of cellulose, maybe due to they were all composed of glucose monomers.

Except for PVC, the pyrolysis processes of other plastics were simple, with the main pyrolytic temperature range in 400–550 °C. The thermal stability from high to low was PE > PET > PS, with the DTG peak at 509.1, 467.4, and 463.1 °C, respectively. PVC pyrolysis was complex, which could be divided into three stages from 300 to 550 °C, with two obvious peaks at 341.5 and 495.6 °C.

3.1.2.2 Kinetics

The kinetic parameters of slow pyrolysis of basic components in Macro-TGA were calculated by PA-LSM. Hemicellulose pyrolysis could be fitted by two peaks, as shown in Fig. 3.5a. Cellulose pyrolysis could be simulated by a single peak, while lignin pyrolysis needed three peaks for simulation, with the R^2 0.9670. The pyrolysis of pectin and starch could be fitted by a single peak.

The kinetics calculation of plastic basic components is shown in Fig. 3.6. The pyrolysis of PE, PS, and PET could be simulated by a single peak with high R^2 values, while PVC pyrolysis needed two peaks for simulation, as shown in Fig. 3.6c.

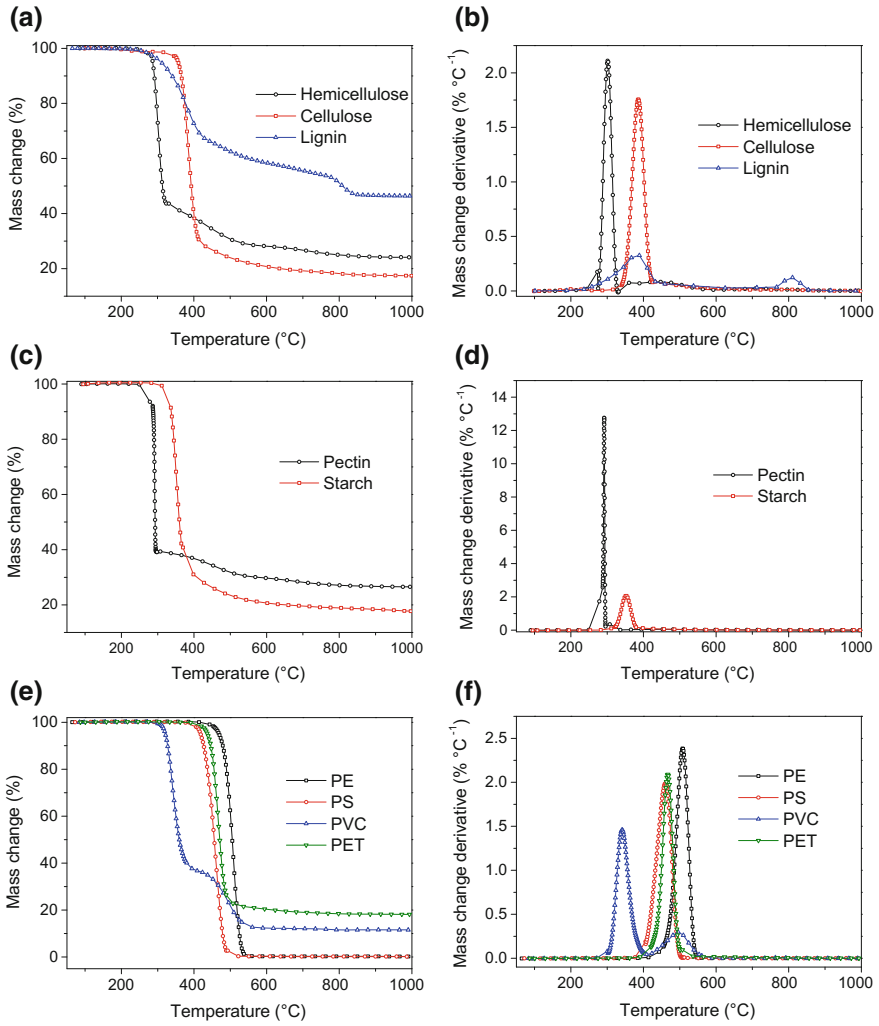

Fig. 3.4 Slow pyrolytic TG and DTG curves of basic components in Macro-TGA

The kinetic parameters of slow pyrolysis of basic components in Macro-TGA were shown in Table 3.2. The *ADI* values were all smaller than 2, which meant the calculated values agreed well with the experimental values. For most reactions, the AE varied from 18 to 588 kJ mol^{-1}, while the AE of pectin pyrolysis was special, as high as 2249 kJ mol^{-1}. As shown in Fig. 3.5f, the DTG curve of pectin pyrolysis was very sharp. The reaction orders n varied from 0.94 to 1.66.

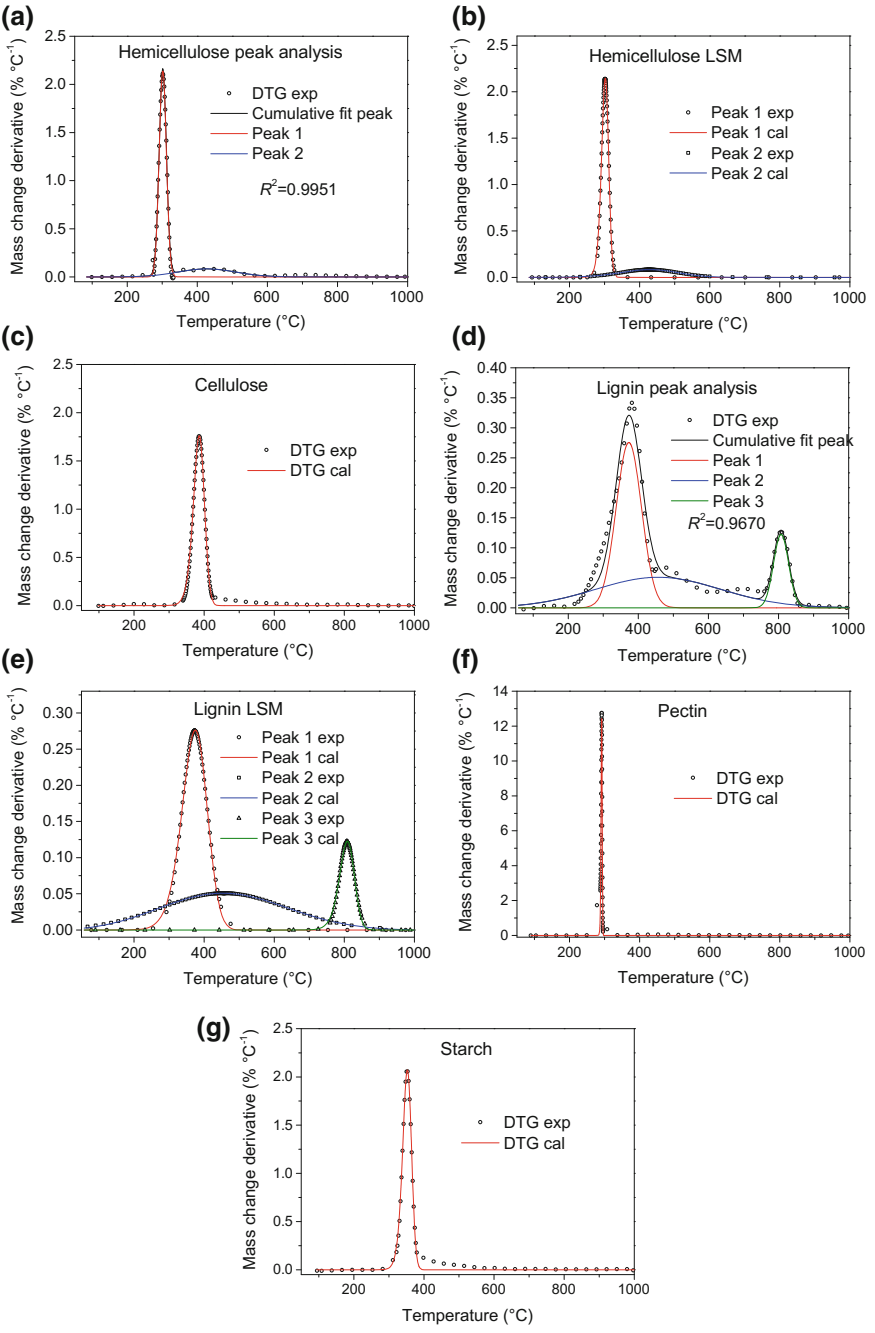

Fig. 3.5 Kinetic calculation of slow pyrolysis of biomass basic components in Macro-TGA

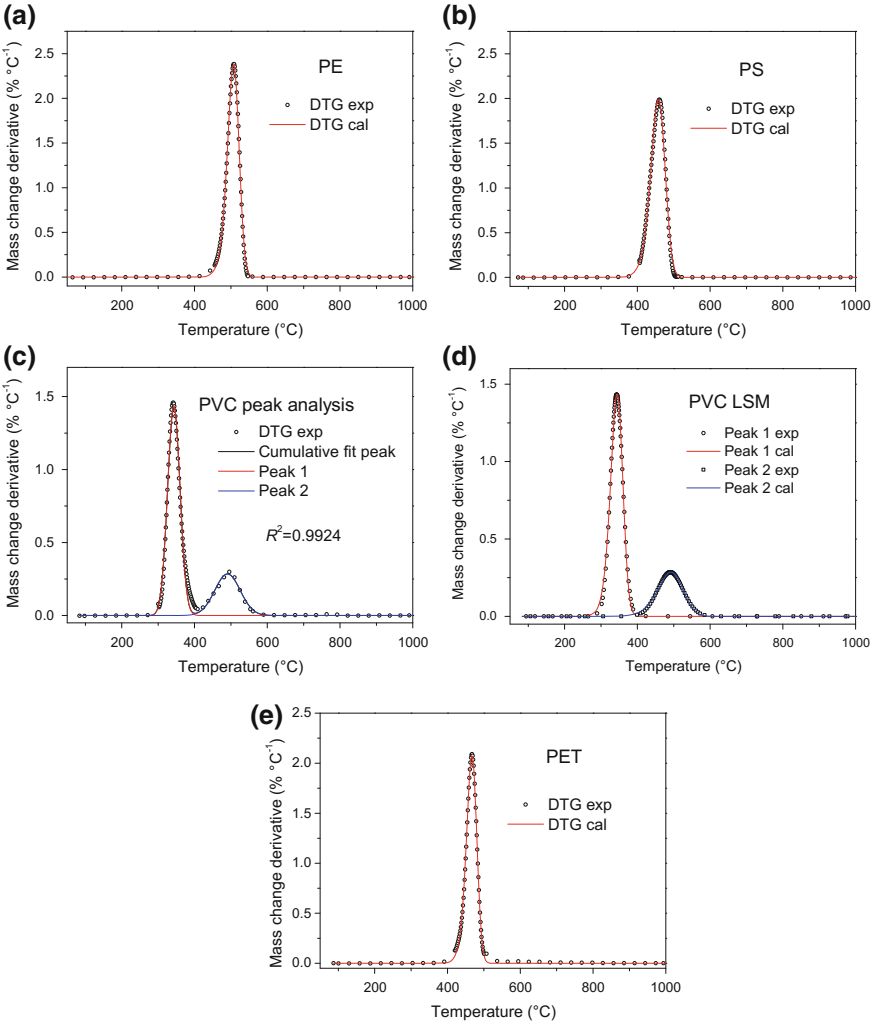

Fig. 3.6 Kinetic calculation of slow pyrolysis of plastic basic components in Macro-TGA

3.1.3 Kinetics of Fast Pyrolysis in Macro-TGA

3.1.3.1 TG and DTG Characteristics

The TG and DTG curves of fast pyrolysis of basic components in Macro-TGA are shown in Fig. 3.7. Hemicellulose pyrolysis ended very fast (∼50 s); cellulose pyrolysis ended at 75 s; while lignin pyrolysis was a slow process (>300 s). As shown in Fig. 3.7c, the pyrolysis of pectin and starch also ended very early. As

Table 3.2 Kinetic parameters of slow pyrolysis of basic components in Macro-TGA

Sample	Reaction	Percentage (%)	Peak temperature (°C)	E (kJ mol^{-1})	A (min^{-1})	n	ADI
Hemicellulose	1	76.1	301.5	350	8.34×10^{31}	1.57	1.65
	2	23.9	427.3	50	5.89×10^{2}	1.22	0.93
Cellulose	1	100.0	385.1	291	8.57×10^{22}	1.53	1.64
Lignin	1	46.3	373.0	113	4.16×10^{8}	1.41	1.46
	2	41.5	456.6	18	8.76×10^{-1}	0.94	0.78
	3	12.2	807.3	588	1.42×10^{28}	1.55	1.78
Pectin	1	100.0	291.7	2249	8.37×10^{208}	1.66	1.91
Starch	1	100.0	351.8	330	3.29×10^{27}	1.56	1.79
PE	1	100.0	506.3	404	8.19×10^{26}	1.56	1.81
PS	1	100.0	456.6	283	988×10^{19}	1.53	1.76
PVC	1	71.1	343.1	236	7.16×10^{19}	1.53	1.76
	2	28.9	490.6	169	1.21×10^{11}	1.45	1.67
PET	1	100.0	466.2	413	1.26×10^{29}	1.56	1.82

shown in Fig. 3.7b, the DTG peak values of hemicellulose, cellulose, and starch were very high.

To evaluate fast pyrolysis quantitatively, some indexes were introduced (Zheng et al. 2009), as shown in Table 3.3. τ_{end} denotes pyrolytic end time (α = 95%); $(d\alpha/d\tau)_{max}$ denotes the maximum mass loss rate; τ_{max} denotes the maximum mass loss time; F denotes pyrolytic factor:

$$F = \frac{(d\alpha/d\tau)_{max}}{\tau_{end} \times \tau_{max}} \tag{3.1}$$

Pyrolytic factor F was determined by the maximum mass loss rate, the maximum mass loss time, and end time, which represented the difficulty of pyrolysis. Larger F meant pyrolytic reaction was more easy to happen (Zheng et al. 2009).

Hemicellulose pyrolysis ended very early (48.3 s); lignin pyrolysis lasted longer time (208.4 s); while starch pyrolysis was the fastest (24.6 s). The maximum mass loss rate of starch was the largest, while the maximum loss rate of lignin was the smallest. The maximum mass loss of starch occurred very early (14.2 s), while that of cellulose occurred the latest (39.9 s). The pyrolytic factor, which represented the difficulty of pyrolysis, from high to low followed the order of starch, pectin, hemicellulose, cellulose, and lignin.

The pyrolytic TG and DTG curves of plastic basic components are shown in Fig. 3.7e and f. The pyrolysis of PE, PS, and PET could be regarded as only one stage, and the maximum mass loss time from early to late followed the order of PET, PS, and PE. PVC pyrolysis was very slow, with two obvious peaks. The pyrolytic indexes are shown in Table 3.3. The order of pyrolytic end time was PET < PS < PE < PVC; the order of the maximum mass loss time was PVC < PET < PS < PE; and the order of pyrolytic factor was PET > PE > PS > PVC.

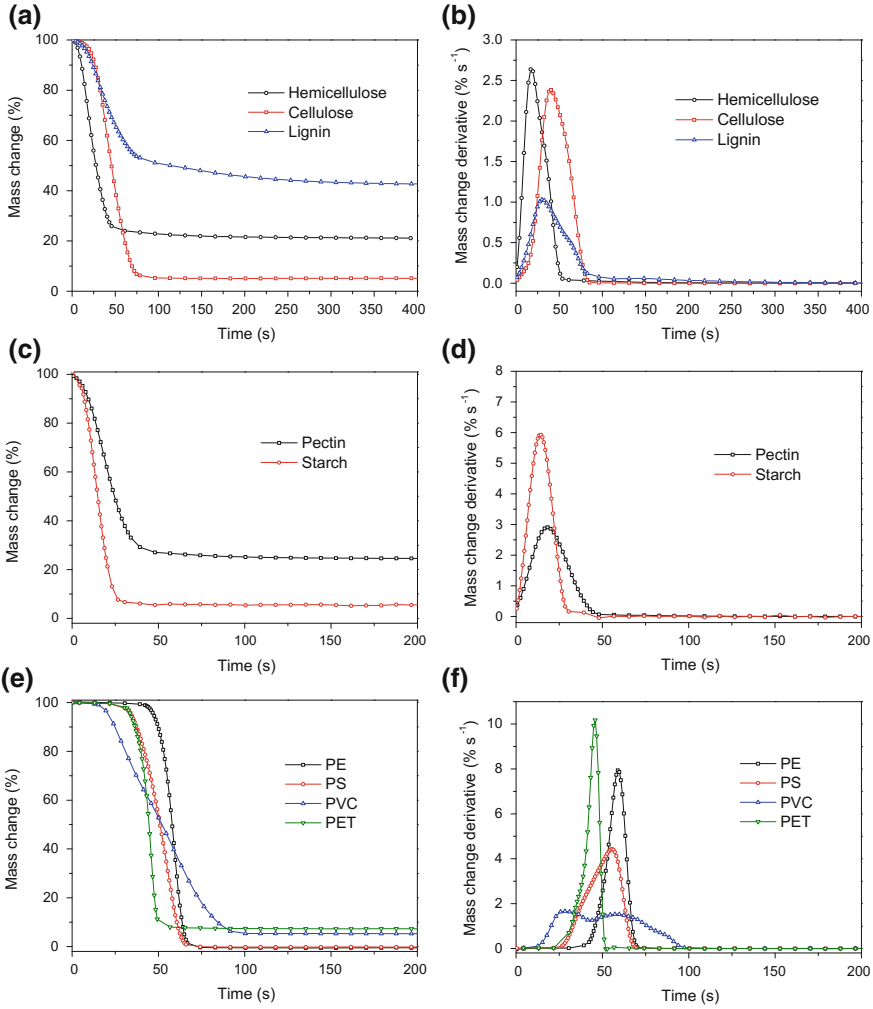

Fig. 3.7 TG and DTG curves of fast pyrolysis of basic components in Macro-TGA

3.1.3.2 Kinetics

The kinetic parameters calculated by PA-LSM are shown in Table 3.4. For biomass basic components, the pyrolysis of hemicellulose, cellulose, and lignin could be regarded as a single peak, as shown in Fig. 3.8a, b, e, and f. The fast pyrolysis of lignin could be regarded as two peaks, as shown in Fig. 3.8c and d. The high R^2 values in Table 3.4 showed that the calculated values of kinetic parameters agreed well with the experimental values.

Table 3.3 Indexes of fast pyrolysis of basic components

Sample	τ_{end} (s)	$(d\alpha/d\tau)_{max}$ (% s^{-1})	τ_{max} (s)	F (% s^{-3})
Hemicellulose	48.3	2.7	17.9	3.1×10^{-3}
Cellulose	69.5	2.4	39.9	8.6×10^{-4}
Lignin	208.4	1.0	30.7	1.6×10^{-4}
Pectin	40.6	2.9	18.3	3.9×10^{-3}
Starch	24.6	5.9	14.2	1.7×10^{-2}
PE	65.3	8.0	59.2	2.1×10^{-3}
PS	62.8	4.4	55.7	1.3×10^{-3}
PVC	84.4	1.7	27.3	7.2×10^{-4}
PET	49.3	10.2	45.7	4.5×10^{-3}

Table 3.4 Kinetic parameters of fast pyrolysis of basic kinetics in Macro-TGA

Sample	Reaction	Percentage (%)	k	n	R^2
Hemicellulose	1	100.0	1.19×10^{-3}	2.03	0.9995
Cellulose	1	100.0	2.21×10^{-6}	3.32	0.9994
Lignin	1	59.9	1.25×10^{-4}	2.57	0.9996
	2	40.1	2.84×10^{-6}	3.12	0.9970
Pectin	1	100.0	1.56×10^{-3}	2.04	0.9990
Starch	1	100.0	5.74×10^{-4}	2.67	0.9997
PE	1	100.0	7.06×10^{-23}	12.47	0.9999
PS	1	100.0	1.22×10^{-12}	6.88	0.9967
PVC	1	27.8	2.55×10^{-6}	3.73	0.9996
	2	72.2	2.43×10^{-7}	3.64	0.9997
PET	1	100.0	1.57×10^{-22}	13.17	0.9967

For plastic basic components, the pyrolysis of PE, PS, and PET could be regarded as a single peak, and the calculated results are shown in Table 3.4 and Fig. 3.9. PVC pyrolysis could be regarded as the superposition of two paralleled reactions, as shown in Fig. 3.9c, d.

3.1.4 Comparison of Kinetics at Different Conditions

3.1.4.1 Comparison of Slow Pyrolysis in TGA and Macro-TGA

For slow pyrolysis in TGA and Macro-TGA, the heating rate and atmosphere were the same, while the reactor scale was different, so the pyrolytic kinetics were different. As shown in Figs. 3.1 and 3.4, the pyrolysis start temperature in Macro-TGA was higher than that in TGA. TGA was regarded as the reactor where heat and mass transfer could be neglected, while the heat and mass transfer in

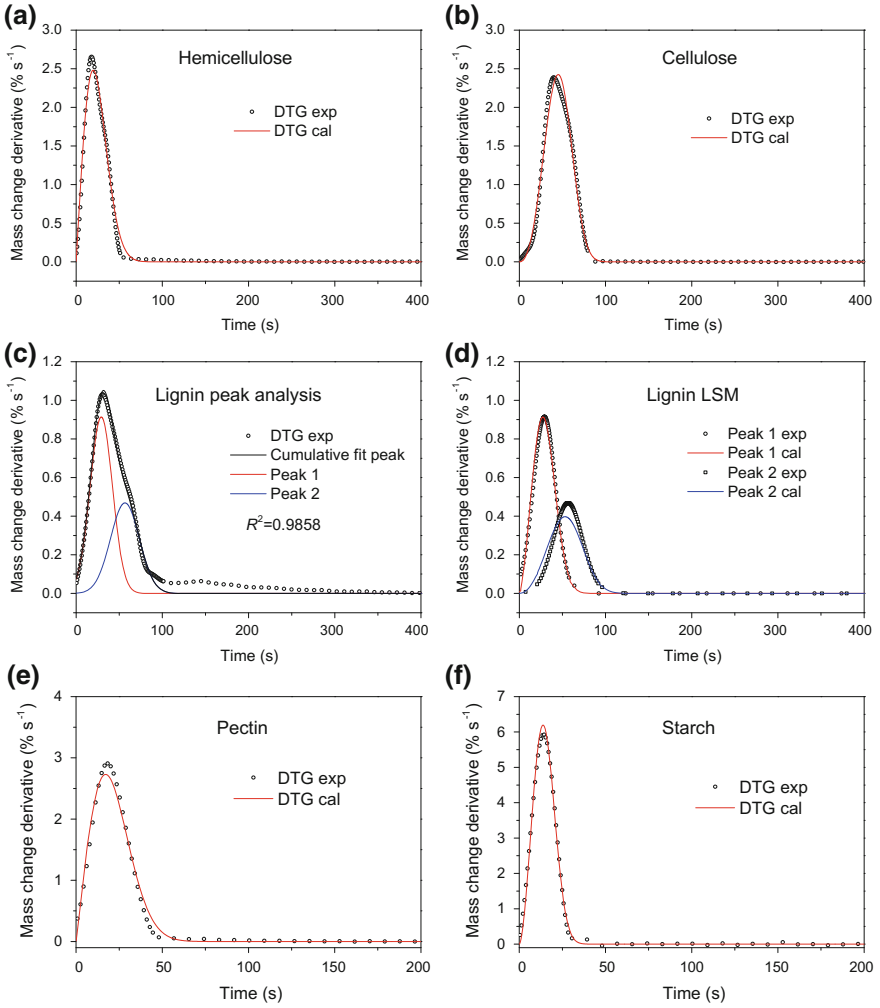

Fig. 3.8 Kinetic calculation of fast pyrolysis of biomass basic components in Macro-TGA

Macro-TGA could not be neglected. The pyrolytic residual mass in Macro-TGA was higher than that in TGA. Especially for cellulose, the residual mass in TGA was 8.6%, and the residual mass in Macro-TGA was 17.4%. The possible reason was the sample mass in Macro-TGA was around a hundred times of that in TGA, and thus the heat and mass transfer effects were significant. In the pyrolytic process, the unreacted sample might be covered by inert char.

As shown in Figs. 3.2a and 3.5a, the two peaks of hemicellulose pyrolysis in TGA merged into one peak in Macro-TGA. The pyrolytic curves of pectin in TGA

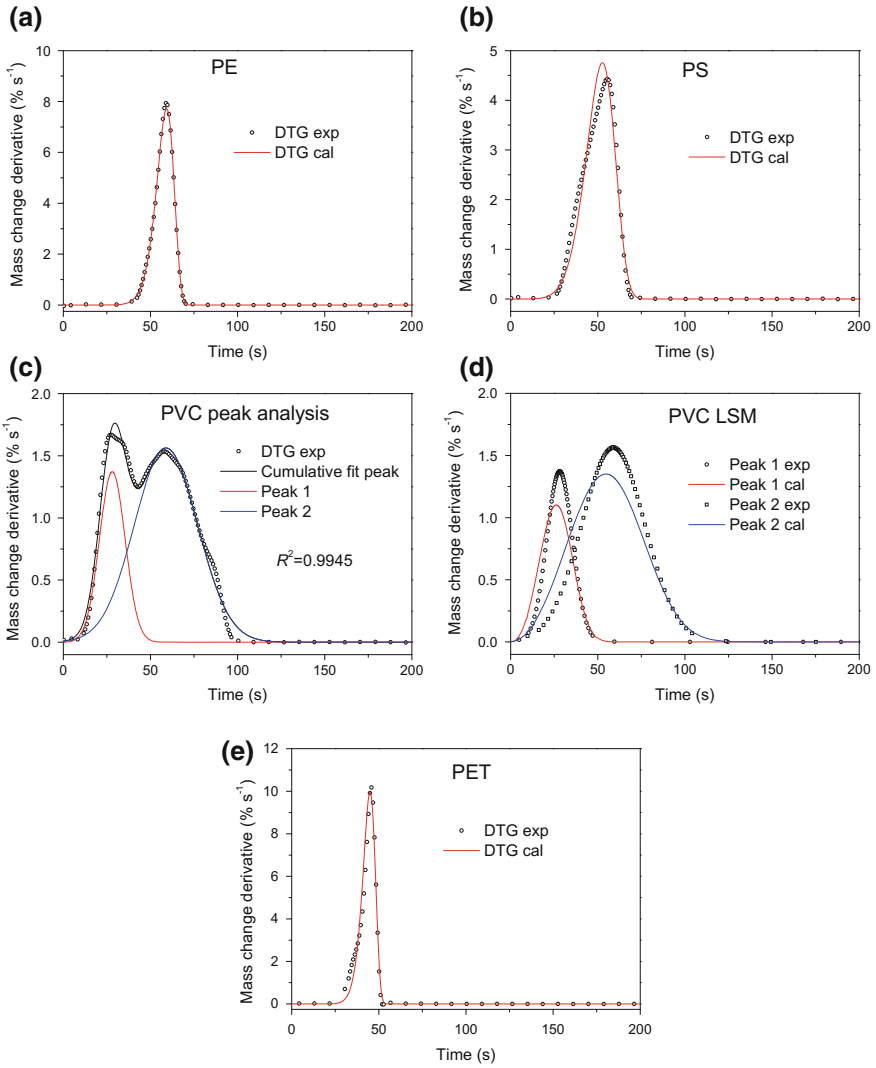

Fig. 3.9 Kinetic calculation of fast pyrolysis of plastic basic components in Macro-TGA

and Macro-TGA were also quite different. For other materials, the curve shape in TGA and Macro-TGA is similar. It should be noted that the DTG peak values of Macro-TGA were much higher than that of TGA, due to the heat transfer effect in Macro-TGA. To investigate this heat transfer process, the values of peaks were compared, as shown in Fig. 3.10.

This relationship could be expressed by $t_{\mathrm{M-TGA}} = t_{\mathrm{TGA}} + (54.7 - 0.033t_{\mathrm{TGA}})$. In this equation, $t_{\mathrm{M-TGA}}$ denotes the peak temperature in Macro-TGA, and t_{TGA}

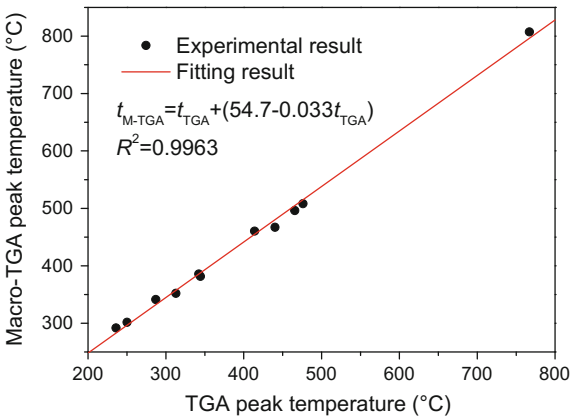

Fig. 3.10 DTG peak temperature comparison of slow pyrolysis in TGA and Macro-TGA

denotes peak temperature in TGA. With the increase in temperature, heat transfer effect was stronger, and thus, the temperature difference was smaller.

3.1.4.2 Comparison of Slow Pyrolysis and Fast Pyrolysis in Macro-TGA

The residual mass of fast pyrolysis was lower than that of slow pyrolysis, especially for cellulose. The study of Wu et al. (2014) has also shown that the residual mass decreased from 25.45 to 21.21% when the heating rate increased from 5 to 40 °C min^{-1}. There might be two reasons: on one hand, during slow pyrolysis, the internal part of sample was heated slowly, which meant the internal part might remain unreacted when the reactions happened on the surface; on the other hand, during the fast pyrolysis process, the high heating rate and drastic reaction had strong disturbance on sample and a large amount of soot was generated. Therefore, the residual mass of fast pyrolysis was lower than that of slow pyrolysis.

The multiple peaks in slow pyrolysis could not be distinguished in fast pyrolysis. The research of Shen et al. (2010) in TGA has also shown that at high heating rates, the two peaks of hemicellulose pyrolysis merged. The reaction orders of fast pyrolysis were usually higher than 2, while the reaction orders of slow pyrolysis were usually lower than 2.

Based on the slow and fast pyrolysis reactions of nine basic components in TGA and Macro-TGA, the kinetic characteristics at different conditions were obtained. The kinetic parameters were calculated from PA-LSM and paralleled-reaction model. Kinetics were basic characteristics of thermochemical reactions, which were the foundation of the following sections.

3.2 Gas, Liquid, and Solid Distribution

The gas, liquid, and solid distribution of basic component pyrolysis were investigated in horizontal fixed bed reactor shown in Fig. 2.19. Meanwhile, the gas products and PAHs formation were investigated. Dry basis samples were used.

The products' (gas, liquid, and solid) mass distribution of basic component pyrolysis is shown in Table 3.5. The products distribution was calculated from the corresponding product (gas, liquid, and solid) divided by the pyrolysis sample mass ($\sim$1 g). The mass balance was calculated from the product mass after reaction divided by the sample mass before reaction. As shown in Table 3.5, the mass balance values were 88.9–102.5%, which could ensure the accuracy of the experiments.

As shown in Table 3.5, for biomass basic components, cellulose and starch produced the most gas amount, while the residual solid amount was low, which was consistent with their proximate analyses and other studies (Liu et al. 2011; Luo et al. 2004). Shen and Gu (2009) reported that when cellulose was pyrolyzed at 730 °C, the char amount was 1.03%. Lignin pyrolysis produced the least gas amount (35.3%); hemicellulose pyrolysis produced the most liquid amount (43.2%); and lignin pyrolysis produced the least liquid amount (22.8%). In addition, the pyrolysis of lignin had the most solid residue (41.3%), which was related to the high amount of fixed carbon and ash in lignin, as shown in Table 2.4. The high amount of volatiles of cellulose pyrolysis and the low amount of volatiles of lignin pyrolysis were consistent with the results of TGA (Fig. 3.1). It should be noted that the pyrolytic product distribution of cellulose and starch was similar, maybe because they were all composed of glucose monomers (Dumitriu, 2004; Shafizadeh and Fu (1973).

For plastic basic components, PVC, PET, and PE produced the most gas, while PS produced the least gas. Accordingly, PS pyrolysis produced the most liquid (84.3%), which was consistent with the result of Scott et al. (1990). PVC pyrolysis generated 46.0% HCl, which was lower than the chlorine amount in PVC (56.96%). Therefore, a portion of chlorine went into liquid or solid. Masuda et al. (2006) have reported similar results. Iida et al. (1974) studied the pyrolysis of PVC at 700 °C in pyrolysis-gas chromatography (Py–GC) and detected various kinds of chlorobenzene in tar.

According to the pyrolytic experiments of nine basic components in horizontal fixed bed reactor, the product distribution of different basic components was

Table 3.5 Product distribution of basic component pyrolysis. Reprinted from Zhou et al. 2015, Copyright 2015, with permission from Elsevier

Sample	Hemicellulose	Cellulose	Lignin	Pectin	Starch	PE	PS	PVC	PET
Gas (wt%)	45.0	69.5	35.3	44.3	62.2	46.3	5.7	53.1	47.2
Liquid (wt%)	43.2	26.3	22.8	32.3	30.8	42.6	84.3	32.2	38.2
Solid (wt%)	8.6	0.0	41.3	25.3	7.7	0.0	2.3	17.2	4.5
Mass balance (wt%)	96.9	95.7	99.5	101.9	100.7	88.9	92.3	102.5	89.9

compared. The mass balance also verified the accuracy of the experiments. The following Sect. 3.3 and 3.4 was the extension of this section, which analyzed the composition of gas and liquid.

3.3 Gas Production

3.3.1 Gas Production in TGA-FTIR

According to Lambert–Beer Law, gas infrared absorbance at specific wavenumber is linearly dependent on gas concentration. Therefore, in TGA-FTIR, the absorbance change detected by FTIR could reflect the gas formation trend (Chen et al. 2014; Liu et al. 2008). In the FTIR spectrum of biomass basic component pyrolysis, 2384, 2180, 2969, 3018, 1747, and 1182 cm^{-1} could be regarded as the characteristic peaks of CO_2, CO, alkanes, alkenes, carbonyls, and carboxyls, respectively, as shown in Table 3.6. The spectrum of steam was wide and complex, and easily affected by other gases, so it was difficult to find a characteristic peak.

The gas products at DTG peak temperatures of hemicellulose pyrolysis are shown in Fig. 3.11a, b. The gas spectrums at 244.9 and 296.1 °C were similar, which meant the pyrolytic mechanisms of these two points were similar. The gas products included CO_2, H_2O, alkanes, aldehyde ketones, and carboxylic acids. The gas production with temperature is shown in Fig. 3.11c. The peaks of gas generation were consistent with the peak of DTG curve.

As shown in Fig. 3.12a, cellulose produced CO_2, CO, H_2O, alkanes, carbonyls, and carboxyls at 344.2 °C. As shown in Table 2.5, the structure of cellulose contains many hydroxyls and ether bonds, which are the source of carboxyls, CO_2, and CO in Fig. 3.12 (Hansson et al. 2004; Shafizadeh and Fu 1973). All the gases reached the maximum at 344.2 °C, which was consistent with the DTG curve, as shown in Fig. 3.12b.

The pyrolysis of lignin had two processes: the first process was from 100 to 600 °C; the second process was from 700 to 800 °C. As shown in Fig. 3.13a, the gases at 337.9 °C were CO_2, H_2O, CO, and alkanes. CO_2 and CO were mainly from the –OH and –O– in lignin structure (Belgacem and Gandini 2008), and alkanes were mainly from the methyls in lignin structure. The second stage at 767.9 °C was quite different from the first stage. The second stage produced not only CO_2 and H_2O, but also a large amount of CO. Alkanes did not occur at the second stage, which meant the demethylation was finished. The production of different gases was shown in Fig. 3.13c. The carbonyls and carboxyls in pyrolysis of hemicellulose and cellulose did not present in lignin pyrolysis.

As shown in previous Fig. 3.1c, pectin pyrolysis was simple, with only one peak at 236.5 °C. FTIR showed that the main gases at this peak were CO_2, H_2O, alkanes, carbonyls, and carboxyls. As shown in Fig. 3.14b, the production of different gases was similar. Alkanes had two peaks: the first peak was at 236.5 °C, and the second peak was at 400–500 °C. The generation of CO_2 might come from the cracking of –OH, while alkanes, especially methane, came from $–CH_2–$ (Liu et al. 2008).

Table 3.6 Gas characteristic peaks in FTIR

Gas	CO_2	CO	Small molecular alkanes	Small molecular alkenes	Carbonyls	Carboxyls	C_9–C_{14} aliphatics	Styrene	HCl	Benzene
Characteristic peak (cm^{-1})	2384	2180	2969	3018	1747	1182	2933	695	2727	3085

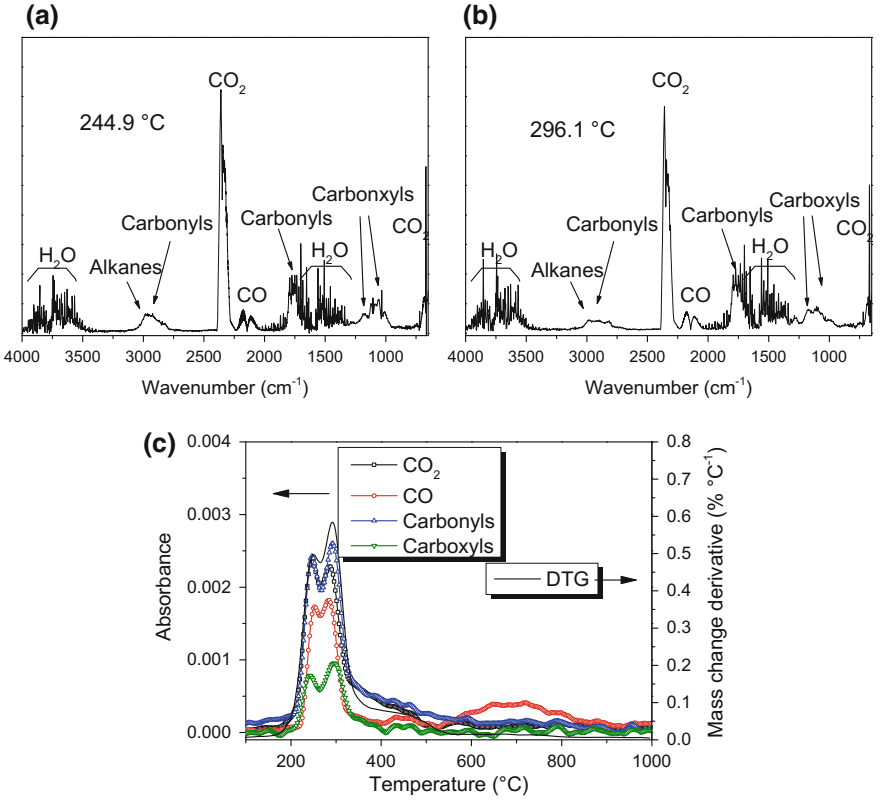

Fig. 3.11 FTIR spectrum of gases from hemicellulose pyrolysis

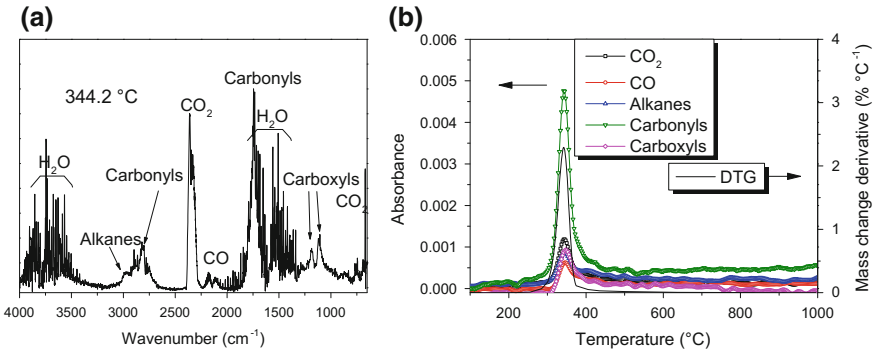

Fig. 3.12 FTIR spectrum of gases from cellulose pyrolysis

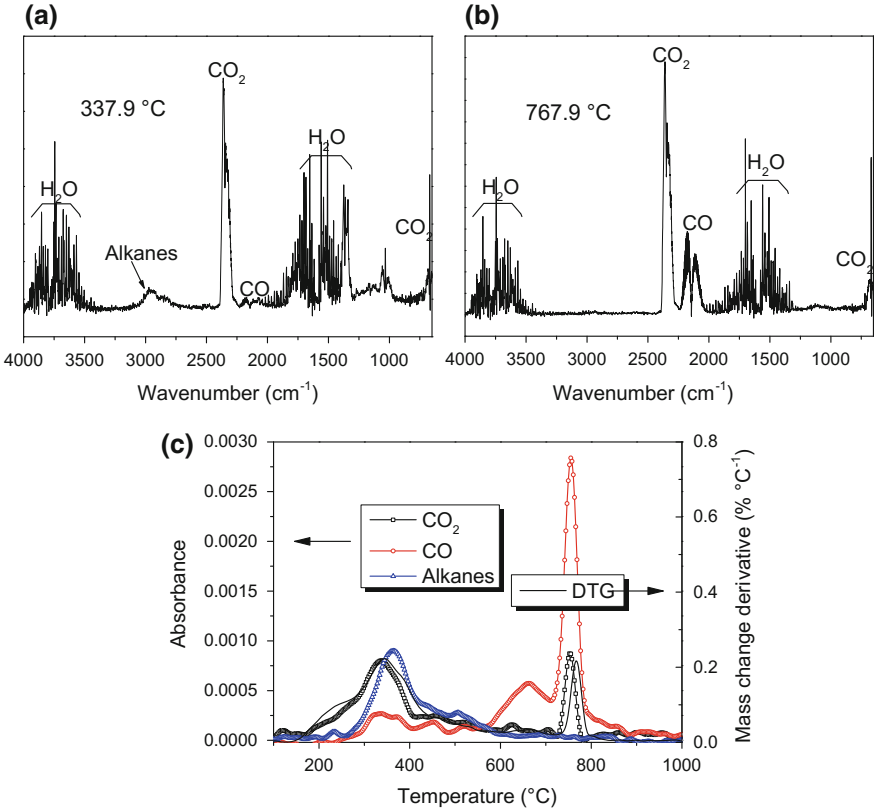

Fig. 3.13 FTIR spectrum of gases from lignin pyrolysis

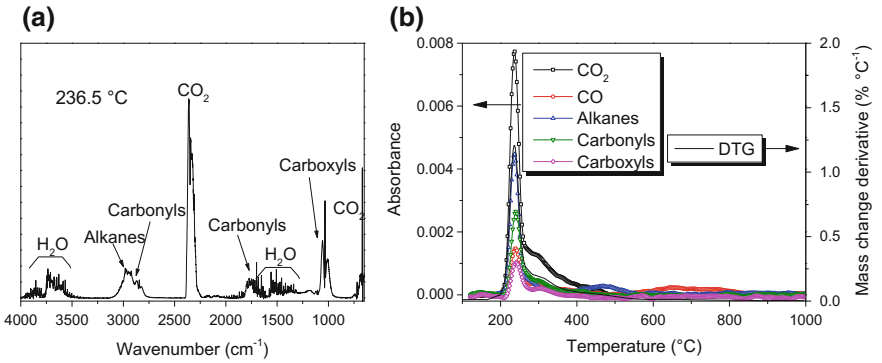

Fig. 3.14 FTIR spectrum of gases from pectin pyrolysis

The gases at DTG peak temperature (312.8 °C) of starch pyrolysis included CO_2, CO, H_2O, carbonyls, and carboxyls. As shown in Fig. 3.15b, CO_2 and carbonyls reached the maximum at this temperature. The monomer of starch was glucopyranose (Dumitriu 2004), with the functional groups –OH, $–CH_2$, –C–OH, $–CH_2OH$, –CHOH, and –O–, as shown in Table 2.5. At low temperatures, the generation of CO came from the breakage of ether bonds (Ferdous et al. 2002; Greenwood et al. 2002). Alkanes, mainly methane, were derived from the cracking of methylene (Liu et al. 2008). The detection of carboxyls was similar to other results (Meng et al. 2013; Siengchum et al. 2013). Carboxyls and CO_2 might be derived from the cracking of –OH. Actually, ethanol could decompose to CO_2 at temperatures higher than 440 °C: $CH_3COOH \rightarrow CO_2 + CH_4$ (Ferry, 1992).

The pyrolysis of PE was simple, with only one DTG peak at 474.0 °C. The gases at this temperature were mainly C_9–C_{14} alkanes and alkenes. Since the FTIR characteristic peaks of these compounds were close, it was difficult to distinguish in detail. As shown in Fig. 3.16, the generation of these aliphatics was consistent with the DTG curve.

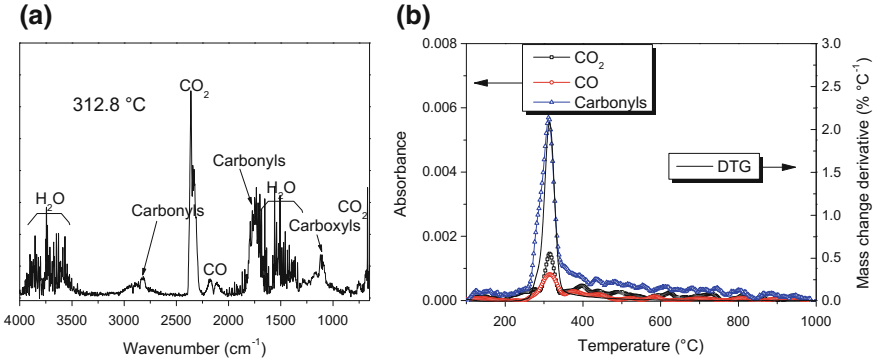

Fig. 3.15 FTIR spectrum of gases from starch pyrolysis

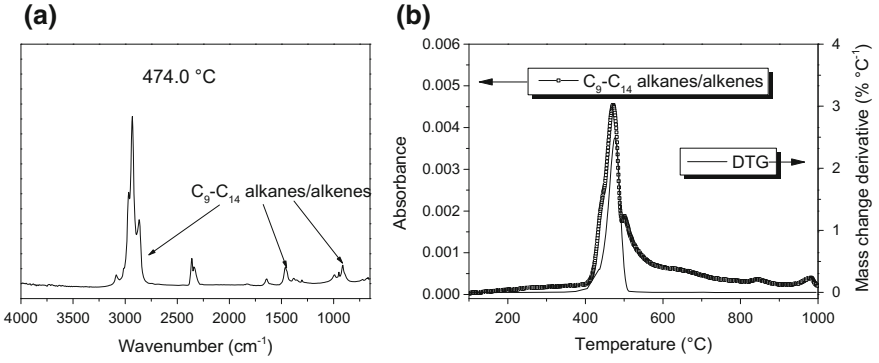

Fig. 3.16 FTIR spectrum of gases from PE pyrolysis

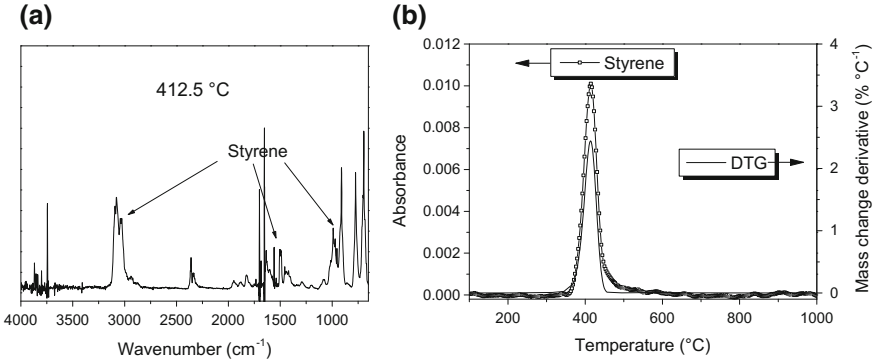

Fig. 3.17 FTIR spectrum of gases from PS pyrolysis

The pyrolysis of PS was similar to that of PE, with a peak at 412.5 °C. The gas product at this point was mainly styrene. As shown in Fig. 3.17b, the generation of styrene was consistent with the DTG curve.

PVC pyrolysis could be divided into two stages. The first stage had mass loss around 56%, with the peak at 286.5 °C. As shown in Fig. 3.18a, the gases at this point were HCl and benzene, which was consistent with other results (Iida et al. 1974; Zhu et al. 2008). This stage was the dechlorination process of PVC. The second peak was at 461.3 °C, with the generation of alkanes and alkenes from the secondary decomposition after chlorination. The generation process of gases was shown in Fig. 3.18c. It has been reported that high temperature would promote the generation of aliphatics (Iida et al. 1974). The first step of PVC pyrolysis was polymer dechlorination reaction, with the generation of HCl and double bonds. The second step was the secondary decomposition of dechlorinated residue with the generation of small molecular hydrocarbons including aliphatics and aromatics (Zhu et al. 2008; Kim 2001).

PET pyrolysis generated various kinds of gases, as shown in Fig. 3.19a. At 437.7 °C, the main gases included CO_2, CO, H_2O, alkanes, carbonyls, and carboxyls. The generation processes of CO_2, CO, and carbonyls are shown in Fig. 3.19b. It should be noted that CO_2 had another peak at 600 °C besides the peak at 437.7 °C.

3.3.2 *Gas Production in Horizontal Fixed Bed Reactor Fast Pyrolysis*

The gases from pyrolysis in HFBR were measured by GC. As shown in Fig. 3.20, every gram biomass basic components produced approximately 100 ml H_2, more than that from plastic basic components. Cellulose and starch produced the most CO ($\sim$300 ml g^{-1}). The high CO production from cellulose pyrolysis was

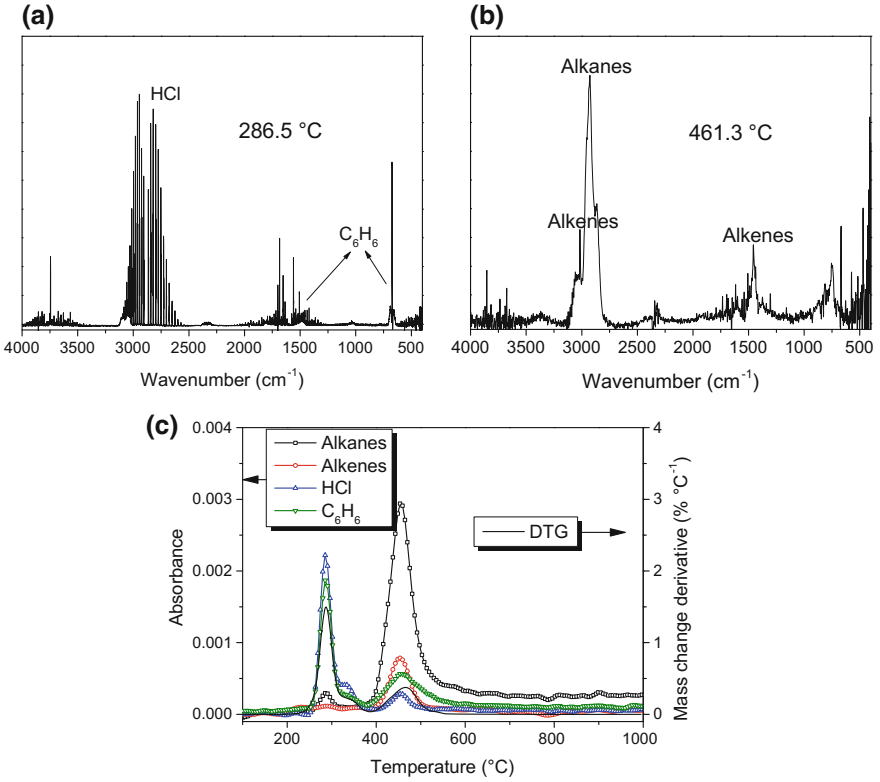

Fig. 3.18 FTIR spectrum of gases from PVC pyrolysis

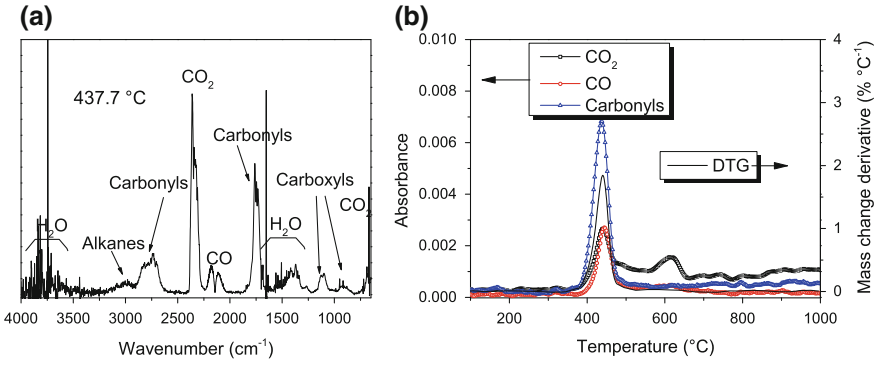

Fig. 3.19 FTIR spectrum of gases from PET pyrolysis

consistent with the report of others (Banyasz et al. 2001). CO was produced from C–O–C functional groups (Ferdous et al. 2002), which were abundant in the structure of cellulose and starch. PET produced the most CO_2, maybe due to the –

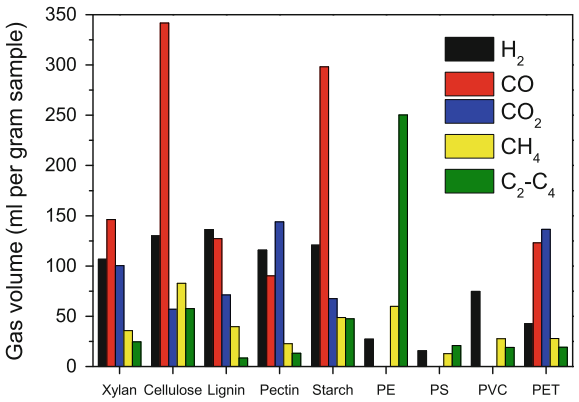

Fig. 3.20 Gas generation characteristics of basic component pyrolysis

COO– groups. For the components except for lignin and PE, the generation characteristics of CH_4 and C_2–C_4 were similar. Lignin produced a large amount of CH_4, due to the $–CH_3$ structure; PE produced a large amount of C_2–C_4.

3.4 PAHs Formation

The PAHs in the tar were measured by GC/MS. As shown in Fig. 3.21, plastic basic components, especially PS and PVC, generated more PAHs. PS generated the most naphthalene, fluorene, phenanthrene, anthracene, and pyrene, while PVC generated the most 1-methylnaphthalene, 2-methylnaphthalene, acenaphthylene, acenaphthene, fluoranthene, and benzo[*a*]anthrathene + chrysene.

The pyrolyzed tar of PE contained naphthalene, 1-methylnaphthalene, acenaphthylene, acenaphthene, fluorene, and phenanthrene. These PAHs were also identified by Williams and Williams (1999) in PE pyrolysis in fluidized bed reactor at 700 °C.

In biomass basic components, lignin generated all kinds of PAHs except fluoranthene. Another important biomass basic component, cellulose generated a small amount of naphthalene, acenaphthylene, fluorene, phenanthrene, and anthracene, which was consistent with the results of Stefanidis et al. (2014). Pectin pyrolysis generated naphthalene, methylnaphthalenes, acenaphthylene, phenanthrene, pyrene, benzo[*a*]anthracene, and chrysene. Compared to the pectin pyrolysis at 600–800 °C by McGrath et al. (2001), this study obtained more naphthalene, acenaphthylene, fluorene, phenanthrene, and pyrene, while anthracene and fluoranthene were not detected. Hemicellulose pyrolysis generated naphthalene, methylnaphthalene, acenaphthylene, acenaphthene, fluorene, phenanthrene, anthracene, and pyrene, while fluoranthene, benzo[*a*]anthracene, and chrysene were not detected. However, the study of Yu et al. (2014) has detected fluoranthene and benzo[*a*]anthracene during

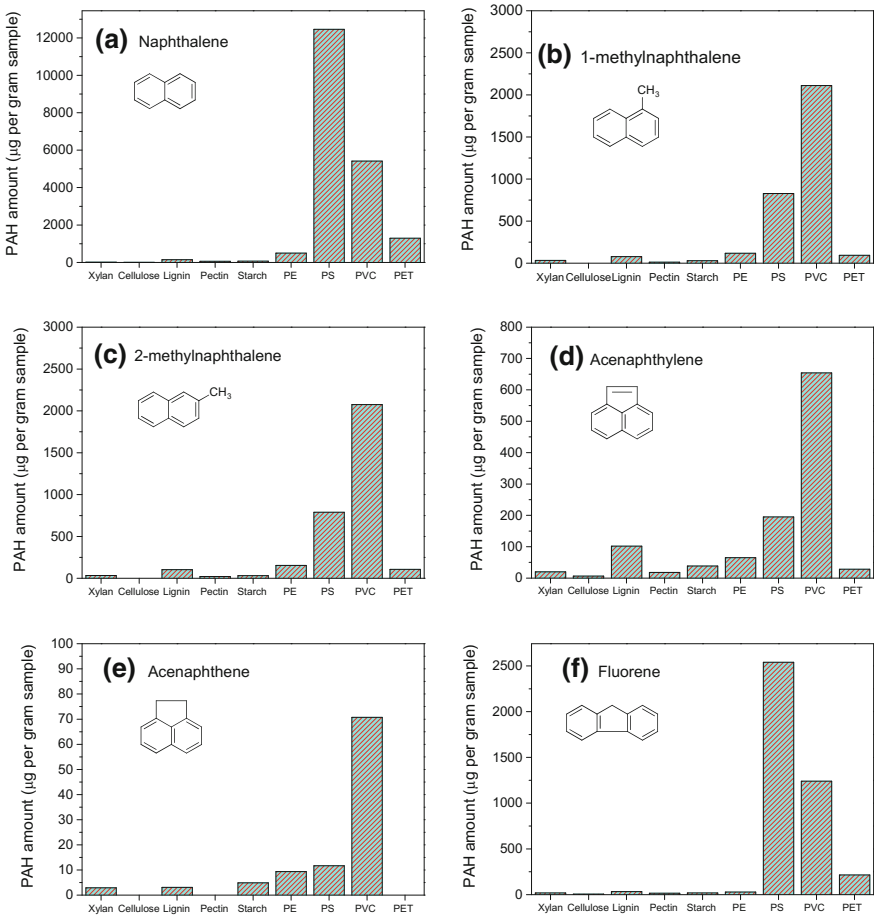

Fig. 3.21 PAHs generation from pyrolysis processes of basic components. Reprinted from Zhou et al. (2015), Copyright 2015, with permission from Elsevier

hemicellulose gasification in entrained flow gasifier when air stoichiometric ratio was 0.2.

The total amount of PAHs is shown in Fig. 3.21l. PS generated the most PAHs, followed by PVC, PET, PE, and lignin. Overall, plastics generated much more PAHs than biomass.

Naphthalene is the simplest PAH, which was also the most abundant PAH in tar. The high concentration of naphthalene in PVC pyrolysis was also reported by other researchers (Iida et al. 1974). The amount of two naphthalene derivatives was also very high. Phenanthrene and fluorene were the most abundant 3-ring PAHs, while the amount of acenaphthene was very low. Three kinds of 4-ring PAHs, pyrene, benzo[*a*]anthracene, and chrysene were very abundant in the pyrolysis tar of PS, PVC, and PET.

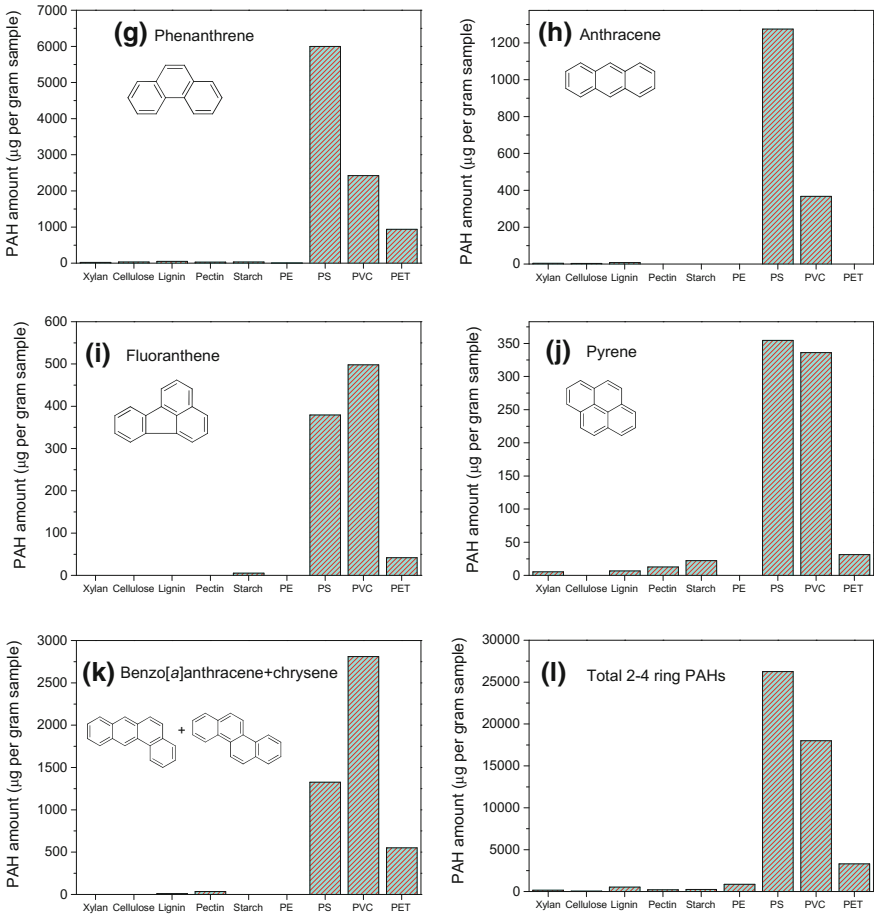

Fig. 3.21 (continued)

The percentage of PAHs with different number of rings is shown in Fig. 3.22. The total mass amount of 2-, 3-, and 4-ring PAHs was regarded as 100%, and then, the percentage of PAHs with certain number of rings was calculated. As shown in Fig. 3.22, the percentage of 2-ring PAHs was the highest. Especially for PE, the percentage of 2-ring PAHs was as high as 90 wt%. Cellulose pyrolysis generated the most 3-ring PAHs (>80 wt%). 4-ring PAHs could be hardly detected in the pyrolysis of cellulose and PE.

This section obtained the PAHs generation characteristics of pyrolysis of nine basic components in horizontal fixed bed reactor and compared the relative percentage of PAHs with different number of rings. The research in this section was not only important to control PAHs as pollutants, but also helpful to further understand the pyrolysis mechanisms of basic components.

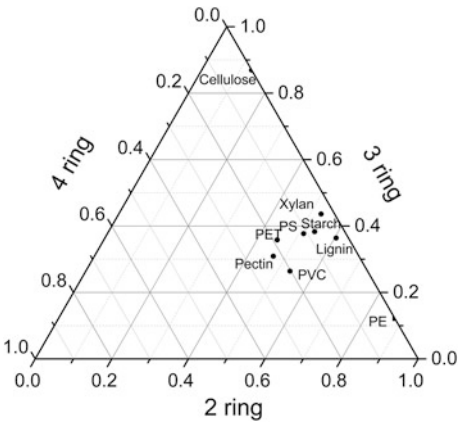

Fig. 3.22 Percentages of PAHs with different number of rings. Reprinted from Zhou et al. (2015), Copyright 2015, with permission from Elsevier

3.5 The Pyrolysis and PAHs Generation Mechanisms of Basic Components

The pyrolysis mechanisms of lignin and PVC will be further investigated in next chapter. In this section, we will focus on the pyrolysis mechanisms of other basic components.

PAHs formation has various mechanisms, and wherein hydrogen abstraction acetylene addition (HACA) is widely acknowledged (Shukla and Koshi 2012). As shown in Eq. (3.2), naphthalene could be generated from benzene through intermediate phenylacetylene, which was abundant in the tar.

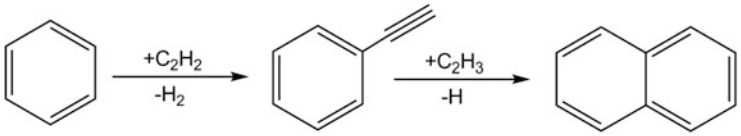

(3.2)

Therefore, single ring compounds (such as benzene and styrene) could be regarded as PAHs precursors. For components with aromatic rings, such as PS, PET, and lignin, PAHs might be formed from aromatic rings through HACA mechanisms (Mastral and Callén 2000; Shukla and Koshi 2012). In these three materials, PS had the highest mass fraction of the aromatic ring, which might be the reason that PS generated the most PAHs. In addition, styrene was regarded as the intermediate of PS pyrolysis, as shown in the FTIR results in Fig. 3.17. According to the study of Shukla and Koshi (2012), styrene could be converted into phenylacetylene through hydrogen adsorption, and the addition of C_2H_3 to phenylacetylene at the *ortho* position could generate naphthalene, which might be the reason that PS pyrolysis generated the most PAHs, as shown in Eq. (3.3).

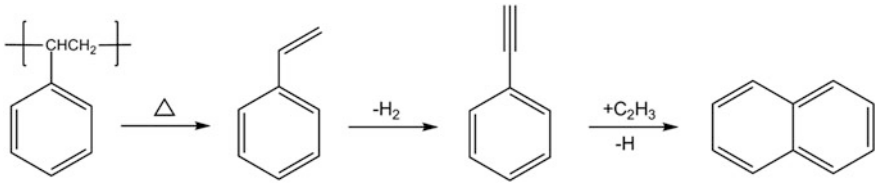

(3.3)

PE might generate PAHs from intermediates alkenes and alkadiene through secondary reaction Diels–Alder Reaction (Cypres 1987; Williams and Williams 1999; Depeyre et al. 1985; Fairburn et al. 1990). In addition, styrene and phenylacetylene might be generated from aliphatics through Eqs. (3.4) and (3.5) (Shukla and Koshi 2012).

$$C_4H_5 + C_4H_4 \rightarrow C_8H_8 + H \tag{3.4}$$

$$C_4H_5 + C_4H_2 \rightarrow C_8H_6 + H \tag{3.5}$$

At high temperature and long residence time, polysaccharides (hemicellulose, cellulose, pectin, and starch) could generate PAHs through two mechanisms: Diels–Alder Reaction and deoxygenation of oxygenated aromatics (Williams and Horne 1995). Since the concentrations of alkenes and alkadienes in the gas phase were very low, Diels–Alder Reaction was unlikely to happen. PAHs might be generated from polysaccharides through benzene and cyclopentadiene (CPD) as intermediates (Stefanidis et al. 2014). In the pyrolyzed tar of these materials, the alkyl substituents of benzene were abundant.

Large molecular PAHs might be generated from small molecular PAHs or single ring aromatics. Naphthalene had different grow routes, which could lead to benzenoid PAHs (Bz-PAHs) or cyclopentaring-fused PAHs (Cp-PAHs).

Acenaphthylene could be generated from acetylene addition reaction of naphthalene, and the detection of vinylnaphthalene proved this mechanism (Kim et al. 2010). For all the basic components, the amount of acenaphthylene was higher than that of acenaphthene, which was consistent with the result of ethene high-temperature pyrolysis (Shukla and Koshi 2012). Therefore, acenaphthene might be generated from the electrophilic addition reaction of acenaphthylene, as shown in Fig. 3.23. Research has shown that it was possible to generate larger PAHs from acenaphthylene through HACA mechanism (Shukla and Koshi 2012). Wang and Violi (2006) reported that the 1, 2 double bond was more active than 4, 5 double bond in acenaphthylene, which explained the formation of fluoranthene, as shown in Fig. 3.23.

The Bz-PAHs from the above mechanism accounted for approximately 25%, while the other 75% belonged to Cp-PAHs (Kislov et al. 2013). Richter and Howard (2000) and Marsh and Wornat (2000) also believed the possibility from naphthalene to phenanthrene by HACA mechanisms was low. However, as shown

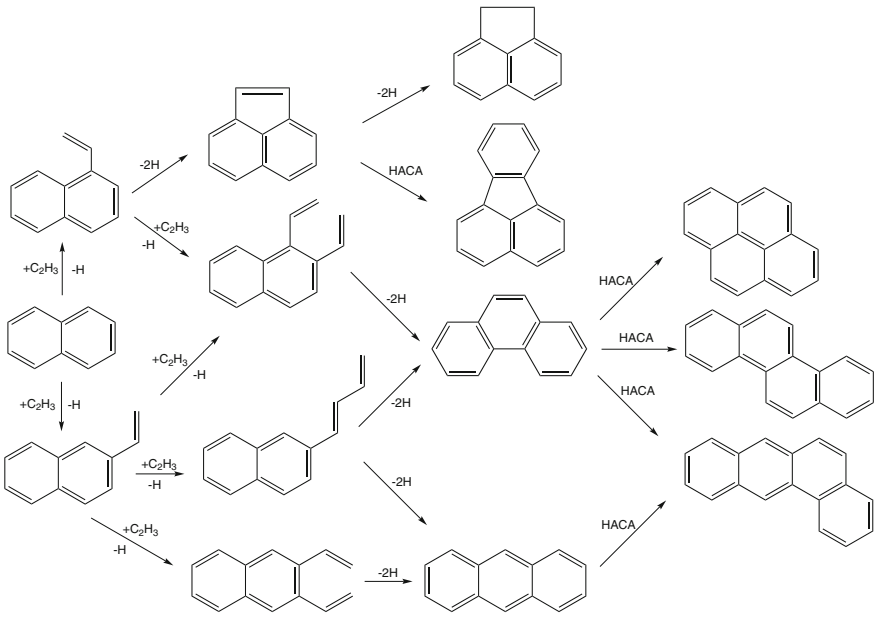

Fig. 3.23 HACA mechanisms from naphthalene. Reprinted from Zhou et al. (2015), Copyright 2015, with permission from Elsevier

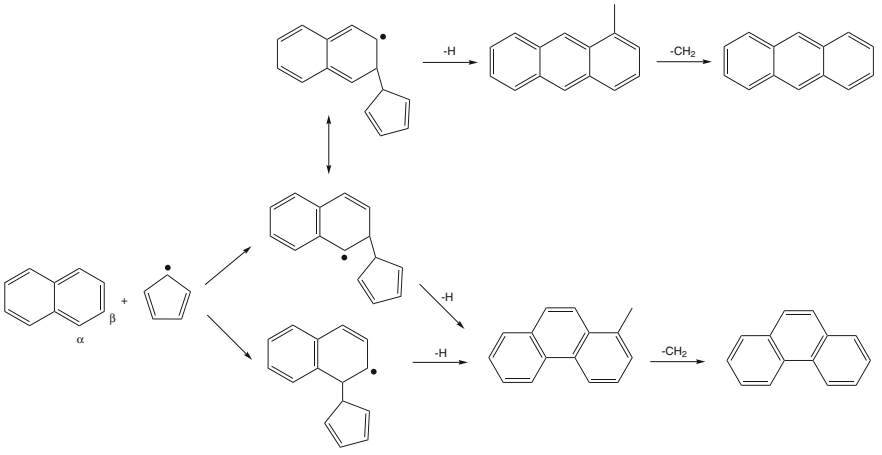

Fig. 3.24 PAHs formation mechanisms from the reaction of naphthalene and CPD. Reprinted from Zhou et al. (2015), Copyright 2015, with permission from Elsevier

in Fig. 3.21g, h, the amounts of phenanthrene and anthracene were considerable. Thus, there might be another mechanism to generate Bz-PAHs. Lu and Mulholland (2004) and Kim et al. (2010) deemed Bz-PAHs might be formed from the interactions of naphthalene/CPD or CPD/indene, as shown in Figs. 3.24 and 3.25. Since

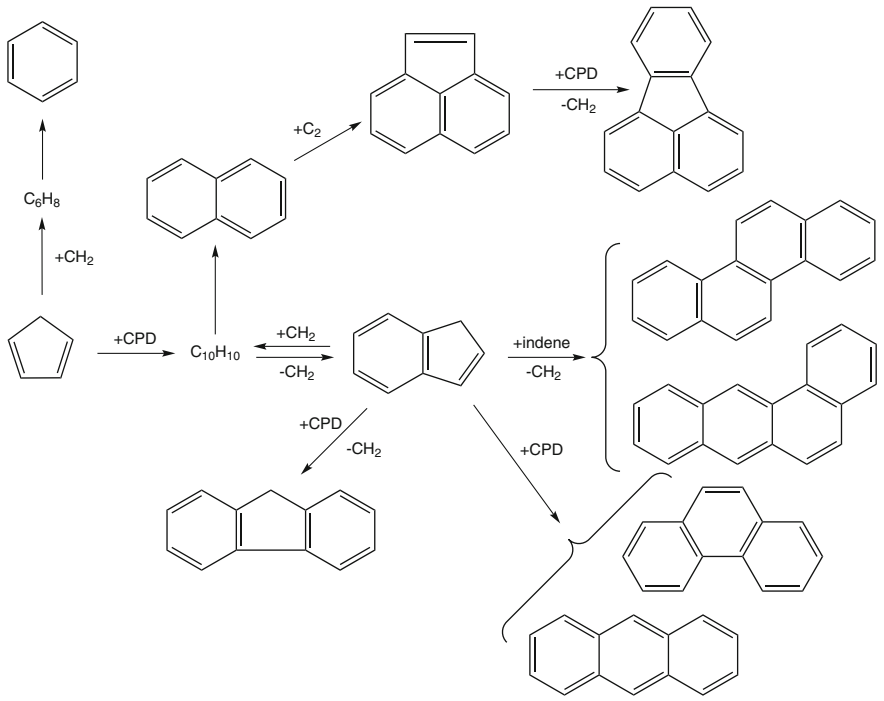

Fig. 3.25 PAHs formation mechanisms from CPD and indene. Reprinted from Zhou et al. (2015), Copyright 2015, with permission from Elsevier

the boiling point of CPD was low, it could not be detected in this study, while a remarkable amount of indene could be detected in the pyrolyzed tar of all the materials except PE.

In the tar from all the components, the amount of phenanthrene was much higher than that of anthracene. The study of Kislov et al. (2013) also found that the concentration of phenanthrene was one order of magnitude higher than that of anthracene. As shown Fig. 3.24, CPD might substitute the α or β position of naphthalene, which could refer to the resonance of intermediates. For α position substituents, there were seven resonance structures, and four of them kept the aromaticity; for β position substituents, there were six resonance structures, and only two of them kept the aromaticity. As shown in Fig. 3.24, α position substitution generated more phenanthrene, while β position substitution generated more anthracene. Therefore, phenanthrene was more likely to be formed than anthracene.

As shown in Fig. 3.22, the PAHs ring number distribution of PE was quite different from those of other components. PE generated a large amount of naphthalene and a certain amount of acenaphthylene and acenaphthene, while the amounts of phenanthrene and anthracene were quite low, which meant HACA process did happen, while the mechanisms shown in Figs. 3.24 and 3.25 did not

happen. During PE pyrolysis, indene was not detected in tar, which proved this conjecture.

For the pyrolysis of all components, the amounts of 1-methylnaphthalene and 2-methylnaphthalene were lower than that of naphthalene. Shukla and Koshi (2012) reported that the low concentration of PAHs with aliphatic chains might be due to the fast consumption of them, which could generate more stable products or soot. The study of Chung and Violi (2011) has shown that aromatics with aliphatic chains presented much faster nucleation rate than those without aliphatic chains, which might be responsible for the lower concentration of methylnaphthalenes than naphthalene.

3.6 Summary

This chapter investigated the kinetics, product distribution, gas production, and PAHs formation characteristics of the pyrolysis of nine basic components in TGA-FTIR, Macro-TGA, and HFBR. Meanwhile, the results from different reactors were compared, and the pyrolysis mechanisms were proposed.

(1) The thermochemical mass loss characteristics of basic components in TGA and Macro-TGA were investigated, wherein the slow pyrolysis and fast pyrolysis were both studied in Macro-TGA. A novel kinetic calculation method PA-LSM was proposed. Complex pyrolysis reactions could be described by a series of paralleled reactions, and each reaction could be expressed by a Gaussian peak. The kinetic parameters were then determined by LSM, and the calculation results agreed quite well with the experimental results. Finally, the kinetic characteristics at different conditions were compared.

(2) The fast pyrolysis of nine basic components was studied at 800 °C and N_2 atmosphere in a horizontal fixed bed reactor. For biomass components, cellulose and starch generated the most gases, and hemicellulose generated the most tar. For plastic components, PE, PVC, and PET generated the most gases, while PS generated the most tar.

(3) The gas products from the slow pyrolysis of basic components were investigated in TGA-FTIR. The detected gases included CO_2, CO, H_2O, alkanes, alkenes, aldehyde ketones, carboxylic acid, HCl, benzene, and styrene. In horizontal fixed bed reactor, the hydrogen production from biomass basic components was approximately 100 ml g^{-1}, higher than that from plastics. Cellulose and starch produced the most CO (around 300 ml g^{-1}); PET produced the most CO_2, and PE generated the most C_2–C_4 hydrocarbons.

(4) In horizontal fixed bed reactor, PS generated the most PAHs, followed by PVC, PET, PE, and lignin. Naphthalene was the most abundant PAH in the tar, and the amounts of naphthalene derivatives were also very high. Phenanthrene and fluorene were the most abundant 3-ring PAHs. 4-ring PAHs

benzo[*a*]anthracene and chrysene were abundant in the tar from the pyrolysis of PS, PVC, and PET.

(5) PAHs could be formed from the aromatic ring in the structure of PS, PET, and lignin, or from Diels–Alder Reaction for PE. For polysaccharides (hemicellulose, cellulose, starch, and pectin), PAHs could be formed through intermediates benzene and CPD. PAHs could grow from HACA mechanisms, or the interactions of naphthalene/CPD or CPD/indene.

Overall, this chapter investigated the pyrolytic characteristics of basic components, which was the foundation of Chaps. 4 and 5.

References

Banyasz JL, Li S, Lyons-Hart J et al (2001) Gas evolution and the mechanism of cellulose pyrolysis. Fuel 80:1757–1763

Belgacem MN, Gandini A (2008) Monomers, polymers and composites from renewable resources. Elsevier Ltd, Oxford

Chen T, Wu J, Zhang J et al (2014) Gasification kinetic analysis of the three pseudocomponents of biomass-cellulose, semicellulose and lignin. Bioresource Technol 153:223–229

Chung S, Violi A (2011) Peri-condensed aromatics with aliphatic chains as key intermediates for the nucleation of aromatic hydrocarbons. P Combust Inst 33:693–700

Cypres R (1987) Aromatic hydrocarbons formation during coal pyrolysis. Fuel Process Technol 15:1–15

Depeyre D, Flicoteaux C, Chardaire C (1985) Pure n-hexadecane thermal steam cracking. Ind Eng Chem Process Design Dev 24:1251–1258

Dumitriu S (2004) Polysaccharides: structural diversity and functional versatility. CRC Press, Boca Raton, Florida

Encinar JM, González JF (2008) Pyrolysis of synthetic polymers and plastic wastes. Kinetic study. Fuel Process Technol 89:678–686

Fairburn JA, Behie LA, Svrcek WY (1990) Ultrapyrolysis of n-hexadecane in a novel micro-reactor. Fuel 69:1537–1545

Ferdous D, Dalai AK, Bej SK et al (2002) Pyrolysis of lignins: experimental and kinetics studies. Energ Fuel 16:1405–1412

Ferry JG (1992) Methane from acetate. J Bacteriol 174:5489–5495

Greenwood PF, van Heemst JDH, Guthrie EA et al (2002) Laser micropyrolysis GC–MS of lignin. J Anal Appl Pyrol 62:365–373

Hansson K, Samuelsson J, Tullin C et al (2004) Formation of HNCO, HCN, and NH3 from the pyrolysis of bark and nitrogen-containing model compounds. Combust Flame 137:265–277

Iida T, Nakanishi M, Got OK (1974) Investigations on poly (vinyl chloride). I. Evolution of aromatics on pyrolysis of poly (vinyl chloride) and its mechanism. J Polym Sci Polym Chem E 12:737–749

Kim DH, Mulholland JA, Wang D et al (2010) Pyrolytic hydrocarbon growth from cyclopentadiene. J Phys Chem A 114:12411–12416

Kim S (2001) Pyrolysis kinetics of waste PVC pipe. Waste Manage 21:609–616

Kislov VV, Sadovnikov AI, Mebel AM (2013) Formation mechanism of polycyclic aromatic hydrocarbons beyond the second aromatic ring. J Phys Chem A 117:4794–4816

Liu Q, Wang SR, Zheng Y et al (2008) Mechanism study of wood lignin pyrolysis by using TG-FTIR analysis. J Anal Appl Pyrol 82:170–177

Liu Q, Zhong ZP, Wang SR et al (2011) Interactions of biomass components during pyrolysis: a TG-FTIR study. J Anal Appl Pyrol 90:213–218
Lu M, Mulholland JA (2004) PAH Growth from the pyrolysis of CPD, indene and naphthalene mixture. Chemosphere 55:605–610
Luo Z, Wang S, Liao Y et al (2004) Mechanism study of cellulose rapid pyrolysis. Ind Eng Chem Res 43:5605–5610
Marsh ND, Wornat MJ (2000) Formation pathways of ethynyl-substituted and cyclopenta-fused polycyclic aromatic hydrocarbons. P Combust Inst 28:2585–2592
Mastral AM, Callén MS (2000) A review on polycyclic aromatic hydrocarbon (PAH) emissions from energy generation. Environ Sci Technol 34:3051–3057
Masuda Y, Uda T, Terakado O et al (2006) Pyrolysis study of poly(vinyl chloride)–metal oxide mixtures: Quantitative product analysis and the chlorine fixing ability of metal oxides. J Anal Appl Pyrol 77:159–168
McGrath T, Sharma R, Hajaligol M (2001) An experimental investigation into the formation of polycyclic-aromatic hydrocarbons (PAH) from pyrolysis of biomass materials. Fuel 80:1787–1797
Meng A, Zhou H, Qin L et al (2013) Quantitative and kinetic TG-FTIR investigation on three kinds of biomass pyrolysis. J Anal Appl Pyrol 104:28–37
Richter H, Howard J (2000) Formation of polycyclic aromatic hydrocarbons and their growth to soot—a review of chemical reaction pathways. Prog Energ Combust 26:565–608
Scott DS, Czernik SR, Piskorz J et al (1990) Fast pyrolysis of plastic wastes. Energ Fuel 4:407–411
Shafizadeh F, Fu YL (1973) Pyrolysis of cellulose. Carbohyd Res 29:113–122
Shen DK, Gu S (2009) The mechanism for thermal decomposition of cellulose and its main products. Bioresource Technol 100:6496–6504
Shen DK, Gu S, Bridgwater AV (2010) Study on the pyrolytic behaviour of xylan-based hemicellulose using TG-FTIR and Py-GC-FTIR. J Anal Appl Pyrol 87:199–206
Shukla B, Koshi M (2012) A novel route for PAH growth in HACA based mechanisms. Combust Flame 159:3589–3596
Siengchum T, Isenberg M, Chuang S (2013) Fast pyrolysis of coconut biomass—an FTIR study. Fuel 105:559–565
Stefanidis SD, Kalogiannis KG, Iliopoulou EF et al (2014) A study of lignocellulosic biomass pyrolysis via the pyrolysis of cellulose, hemicellulose and lignin. J Anal Appl Pyrol 105:143–150
Varhegyi G, Antal MJ, Sezekely T et al (1989) Kinetics of the thermal-decomposition of cellulose, hemicellulose, and sugar-cane bagasse. Energ Fuel 3:329–335
Wang C, Dou B, Song Y et al (2014) Kinetic study on nonisothermal pyrolysis of sucrose biomass. Energ Fuel 28:3793–3801
Wang D, Violi A (2006) Radical—molecule reactions for aromatic growth: a case study for cyclopentadienyl and acenaphthylene. J Org Chem 71:8365–8371
Williams P, Horne PA (1995) Analysis of aromatic hydrocarbons in pyrolytic oil derived from biomass. J Anal Appl Pyrol 31:15–37
Williams PT, Williams EA (1999) Fluidised bed pyrolysis of low density polyethylene to produce petrochemical feedstock. J Anal Appl Pyrol 51:107–126
Wu C, Budarin VL, Gronnow MJ et al (2014) Conventional and microwave-assisted pyrolysis of biomass under different heating rates. J Anal Appl Pyrol 107:276–283
Yang H, Yan R, Chen H et al (2007) Characteristics of hemicellulose, cellulose and lignin pyrolysis. Fuel 86:1781–1788
Yu H, Zhang Z, Li Z et al (2014) Characteristics of tar formation during cellulose, hemicellulose and lignin gasification. Fuel 118:250–256
Zhang J, Chen T, Wu J et al (2014) A novel Gaussian-DAEM-reaction model for the pyrolysis of cellulose, hemicellulose and lignin. RSC Adv 4:17513–17520

Zheng J, Jin YQ, Chi Y et al (2009) Pyrolysis characteristics of organic components of municipal solid waste at high heating rates. Waste Manage 29:1089–1094
Zhou H, Wu C, Onwudili JA et al (2015) Polycyclic aromatic hydrocarbons (PAH) formation from the pyrolysis of different municipal solid waste fractions. Waste Manage 36:136–146
Zhu HM, Jiang XG, Yan JH et al (2008) TG-FTIR analysis of PVC thermal degradation and HCl removal. J Anal Appl Pyrol 82:1–9

Chapter 4
Influential Factors of Thermochemical Conversion of Basic Components

Abstract Chapter 3 investigated the pyrolytic characteristics and mechanisms of basic components, while the reaction conditions were constant, which simplified the comparison of different components. Then, which factors could influence the pyrolytic process of basic components? This chapter will try to provide an answer to this question. Actually, part of the content was involved in Chap. 3. For example, during the study of kinetics in 3.1, the pyrolysis in thermogravimetric analyzer (TGA), slow pyrolysis in Macro-TGA, and fast pyrolysis in Macro-TGA were compared. This chapter aims to investigate this question systematically. Limited by the number of experiments, we could not study the influential factors of all the basic components. Lignin and polyvinyl chloride (PVC) account for high fractions in combustible solid waste (CSW); the thermochemical conversion processes of them are complicated; and a large amount of polycyclic aromatic hydrocarbons (PAHs) are formed during the thermochemical processes. In particular for PVC, the chlorine in its structure is the main chlorine source of dioxins. Therefore, this chapter chose lignin as the representative of biomass basic components and PVC as the representative of biomass basic components. Investigation of different influence factors could help us determine suitable factors to enhance efficiency and control pollution in industrial applications. In addition, understanding the effect of different factors could help to further explore the pyrolytic mechanisms of basic components. It should be noted that the study of influence factor in this chapter was limited to single component, and the interactions of basic components were the research focus of next chapter.

Keywords Combustible solid waste (CSW) · Basic component · Pyrolysis · Gasification · Polycyclic aromatic hydrocarbons (PAHs)

H. Zhou, *Combustible Solid Waste Thermochemical Conversion*, Springer Theses,
DOI 10.1007/978-981-10-3827-3_4

4.1 Influence of Temperature

Since slow pyrolysis is a linearly heating process, the study of the final temperature is meaningless. Therefore, the influence of temperature focuses on fast pyrolysis (isothermal pyrolysis). This chapter investigated the influence of temperature on kinetics, product distribution, gas production, and PAHs formation characteristics. The studied temperature included 500, 600, 700, 800, and 900 °C. The temperature range covered the reaction temperature of pyrolysis, gasification, and combustion of CSW. The carrier gas in this part was N_2.

4.1.1 Influence of Temperature on Lignin Pyrolysis

4.1.1.1 Influence of Temperature on Kinetics of Lignin Pyrolysis

The TG and derivative thermogravimetric (DTG) curves of lignin pyrolysis at different temperatures are shown in Fig. 4.1. It could be observed that the pyrolytic processes were significantly different at different temperatures. If the pyrolytic temperature was higher, the pyrolysis started earlier, the residue mass was lower, and the DTG peak was higher.

Similar to 3.1, pyrolytic indexes were calculated, as shown in Fig. 4.2. Reaction end time represented the time from start to end. As shown in Fig. 4.2a, reaction end time did not change with temperature monotonously and had a maximum value at 700–800 °C. Reaction end time was determined by two factors: reaction rate and final conversion rate. When temperature increased from 500 to 900 °C, reaction rate

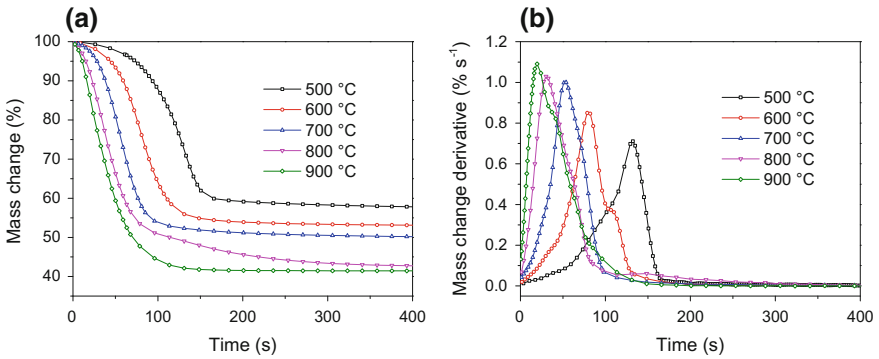

Fig. 4.1 TG and DTG curves of lignin fast pyrolysis at different temperatures

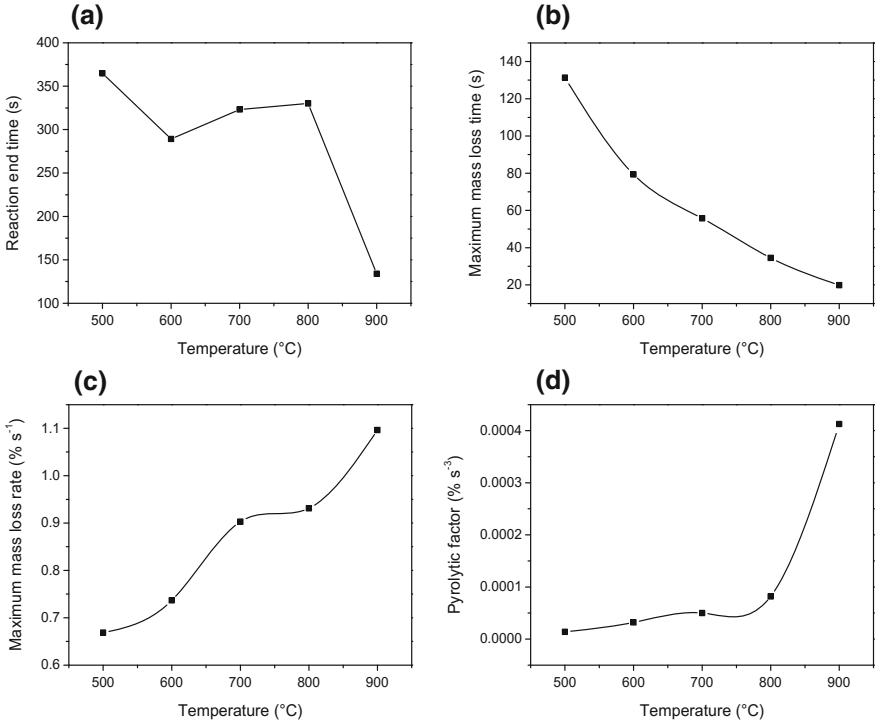

Fig. 4.2 Lignin pyrolytic indexes at different temperatures

was increased, while the final conversion rate was increased, too, since there were new reactions in this temperature range, as shown in TG and DTG curves in Fig. 3.1 in Chap. 3.

Reaction maximum mass loss time decreased with the increase in temperature linearly. The higher the reaction temperature was, the earlier the maximum mass

Table 4.1 Lignin fast pyrolysis kinetic parameters at different temperatures in Macro-TGA

Temperature (°C)	Reaction	Percentage (%)	k	n	R^2
500	1	63.6	1.63×10^{-8}	3.78	0.9996
	2	36.4	1.02×10^{-24}	11.21	0.9947
600	1	15.7	4.10×10^{-19}	9.59	0.9952
	2	84.3	9.39×10^{-7}	3.09	1.0000
700	1	100.0	1.63×10^{-6}	3.23	0.9999
800	1	59.9	1.25×10^{-4}	2.57	0.9996
	2	40.1	2.84×10^{-6}	3.12	0.9970
900	1	20.6	2.39×10^{-4}	2.71	0.9998
	2	79.4	2.84×10^{-4}	2.10	0.9990

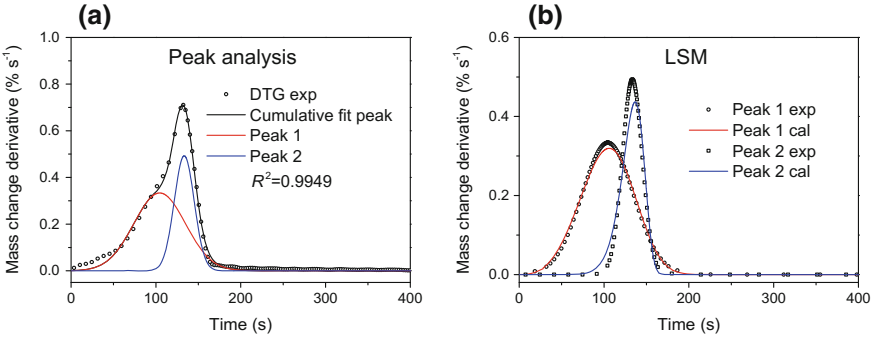

Fig. 4.3 Kinetic calculation of lignin pyrolysis at 500 °C

loss happened. Accordingly, maximum mass loss rate, i.e., the DTG peak value in Fig. 4.1b was higher. Pyrolytic factor was the integrated index to evaluate the difficulty of pyrolysis. As shown in Fig. 4.2d, with the increase in temperature, pyrolytic factor increased, which meant reaction was easier. In particular from 800 to 900 °C, pyrolytic factor increased significantly.

The lignin pyrolytic kinetic parameters at different temperatures were calculated by peak analysis–least square method (PA-LSM), and the results are shown in Table 4.1. Lignin pyrolysis at 500 and 600 °C could be described by two paralleled reactions. From the R^2 values in the table, the kinetic parameters from LSM agreed well with the experimental values. The results of peak analysis and kinetic parameters were shown in Figs. 4.3, 4.4, 4.5, 4.6, and 4.7.

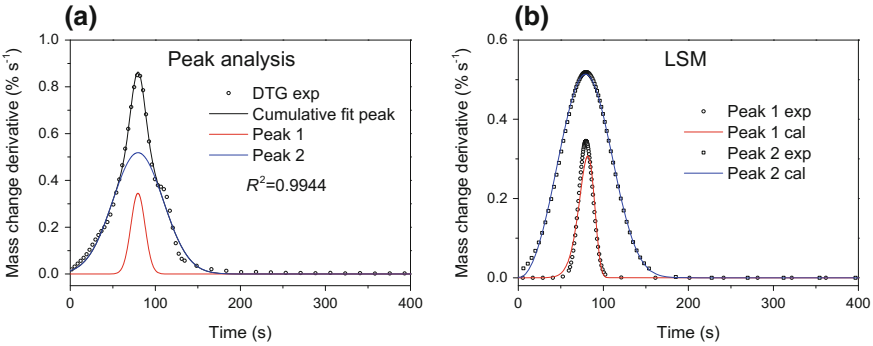

Fig. 4.4 Kinetic calculation of lignin pyrolysis at 600 °C

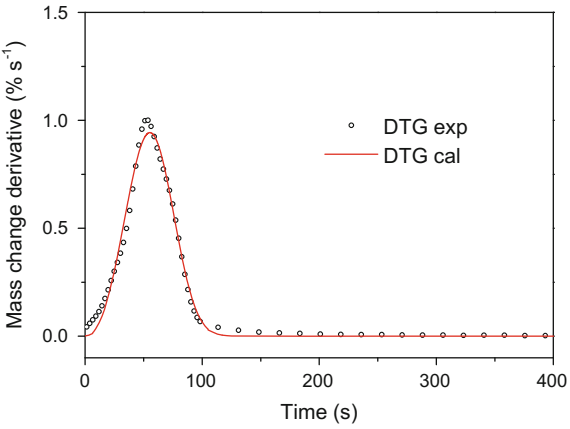

Fig. 4.5 Kinetic calculation of lignin pyrolysis at 700 °C

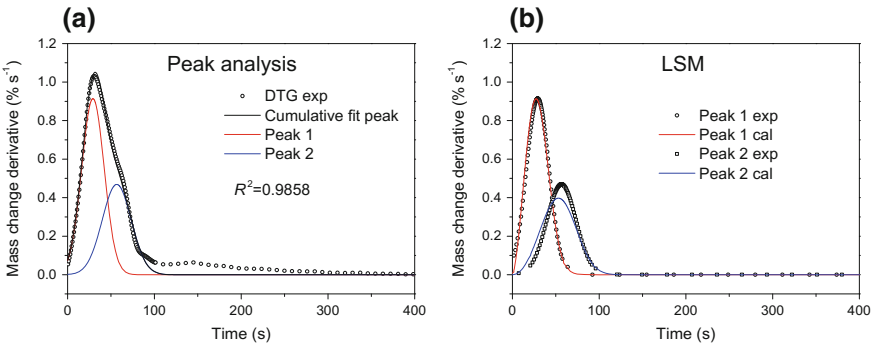

Fig. 4.6 Kinetic calculation of lignin pyrolysis at 800 °C

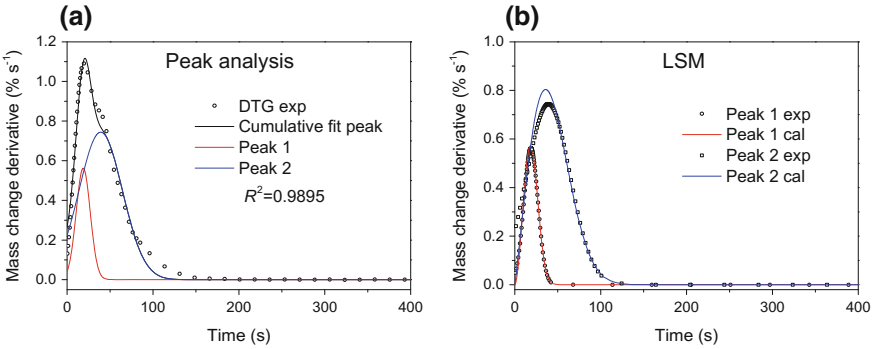

Fig. 4.7 Kinetic calculation of lignin pyrolysis at 900 °C

4.1.1.2 Influence of Temperature on Product Distribution of Lignin Pyrolysis

As shown in Fig. 4.8, when the temperature was increased from 500 to 900 °C, gas production increased, and tar and solid decreased accordingly. The TG curve of lignin pyrolysis in Fig. 3.1 has shown that lignin pyrolysis happened from 200 to 900 °C, which was consistent with the decrease in solid with the increase in temperature as shown in Fig. 4.8. Research has shown that in circulation fluidized bed gasifier, the amount of tar decreased with the increase in temperature at 700–850 °C (Li et al. 2004). The reason might be that with the increase in temperature, the secondary reactions of tar were promoted, and thus more gas was generated (Han and Kim 2008).

4.1.1.3 Influence of Temperature on Gas Production of Lignin Pyrolysis

The gas production of lignin pyrolysis at different temperatures is shown in Fig. 4.9. With the increase in temperature, H_2 and CO increased significantly, and CO_2 increased slightly. Lignin pyrolysis generated a certain amount of CH_4, which increased with the increase in temperature. Research has shown that the formation of CH_4 might come from demethylation reactions (Asmadi et al. 2011a). The amount of C_2–C_4 from lignin pyrolysis was low and increased slightly with the increase in temperature. The increase in gases with temperature agreed well with the results in Fig. 4.8.

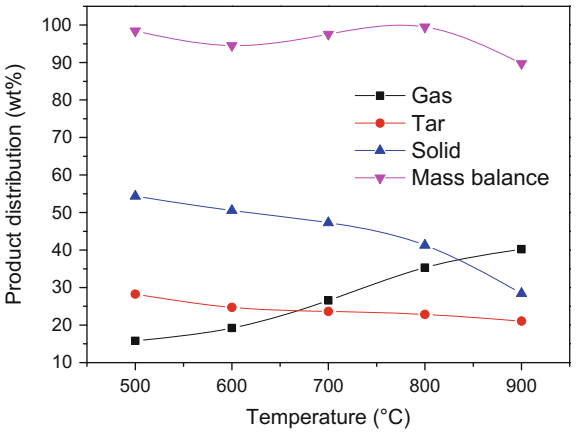

Fig. 4.8 Product distribution of lignin pyrolysis at different temperatures. Reprinted with the permission from Zhou et al. (2014b). Copyright 2014 American Chemical Society

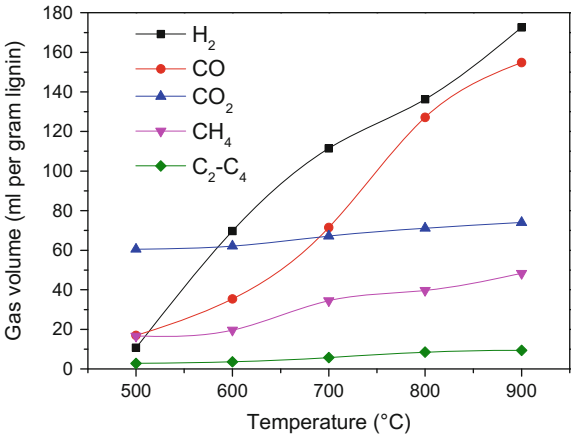

Fig. 4.9 Gas production of lignin pyrolysis at different temperatures. Reprinted with the permission from Zhou et al. (2014b). Copyright 2014 American Chemical Society

4.1.1.4 Influence of Temperature on PAHs Formation of Lignin Pyrolysis

The tar molecular weight distribution was measured by size-exclusion chromatography (SEC), as shown in Fig. 4.10. The *x*-axis was tar molecular weight, and *y*-axis was the mass fraction. Figure 4.10 focused on the molecular weight distribution in 100–250 g mol^{-1}. The tar molecular weight was distributed in 120–180 g mol^{-1}, with the peak value at 140–160 g mol^{-1}, maybe due to the generation of naphthalene (Asmadi et al. 2011c). With the increase in temperature, tar molecular weight increased. In particular when the temperature was increased from 800 to 900 °C, tar molecular weight increased significantly. The possible reason was that the secondary reactions of PAHs growth were promoted with the increase in temperature (Sharma and Hajaligol 2003).

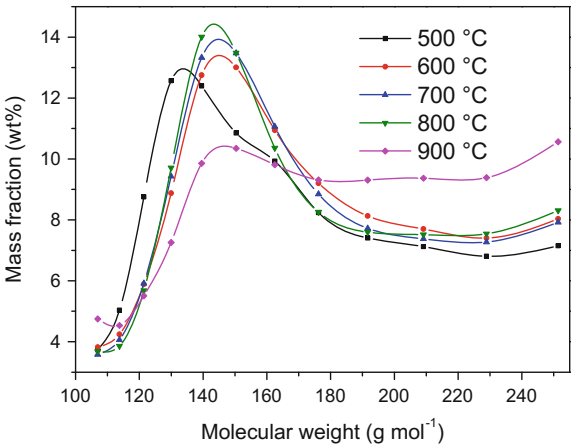

Fig. 4.10 Tar molecular weight distribution of lignin pyrolysis at different temperatures. Reprinted with the permission from Zhou et al. (2014b). Copyright 2014 American Chemical Society

The PAHs generation from lignin pyrolysis at different temperatures is shown in Fig. 4.11. As shown in Fig. 4.11a, with the increase in temperature, the generation of naphthalene increased, especially from 700 to 900 °C. With the increase in temperature from 500 to 800 °C, the generation of 1-methylnaphthalene and 2-methylnaphthalene increased. However, when the temperature was increased from 800 to 900 °C, the generation of 1-methylnaphthalene and 2-methylnaphthalene decreased slightly, likely due to demethylation reactions. When the temperature was lower than 700 °C, 3-ring PAHs could not be detected. Nevertheless, with the increase in temperature from 700 to 900 °C, the generation of acenaphthylene, fluorene, phenanthrene, and anthracene increased. The results were similar for 4-ring PAHs. Fluoranthene, pyrene, benzo[*a*]anthracene, and chrysene could only be detected above 700 °C.

The total PAHs amounts from lignin pyrolysis at different temperatures are shown in Fig. 4.11d. The increasing trend of PAHs could be fitted by a quadric curve, which indicated that the increase in PAHs at high temperatures was more significant. Sharma and Hajaligol (2003) investigated lignin pyrolysis in a two-stage reactor. Reactor 1 was isothermal at 600 °C, and when the temperature of Reactor 2 increased from 700 to 900 °C, most PAHs increased. Ledesma et al.

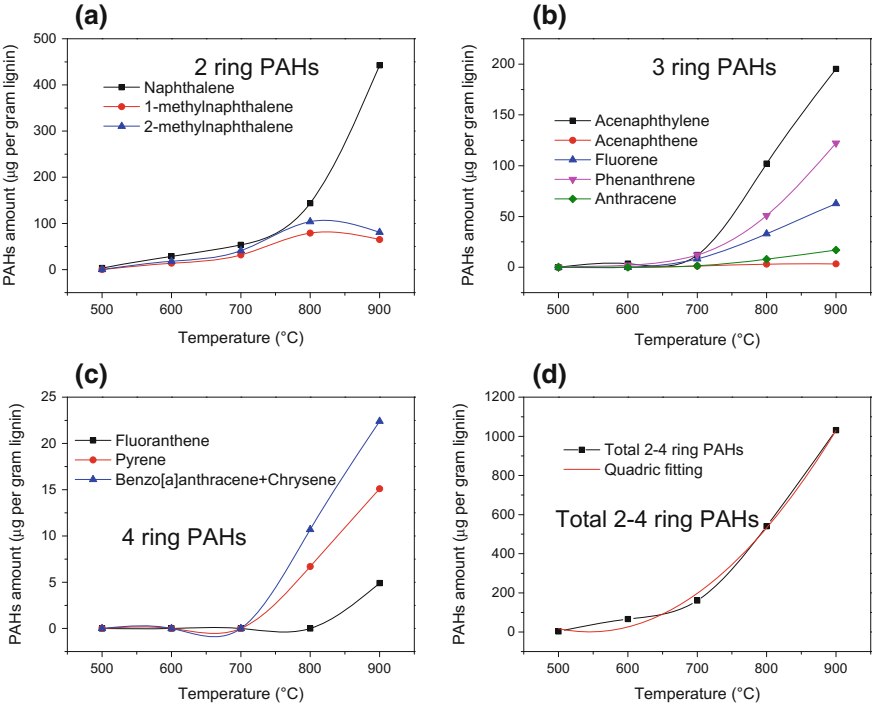

Fig. 4.11 PAHs generation of lignin pyrolysis at different temperatures. Reprinted with the permission from Zhou et al. (2014b). Copyright 2014 American Chemical Society

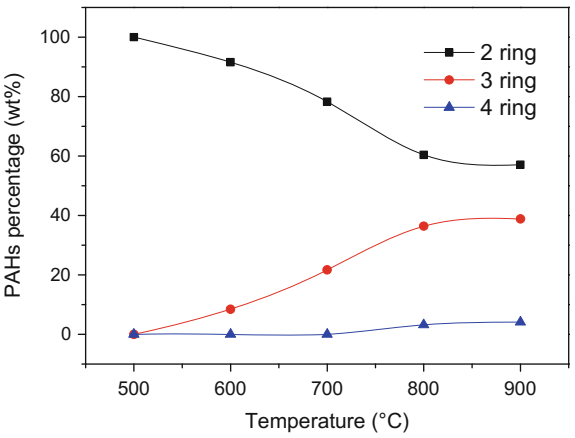

Fig. 4.12 Percentages of PAHs with different number of rings at different temperatures. Reprinted with the permission from Zhou et al. (2014b). Copyright 2014 American Chemical Society

(2002) pyrolyzed catechol (a model compound of lignin) in a tubular reactor. With the increase in temperature, the amount of PAHs increased significantly.

The change in PAHs percentage of different number of rings with the change in temperature is shown in Fig. 4.12. With the increase in temperature, 2-ring PAHs percentage decreased, and the percentages of 3- and 4-ring PAHs increased, which was consistent with tar molecular increase from SEC measurement as shown in Fig. 4.10. The mechanisms will be analyzed at the end of this chapter.

4.1.2 Influence of Temperature on PVC Pyrolysis

4.1.2.1 Influence of Temperature on Kinetics of PVC Pyrolysis

The influence of temperature on lignin fast pyrolysis kinetics was investigated above, and here we are going to discuss the influence of temperature on PVC fast pyrolysis kinetics. As shown in Fig. 4.13, the trend in TG and DTG curves of PVC pyrolysis at different temperatures was monotonic. We introduced similar pyrolytic parameters as shown in Fig. 4.14: reaction end time, the maximum mass loss time, the maximum mass loss rate, and pyrolytic factor. With the increase in temperature, the reaction was faster and reaction ended earlier. The trend was different from lignin pyrolysis, and the reason was that lignin pyrolysis had new reactions between 500 and 900 °C, which was different from PVC pyrolysis. As shown in Fig. 4.13a, the final residue mass of PVC pyrolysis was similar from 500 to 900 °C.

Similar to lignin pyrolysis, with the increase in temperature, the maximum mass loss time of PVC pyrolysis decreased linearly. The maximum mass loss rate and

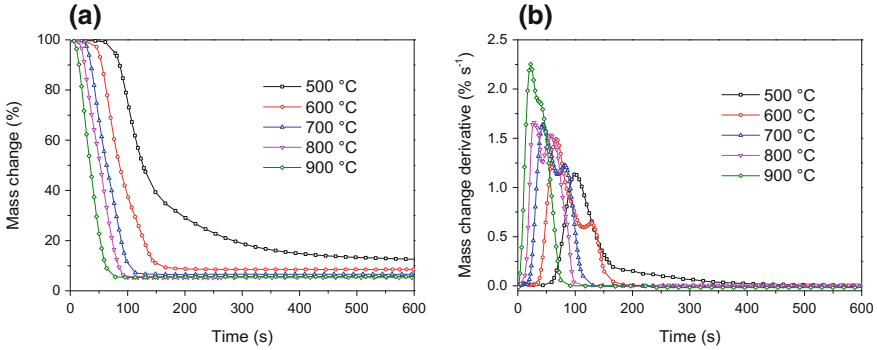

Fig. 4.13 TG and DTG curves of PVC fast pyrolysis at different temperatures

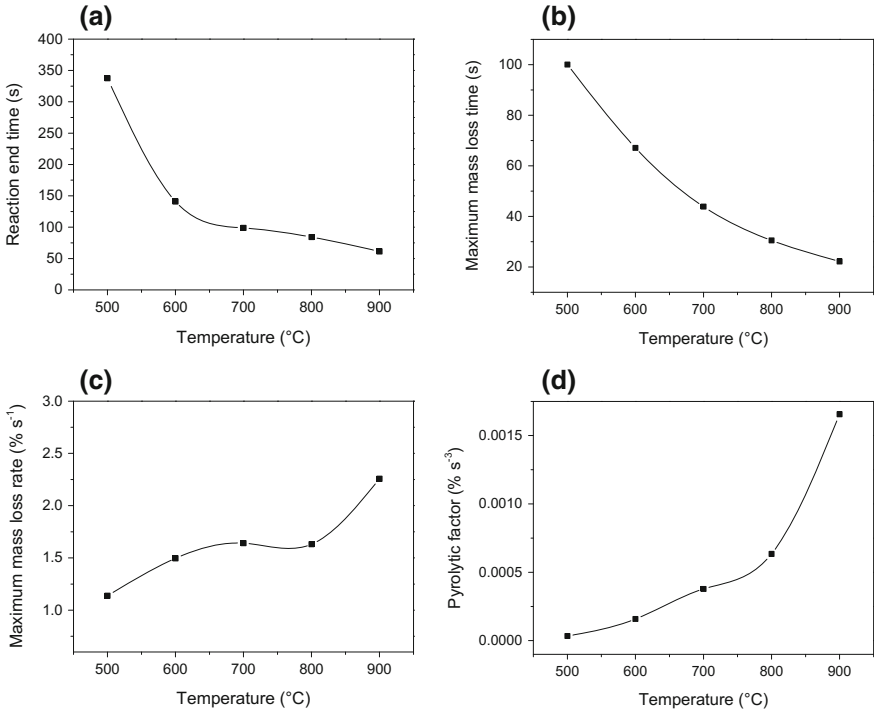

Fig. 4.14 PVC pyrolytic indexes at different temperatures

pyrolytic factor increased with the increase in temperature. In particular from 800 to 900 °C, pyrolytic factor increased considerably.

The kinetic parameters of fast pyrolysis by PA-LSM are shown in Table 4.2. At different temperatures, PVC pyrolysis could be described by two paralleled reactions with the reaction order in the range 3–6 and the R^2 values more than 0.9980.

Table 4.2 PVC fast pyrolysis kinetic parameters at different temperatures in Macro-TGA

Temperature (°C)	Reaction	Percentage (%)	k	n	R^2
500	1	64.0	1.23×10^{-11}	5.33	0.9981
	2	36.0	8.70×10^{-8}	3.04	1.0000
600	1	51.6	4.63×10^{-10}	5.04	0.9984
	2	48.4	3.66×10^{-10}	4.54	0.9993
700	1	48.1	8.52×10^{-8}	4.20	0.9992
	2	51.9	5.19×10^{-11}	5.32	0.9982
800	1	27.8	2.55×10^{-6}	3.73	0.9996
	2	72.2	2.43×10^{-7}	3.64	0.9997
900	1	30.5	7.57×10^{-5}	3.07	1.0000
	2	69.5	4.82×10^{-6}	3.20	0.9999

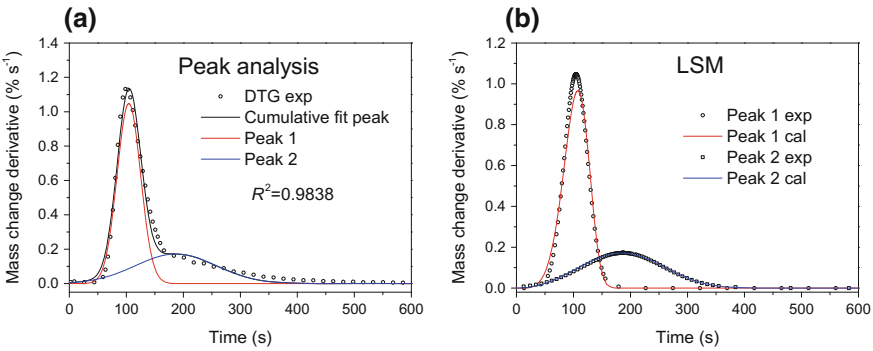

Fig. 4.15 Kinetic calculation of PVC pyrolysis at 500 °C

The results of peak analysis are shown in Figs. 4.15a, 4.16a, 4.17a, 4.18a, and 4.19a with the R^2 values more than 0.9800. The peaks reproduced from kinetic parameters by LSM were shown in Fig. 4.15b, 4.16b, 4.17b, 4.18b, and 4.19b, which indicated that the calculation results agreed well with experimental results.

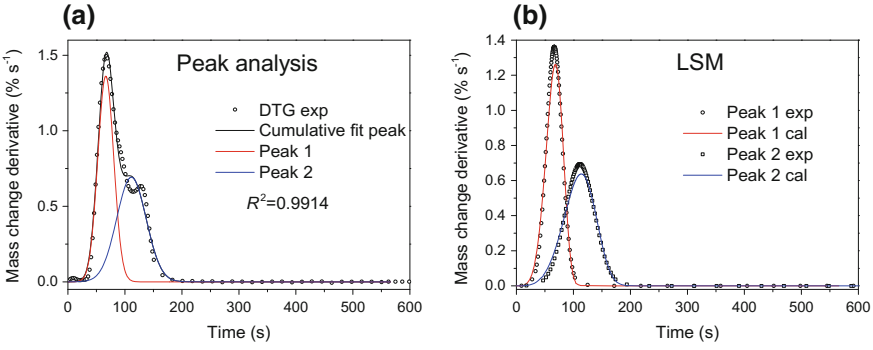

Fig. 4.16 Kinetic calculation of PVC pyrolysis at 600 °C

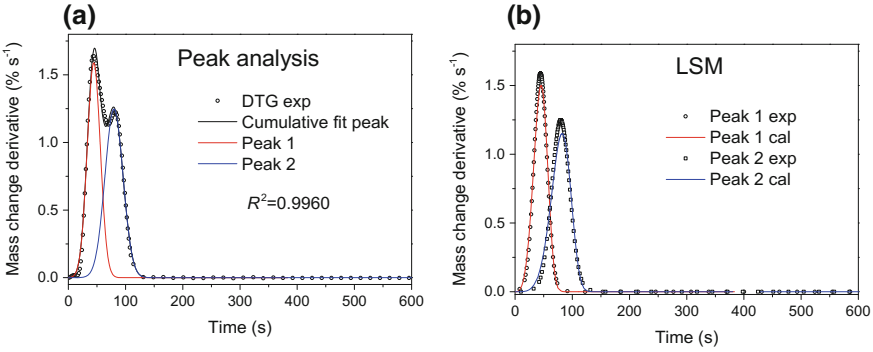

Fig. 4.17 Kinetic calculation of PVC pyrolysis at 700 °C

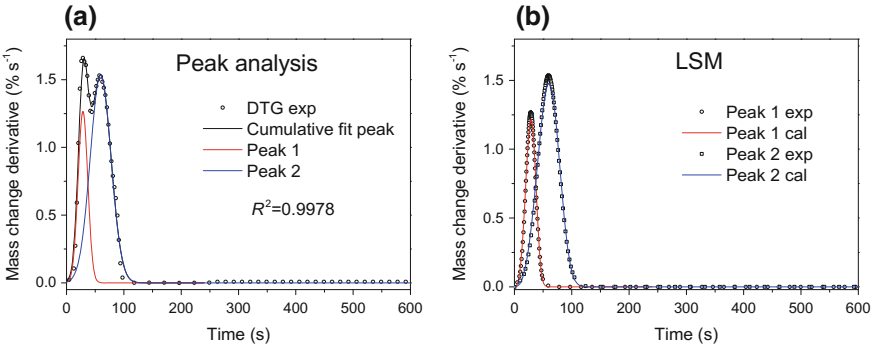

Fig. 4.18 Kinetic calculation of PVC pyrolysis at 800 °C

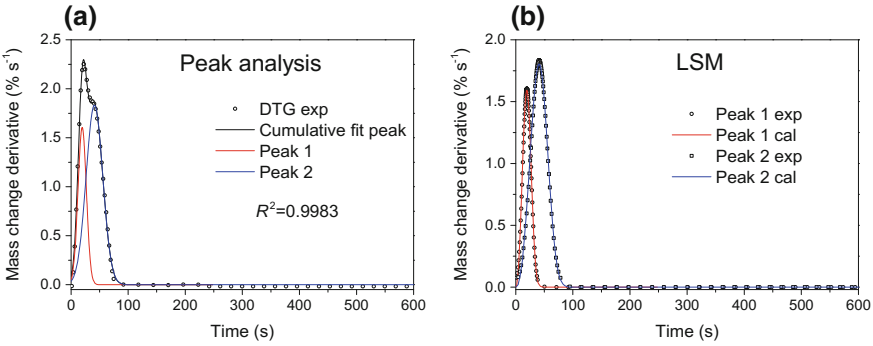

Fig. 4.19 Kinetic calculation of PVC pyrolysis at 900 °C

4.1.2.2 Influence of Temperature on Product Distribution of PVC Pyrolysis

The product mass distribution of PVC fast pyrolysis at 500–900 °C is shown in Fig. 4.20. The mass balance of all the experiments was 91.8–102.5%, which indicated the good accuracy of the experiments. With the increase in temperature from 500 to 900 °C, HCl amount decreased from 54.7 to 30.2%. On the contrary, the amount of gas and tar increased with the increase in temperature, and solid amount decreased with the increase in temperature.

4.1.2.3 Influence of Temperature on Gas Production of PVC Pyrolysis

As shown in Fig. 4.21, with the temperature being increased from 500 to 900 °C, all the gases increased. Therein, H_2 amount increased by 10 times from 11.2 to 114.1 ml/g PVC. H_2 generation was mainly due to secondary reactions. For example, during the reaction from small aromatics to large aromatics or even soot, H_2 was formed as a by-product. The amounts of CH_4 and C_2–C_4 were similar and increased with the increase in temperature slightly. Ma et al. (2002) compared PVC fast pyrolysis at 600 and 800 °C, and found that more CH_4, C_2H_4, C_2H_6, C_3H_6, and C_3H_8 are generated at 800 °C, which was consistent with this study. At high temperatures, more aliphatic groups were disconnected from aromatic rings, and thus some molecular hydrocarbons were formed.

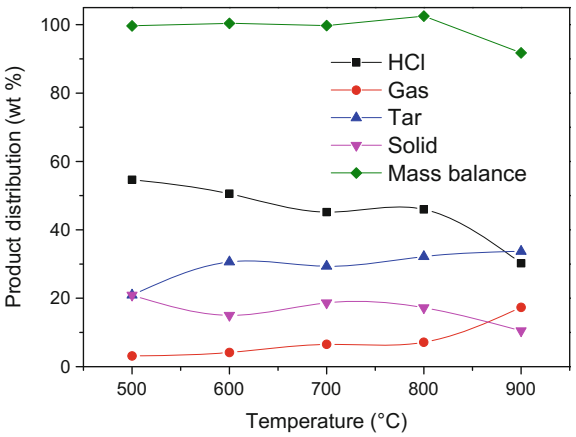

Fig. 4.20 Product distribution of PVC pyrolysis at different temperatures. Reprinted from Zhou et al. (2016), Copyright 2016, with permission from Elsevier

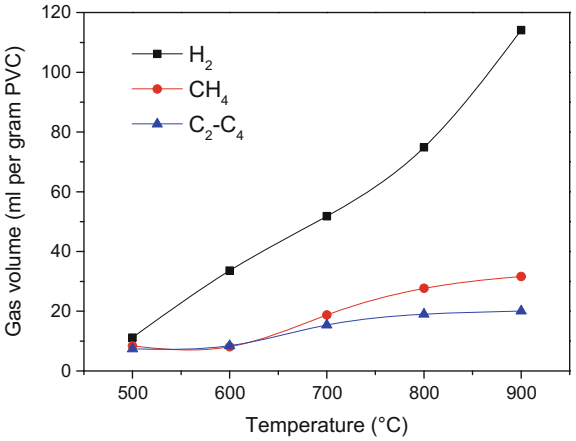

Fig. 4.21 Gas production of PVC pyrolysis at different temperatures. Reprinted from Zhou et al. (2016), Copyright 2016, with permission from Elsevier

4.1.2.4 Influence of Temperature on PAHs Formation of PVC Pyrolysis

As shown in Fig. 4.22, 2 to 4-ring PAHs from PVC pyrolysis tar were quantitatively measured. When the temperature was increased from 500 to 600 °C, naphthalene amount decreased from 1779.5 to 755.8 μg/g PVC. When the temperature was further increased from 600 to 900 °C, naphthalene increased to 7960.8 μg/g PVC. Two naphthalene derivatives, 1-methylnaphthalene and 2-methylnapthalene, increased with temperature from 500 to 700 °C, while they decreased with temperature from 700 to 900 °C, which may be due to demethylation reactions. This result was consistent with the result of lignin pyrolysis as shown in Sect. 4.1.1. When the temperature was increased from 500 to 900 °C, 3-ring PAHs increased. In particular, phenanthrene amount increased from 365.5 to 4242.1 μg/g PVC. 4-ring PAHs also increased with temperature: The amount of benzo[*a*]anthracene +chrysene increased from 209.3 to 6137.0 μg/g PVC significantly. With the increase in temperature from 500 to 900 °C, total PAHs amount increased from 4074.4 to 26,506.1 μg/g PVC. Wang et al. (2003) have reported that PAHs decreased with the increase in temperature during PVC combustion process. Therefore, it could be concluded that the effects of temperature on PAHs release were different for PVC pyrolysis and combustion.

This section studied the influence of temperature on the pyrolysis of lignin and PVC, and some universal conclusions were obtained. The higher the pyrolytic temperature was, the earlier the maximum mass loss peak occurred, and the higher the maximum mass loss rate was. With the increase in temperature from 500 to 900 °C, gas production increased, tar molecular weight increased, and PAHs

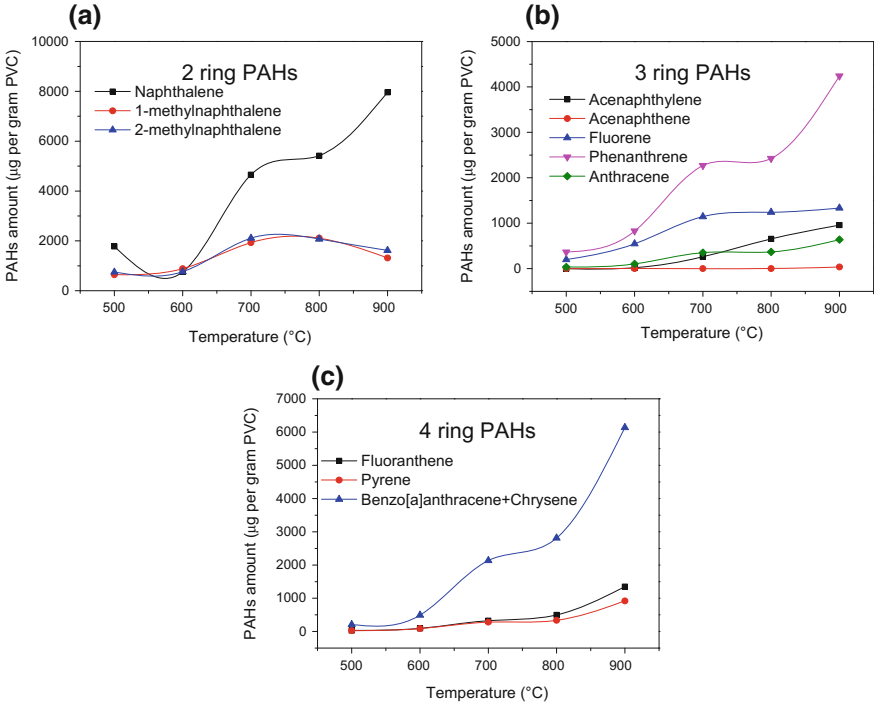

Fig. 4.22 PAHs generation of PVC pyrolysis at different temperatures. Reprinted from Zhou et al. (2016), Copyright 2016, with permission from Elsevier

amount increased. The different part was that tar amount decreased with the increase in temperature for lignin pyrolysis, while for PVC pyrolysis, HCl amount decreased and tar amount increased with the increase in temperature.

4.2 Influence of Heating Rate

Both slow pyrolysis and fast pyrolysis are widely applied in industrial appliances. For slow pyrolysis, the sample was placed in the reactor first, and then the temperature was ramped up at 10 °C min^{-1}. For fast pyrolysis, when furnace temperature was stable at 800 °C, the sample was put into reactor very fast. The detailed procedure could be found at 2.2.3. For both slow pyrolysis and fast pyrolysis, the carrier gas was 100 ml min^{-1} N_2. The influence of heating rate on the kinetics of basic components has been discussed in 3.1, so this section will focus on the influence of heating rate on pyrolysis reaction product distribution, gas products, and PAHs generation.

4.2.1 Influence of Heating Rate on Lignin Pyrolysis

4.2.1.1 Influence of Heating Rate on Product Distribution of Lignin Pyrolysis

The product distribution of lignin pyrolysis at different heating rates is shown in Fig. 4.23. Compared to fast pyrolysis, slow pyrolysis generated more tar and less gas.

4.2.1.2 Influence of Heating Rate on Gas Production of Lignin Pyrolysis

The gas products from lignin pyrolysis at different heating rates are shown in Fig. 4.24. Compared to fast pyrolysis, slow pyrolysis generated a similar amount of H_2 and C_2–C_4, while the generation of CO, CO_2, and CH_4 was lower.

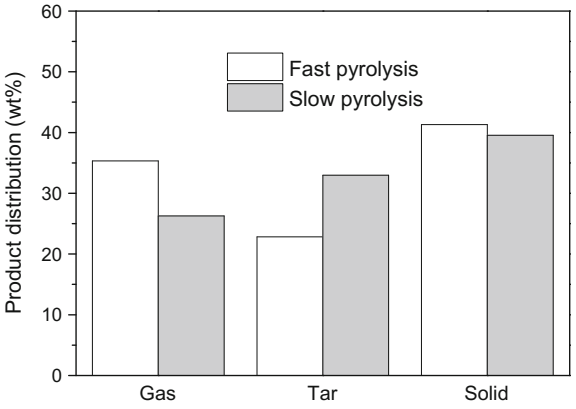

Fig. 4.23 Product distribution of lignin pyrolysis at different heating rates

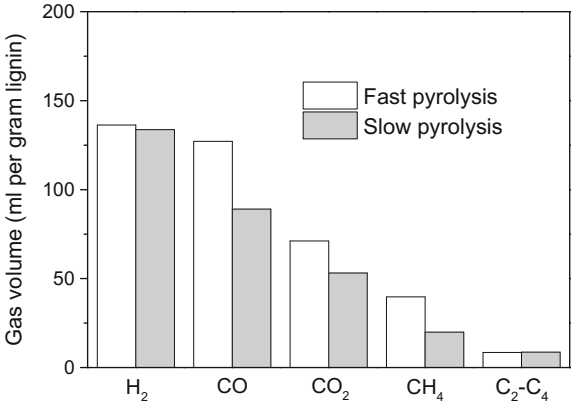

Fig. 4.24 Gas production of lignin pyrolysis at different heating rates

4.2.1.3 Influence of Heating Rate on PAHs Formation of Lignin Pyrolysis

SEC provided tar molecular weight distribution, as shown in Fig. 4.25. Compared to fast pyrolysis, slow pyrolysis generated a higher percentage of molecules in 140–160 g mol^{-1} (21%), which indicated that slow pyrolysis generated a higher percentage of small molecules.

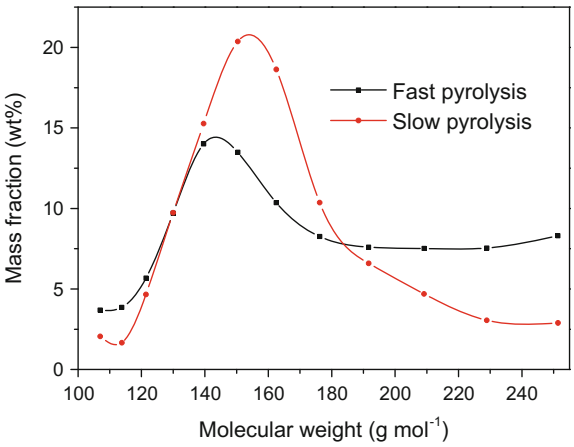

Fig. 4.25 Tar molecular weight distribution of lignin pyrolysis at different heating rates

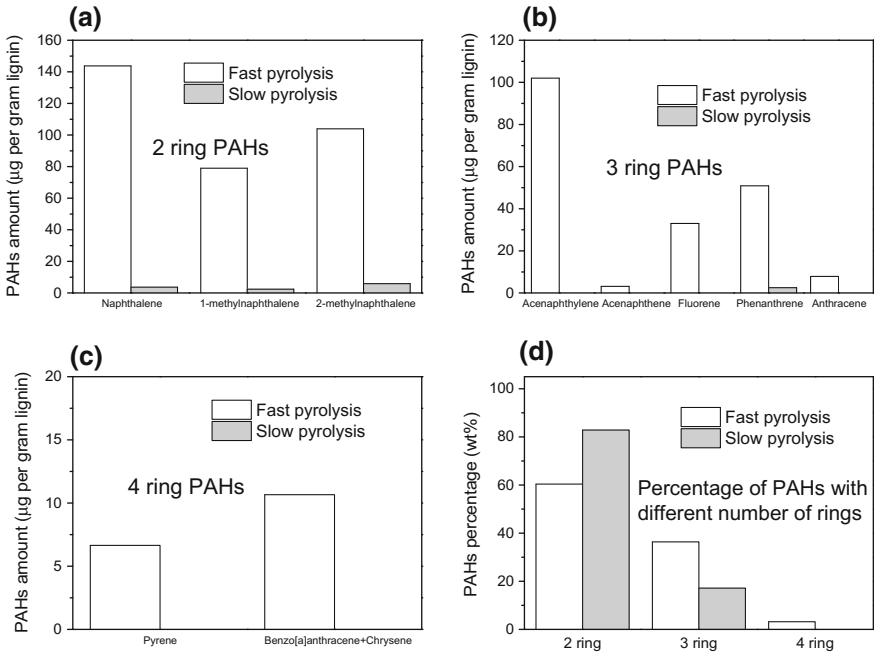

Fig. 4.26 PAHs generation of lignin pyrolysis at different heating rates

The PAHs generation from lignin pyrolysis at different heating rates is shown in Fig. 4.26. Slow pyrolysis generated much less 2-ring PAHs than fast pyrolysis. The results were similar for 3-ring PAHs. In addition, 4-ring PAHs could be hardly detected in the tar of slow pyrolysis. The percentages of 2-, 3-, and 4-ring PAHs are shown in Fig. 4.26d. Compared to fast pyrolysis, 2-ring PAHs percentage for slow pyrolysis was higher, while the percentages of 3- and 4-ring PAHs were lower, which was consistent with SEC results in Fig. 4.25. The mechanisms will be analyzed at the end of this chapter.

4.2.2 Influence of Heating Rate on PVC Pyrolysis

4.2.2.1 Influence of Heating Rate on Product Distribution of PVC Pyrolysis

The product distribution of PVC pyrolysis at different heating rates is shown in Fig. 4.27. Compared to fast pyrolysis, slow pyrolysis generated more HCl (52.7%), which was close to the chlorine content in PVC (Table 2.4) and similar to the report of Williams and Williams (1999). In addition, compared to fast pyrolysis, slow pyrolysis generated more gas and less tar. The final residue amounts for fast pyrolysis and slow pyrolysis were similar (~17%).

4.2.2.2 Influence of Heating Rate on Gas Production of PVC Pyrolysis

The gas production from PVC pyrolysis at different heating rates is shown in Fig. 4.28. Compared to fast pyrolysis, slow pyrolysis generated less H_2, CH_4, and C_2–C_4, which was consistent with the results of lignin pyrolysis as shown in Fig. 4.24.

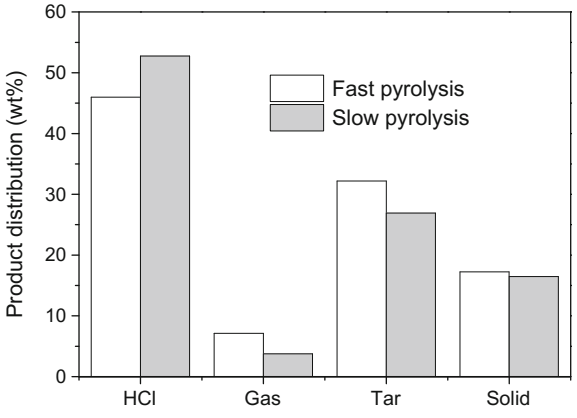

Fig. 4.27 Product distribution of PVC pyrolysis at different heating rates. Reprinted from Zhou et al. (2016), Copyright 2016, with permission from Elsevier

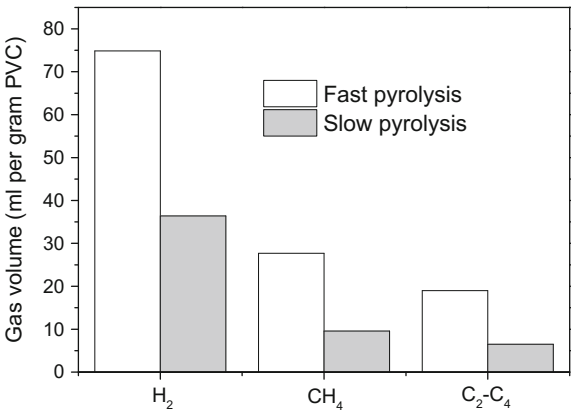

Fig. 4.28 Gas production of PVC pyrolysis at different heating rates. Reprinted from Zhou et al. (2016), Copyright 2016, with permission from Elsevier

4.2.2.3 Influence of Heating Rate on PAHs Formation of PVC Pyrolysis

The PAHs generation from PVC fast pyrolysis and slow pyrolysis is shown in Fig. 4.29. Compared to fast pyrolysis, slow pyrolysis generated less 2-ring PAHs. Particularly slow pyrolysis generated less naphthalene (291.4 μg/g PVC) than fast pyrolysis (5419.6 μg/g PVC). The trend was similar for 3-ring and 4-ring PAHs.

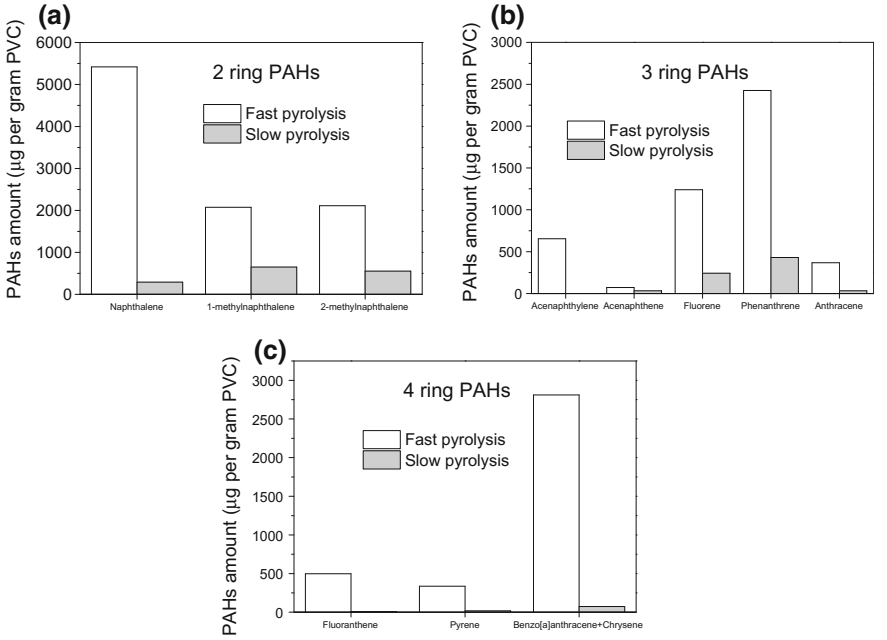

Fig. 4.29 PAHs generation of PVC pyrolysis at different heating rates. Reprinted from Zhou et al. (2016), Copyright 2016, with permission from Elsevier

The total 2- to 4-ring PAHs amount from slow pyrolysis (2334.3 μg/g PVC) was approximately an eighth of that from fast pyrolysis (18,009.1 μg/g PVC).

This section discusses the influence of heating rate on pyrolysis of lignin and PVC. The common part is that slow pyrolysis generated less gas and PAHs compared to fast pyrolysis. The different part is that slow pyrolysis of lignin generated more tar than fast pyrolysis, while slow pyrolysis of PVC generated more HCl than fast pyrolysis. Accordingly, PVC slow pyrolysis generated less tar compared to fast pyrolysis. The mechanisms will be discussed in Sect. 4.5.

4.3 Influence of Atmosphere

4.3.1 Influence of Atmosphere on Lignin Thermochemical Conversion

4.3.1.1 Influence of Atmosphere on Kinetics of Lignin Thermochemical Conversion

To study the influence of atmosphere on lignin thermochemical conversion, except the aforementioned experiments in N_2, experiments in air and CO_2 were carried out. In TGA, the flow rate of air or CO_2 was still 100 ml min^{-1}. As shown in Fig. 4.30, the TG curves of three atmospheres were coincident below 350 °C. After that, the experiment in air had an obvious fast mass loss until the finish at 500 °C. It was due to the combustion in air, and the residue was only ash. For CO_2 atmosphere, the mass loss was inhabited in 350–700 °C and promoted from 700 °C. The reason was gasification of C in CO_2 to form CO. The residue mass in CO_2 was similar to that in air, which indicated the completed gasification at 1000 °C. Comparing the DTG curves in Fig. 4.30b, there were a pyrolysis peak and a combustion peak in air. While in CO_2, except a pyrolysis peak similar to that in N_2, there was an obvious gasification peak at 750–800 °C.

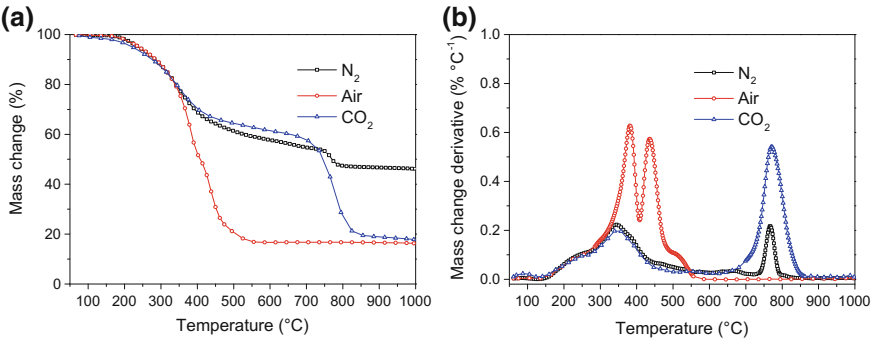

Fig. 4.30 TG and DTG curves of lignin thermochemical conversion in TGA under different atmospheres

Table 4.3 Kinetic parameters of lignin thermochemical conversion in TGA under different atmospheres

Atmosphere	Reaction	Percentage (%)	Peak temperature (°C)	E (kJ mol^{-1})	A (min^{-1})	n	ADI
N_2	1	13.6	227.7	62	8.61×10^5	1.35	1.32
	2	52.8	344.3	73	3.05×10^5	1.34	1.29
	3	9.0	478.4	144	3.04×10^9	1.43	1.48
	4	13.9	649.3	81	3.91×10^3	1.27	1.13
	5	10.7	767.1	1090	5.85×10^{54}	1.6	1.87
Air	1	55.1	354.0	38	1.55×10^2	1.18	0.81
	2	18.8	378.7	302	1.11×10^{24}	1.55	1.78
	3	19.4	438.4	375	2.88×10^{27}	1.56	1.81
	4	6.6	493.5	189	2.78×10^{12}	1.47	1.68
CO_2	1	48.1	336.6	35	1.17×10^2	1.17	0.76
	2	51.9	773.8	392	1.41×10^{19}	1.52	1.83

The kinetic parameters in air and CO_2 calculated by PA-LSM are shown in Table 4.3. The reaction in air could be described by four paralleled reactions, with the overlay of the pyrolytic process and combustion process. The pyrolytic process and gasification process were separated. Pyrolysis reaction could be described by Reaction 1, and gasification reaction could by described by Reaction 2. It could be found that the activation energy of gasification reaction was much higher than that of pyrolysis reaction. The reaction orders were between 1 and 2, and the average deviation indexes (*ADIs*) were less than 2. The results of PA-LSM are shown in Fig. 4.31.

The TG and DTG curves of fast pyrolysis/gasification in Macro-TGA are shown in Fig. 4.32. Before 100 s, the mass loss characteristics in three atmospheres were similar. In 100–350 s, the reactions in N_2 and air were similar. After that, the gasification effect of air came out. In 100–450 s, CO_2 inhabited the thermochemical conversion, which was consistent with the result in TGA, as shown in Fig. 4.30a. As time went by, the gasification effect of CO_2 made the mass loss surpass that in N_2. At 600 s, the reaction in N_2 was completed, while the reactions in air and CO_2 were not finished.

The thermochemical indexes in different atmospheres were shown in Fig. 4.33. Since the reactions in air and CO_2 were not finished, reaction end time and pyrolysis/gasification factor were not calculated here. The maximum mass loss rates in air and CO_2 were much higher than that in N_2, and the maximum mass loss time in air was much shorter than that in N_2 and CO_2.

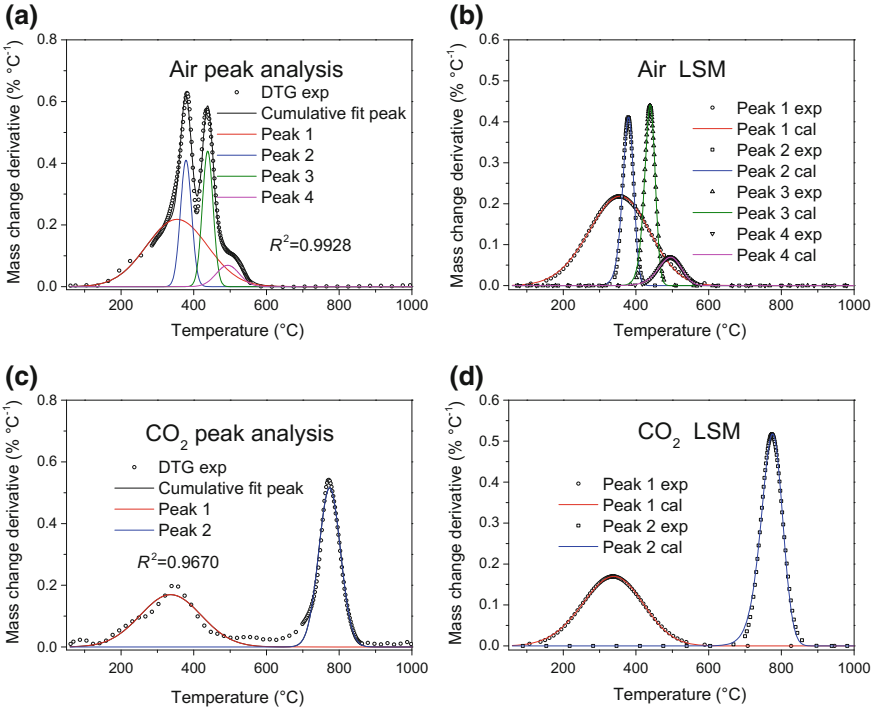

Fig. 4.31 Kinetic calculation of lignin thermochemical conversion in TGA under air and CO_2

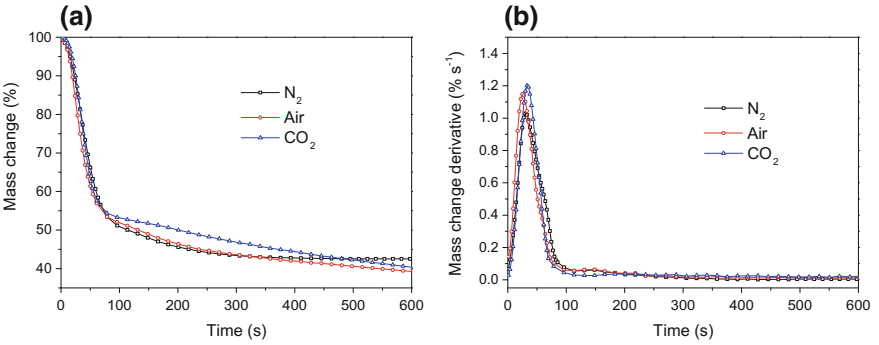

Fig. 4.32 TG and DTG curves of lignin thermochemical conversion in Macro-TGA under different atmospheres

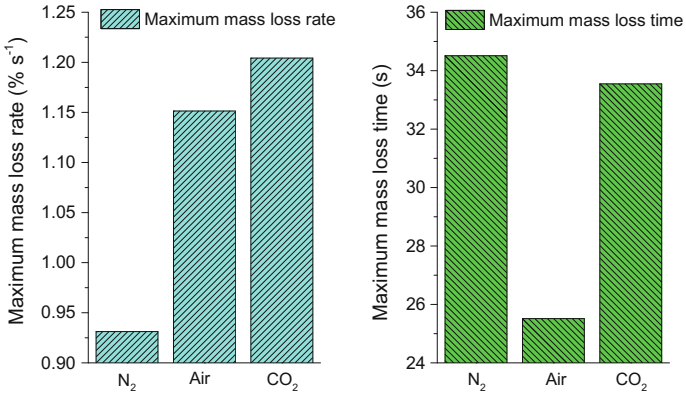

Fig. 4.33 Lignin thermochemical conversion indexes under different atmospheres

Table 4.4 Kinetic parameters of lignin thermochemical conversion in Macro-TGA under different atmospheres

Temperature (°C)	Reaction	Percentage (%)	k	n	R^2
N_2	1	59.9	1.25×10^{-4}	2.57	0.9996
	2	40.1	2.84×10^{-6}	3.12	0.9970
Air	1	47.5	1.66×10^{-4}	2.61	0.9998
	2	52.5	3.85×10^{-5}	2.60	0.9998
CO_2	1	100.0	3.88×10^{-5}	2.73	0.9999

The kinetic parameters in three atmospheres calculated by PA-LSM are shown in Table 4.4. The kinetics in air were similar to those in N_2, which could be described by two peaks. The reaction in CO_2 could be described by single reaction with very high R^2 value. The results of peak analysis and LSM are shown in Fig. 4.34, which indicated that the calculation results agreed well with experimental results.

4.3.1.2 Influence of Atmosphere on Product Distribution of Lignin Thermochemical Conversion

The product distribution from different atmospheres is shown in Fig. 4.35. The y-axis was the ratio of products to original lignin mass. Since gasifying agent air and CO_2 might participate in the reaction, the values could be more than 100%. As shown in Fig. 4.35, compared to pyrolysis in N_2, gasification in air or CO_2 produced less final residue, due to the reaction of char and air or CO_2. Accordingly, the production of gas and tar increased. The study by Gordillo and Annamalai (2010) has shown that with the increase in air, tar amount increased at 800 °C. However,

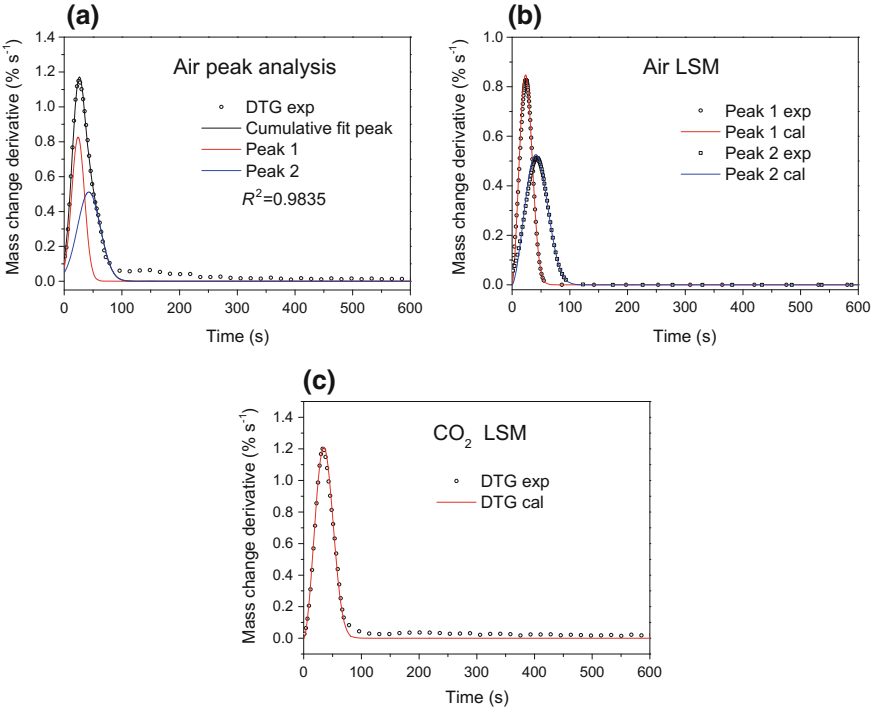

Fig. 4.34 Kinetic calculation of lignin thermochemical conversion in Macro-TGA under air and CO_2

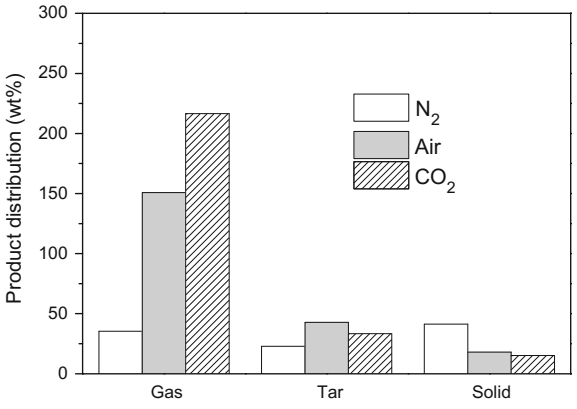

Fig. 4.35 Product distribution of lignin thermochemical conversion under different atmospheres

Yu et al. (2014) have reported different results that in an entrained flow reactor, tar amount decreased with an increase in excess air coefficient. With the increase in air flow rate, there might be a maximum value of tar amount (Lv et al. 2007). Due to the generation of oxygenates, the participation of O_2 might increase tar amount. However, with the increase in O_2, these compounds might be further oxidized into

CO_2 or CO. It should be noted that in our reaction system, a fuel-rich atmosphere might be formed partially because of 1 g lignin in the small reactor (inner diameter 1 cm). As shown in Fig. 4.35, gasification in CO_2 released more gas, due to the reaction of CO_2 and char.

4.3.1.3 Influence of Atmosphere on Gas Production of Lignin Thermochemical Conversion

The gas generation of lignin in different atmospheres is shown in Fig. 4.36. Gasification in air generated less H_2, but more CO_2 and CO. Compared to pyrolysis in N_2, gasification in CO_2 generated more CO, due to the reaction of CO_2 and char (Kwon and Castaldi 2012).

4.3.1.4 Influence of Atmosphere on PAHs Formation of Lignin Thermochemical Conversion

The SEC results of tar of lignin pyrolysis/gasification are shown in Fig. 4.37. In air atmosphere, the tar molecules were smaller than those in N_2, while the tar molecules were smallest under CO_2 atmosphere.

The PAHs amount of tar from lignin pyrolysis/gasification under different atmospheres is shown in Fig. 4.38. The 2-ring PAHs from air atmosphere were less than that from N_2, while the 2-ring PAHs amount from CO_2 atmosphere was the lowest. For 3-ring PAHs, compared to pyrolysis under N_2, gasification under air or CO_2 generated less acenaphthylene, acenaphthene, and fluorene, while the generation of phenanthrene (~45 μg/g lignin) and anthracene (~7 μg/g lignin) from different atmospheres was similar. Under CO_2 atmosphere, 4-ring PAHs could not be detected, and only a small amount of pyrene could be detected under air atmosphere, as shown in Fig. 4.38c.

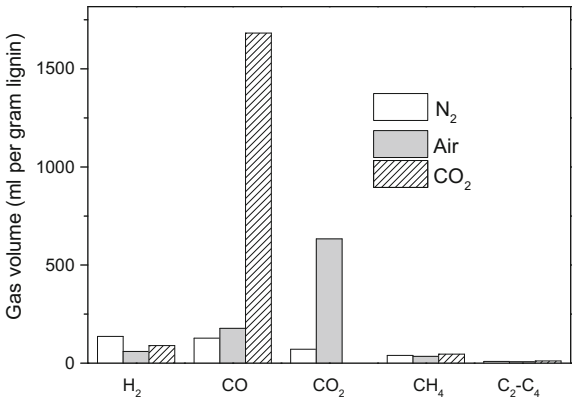

Fig. 4.36 Gas production of lignin thermochemical conversion under different atmospheres

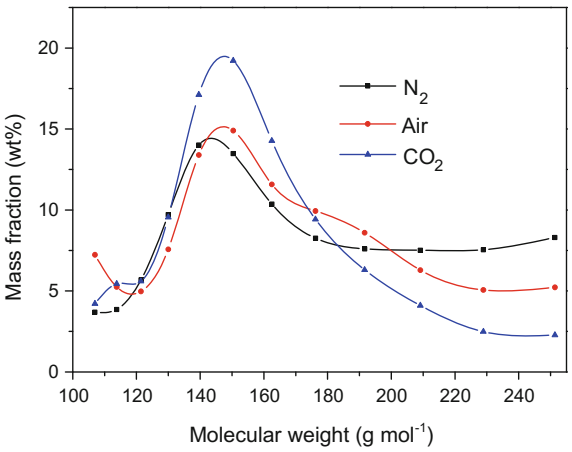

Fig. 4.37 Tar molecular weight distribution of lignin thermochemical conversion under different atmospheres

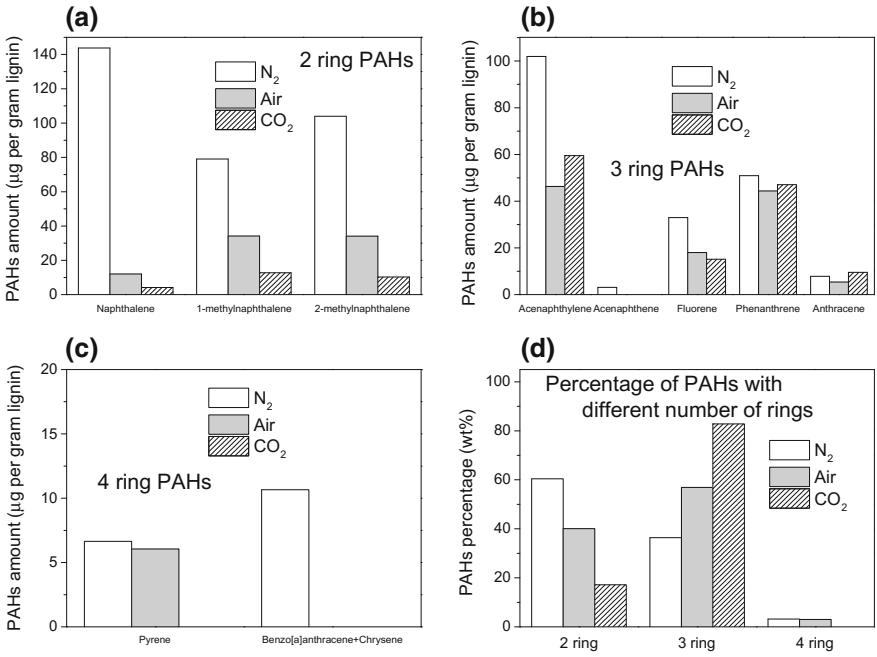

Fig. 4.38 PAHs generation of lignin thermochemical conversion under different atmospheres

The percentages of PAHs with different number of rings are shown in Fig. 4.38d. Air and CO_2 atmosphere had lower 2-ring PAHs percentages, which was consistent with the SEC results in Fig. 4.37.

4.3.2 *Influence of Atmosphere on PVC Thermochemical Conversion*

4.3.2.1 Influence of Atmosphere on Kinetics of PVC Thermochemical Conversion

The TG and DTG curves of PVC thermochemical conversion under air and CO_2 atmosphere are shown in Fig. 4.39. Similar to lignin, three curves were overlapped at beginning. At 300–350 °C, CO_2 presented inhibition effect on mass loss. Above 400 °C, air had obvious inhibition effect on PVC mass loss. Finally, the residue under air atmosphere was almost zero, while the gasification in CO_2 did not finish at 1000 °C. As shown by the DTG curves in Fig. 4.39, reactions in N_2 and air were similar below 400 °C, while reactions in N_2 and CO_2 were similar above 400 °C.

The kinetic parameters of PVC thermochemical conversion under different atmospheres are shown in Table 4.5. The reactions under every atmosphere could be described by three paralleled reactions, while the percentage of each paralleled reaction was different, which indicated that the paralleled reactions were not real independent reactions. The activated energies of these paralleled reactions varied from 142 to 268 kJ mol^{-1}, the reaction orders were around 1.5, and the *ADIs* were less than 2. The calculation results from PA-LSM are shown in Fig. 4.40.

The TG and DTG curves of PVC pyrolysis/gasification in Macro-TGA under different atmospheres are shown in Fig. 4.41. The mass loss in air was the fastest, followed by CO_2 and N_2, which was different from the slow reaction in TGA. Under different conditions, the residue mass was similar. The thermochemical

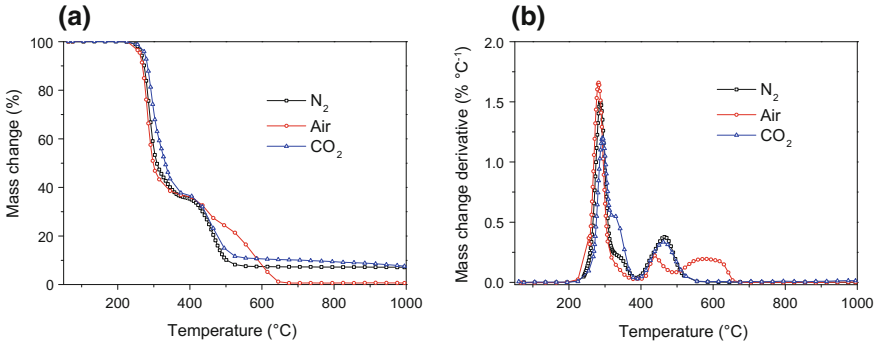

Fig. 4.39 TG and DTG curves of PVC thermochemical conversion in TGA under different atmospheres

Table 4.5 Kinetic parameters of PVC thermochemical conversion in TGA under different atmospheres

Atmosphere	Reaction	Percentage (%)	Peak temperature (°C)	E (kJ mol^{-1})	A (min^{-1})	n	ADI
N_2	1	55.3	286.5	244	4.99×10^{22}	1.54	1.76
	2	13.5	335.9	179	1.13×10^{15}	1.50	1.72
	3	31.4	461.3	181	2.93×10^{12}	1.47	1.68
Air	1	61.0	282.2	234	8.74×10^{21}	1.54	1.76
	2	11.1	442.5	265	1.32×10^{19}	1.52	1.75
	3	27.9	573.7	142	1.15×10^{8}	1.41	1.60
CO_2	1	41.7	292.0	268	4.82×10^{24}	1.55	1.77
	2	28.1	332.2	210	7.40×10^{17}	1.52	1.74
	3	30.2	461.8	177	1.33×10^{12}	1.47	1.67

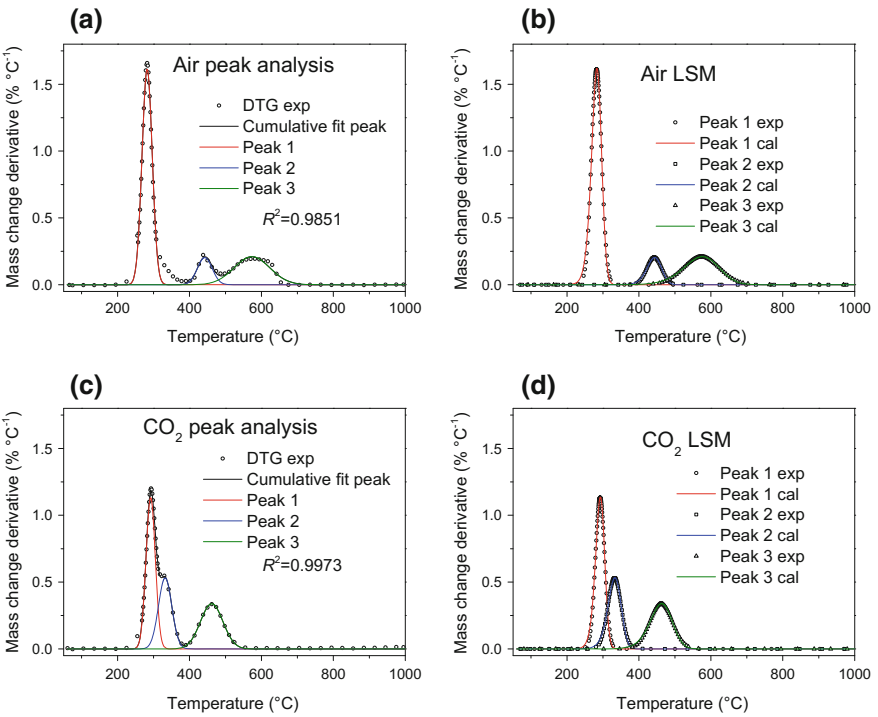

Fig. 4.40 Kinetic calculation of PVC thermochemical conversion in TGA under air and CO_2

conversion indexes are shown in Fig. 4.42. The reaction end time in air was shortest and that in N_2 was the longest. The maximum mass loss time in air was the earliest. For maximum mass loss rates and thermochemical conversion indexes,

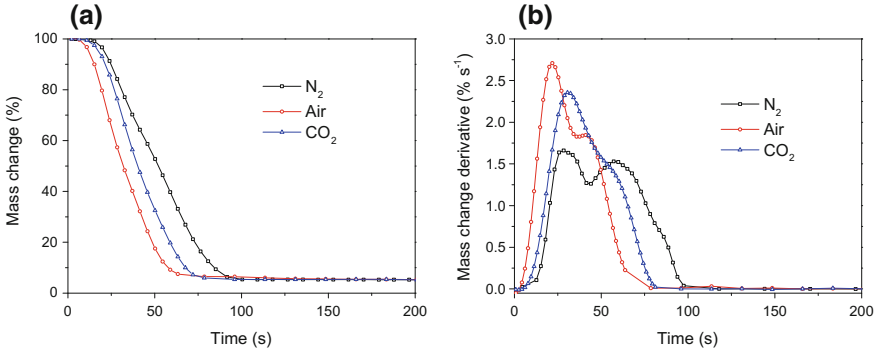

Fig. 4.41 TG and DTG curves of PVC thermochemical conversion in Macro-TGA under different atmospheres

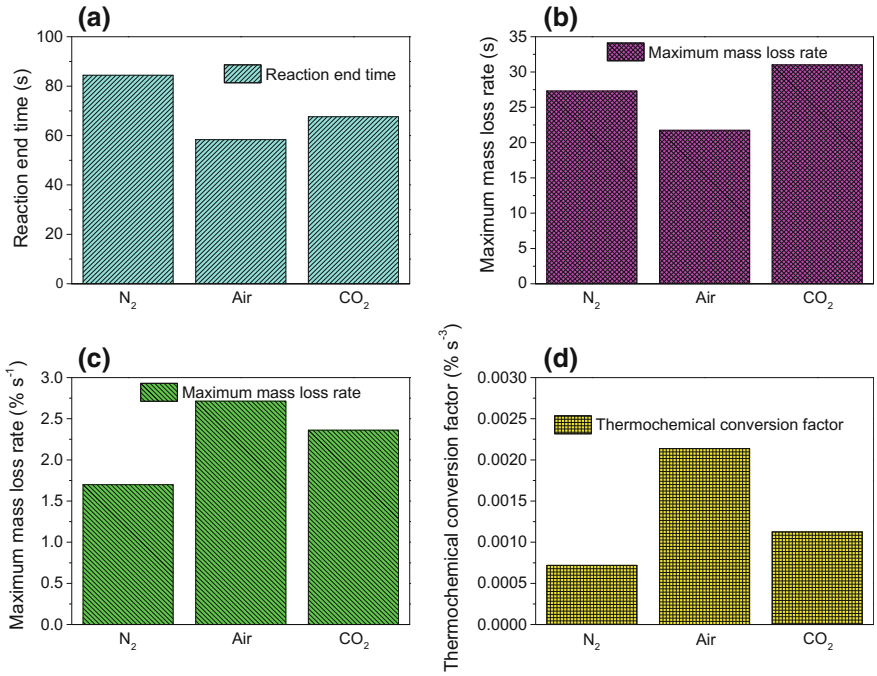

Fig. 4.42 PVC thermochemical conversion indexes under different atmospheres

air > CO_2 > N_2. The reason was that for thermochemical conversion in air or CO_2 at a high temperature (800 °C), gasification and pyrolysis almost happened at the same time.

The kinetic parameters are shown in Table 4.6. Each reaction could be simulated by two paralleled reactions, with the reaction order between 3 and 4. The results of

Table 4.6 Kinetic parameters of PVC thermochemical conversion in Macro-TGA under different atmospheres

Temperature (°C)	Reaction	Percentage (%)	k	n	R^2
N_2	1	27.8	2.55×10^{-6}	3.73	0.9996
	2	72.2	2.43×10^{-7}	3.64	0.9997
Air	1	46.2	3.90×10^{-5}	3.24	0.9999
	2	53.8	1.54×10^{-7}	4.11	0.9993
CO_2	1	55.2	5.10×10^{-6}	3.48	0.9998
	2	44.8	2.37×10^{-9}	4.88	0.9986

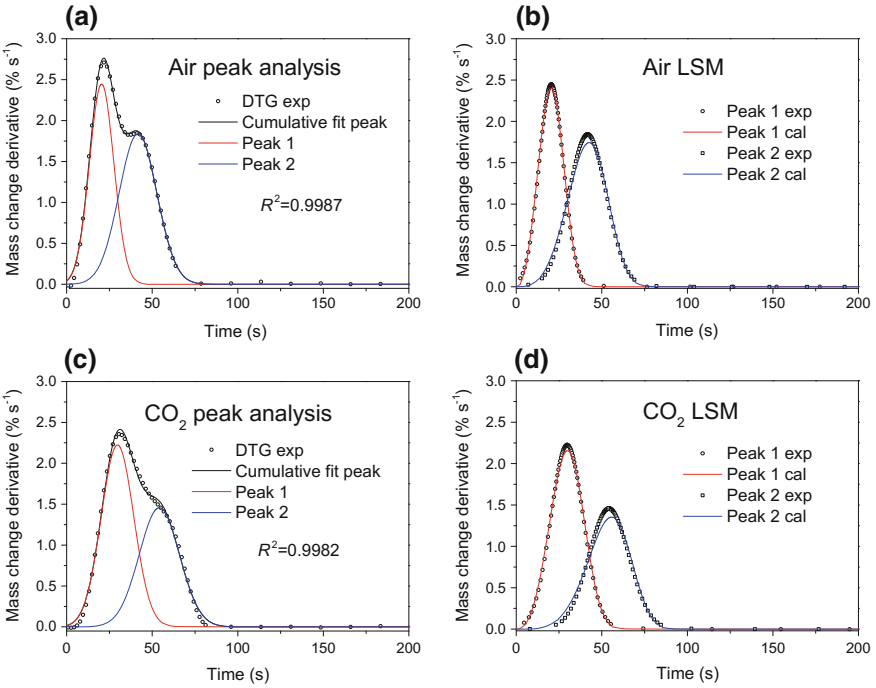

Fig. 4.43 Kinetic calculation of PVC thermochemical conversion in Macro-TGA under air and CO_2

kinetic calculation are shown in Fig. 4.43, which indicated that the mass loss characteristics could be simulated quite accurately by kinetic parameters.

4.3.2.2 Influence of Atmosphere on Product Distribution of PVC Thermochemical Conversion

The influence of different atmospheres on product distribution is shown in Fig. 4.44. For reactions under air or CO_2 atmosphere, HCl decreased by 31.6 and

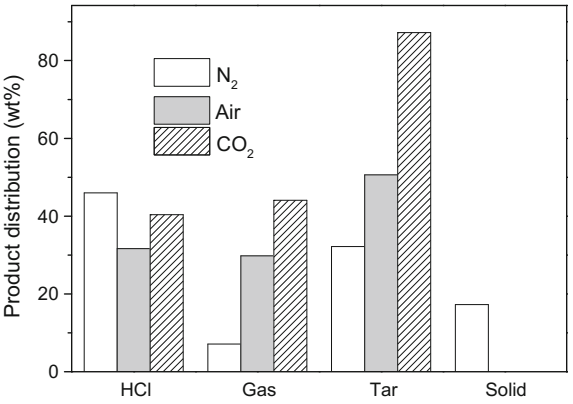

Fig. 4.44 Product distribution of PVC thermochemical conversion under different atmospheres

40.4%, respectively. The gasification under air atmosphere generated more gas (29.8%) and tar (50.6%), while the gasification under CO_2 atmosphere generated the most gas (44.1%) and tar (87.6%), due to the reaction between CO_2 and char.

4.3.2.3 Influence of Atmosphere on Gas Production of PVC Thermochemical Conversion

The gas products from PVC under different atmospheres are shown in Fig. 4.45. Some CO (63.8 ml/g PVC) and CO_2 (74.6 ml/g PVC) were generated under air atmosphere, while the gasification under CO_2 atmosphere generated the most CO (322.7 ml/g PVC). The large amount of CO came from the reaction between CO_2 and char (Kwon and Castaldi 2012).

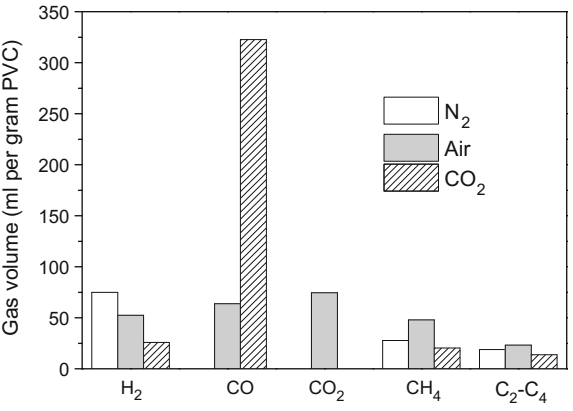

Fig. 4.45 Gas production of PVC thermochemical conversion under different atmospheres

4.3.2.4 Influence of Atmosphere on PAHs Formation of PVC Thermochemical Conversion

The 2, 3, and 4-ring PAHs from PVC under different atmospheres are shown in Fig. 4.46. Compared to the pyrolysis in N_2, gasification in air generated more naphthalene, while the amount of methylnaphthalene was comparable. Reaction in air generated less fluorene and phenanthrene and far less other PAHs than those in N_2. Gasification in CO_2 generated less 2-ring PAHs and more other PAHs than that in air.

The percentages of 2, 3, and 4-ring PAHs are shown in Fig. 4.46d. Compared to that in N_2, the reaction in air generated more percentage of 2-ring PAHs (80.1%) and less percentages of 3-ring PAHs (18.9%) and 4-ring PAHs (1.1%). On the contrary, compared to that in N_2 atmosphere, gasification in CO_2 generated more percentage of 3-ring PAHs (43.8%) and less percentage of 4-ring PAHs (3.3%).

This section obtained the influence of different atmospheres (N_2, air, and CO_2) on the thermochemical conversion of lignin and PVC on TGA and fixed bed reactor. Gasification in air or CO_2 generated more gas and tar, while pyrolysis in N_2 generated more PAHs.

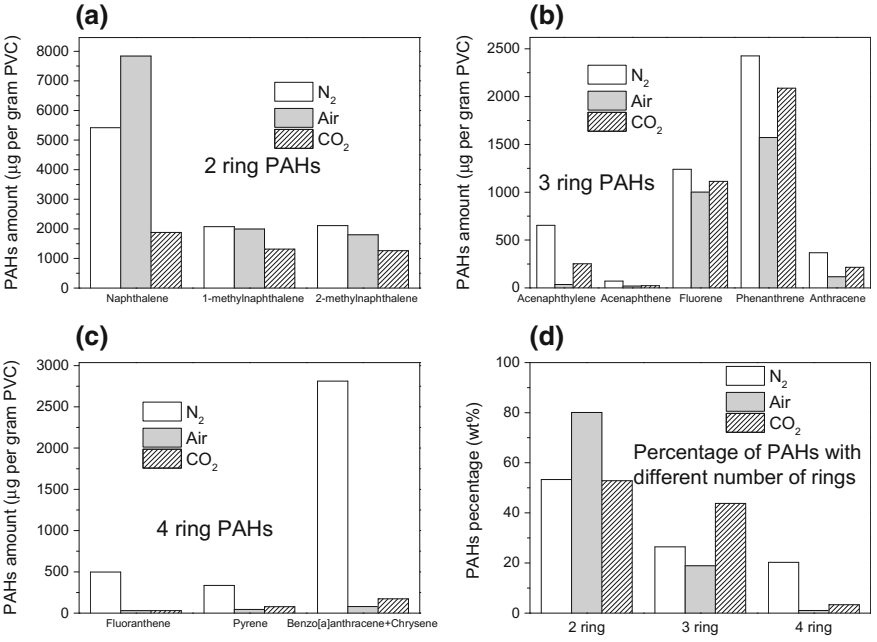

Fig. 4.46 PAHs generation of PVC thermochemical conversion under different atmospheres

4.4 Influence of Inorganics

CSW contains more chlorine (0.8–2.5%) than coal and biomass (Zhou et al. 2014a). Chlorine may have a significant influence on the generation of PAHs. The common chlorine forms in CSW are organic chlorine (such as PVC) and inorganic chlorine (such as NaCl). Organic chlorine itself could lead to PAHs, as discussed in Chap. 3. This section investigated the effect of inorganic chlorine (NaCl). Lignin and PVC were also selected as the representatives. NaOH was investigated to compare with NaCl. The reason for choosing NaOH was due to only H_2O was generated during the thermochemical conversion process. Meanwhile, some studies have shown that Cu^{2+} might have a remarkable influence on PAHs generation (Wang et al. 2002). Therefore, the influence of $CuCl_2$ was also investigated.

During the experiments, the concentration of additives was 0.001 mol g^{-1}. The inorganics were added in the form of solution and then dried to have uniform dispersion.

4.4.1 Influence of Inorganics on Lignin Pyrolysis

4.4.1.1 Influence of Inorganics on Product Distribution of Lignin Pyrolysis

The mass balances of lignin pyrolysis with the addition of NaCl, NaOH, and $CuCl_2$ are shown in Table 4.7. The mass balances were between 94.5 and 99.7%, which indicated the accuracy of the experiments. The influence of different additives on product distribution is shown in Fig. 4.47. As shown in Fig. 4.47, NaCl and NaOH had no significant influence on pyrolysis product distribution. Kleen (1995) investigated lignin pyrolysis and found that Na^+ had no considerable influence on the volatile generation. However, some studies have shown that the addition of NaCl could increase the formation of char during cellulose pyrolysis (Williams and Horne 1994), which indicated that the influence of NaCl on cellulose and lignin pyrolysis was different. When $CuCl_2$ was added, solid amount decreased and tar amount increased. The reason might be that at high temperatures, low boiling point (430 °C) CuCl was generated from $CuCl_2$, which would go into tar.

Table 4.7 Mass balance of lignin pyrolysis with different additives

Additives	w/o Inorganics	NaCl	NaOH	$CuCl_2$
Mass balance (wt%)	99.5	99.7	94.5	99.1

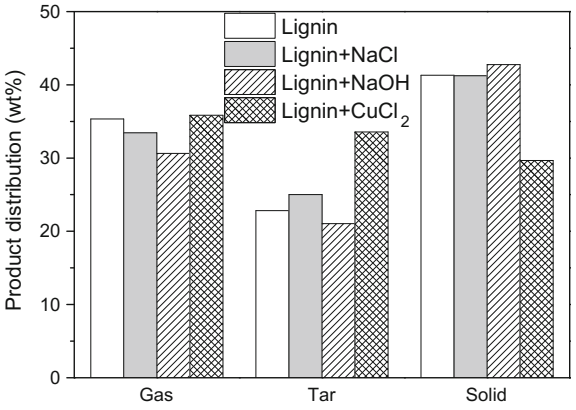

Fig. 4.47 Product distribution of lignin pyrolysis with different inorganics

4.4.1.2 Influence of Inorganics on PAHs Formation of Lignin Pyrolysis

The influence of different additives on PAHs generation from lignin pyrolysis is shown in Fig. 4.48. With the addition of NaCl, the generation of all PAHs decreased significantly. For example, naphthalene amount decreased from 143.8 to 2.5 μg/g lignin, and acenaphthylene amount decreased from 102.0 to 26.9 μg/g lignin. Benzo[*a*]anthrathene and chrysene were not detected with the addition of NaCl. The experiments of Kuroda et al. (1990) have shown that NaCl could inhibit the generation of guaiacol from lignin pyrolysis at 500 °C, while PAHs were typical guaiacol derivatives. The inhibited effect of NaOH was similar with that of NaCl. With the addition of NaCl or NaOH, PAHs total amount decreased from 541.0 to ~80 μg/g lignin. With the addition of $CuCl_2$, all PAHs decreased and the total amount decreased from 541.0 to 267.0 μg/g lignin. As shown in Fig. 4.47 and 4.48, cation was the main factor that affected lignin pyrolysis, while the mechanisms needed further study.

With different additives in lignin, the morphologies of residue are shown in Fig. 4.49, and the energy dispersive X-ray spectroscopy (EDX) results are shown in Table 4.8. With the addition of NaCl, the morphology of residue did not change significantly, while the EDX results showed that Na presented mainly in the solid in the form of chloride or oxide. With the addition of NaOH, the morphology of residue changed significantly. There were many short fibers, as shown in Fig. 4.49c. The EDX showed that Na was mainly in the form of oxide. With the addition of $CuCl_2$, some fine particles occurred in the solid, and Cu presented in the forms of both chloride and oxide.

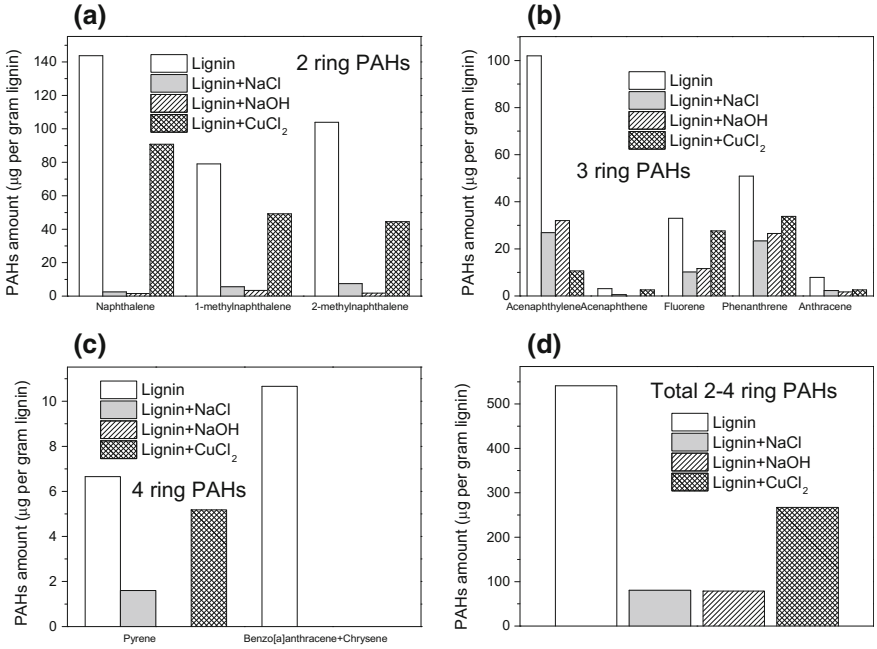

Fig. 4.48 PAHs generation of lignin pyrolysis with different inorganics

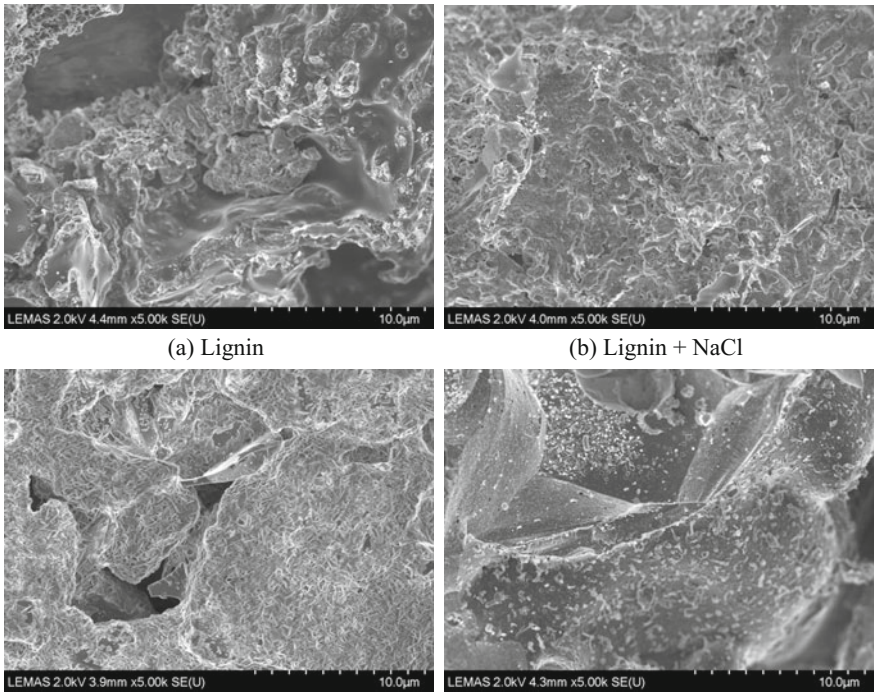

(a) Lignin (b) Lignin + NaCl

(c) Lignin + NaOH (d) Lignin + $CuCl_2$

Fig. 4.49 Char morphology of lignin pyrolysis with different inorganics

Table 4.8 Influence of different additives on composition of solid residue of lignin pyrolysis

Sample	C (wt%)	O (wt%)	Na (wt%)	Cl (wt%)	S (wt%)	Cu (wt%)
Lignin	82.42	2.36	4.71	–	0.06	–
Lignin + NaCl	59.76	12.00	11.26	15.24	1.14	–
Lignin + NaOH	47.94	29.36	17.44	–	4.57	–
Lignin + $CuCl_2$	66.71	11.57	5.49	5.35	3.83	7.06

4.4.2 Influence of Inorganics on PVC Pyrolysis

4.4.2.1 Influence of Inorganics on Product Distribution of PVC Pyrolysis

With the addition of NaCl, NaOH, or $CuCl_2$, the mass balance of PVC pyrolysis is shown in Table 4.9. The mass balance was between 97.1 and 102.5%, which indicated the good accuracy of the experiments. As shown in Fig. 4.50, with the addition of NaCl, HCl decreased, while tar and solid increased. With the addition of NaOH, HCl and solid decreased, and the amount of tar increased. The reason might be that water was formed from the reaction of NaOH and HCl, which presented in the tar (Masuda et al. 2006; Hayashi et al. 2010). However, the inhibited mechanism of NaCl on HCl generation was not clear. With the addition of $CuCl_2$, HCl generation did not change significantly. The amount of tar decreased, and solid residue amount increased. Cheng and Liang (2000) also reported that $CuCl_2$ addition led to the increase in solid residue amount, as $CuCl_2$ was a Lewis acid (Müller et al. 1997; Müller and Dongmann 1998). Lewis acid could catalyze the Friedel–Crafts alkylation reaction: The positively charged carbon atoms could react with the alkene-rich sequence with an electron, which could catalyze intermolecular cross-linking reactions and form char eventually (Montaudo and Puglisi 1991; Müller and Dongmann 1998). From Figs. 4.47 and 4.50, it could also be concluded that the influence of inorganics on pyrolysis of lignin and PVC was different.

4.4.2.2 Influence of Inorganics on PAHs Formation of PVC Pyrolysis

The influence of three inorganics on PAHs generation from PVC pyrolysis is shown in Fig. 4.51. The addition of NaCl had a significant influence on PAHs generation

Table 4.9 Mass balance of PVC pyrolysis with different additives

Sample	PVC	PVC + NaCl	PVC + NaOH	PVC + $CuCl_2$
Mass balance (wt%)	102.5	97.1	99.0	99.8

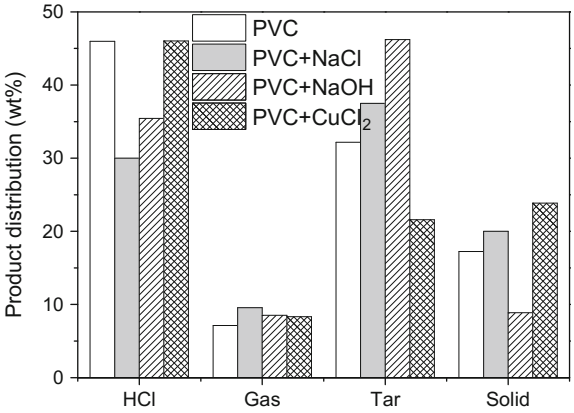

Fig. 4.50 Product distribution of PVC pyrolysis with different inorganics

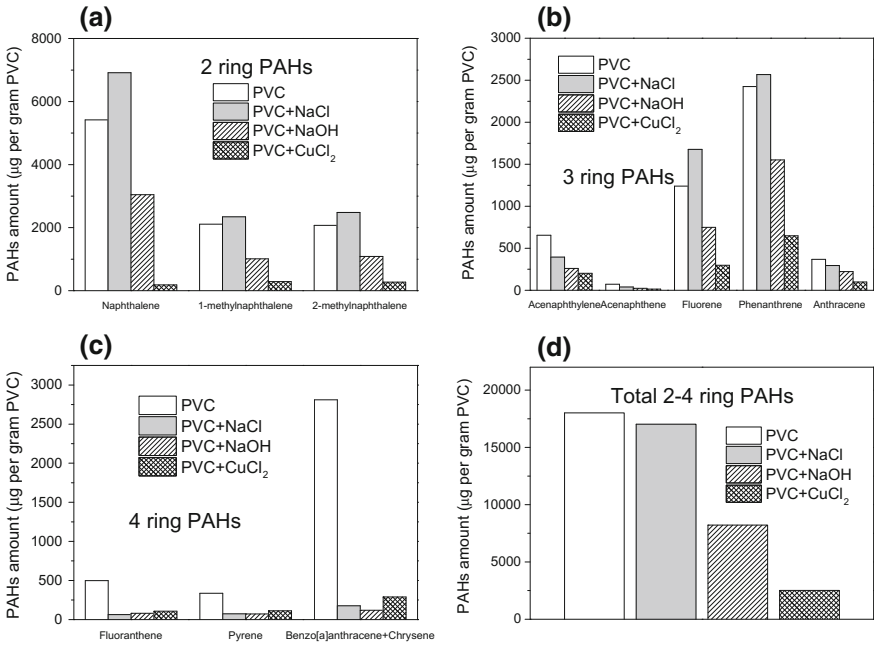

Fig. 4.51 PAHs generation of PVC pyrolysis with different inorganics

from PVC pyrolysis. Therein, it had an obvious inhibited effect on the generation of 2-ring and 3-ring PAHs and promoted effect on the generation of 4-ring PAHs. NaOH had inhibited effect on all the PAHs. It had been reported by Masuda et al. (2006) that during PVC pyrolysis, with the addition of oxides, the generation of benzene was inhibited, while benzene was proved to be the precursor of PAHs

(Shukla and Koshi 2012). $CuCl_2$ had the most obvious inhibited effect on PAHs generation, as shown in Fig. 4.51. The research of Cheng and Liang (2000) has shown that $CuCl_2$ could inhibit the second step reaction of PVC pyrolysis (chain scission reaction). According to the report of Montaudo and Puglisi (1991), the inhibition on PAHs was due to the catalytic effect of Lewis acids. Therefore, with the addition of $CuCl_2$, the amount of tar and PAHs decreased. The total amount of PAHs is shown in Fig. 4.51d. The total PAHs amount from high to low was: without additives > NaCl > NaOH > $CuCl_2$.

The morphologies of solid residue from PVC pyrolysis with different additives are shown in Fig. 4.52. Without additives, the main composition of the solid was carbon; with the addition of NaCl, crystalline could be found, as shown in Fig. 4.52b. With the addition of NaOH, there were some fine particles; with the addition of $CuCl_2$, the particles were larger. From Fig. 5.52, the influences of different inorganics on solid residue morphology were significantly different.

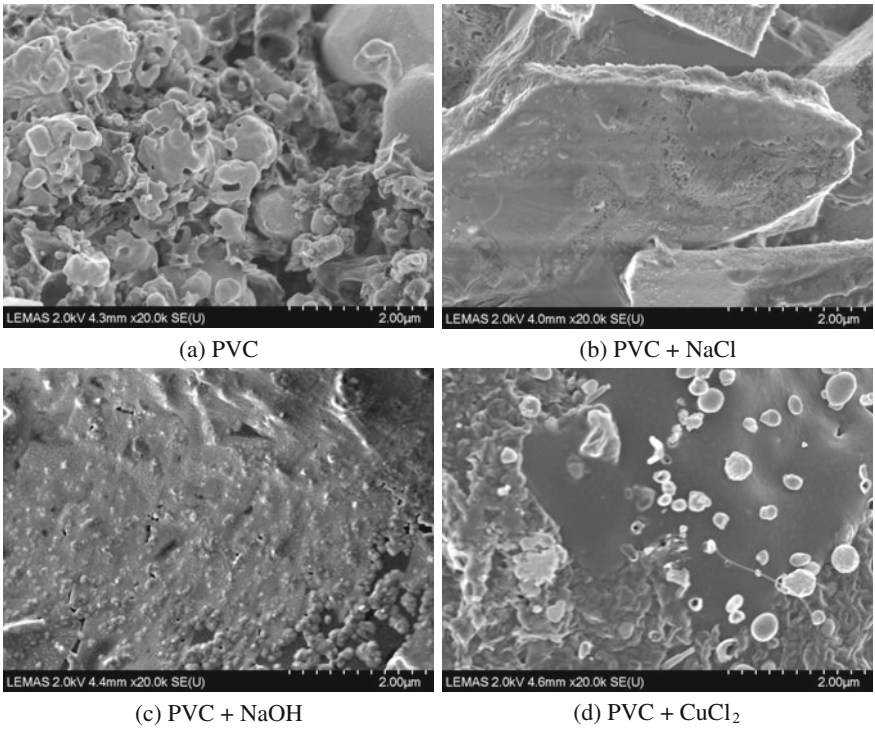

(a) PVC (b) PVC + NaCl

(c) PVC + NaOH (d) PVC + $CuCl_2$

Fig. 4.52 Char morphology of PVC pyrolysis with different inorganics

4.5 The Mechanisms of Lignin and PVC Pyrolysis and PAHs Formation

4.5.1 The Mechanisms of Lignin Pyrolysis and PAHs Formation

From the pyrolysis tar of lignin, phenol, *o*-cresol, *p*-cresol, *m*-cresol, guaiacol, 3,5-xylenol, 3,4-xylenol, 2,5-xylenol, and 3-ethyl-5-methylphenol could be clearly detected. Asmadi et al. (2011b, c) proposed that cresol and xylenol were PAHs precursors. The generation of derivatives of benzenes and phenols at different temperatures is shown in Fig. 4.53. Phenol could be detected at all the temperatures. The study by Jiang et al. (2010) has shown that in pyrolysis-gas chromatography/mass spectrometry (Py-GC/MS) experiments, the generation of phenol increased with the increase in reaction temperature from 400 to 800 °C. As shown in Fig. 4.53, at 500 °C, ethylguaiacol, dimethoxytoluene, methylguaiacol, and xylene could be identified in the tar. When the temperature increased to 600 °C, these four compounds disappeared, while alkylbenzene, guaiacol, and anisole were formed from demethylation and demethoxylation. With the increase in temperature to 700 °C, guaiacol and anisole could not be detected anymore, which indicated the completion of demethoxylation. At 900 °C, xylenol and cresol could not be detected due to the dehydroxylation reaction.

Asmadi et al. (2011b) have reported that from 400 to 600 °C, syringols and guaiacols decreased. In our study, catechols and pyrogallols could not be detected because they were very reactive. As shown in Fig. 4.53, there were three different secondary reactions: dehydroxylation, demethoxylation (including OCH_3 homolysis), and demethylation, and these three secondary reactions could happen

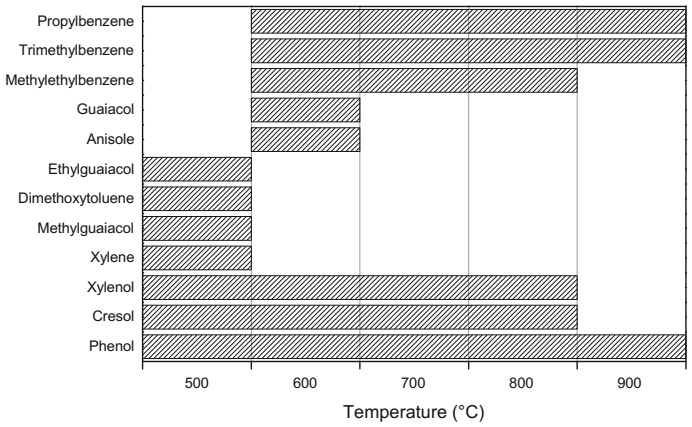

Fig. 4.53 Generation of benzene and phenol derivatives from lignin pyrolysis at different temperatures. Reprinted with the permission from Zhou et al. (2014b). Copyright 2014 American Chemical Society

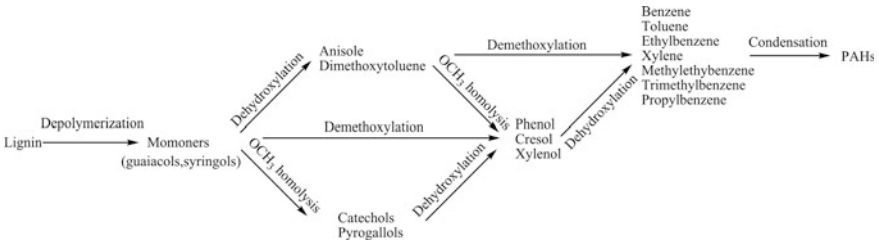

Fig. 4.54 PAHs generation mechanisms from lignin pyrolysis. Reprinted with the permission from Zhou et al. (2014b). Copyright 2014 American Chemical Society

simultaneously. The pyrolysis/gasification mechanisms of lignin are summarized in Fig. 4.54. Demethylation processes are not noted in the figure to simplify the discussion. Monomers (such as catechol and pyrogallols) were formed from lignin pyrolysis at first; then benzene derivatives were formed from dehydroxylation and demethoxylation; and demethylation happened at the same time. As shown in Fig. 4.54, methoxyls could only be detected below 700 °C, which indicated that demethoxylation reactions were completed below 700 °C. More hydroxyls and methyls were detected at low temperatures, and more derivatives of benzene were detected at high temperatures. With the increase in temperature, secondary reactions (demethoxylation, dehydroxylation, and demethylation) were promoted. Research has shown that PAHs could be formed from benzene, as shown in 3.5, and these reactions were also promoted at higher temperatures (Mastral and Callén 2000). Therefore, with the increase in temperature, PAHs generation increased. In addition, due to demethylation, methylnaphthalene decreased at 900 °C. The gas product amount from lignin pyrolysis was low, which demonstrated PAHs were not formed from the condensation of alkenes. Taking coniferyl alcohol monomer as an example, the secondary reactions are shown in Fig. 4.55. This figure provides a more intuitional explanation.

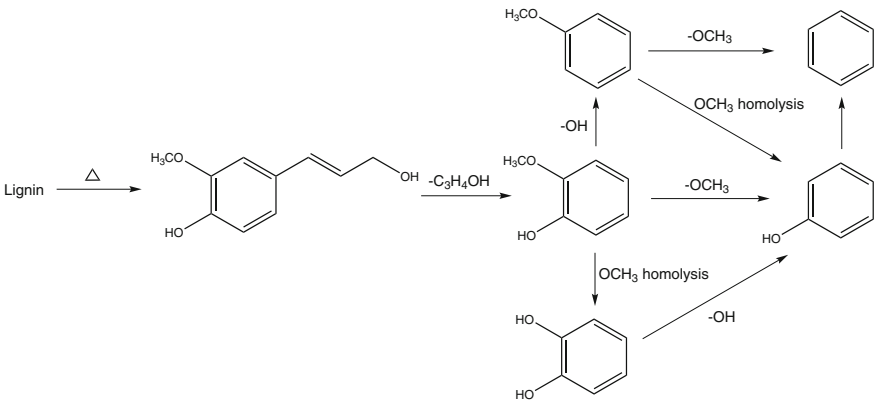

Fig. 4.55 Pyrolysis mechanisms of coniferyl alcohol

For lignin slow pyrolysis, monomers could be formed at a relatively low temperature (300–350 °C) (Asmadi et al. 2011c), while secondary reactions needed a higher temperature. Compared to fast pyrolysis, slow pyrolysis generated more tar, less gas, and less PAHs. At a low temperature, monomers could be formed while secondary reactions are unlikely to happen, and thus the intermediates could come out from reactor to tar condenser. The analysis of slow pyrolysis tar proved this process, where large amounts of methylguaiacols, demethoxytoluene, ethylguaiacol, and syringol were detected, while the concentrations of benzene derivatives were low.

With the presence of oxidizers (air or CO_2), the intermediates from lignin pyrolysis (Fig. 5.53) might be oxidized, and thus less PAHs were generated. GC/MS results showed that the amounts of benzenes and phenols were very low in the tar, which proved this speculation.

4.5.2 *The Mechanisms of PVC Pyrolysis and PAHs Formation*

The mechanisms of PVC pyrolysis are shown in Fig. 4.56. Research has shown that PVC pyrolysis had two steps: dechlorination and chain scission (Ma et al. 2002). In the process of slow pyrolysis, dechlorination is a slow process, and thus all the Cl will be present in the form of HCl (Williams and Williams 1999; McNeill et al. 1995). In the process of fast pyrolysis, chlorination and chain scission happen simultaneously in a short time, and thus the chlorination may be not completed, as shown in Fig. 4.56. The influence of fast pyrolysis temperature on HCl generation also supported this speculation, because high pyrolysis temperature meant high heating rate.

During dechlorination process, C=C double bonds were formed at the same time, which were the source of aromaticity. It should be noted that aliphatics could be hardly detected in the tar from PVC pyrolysis, and the amount of alkenes in the gas phase was also very low (Fig. 3.20), which demonstrated that during PVC pyrolysis, aromatic rings could be formed directly from polymer molecular reactions instead of Diels–Alder reactions.

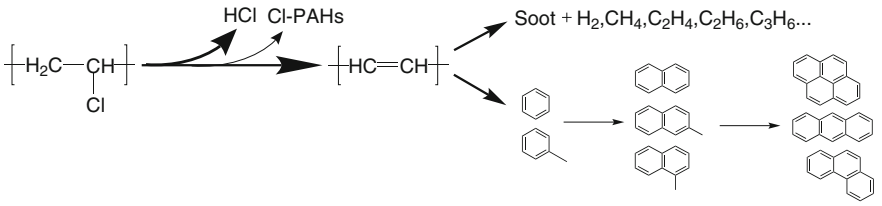

Fig. 4.56 Proposed mechanism of PAHs formation from pyrolysis of PVC. Reprinted from Zhou et al. (2016), Copyright 2016, with permission from Elsevier

The study by Gui et al. (2013) has shown that in PVC pyrolysis, 2-ring aromatics increased from 7.02 to 31.75% with the increase in temperature from 500 to 800 °C. At 500 °C, 2-ring aromatics increased from 7.02 to 50.33% with residence time increased to 300 s. Large amounts of soot and benzenes were detected from PVC pyrolysis, which suggested that benzenes and soot might be formed simultaneously during chain scission process. With the increase in temperature, secondary reactions would be promoted, and thus more PAHs would be generated (Han and Kim 2008). With the increase in temperature from 700 to 900 °C, methylnaphthalenes were converted to naphthalene, due to the demethylation at high temperatures.

4.6 Summary

This chapter investigated the influence of temperature, heating rate, atmosphere, and inorganics on thermochemical reaction characteristics of lignin (representative of biomass) and PVC (representative of plastics). The thermochemical reaction characteristics here include kinetics in TGA and Macro-TGA, product distribution characteristics, gas production characteristics, and PAHs formation characteristics. Furthermore, the pyrolytic mechanisms of these two substances were explored.

(1) The influence of temperature (500–900 °C) on the pyrolysis of lignin and PVC was obtained. With the increase in temperature, the maximum mass loss time decreased, the maximum mass loss rate increased, and the pyrolytic index increased. With the increase in temperature from 500 to 900 °C, the gas amount increased and total PAHs amount increased. For lignin, tar amount decreased with temperature due to secondary reactions; while for PVC, HCl amount decreased and tar amount increased with the increase in temperature.
(2) The influence of heating rate on the pyrolysis of lignin and PVC was obtained. Compared to fast pyrolysis, slow pyrolysis generated less gas and PAHs. For lignin, the tar amount from slow pyrolysis was higher than that from fast pyrolysis; for PVC, slow pyrolysis generated more HCl and less tar compared to fast pyrolysis.
(3) The influence of atmosphere (N_2, air, and CO_2) on thermochemical conversion of lignin and PVC was obtained. At low temperatures in TGA, the influence of atmosphere on mass loss was not significant; at high temperatures, both air and CO_2 promoted the mass loss. Compared to N_2, more gas and tar were generated in air of CO_2. Overall, less PAHs were generated in air than in N_2, while gasification in CO_2 generated the least PAHs.
(4) The influence of three inorganics (NaCl, NaOH, and $CuCl_2$) on the pyrolysis of lignin and PVC was obtained. NaCl and NaOH had no significant influence on the product distribution of lignin pyrolysis, while the addition of $CuCl_2$ decreased the solid amount and increased the tar amount. NaCl, NaOH, and $CuCl_2$ all presented inhibited effect on the PAHs formation from pyrolysis of lignin and PVC.

(5) The thermochemical mechanisms of lignin and PVC were obtained. Monomers were first released from lignin pyrolysis. With the increase in temperature, secondary reactions (demethoxylation, dehydroxylation, and demethylation) would be promoted. PAHs could be formed from benzenes, and these reactions were also promoted at higher temperatures. The slow pyrolysis of lignin could release monomers at low temperatures (300–350 °C), while secondary reactions could hardly happen at low temperatures. Therefore, slow pyrolysis generated more tar, less gases, and less PAHs. For gasification in air or CO_2, the intermediates from lignin pyrolysis might be oxidized, and thus less PAHs were formed. PVC pyrolysis had two steps: dechlorination and chain scission. In slow pyrolysis process, dechlorination was a slow process, and thus all the Cl presented in the form of HCl. In fast pyrolysis process, dechlorination and chain scission happened simultaneously in a short time, which meant the dechlorination was not completed, and less HCl was released.

In summary, this chapter obtained the influence of temperature (500, 600, 700, 800, and 900 °C), heating rate (fast, slow), atmosphere (N_2, air, and CO_2), and inorganics (NaCl, NaOH, and $CuCl_2$) on the thermochemical characteristics of lignin and PVC. This chapter was the further exploration based on Chap. 3 and provided the basis for the condition selection for Chaps. 3 and 5.

References

Asmadi M, Kawamoto H, Saka S (2011a) Thermal reactivities of catechols/pyrogallols and cresols/xylenols as lignin pyrolysis intermediates. J Anal Appl Pyrol 92:76–87

Asmadi M, Kawamoto H, Saka S (2011b) Thermal reactions of guaiacol and syringol as lignin model aromatic nuclei. J Anal Appl Pyrol 92:88–98

Asmadi M, Kawamoto H, Saka S (2011c) Gas- and solid/liquid-phase reactions during pyrolysis of softwood and hardwood lignins. J Anal Appl Pyrol 92:417–425

Cheng WH, Liang YC (2000) Catalytic pyrolysis of polyvinylchloride in the presence of metal chloride. J Appl Polym Sci 77:2464–2471

Gordillo G, Annamalai K (2010) Adiabatic fixed bed gasification of dairy biomass with air and steam. Fuel 89:384–391

Gui B, Qiao Y, Wan D et al (2013) Nascent tar formation during polyvinylchloride (PVC) pyrolysis. Proc Combust Inst 34:2321–2329

Han J, Kim H (2008) The reduction and control technology of tar during biomass gasification/pyrolysis: an overview. Renew Sustain Energy Rev 12:397–416

Hayashi S, Amano H, Niki T et al (2010) A new pyrolysis of metal hydroxide-mixed waste biomass with effective chlorine removal and efficient heat recovery. Ind Eng Chem Res 49:11825–11831

Jiang G, Nowakowski DJ, Bridgwater AV (2010) Effect of the temperature on the composition of lignin pyrolysis products. Energy Fuels 24:4470–4475

Kleen M (1995) Influence of inorganic species on the formation of polysaccharide and lignin degradation products in the analytical pyrolysis of pulps. J Anal Appl Pyrol 35:15–41

Kuroda K, Inoue Y, Sakai K (1990) Analysis of lignin by pyrolysis-gas chromatography. I. Effect of inorganic substances on guaiacol-derivative yield from softwoods and their lignins. J Anal Appl Pyrol 18:59–69

Kwon EE, Castaldi MJ (2012) Urban energy mining from municipal solid waste (MSW) via the enhanced thermo-chemical process by carbon dioxide (CO2) as a reaction medium. Bioresour Technol 125:23–29

Ledesma EB, Marsh ND, Sandrowitz AK et al (2002) Global kinetic rate parameters for the formation of polycyclic aromatic hydrocarbons from the pyrolyis of catechol, a model compound representative of solid fuel moieties. Energy Fuels 16:1331–1336

Li XT, Grace JR, Lim CJ et al (2004) Biomass gasification in a circulating fluidized bed. Biomass Bioenerg 26:171–193

Lv P, Yuan Z, Ma L et al (2007) Hydrogen-rich gas production from biomass air and oxygen/steam gasification in a downdraft gasifier. Renewable Energy 32:2173–2185

Ma S, Lu J, Gao J (2002) Study of the low temperature pyrolysis of PVC. Energy Fuels 16:338–342

Mastral AM, Callén MS (2000) A review on polycyclic aromatic hydrocarbon (PAH) emissions from energy generation. Environ Sci Technol 34:3051–3057

Masuda Y, Uda T, Terakado O et al (2006) Pyrolysis study of poly(vinyl chloride)–metal oxide mixtures: quantitative product analysis and the chlorine fixing ability of metal oxides. J Anal Appl Pyrol 77:159–168

McNeill IC, Memetea L, Cole WJ (1995) A study of the products of PVC thermal degradation. Polym Degrad Stab 49:181–191

Montaudo G, Puglisi C (1991) Evolution of aromatics in the thermal degradation of poly(vinyl chloride): a mechanistic study. Polym Degrad Stab 33:229–262

Müller J, Dongmann G (1998) Formation of aromatics during pyrolysis of PVC in the presence of metal chlorides. J Anal Appl Pyrol 45:59–74

Müller J, Dongmann G, Frischkorn CGB (1997) The effect of aluminium on the formation of PAH, Methyl-PAH and chlorinated aromatic compounds during thermal decomposition of PVC. J Anal Appl Pyrol 43:157–168

Sharma RK, Hajaligol MR (2003) Effect of pyrolysis conditions on the formation of polycyclic aromatic hydrocarbons (PAHs) from polyphenolic compounds. J Anal Appl Pyrol 66:123–144

Shukla B, Koshi M (2012) A novel route for PAH growth in HACA based mechanisms. Combust Flame 159:3589–3596

Wang D, Xu X, Zheng M et al (2002) Effect of copper chloride on the emissions of PCDD/Fs and PAHs from PVC combustion. Chemosphere 48:857–863

Wang Z, Wang J, Richter H et al (2003) Comparative study on polycyclic aromatic hydrocarbons, light hydrocarbons, carbon monoxide, and particulate emissions from the combustion of polyethylene, polystyrene, and poly(vinyl chloride). Energy Fuels 17:999–1013

Williams PT, Horne PA (1994) The role of metal salts in the pyrolysis of biomass. Renewable Energy 4:1–13

Williams PT, Williams EA (1999) Interaction of plastics in mixed-plastics pyrolysis. Energy Fuels 13:188–196

Yu H, Zhang Z, Li Z et al (2014) Characteristics of tar formation during cellulose, hemicellulose and lignin gasification. Fuel 118:250–256

Zhou H, Meng A, Long Y et al (2014a) An overview of characteristics of municipal solid waste fuel in China: physical, chemical composition and heating value. Renew Sustain Energy Rev 36:107–122

Zhou H, Wu C, Onwudili JA et al (2014b) Polycyclic aromatic hydrocarbon formation from the pyrolysis/gasification of lignin at different reaction conditions. Energy Fuels 28:6371–6379

Zhou H, Wu C, Onwudili JA et al (2016) Influence of process conditions on the formation of 2–4 ring polycyclic aromatic hydrocarbons from the pyrolysis of polyvinyl chloride. Fuel Process Technol 144:299–304

Chapter 5
Influence of Interactions on the Pyrolytic Characteristics of Basic Components

Abstract In real combustible solid waste (CSW), basic components do not exist independently. Therefore, how to describe real mixtures from basic components involves the interactions of basic components. The interaction effect is a complicated problem involving a large amount of experiments, and the mechanisms are also very complex. In this chapter, we are trying to have a preliminary understand of this problem. Since the number of interaction experiments is large, according to the preliminary tests, we choose two kinds of interacted effect for study. One is the interactions of lignocellulosic components (hemicellulose, cellulose, and lignin), which have high fractions in CSW and usually present together. The other interactions studied in this chapter are the interactions between polyvinyl chloride (PVC) and lignocellulosic basic components. PVC is special due to the high chlorine content. In addition, the preliminary tests have shown that the interactions between PVC and biomass are strong. Limited by the number of experiments, this chapter only studies the mixture of 1:1, as the representative of interactions. Generally speaking, 1:1 is the ratio with relatively strong interacted effect. In this chapter, the slow pyrolysis characteristics in thermogravimetric analyzer (TGA), the fast pyrolysis characteristics in Macro-TGA, and the fast pyrolysis in the horizontal fixed bed reactor are investigated. To study the interacted effect, the experimental results of mixtures are compared with the superposition of single components.

Keywords Combustible solid waste (CSW) · Basic component · Pyrolysis · Polycyclic aromatic hydrocarbons (PAHs) · Interactions

The pyrolysis characteristics of basic components were investigated in Chap. 3, while the influences of temperature, heating rate, atmosphere, and inorganics on thermochemical conversion characteristics of basic components were investigated in Chap. 4. In real combustible solid waste (CSW), basic components do not exist independently. Therefore, how to describe real mixtures from basic components involves the interactions of basic components. The interaction effect is a complicated problem involving a large number of experiments, and the mechanisms are also very complex. In this chapter, we are trying to have a preliminary understand

H. Zhou, *Combustible Solid Waste Thermochemical Conversion*, Springer Theses,
DOI 10.1007/978-981-10-3827-3_5

for this problem. Since the number of interaction experiments is large, according to the preliminary tests, we choose two kinds of interacted effect for study. One is the interactions of lignocellulosic basic components (LBCs) (hemicellulose, cellulose, and lignin), which have high fractions in CSW and usually present together. The other interactions studied in this chapter are the interactions between polyvinyl chloride (PVC) and LBCs. PVC is special due to the high chlorine content. In addition, the preliminary tests have shown that the interactions between PVC and biomass are strong.

Limited by the number of experiments, this chapter only studies the mixture of 1:1, as the representative of interactions. Generally speaking, 1:1 is the ratio with relatively strong interacted effect. In this chapter, the slow pyrolysis characteristics in thermogravimetric analyzer-Fourier transform infrared spectroscopy (TGA-FTIR), the fast pyrolysis characteristics in Macro-TGA, and the fast pyrolysis in the horizontal fixed bed reactor (HFBR) are investigated. To study the interacted effect, the experimental results of mixtures are compared with the superposition of single components, which was widely applied in the previous studies of interactions (Giudicianni et al. 2013; Wang et al. 2011; Hosoya et al. 2007).

5.1 The Interactions of Lignocellulosic Basic Components

5.1.1 Interacted Effects in TGA-FTIR

5.1.1.1 Influence of Interactions on Kinetics

To investigate the interactions of basic components during pyrolysis, the binary mixtures of hemicellulose, cellulose, and lignin were experimental studies with the ratio of 1:1. If there were no interactions of basic components, the TG and derivative thermogravimetric (DTG) curves from the mixture experiments should be overlapped with the linear superposition results. The comparisons of mixture experiments and linear superposition results of basic components are shown in Figs. 5.1, 5.2, and 5.3. To describe the influence of interactions on thermal mass loss quantitatively, TG curve overlap ratio (*OR*) was introduced, which was described as follows:

$$OR = 1 - \frac{\text{The area sandwiched by two curves}}{\text{The total area}} = 1 - \frac{\int_{t_s}^{t_e} |\Delta m(t)| \mathrm{d}t}{(t_e - t_s)(m_s - m_e)} \quad (5.1)$$

In this equation, $|\Delta m(t)|$ denoted the absolute value of the vertical coordinate difference of two curves at corresponding temperatures; t_s, t_e, m_s, and m_e denoted start temperature, end temperature, initial mass (100%), and residue mass,

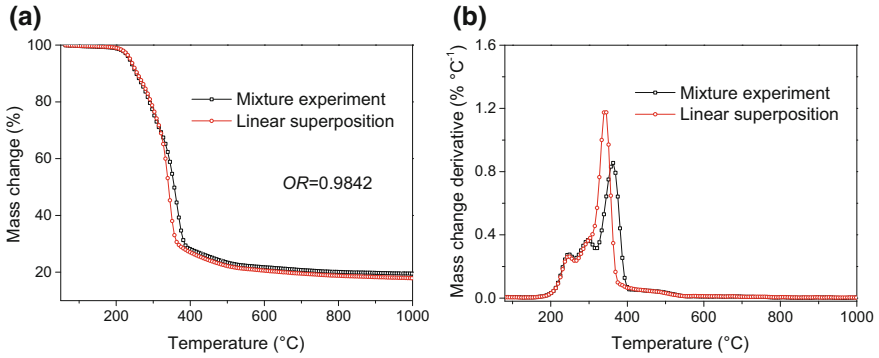

Fig. 5.1 The pyrolysis TG and DTG curves of hemicellulose/cellulose mixture in TGA. Reprinted from Long et al. (2016), with kind permission from Springer Science + Business Media

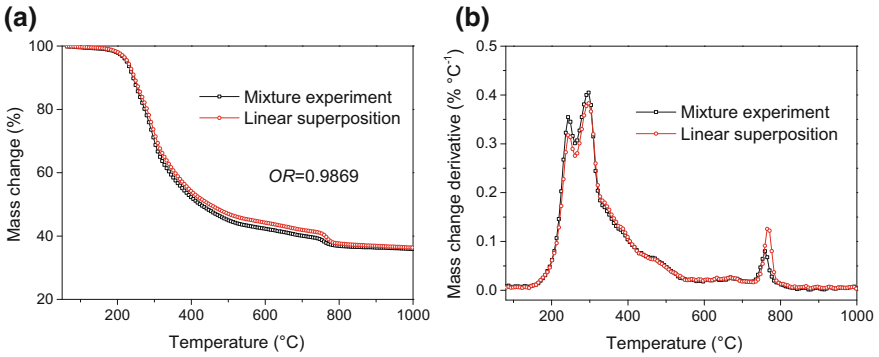

Fig. 5.2 The pyrolysis TG and DTG curves of hemicellulose/lignin mixture in TGA. Reprinted from Long et al. (2016), with kind permission from Springer Science + Business Media

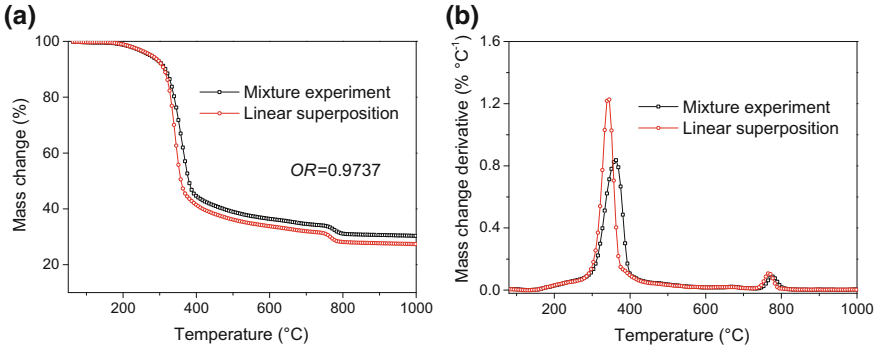

Fig. 5.3 The pyrolysis TG and DTG curves of cellulose/lignin mixture in TGA. Reprinted from Long et al. (2016), with kind permission from Springer Science + Business Media

respectively. $OR = 1$ denoted that two curves were overlapped and $0 \leq OR < 1$ in other conditions.

N sets of data were exported from TG curve, and OR could be defined as follows:

$$OR = 1 - \frac{(t_e - t_s)\lim\limits_{N\to\infty}\frac{\sum\limits_{N}|\Delta m(t)|}{N}}{(t_e - t_s)(m_s - m_e)} = 1 - \lim_{N\to\infty}\frac{\sum\limits_{N}|\Delta m(t)|}{N} \tag{5.2}$$

In the real calculation, N was chosen as 16,000, which was large enough to reflect the complete characteristics of a TG curve. Preliminary tests have shown that the influence was small when N was larger.

As shown in Fig. 5.1, the difference between mixture experiment and linear superposition of hemicellulose and cellulose was insignificant, with the OR 0.9842. While the difference of the corresponding DTG curves was relatively significant, which demonstrated that DTG curve was more sensitive than TG curve. Stefanidis et al. (2014) studied the co-pyrolysis of hemicellulose and cellulose in TGA and found that the TG curves from mixture experiments agreed well with those from linear superposition, while there was a significant difference between DTG curves. Interactions had no significant influence on the pyrolytic peak of hemicellulose, while moved the pyrolytic peak of cellulose later (from 342 to 362 °C).

The TG overlap ratio of hemicellulose and lignin was as high as 0.9869, and the DTG curves were almost coincident, as shown in Fig. 5.2. The final residue mass at 1000 °C of mixture experiment and linear superposition result was similar, which was consistent with the steam gasification of Giudicianni et al. (2013). Wang et al. (2008) investigated the co-pyrolysis of hemicellulose and lignin in TGA and also found that they did not present significant interactions.

In comparison, the co-pyrolysis of cellulose and lignin presented strong interactions in TGA, with the OR 0.9737. As shown in Fig. 5.3, the mixture of cellulose and lignin had inhibited effect on co-pyrolysis, and the residue mass was increased. Worasuwannarak et al. (2007) studied the pyrolysis of cellulose and lignin with the heating rate of 10 °C min^{-1} and found that interactions decreased tar amount and increased char formation, which was consistent with our study. As shown in Figs. 5.2b and 5.3b, the interaction effect of cellulose and lignin was similar to that of hemicellulose and lignin.

Considering the results in Figs. 5.1b and 5.2b, the pyrolysis of hemicellulose was not affected significantly by cellulose or lignin, and thus, the peak below 300 °C did not change obviously. However, considering the results in Figs. 5.1b and 5.3b, the pyrolysis of cellulose was inhibited by the presence of hemicellulose or lignin. The reason might be that the start temperature of the pyrolysis of hemicellulose or lignin was low, and the char formed could impede the heat and mass transfer of unreacted cellulose. Hosoya et al. (2007) and Wang et al. (2011) emphasized the influence of mass transfer, while Stefanidis et al. (2014) deemed that the effect of heat transfer was also very important.

Many studies involved the effect of ash during biomass pyrolysis, and the common conclusion was that ash could catalyze biomass pyrolysis and made DTG peak move earlier (Horne and Williams 1996). In Figs. 5.1b and 5.3b, the catalytic effect of ash from hemicellulose and lignin on cellulose pyrolysis was not observed, and the reason might be that the mechanical mixture of ash and cellulose could not give play to the catalytic effect of ash. The study of Couhert et al. (2009) has shown that ash had only slight effect on biomass pyrolysis when they were mechanically mixed.

5.1.1.2 Influence of Interactions on Gas Production

To investigate the influence of interactions on pyrolysis gas products, the gas production from mixture experiments and linear superposition results in TGA-FTIR was compared. The mixture results of hemicellulose and cellulose are shown in Fig. 5.4. As shown in Fig. 5.4a, the third peak of CO_2 production obtained from mixture experiment was higher than that of linear superposition. Combining Fig. 5.4b and c, the third peaks of CO and carbonyls from mixture experiments were also higher. The third peak at around 350 °C was from the pyrolysis of cellulose, which indicated that the addition of hemicellulose promoted the gas production of cellulose pyrolysis. Giudicianni et al. (2013) conducted the co-gasification of hemicellulose and cellulose and found that CO_2 and CO were all increased in mixture experiments, which was consistent with the results of this study.

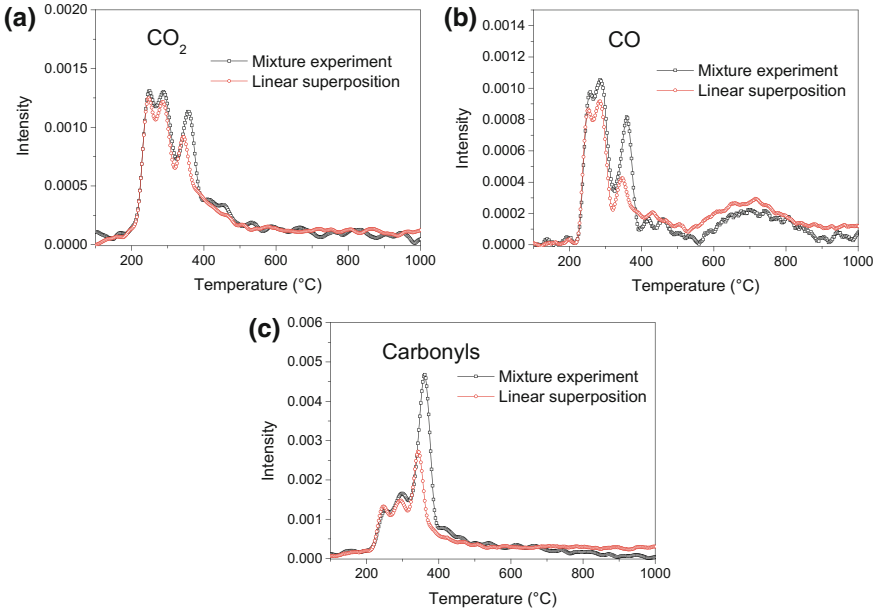

Fig. 5.4 The pyrolysis gas products of hemicellulose/cellulose mixture in TGA-FTIR

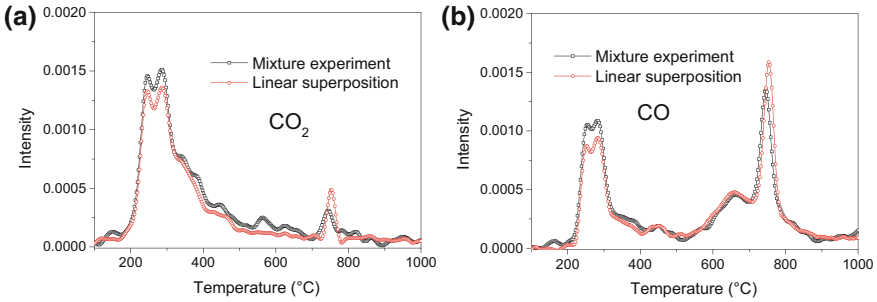

Fig. 5.5 The pyrolysis gas products of hemicellulose/lignin mixture in TGA-FTIR

As shown in Fig. 5.2, the interaction between hemicellulose and lignin was not significant. The CO_2 and CO production from mixture experiment is shown in Fig. 5.5. The results of mixture experiment were similar with those of linear superposition. At 200–400 °C, interaction promoted gas production slightly, while at 700–800 °C, interaction inhibited gas production slightly.

As shown in the TG and DTG curves in Fig. 5.3, the interaction between cellulose and lignin was significant. The gas production from FTIR is shown in Fig. 5.6. Interaction promoted CO_2 production remarkably at 300–400 °C, and the production of CO and carbonyls was also promoted in this temperature range.

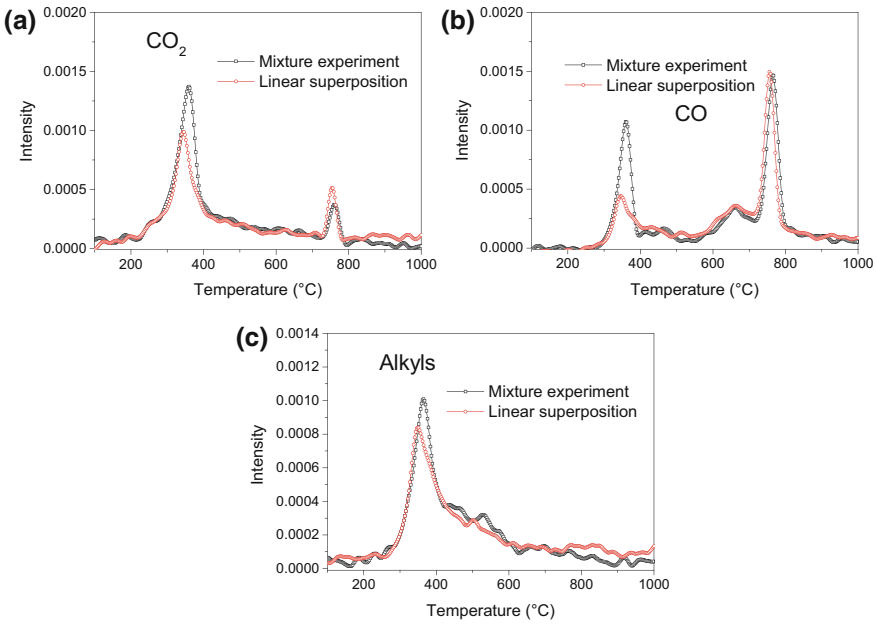

Fig. 5.6 The pyrolysis gas products of cellulose/lignin mixture in TGA-FTIR

5.1.2 *Interacted Effects in Fixed Bed*

The experiments in fixed bed reactor included two parts: experiments in Macro-TGA and horizontal fixed bed reactor. All the experiments kept the same reaction conditions: the reaction temperature was 800 °C and the atmosphere was N_2.

5.1.2.1 Influence of Interactions on Kinetics

Similar to the above comparisons, the mixture experiments in Macro-TGA were compared with the linear superposition results. The TG and DTG curves of the mixture of hemicellulose and cellulose were shown in Fig. 5.7, and the *OR* was 0.9674. Comparing results of the mixture experiments and linear superposition, the residue mass of mixture experiment was higher than that of linear superposition, which was consistent with the fast pyrolysis result in fixed bed reactor of Stefanidis et al. (2014). For the DTG curves in Fig. 5.7b, the peak of mixture experiment occurred earlier.

In TGA, the interaction between hemicellulose and lignin was not significant, while the interaction was significant in Macro-TGA, as shown in Fig. 5.8. The DTG peak of mixture experiment was lower than that of linear superposition.

The TG and DTG curves of the mixture of cellulose and lignin in Macro-TGA are shown in Fig. 5.9. The interaction between these two components was significant, with the *OR* 0.9655. Interaction promoted pyrolysis at first and inhibited pyrolysis later. Finally, the char amount from the mixture experiment was higher than that from the linear superposition, which was consistent with the result in TGA (Fig. 5.3).

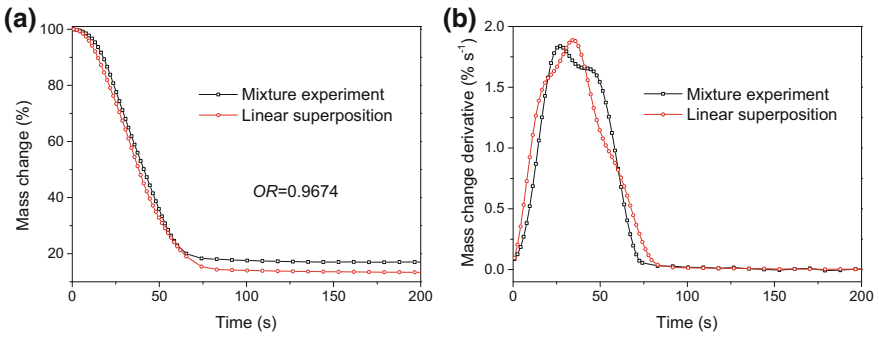

Fig. 5.7 The pyrolysis TG and DTG curves of hemicellulose/cellulose mixture in Macro-TGA. Reprinted from Long et al. (2016), with kind permission from Springer Science + Business Media

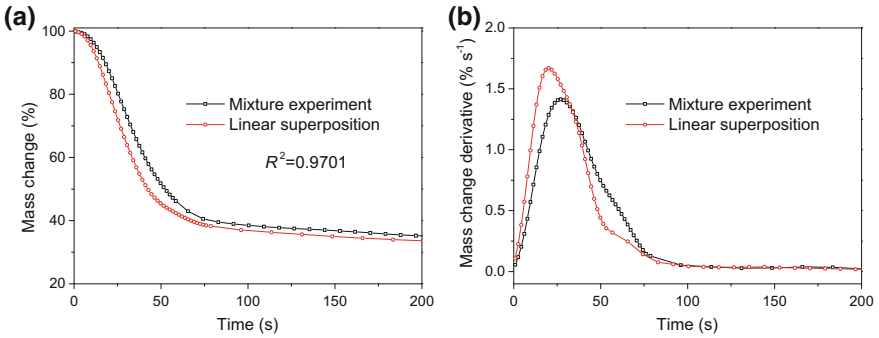

Fig. 5.8 The pyrolysis TG and DTG curves of hemicellulose/lignin mixture in Macro-TGA. Reprinted from Long et al. (2016), with kind permission from Springer Science + Business Media

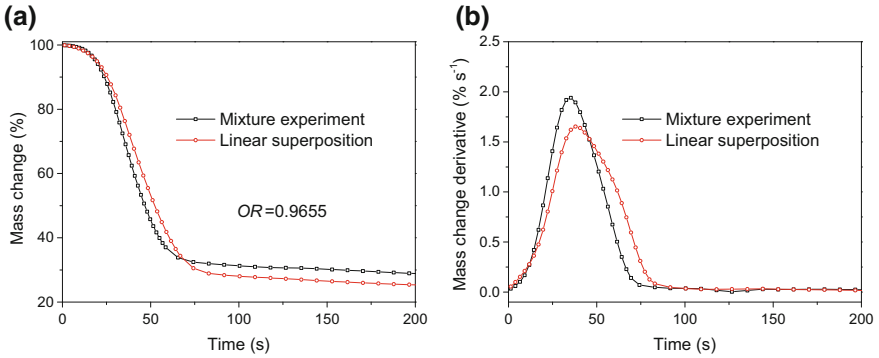

Fig. 5.9 The pyrolysis TG and DTG curves of cellulose/lignin mixture in Macro-TGA. Reprinted from Long et al. (2016), with kind permission from Springer Science + Business Media

Based on the results in Sects. 5.2.1.1 and 5.2.2.1, the interactions of biomass basic components in Macro-TGA were considerable. In TGA, the inhibition effect of interactions on pyrolysis might be due to the inhibition of heat and mass transfer process. In Macro-TGA with higher heating rate and larger sample mass, the inhibited effect of heat and mass transfer on co-pyrolysis was stronger.

5.1.2.2 Influence of Interactions on Product Distribution

The mass balance of mixture experiments has shown that the accuracy of experiments was quite good, as shown in Table 5.1. As shown in Fig. 5.10a, the co-pyrolysis of hemicellulose and cellulose had no significant influence on product distribution (<5 wt%), which was also reported by others (Giudicianni et al. 2013; Hosoya et al. 2007). The interaction between hemicellulose and lignin was also

Table 5.1 Mass balance of mixture experiments of lignocellulosic basic components

Sample	Hemicellulose + cellulose	Hemicellulose + lignin	Cellulose + lignin
Mass balance (wt%)	99.6	104.5	99.2

weak, as shown in Fig. 5.10b, which was consistent with the result in TGA (Wang et al. 2008; Worasuwannarak et al. 2007). However, the interaction between cellulose and lignin was obvious. Due to interacted effect, gas amount decreased by 7 wt%; tar amount increased by 15%; and solid amount decreased by 6%. Hosoya et al. (2007) studied the co-pyrolysis of cellulose and milled wood lignin at 800 °C and obtained similar results. It was believed that lignin inhibited the formation of levoglucosan from cellulose, decreased char amount, and promoted the generation of small molecules by changing secondary cracking of volatiles (Giudicianni et al. 2013; Wang et al. 2011).

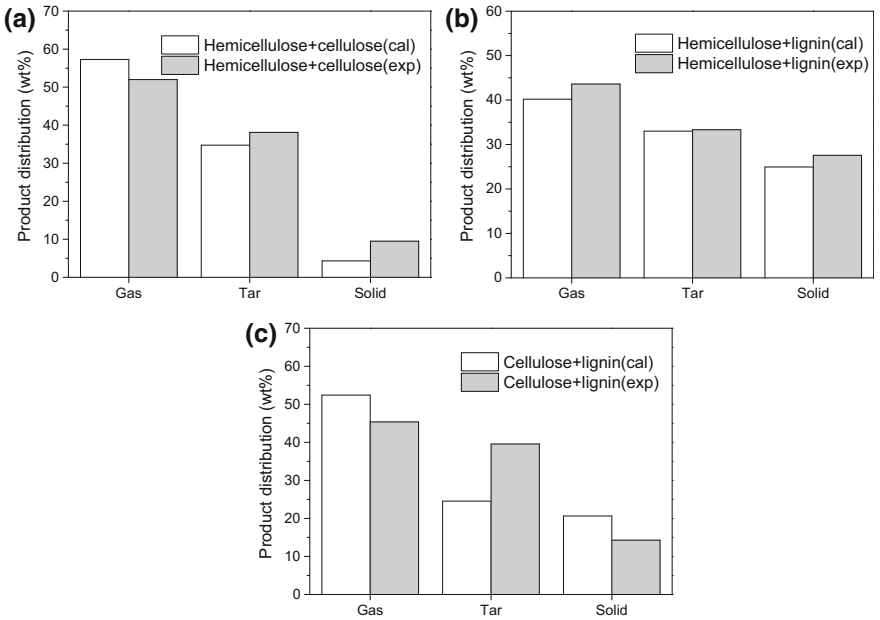

Fig. 5.10 The influence of interactions of lignocellulosic basic components on product distribution during co-pyrolysis. Reprinted from Zhou et al. (2014), Copyright 2014, with permission from Elsevier

5.1.2.3 Influence of Interactions on Gas Production

The comparison of gas products from mixture experiment and linear superposition of single components is shown in Fig. 5.11. For hemicellulose and cellulose, mixture experiment generated less CO. Giudicianni et al. (2013) studied the steam gasification of the mixture of hemicellulose and cellulose and obtained similar results. Figure 5.11 showed that the interacted effect of hemicellulose and lignin on gas composition was not significant. However, compared to linear superposition results, mixture experiment of cellulose and lignin generated less H_2 and CO. The reason was unknown, which needed further study.

5.1.2.4 Influence of Interactions on PAH Formation

Figure 5.12a presents the fast pyrolysis of hemicellulose/cellulose mixture generated more PAHs than superposition. For example, the amount of naphthalene increased from 11.9 to 44.0 μg per gram sample, and the amount of acenaphthylene increased from 13.2 to 48.8 μg per gram sample. At present, the studies on the

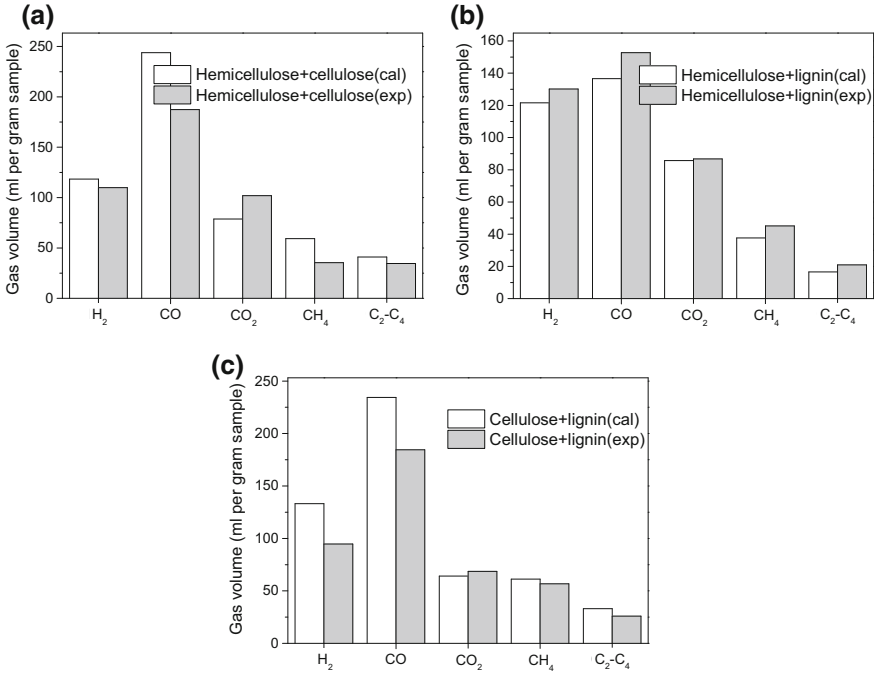

Fig. 5.11 The influence of interactions of lignocellulosic basic components on gas production during co-pyrolysis. Reprinted from Zhou et al. (2014), Copyright 2014, with permission from Elsevier

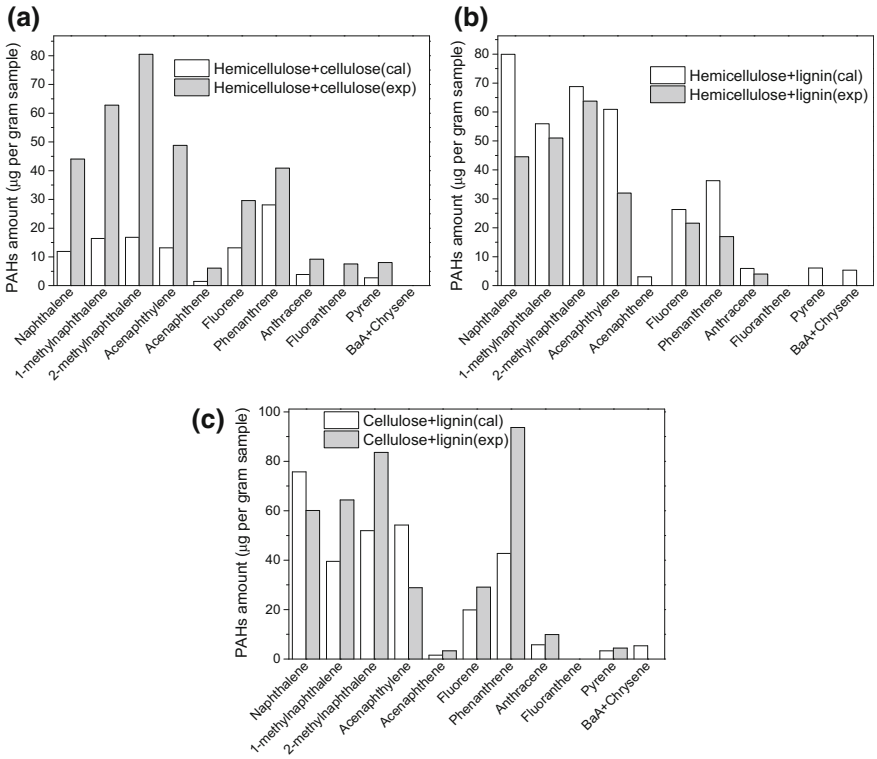

Fig. 5.12 The influence of interactions of lignocellulosic basic components on PAH formation during co-pyrolysis (BaA, benzo[*a*]anthracene). Reprinted from Zhou et al. (2014), Copyright 2014, with permission from Elsevier

interacted effect of lignocellulosic on PAH generation were few. Wang et al. (2011) studied the mixture of hemicellulose and cellulose in TGA. When the amount of cellulose was kept constant, the concentration of 2,5-diethoxytetrahydrofuran increased with the increase in hemicellulose amount. In addition, the addition of cellulose promoted the generation of acetic acid and 2-furfural. Stefanidis et al. (2014) have reported that the interaction between hemicellulose and cellulose could promote the formation of phenols, while phenols were regarded as PAH precursors.

Compared to superposition results, some PAHs decreased during the co-pyrolysis of hemicellulose and lignin. In particular, the amount of naphthalene decreased from 79.9 to 44.5 μg per gram sample; the amount of acenaphthylene decreased from 54.2 to 28.9 μg per gram sample; and the amount of phenanthrene decreased from 36.3 to 16.9 μg per gram sample, which was different from the interaction between hemicellulose and cellulose. In addition, the interacted effects of cellulose and lignin on the generation of different PAHs were different (Fig. 5.12c). For example, the amounts of naphthalene, acenaphthylene, chrysene,

and benzo[*a*]anthracene decreased, while the amounts of methylnaphthalene, acenaphthene, fluorene, phenanthrene, anthracene, and pyrene increased.

At present, the mechanisms of interacted effect of co-pyrolysis of lignocellulosic basic components on PAH formation remain unknown. Hosoya et al. (2009) investigated phenol derivatives from the interaction between lignin and cellulose and found that some compounds (such as catechol) increased compared to superposition result, while some compounds such as (*o*-cresol) decreased compared to superposition result. Asmadi et al. (2011a, b) deemed that catechol and pyrogallol from lignin pyrolysis could further decompose to PAHs. Stefanidis et al. (2014) also believed that benzenes and phenols might be PAH precursors during hemicellulose or cellulose pyrolysis. The interactions among lignocellulosic basic components were very complicated, especially on PAH formation. Therefore, more work needs to be done to further explore the mechanisms.

This section investigated the interaction between the lignocellulosic basic components in TGA and fixed bed reactor. In TGA-FTIR, the interaction between cellulose and lignin was significant, and the results of fast pyrolysis in Macro-TGA were consistent with the results of slow pyrolysis in TGA. In horizontal fixed bed reactor, cellulose and lignin also presented the strongest interacted effect. The study in this section provided a basis for the description of biomass from lignocellulosic basic components. However, the interacted mechanisms needed further exploration.

5.2 The Interactions of PVC and Lignocellulosic Basic Components

Preliminary experiments have shown that the interacted effects between PVC and lignocellulosic basic components (hemicellulose, cellulose, and lignin) were significant, and thus, this problem would be systematically discussed here. Similar to the last section, the kinetics and gas production were studied in TGA-FTIR; fast pyrolysis mass loss kinetics was studied in Macro-TGA; and product distribution, gas production, and PAH formation characteristics were studied in horizontal fixed bed reactor. Finally, the possible interacted mechanisms would be proposed.

5.2.1 Interacted Effects in TGA-FTIR

5.2.1.1 Influence of Interactions on Kinetics

The co-pyrolysis TG and DTG curves of PVC and hemicellulose are shown in Fig. 5.13. Some interacted effect could be observed, with the *OR* 0.9776. As shown in Fig. 5.13a, interaction promoted pyrolysis slightly at first, while inhibited pyrolysis later. DTG curve showed that the interaction made the mass loss peak

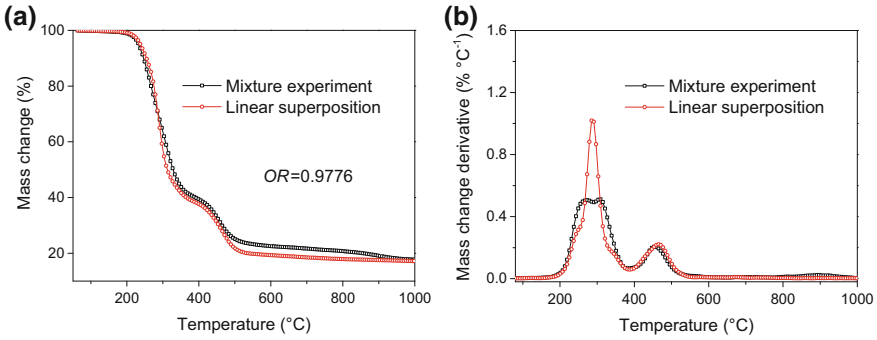

Fig. 5.13 The pyrolysis TG and DTG curves of PVC/hemicellulose mixture in TGA

flatter. The interaction between PVC and cellulose was considerable, with the *OR* only 0.9450, as shown in Fig. 5.14. Obviously, interaction promoted pyrolysis first and inhibited pyrolysis later, with the demarcation point around 350 °C, which was similar to the interaction between cellulose and PVC, but stronger. Meanwhile, the char amount from mixture experiment was higher than that of superposition. DTG curve showed that two mass loss peaks were combined into a single peak in mixture experiment. The main pyrolytic temperature ranges of cellulose and PVC were overlapped, which might be the reason that their interaction was strong. The interaction between PVC and cellulose during co-pyrolysis in this study was the same with the interaction between PVC and newspaper in TGA (Sorum et al. 2001), while the main composition of newspaper is just cellulose. McGhee et al. (1995) believed that HCl from PVC pyrolysis could participate in cellulose pyrolysis and catalyze acid hydrolysis reaction to lower its stability. Conversely, the interaction

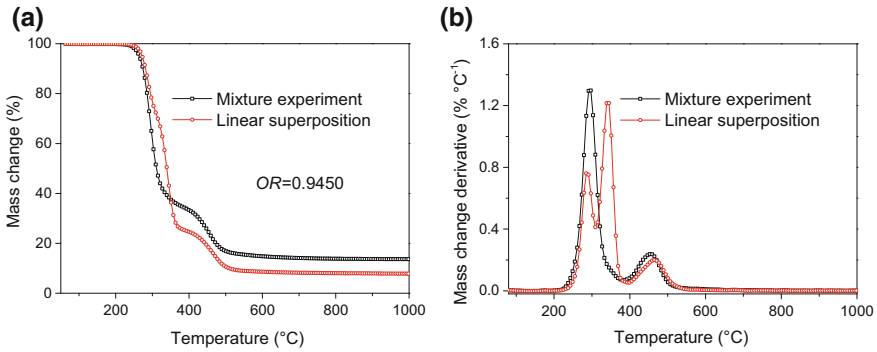

Fig. 5.14 The pyrolysis TG and DTG curves of PVC/cellulose mixture in TGA

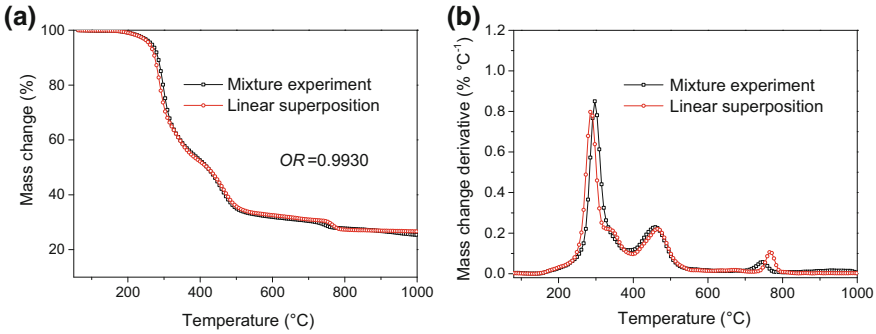

Fig. 5.15 The pyrolysis TG and DTG curves of PVC/lignin mixture in TGA

between lignin and PVC was not significant, with the *OR* as high as 0.9930, as shown in Fig. 5.15.

5.2.1.2 Influence of Interactions on Gas Production

In TGA-FITR, the gas production from the mixture of hemicellulose and PVC is shown in Fig. 5.16. CO_2, CO, carbonyls, and carboxyls were mainly derived from hemicellulose, and interaction promoted the production of these gases. For HCl and benzene, interaction slowed down the release of these two.

For the mixture of PVC and cellulose, interaction made the release of alkyls and carbonyls earlier, as shown in Fig. 5.17. For HCl and benzene, the overall trends were consistent. The interaction made these two gases release later, which was similar to the mixture of PVC and hemicellulose. As shown in Fig. 5.14, the char amount from mixture experiment was higher than that of linear superposition result. At the same experimental conditions, we carried out the co-pyrolysis of PVC and tissue paper and obtained similar results (Zhou et al. 2015a), while the main composition of tissue paper was cellulose. The study of Matsuzawa et al. (2001, 2004) showed that the char from co-pyrolysis of PVC and cellulose had fewer hydroxyls and more C = O and C = C bonds than the char from cellulose pyrolysis. The HCl from PVC pyrolysis might induce dehydration reaction and cut the inner ring of glucose unit, which would lead to the increase in char amount.

Three kinds of gases from the interaction between PVC and lignin are shown in Fig. 5.18: alkyls, HCl, and benzene. Interaction did not have a significant influence on these three gases, which was consistent with the result of TG and DTG, as shown in Fig. 5.15.

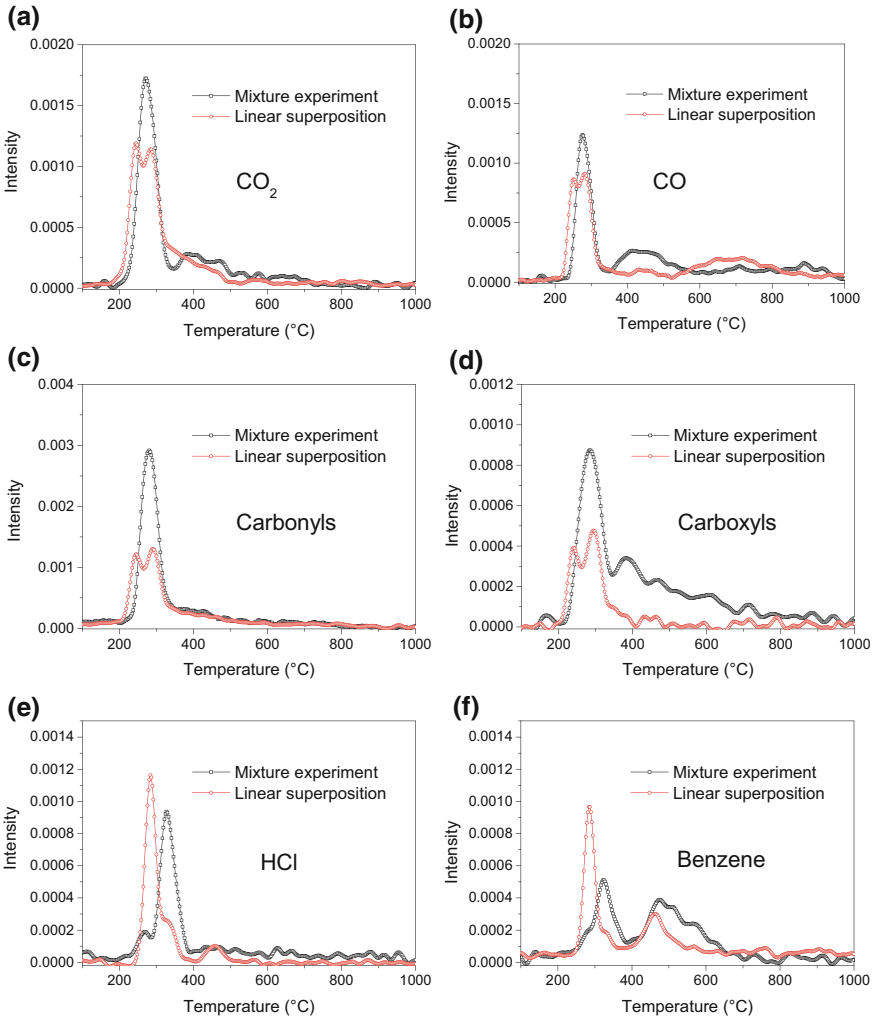

Fig. 5.16 The pyrolysis gas products of PVC/hemicellulose mixture in TGA-FTIR

5.2.2 Interacted Effects in Fixed Bed

5.2.2.1 Influence of Interactions on Kinetics

In Macro-TGA, the TG and DTG curves of PVC and hemicellulose 1:1 mixture are shown in Fig. 5.19. The mixture experiment result of PVC and hemicellulose was quite different from that of linear superposition. At 30–90 s, interaction promoted pyrolysis significantly, while the char amounts from mixture experiment and superposition were similar.

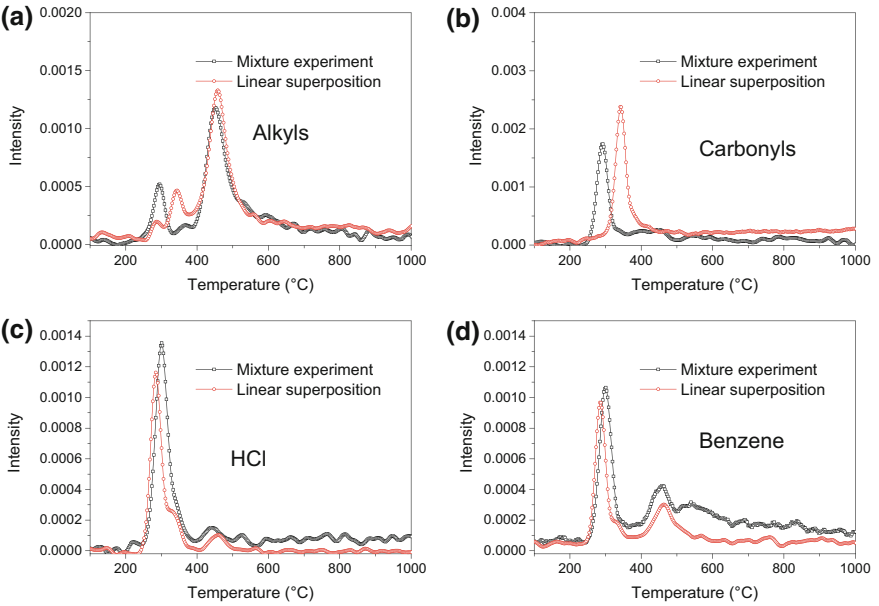

Fig. 5.17 The pyrolysis gas products of PVC/cellulose mixture in TGA-FTIR

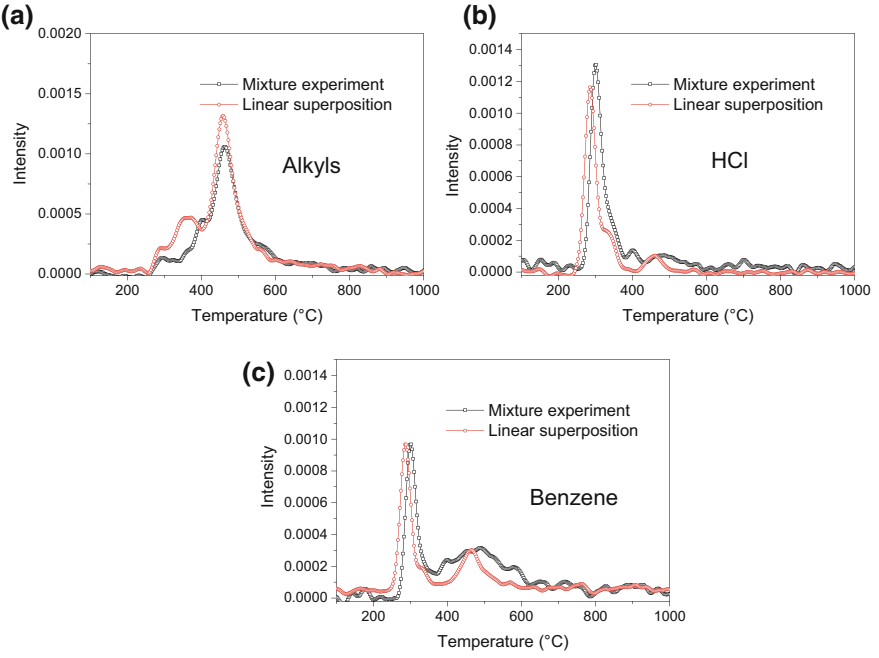

Fig. 5.18 The pyrolysis gas products of PVC/lignin mixture in TGA-FTIR

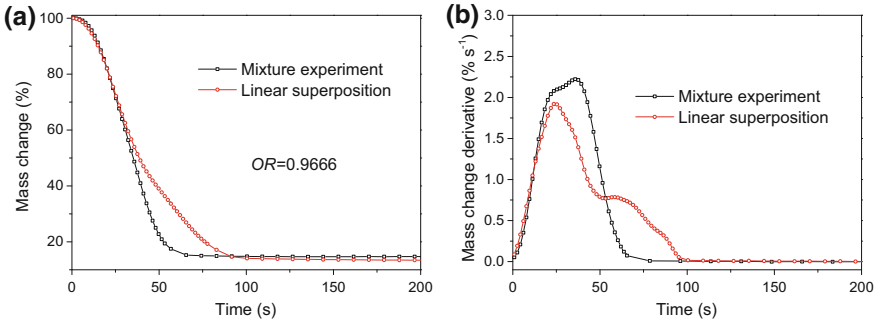

Fig. 5.19 The pyrolysis TG and DTG curves of PVC/hemicellulose mixture in Macro-TGA

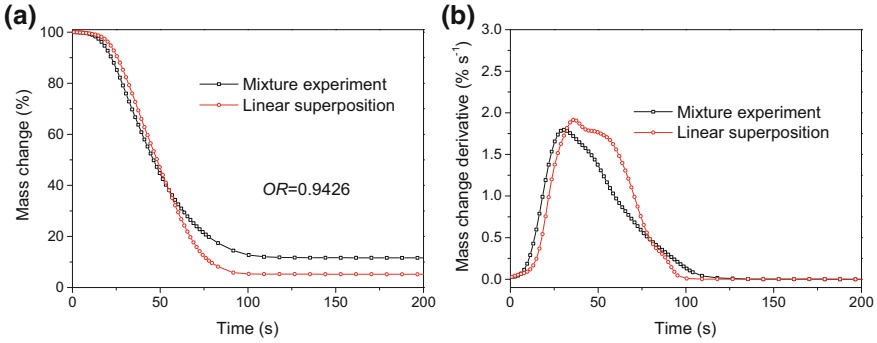

Fig. 5.20 The pyrolysis TG and DTG curves of PVC/cellulose mixture in Macro-TGA

The interaction between PVC and cellulose was also very significant, with the *OR* 0.9426, as shown in Fig. 5.20. Interaction promoted pyrolysis first and inhibited pyrolysis later. Finally, the char amount from mixture experiment was around 6% higher than that from linear superposition, which was similar to the result in TGA.

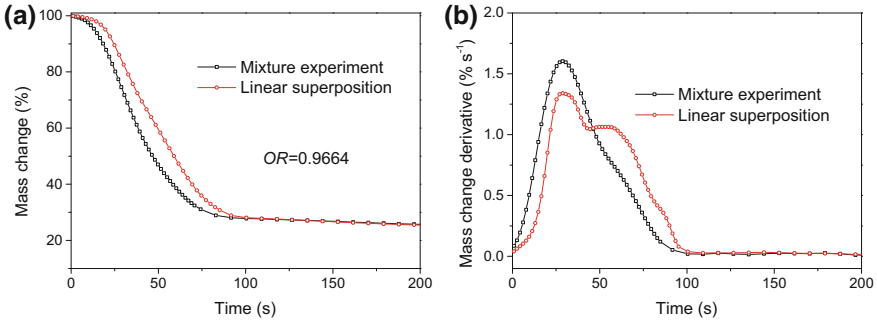

Fig. 5.21 The pyrolysis TG and DTG curves of PVC/lignin mixture in Macro-TGA

The TG and DTG curves of the mixture of PVC/lignin are shown in Fig. 5.21. Similar to the mixture of PVC and hemicellulose, mixture experiment promoted pyrolysis before 90 s, while the interaction had no significant effect on char amount.

The research of Zuo et al. (2004) has shown that the dechlorination of PVC, i.e., the breakage of the branched chain of the polymer, could generate HCl, while HCl had a self-catalytic effect which accelerated reaction rate and made the process finish at low temperatures. Therefore, the release of HCl could accelerate pyrolysis and made co-pyrolysis faster than the pyrolysis of single components.

5.2.2.2 Influence of Interactions on Product Distribution

At 800 °C, the mass balances of 1:1 mixture experiments of PVC and LBCs are shown in Table 5.2. The mass balances of three mixture experiments were in the range of 98.4–100.5%, which indicated the accuracy of the experiments was quite good.

The interacted effects of PVC with hemicellulose, cellulose, and lignin on product distribution of pyrolysis are shown in Fig. 5.22. The experimental results came from the pyrolytic results of the 1:1 mixtures of PVC and lignocellulosic basic components, and the calculated results came from the superposition of single components, that is,

$$X(\text{cal}) = 50\%X_{\text{PVC}} + 50\%X_{\text{hemicellulose/cellulose/lignin}} \tag{5.3}$$

Here, X(cal) denotes experimental result; X_{PVC} denotes the pyrolytic result of PVC; and $X_{\text{hemicellulose/cellulose/lignin}}$ denotes the pyrolytic result of the lignocellulosic basic component.

As shown in Fig. 5.22, when PVC was mixed with hemicellulose, cellulose, or lignin, the generation of HCl decreased significantly. In particular for the mixture of PVC and lignin, the generation of HCl decreased from 23.0 to 9.3%. Correspondingly, the amount of tar increased.

As shown in Fig. 5.22, when PVC was mixed with hemicellulose, cellulose, or lignin, the influence on the amount of char and gas was different. For example, when PVC was mixed with hemicellulose or lignin, the gas amount increased; when PVC was mixed with cellulose, gas amount decreased and char amount increased. In aforementioned TGA experiment, the mixture of PVC and cellulose also promoted the generation of char. When PVC was mixed with lignin, tar amount decreased compared to linear superposition.

Table 5.2 Mass balance of mixture experiments of PVC and lignocellulosic basic components

Sample	PVC + hemicellulose	PVC + cellulose	PVC + lignin
Mass balance (wt%)	99.8	100.5	98.4

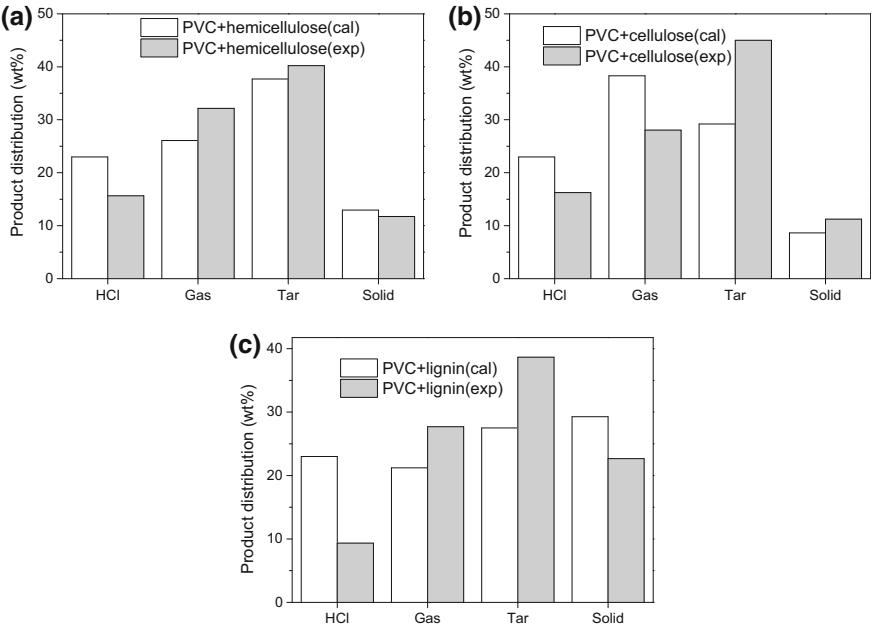

Fig. 5.22 The influence of interactions between PVC and lignocellulosic basic components on product distribution during co-pyrolysis (Zhou et al. 2015b). Reproduced by permission of The Royal Society of Chemistry

5.2.2.3 Influence of Interactions on Gas Production

The influence of the mixture of PVC and lignocellulosic basic components on gas production is complex, as shown in Fig. 5.23. Interactions decreased the amount of H_2. Interactions between PVC and cellulose or lignin increased CO generation, while the interaction between PVC and cellulose decreased CO generation. In addition, during the interaction between PVC and lignin, CO_2 amount increased from 39.9 to 62.0 ml per gram sample.

5.2.2.4 Influence of Interactions on PAH Formation

As shown in Fig. 5.24a, when PVC and hemicellulose were 1:1 mixed, the PAHs produced were decreased compared to linear superposition, and the inhibition of the generation of naphthalene, benzo[*a*]anthracene, and chrysene was the most significant. The amount of naphthalene decreased from 2717.8 to 1361.0 μg per gram sample. The amount of benzo[*a*]anthracene and chrysene decreased from 1405.8 μg per gram sample to zero.

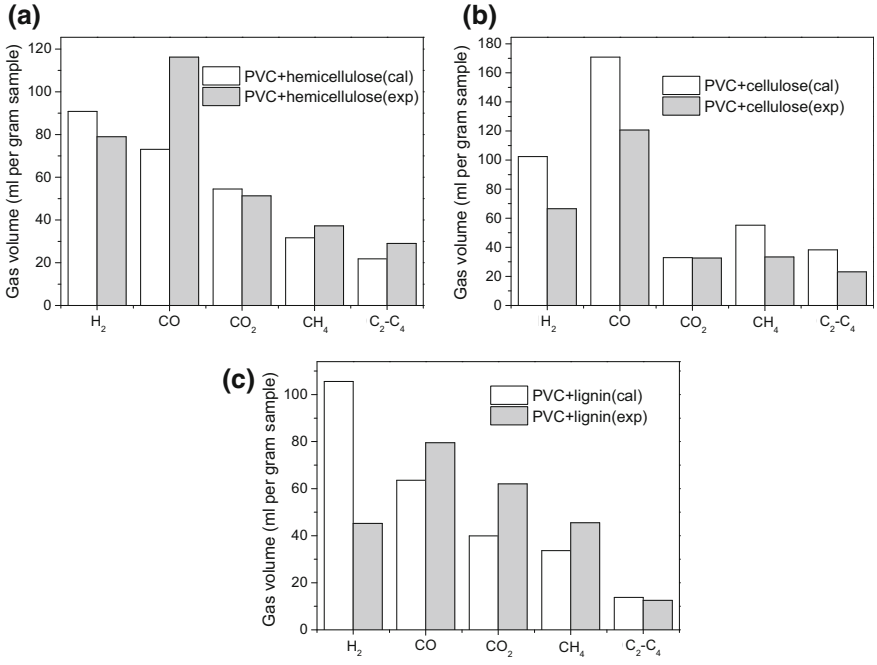

Fig. 5.23 The influence of interactions between PVC and lignocellulosic basic components on gas production during co-pyrolysis (Zhou et al. 2015b). Reproduced by permission of The Royal Society of Chemistry

The influence of the interaction between PVC and cellulose on PAH generation is shown in Fig. 5.24b. When PVC was mixed with cellulose, naphthalene, benzo [*a*]anthracene, and chrysene decreased considerably, while fluorene, phenanthrene, and anthracene increased slightly. Overall, when PVC was mixed with cellulose, total PAH amount decreased from 9034.1 to 6370.2 μg per gram sample.

The influence of interaction between PVC and lignin on PAH generation is shown in Fig. 5.24c. When PVC was 1:1 mixed with lignin, naphthalene, benzo[*a*] anthracene, and chrysene decreased significantly, while the amount of phenanthrene and anthracene increased slightly. Overall, when PVC was mixed with lignin, PAH total amount decreased from 9275.1 to 7181.5 μg per gram sample.

During the pyrolysis of lignocellulosic basic components, volatiles and solid char were generated simultaneously. Therefore, PVC might interact with volatiles or char. In this study, to further explore the interacted mechanisms of PVC and lignocellulose basic components, lignin pyrolysis char (LPC) and PVC were co-pyrolyzed at the same experimental conditions. LPC was derived from lignin pyrolysis at 800 °C under N_2 atmosphere, which could be regarded inert. The product distribution of mixture experiment and linear superposition results is shown in Fig. 5.25. Due to the interaction between PVC and LPC, HCl yield decreased and tar yield increased, which was consistent with the results in Fig. 5.22.

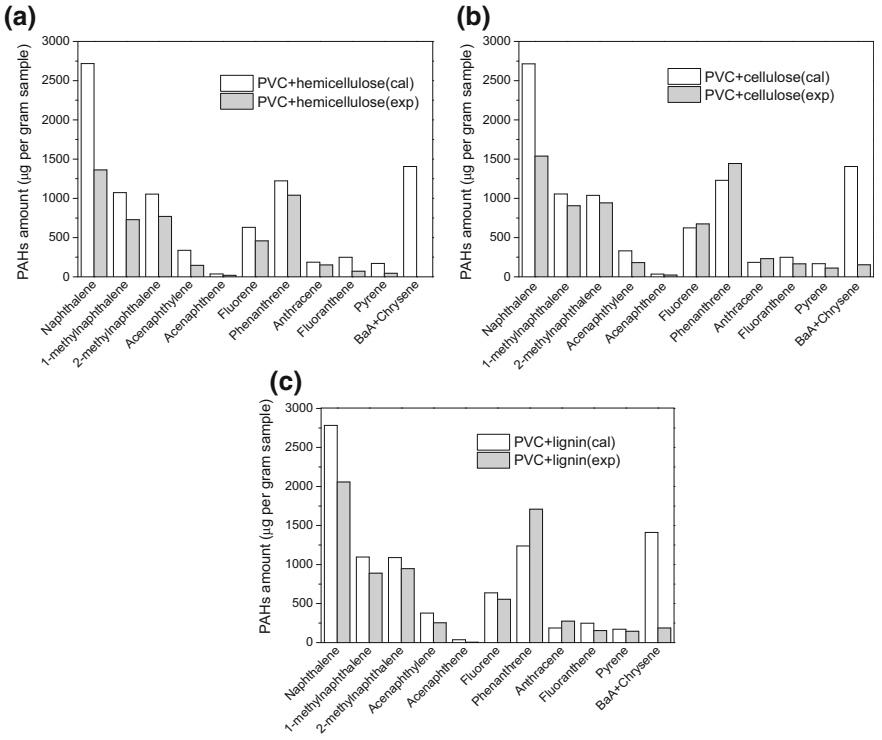

Fig. 5.24 The influence of interactions between PVC and lignocellulosic basic components on PAH formation during co-pyrolysis (BaA, benzo[*a*]anthracene) (Zhou et al. 2015b). Reproduced by permission of The Royal Society of Chemistry

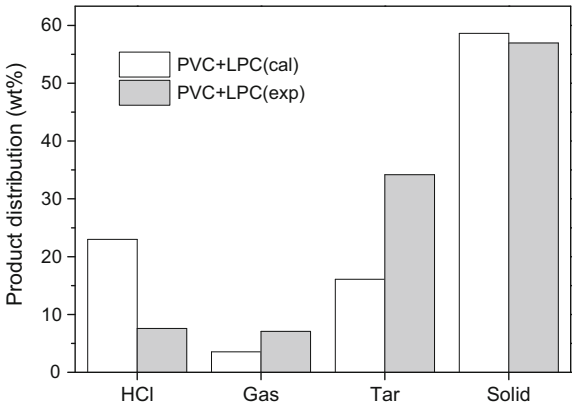

Fig. 5.25 The influence of interactions between PVC and LPC on product distribution during co-pyrolysis (Zhou et al. 2015b). Reproduced by permission of The Royal Society of Chemistry

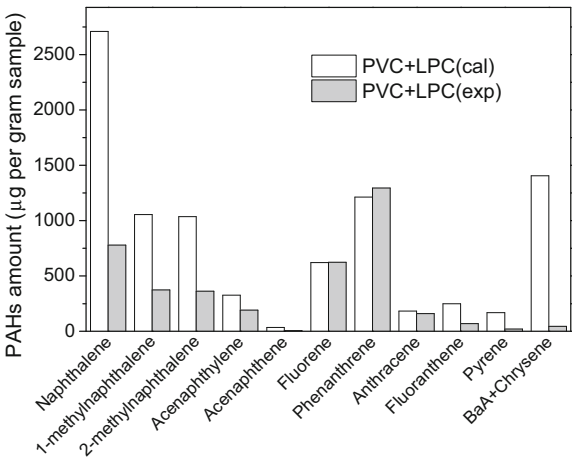

Fig. 5.26 The influence of interactions between PVC and LPC on PAH formation during co-pyrolysis (Zhou et al. 2015b). Reproduced by permission of The Royal Society of Chemistry

The PAH generation comparison of mixture experiment and linear superposition of PVC and LPC is shown in Fig. 5.26. Due to the interaction between PVC and LPC, the generation of most PAHs decreased except fluorene and phenanthrene, which was consistent with the results in Fig. 5.24. The amounts of naphthalene, chrysene, and benzo[*a*]anthracene from mixture experiment were much lower than those from linear superposition.

The decomposition of PVC has two processes: dechlorination and chain scission (Miranda et al. 1999). During slow pyrolysis, dechlorination was a slow process, and almost all the chlorine was converted to HCl (Miranda et al. 1999; McNeil et al. 1995). During fast pyrolysis, dechlorination and chain scission can be finished in a short time with high heating rates. Therefore, the chlorination might be incomplete. The chlorine detected in HCl was lower than the chlorine content in PVC molecular, as shown in Fig. 5.22. During the co-pyrolysis of PVC and other plastics in fluidized bed reactor, a large amount of chlorine presented in the form other than HCl (Williams and Williams 1997).

The research of Matsuzawa et al. (2001, 2004) has shown that after the PVC dechlorination, dehydration and the generation of aldehydes from lignocellulosic basic components were promoted. HCl released from PVC was Lewis acid, which could induce dehydration reaction and lead to scission, cross-linking, and coking of glucose intra-ring, instead of the depolymerization of cellulose. Therefore, during the co-pyrolysis of PVC and cellulose, more solid residue was generated, as shown in Fig. 5.22.

As shown in Figs. 5.22 and 5.25, lignocellulosic materials, no matter hemicellulose, cellulose, lignin, or LPC, could inhibit the generation of HCl from PVC pyrolysis. It was considered that lignocellulosic materials could inhibit the dechlorination or promote chain scission of PVC pyrolysis. Therefore, during PVC pyrolysis, dechlorination was not complete. The study of Jakab et al. (2000) has shown that coal char had a significant influence on the thermal conversion of

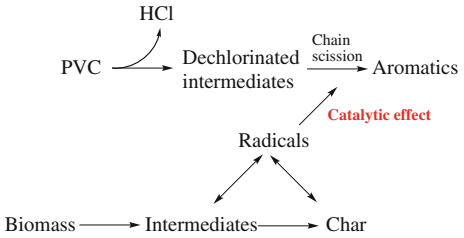

Fig. 5.27 Co-pyrolysis mechanisms of PVC and biomass

polypropylene (PP). With the effect of coal char, the decomposition of PP happened at a lower temperature, which indicated coal char could promote the chain scission. In addition, when carbon black was added, hydrogenation was enhanced, which might be the reason of PAH reduction from the mixture of PVC and biomass.

The interaction mechanisms of PVC and biomass co-pyrolysis are shown in Fig. 5.27. Biomass is typically decomposed earlier than PVC, while during the polymer chain scission, the solid char from biomass pyrolysis could provide radicals, which could promote the chain scission process (Marin et al. 2002).

To further explore the description method of real CSW mixtures from basic components, this section investigated the influence of interactions between PVC and lignocellulosic basic components on thermal mass loss, product distribution, gas products, and PAH formation in TGA and fixed bed. The results showed that in TGA, interactions promoted pyrolysis first and inhibit pyrolysis later. The interactions between PVC and lignocellulosic basic components decreased HCl generation and promoted tar generation considerably, and the amounts of most PAHs decreased. The mechanisms might be that during fast pyrolysis, lignocellulosic basic components could act as a catalyst to promote the chain scission of PVC.

5.3 Summary

To describe real CSW mixtures from basic components, this chapter investigated the interactions of basic components. Two kinds of interactions were studied in TGA and fixed bed reactor: the interactions of LBCs (hemicellulose, cellulose, and lignin) and the interactions between PVC and LBCs. The mixture ratio was 1:1. The results of mixture experiments were compared with the linear superposition results, with the main conclusions as follows:

(1) In TGA, interaction effects from weak to strong were as follows: hemicellulose/lignin < hemicellulose/cellulose < cellulose/lignin. The interaction between cellulose and lignin inhibited the co-pyrolysis and increased the final residue.
(2) The influence of interactions of LBCs on mass loss, product distribution, gas products, and PAH formation was investigated in fixed bed reactor. The interaction effects in Macro-TGA were consistent with those in TGA.

In HFBR, for hemicellulose and cellulose, the product distribution of mixture experiment was similar to that of calculated result. However, the generation of PAHs in tar increased. The interaction effect of hemicellulose and lignin on product distribution was not significant, while some PAHs in tar decreased. The co-pyrolysis of cellulose and lignin presented the strongest interaction effect, with the gas and char decreased and the tar increased. Some PAHs increased, while the other decreased, which suggested the interaction between these two was complicated.

(3) In TGA, the interactions between PVC and hemicellulose or lignin were insignificant, while the interaction between PVC and cellulose was significant: pyrolysis was promoted first and inhibited later, and the release of alkyls and carbonyls was earlier due to interactions. The HCl from PVC pyrolysis might induce dehydration and scission of intra-ring of glucose unit, and thus, the char amount from mixture experiments was higher than that from superposition result.

(4) The interactions between PVC and LBCs decreased the generation of HCl and increased the generation of tar considerably. Most of the PAHs decreased due to these interactions. The co-pyrolysis of PVC and LPC had similar results. During fast pyrolysis, the dechlorination and chain scission of PVC were finished in a short time, and thus, the dechlorination process might be incomplete. LBCs could act as a catalyst and promote the chain scission of PVC.

Overall, this chapter investigated the mixture of LBCs (hemicellulose, cellulose, and lignin) and the mixture of PVC and LBCs. Therein, the interaction between cellulose and lignin was significant, and the interactions between PVC and LBCs were significant. This chapter was the deepening of Chap. 3 and the main part of the basic component system in Chap. 2.

References

Asmadi M, Kawamoto H, Saka S (2011a) Thermal reactions of guaiacol and syringol as lignin model aromatic nuclei. J Anal Appl Pyrol 92:88–98

Asmadi M, Kawamoto H, Saka S (2011b) Gas- and solid/liquid-phase reactions during pyrolysis of softwood and hardwood lignins. J Anal Appl Pyrol 92:417–425

Couhert C, Commandre JM, Salvador S (2009) Is it possible to predict gas yields of any biomass after rapid pyrolysis at high temperature from its composition in cellulose, hemicellulose and lignin? Fuel 88:408–417

Giudicianni P, Cardone G, Ragucci R (2013) Cellulose, hemicellulose and lignin slow steam pyrolysis: thermal decomposition of biomass components mixtures. J Anal Appl Pyrol 100:213–222

Horne PA, Williams PT (1996) Reaction of oxygenated biomass pyrolysis model compounds over a ZSM-5 catalyst. Renew Energ 7:131–144

Hosoya T, Kawamoto H, Saka S (2007) Cellulose–hemicellulose and cellulose–lignin interactions in wood pyrolysis at gasification temperature. J Anal Appl Pyrol 80:118–125

Hosoya T, Kawamoto H, Saka S (2009) Solid/liquid- and vapor-phase interactions between cellulose- and lignin-derived pyrolysis products. J Anal Appl Pyrol 85:237–246
Jakab E, Várhegyi G, Faix O (2000) Thermal decomposition of polypropylene in the presence of wood-derived materials. J Anal Appl Pyrol 56:273–285
Long Y, Zhou H, Meng A et al (2016) Interactions among biomass components during co-pyrolysis in (macro)thermogravimetric analyzers. Korean J Chem Eng 33:2638–2643
Marin N, Collura S, Sharypov VI et al (2002) Copyrolysis of wood biomass and synthetic polymers mixtures. Part II: characterisation of the liquid phases. J Anal Appl Pyrol 65:41–55
Matsuzawa Y, Ayabe M, Nishino J (2001) Acceleration of cellulose co-pyrolysis with polymer. Polym Degrad Stabil 71:435–444
Matsuzawa Y, Ayabe M, Nishino J et al (2004) Evaluation of char fuel ratio in municipal pyrolysis waste. Fuel 83:1675–1687
McGhee B, Norton F, Snape CE et al (1995) The copyrolysis of poly(vinylchloride) with cellulose derived materials as a model for municipal waste derived chars. Fuel 74:28–31
McNeill IC, Memetea L, Cole WJ (1995) A study of the products of PVC thermal degradation. Polym Degrad Stabil 49:181–191
Miranda R, Yang J, Roy C et al (1999) Vacuum pyrolysis of PVC I. Kinetic study. Polym Degrad Stabil 64:127–144
Sorum L, Gronli MG, Hustad JE (2001) Pyrolysis characteristics and kinetics of municipal solid wastes. Fuel 80:1217–1227
Stefanidis SD, Kalogiannis KG, Iliopoulou EF et al (2014) A study of lignocellulosic biomass pyrolysis via the pyrolysis of cellulose, hemicellulose and lignin. J Anal Appl Pyrol 105:143–150
Wang G, Li W, Li B et al (2008) TG study on pyrolysis of biomass and its three components under syngas. Fuel 87:552–558
Wang SR, Guo XJ, Wang KG et al (2011) Influence of the interaction of components on the pyrolysis behavior of biomass. J Anal Appl Pyrol 91:183–189
Williams EA, Williams PT (1997) Analysis of products derived from the fast pyrolysis of plastic waste. J Anal Appl Pyrol 40:347–363
Worasuwannarak N, Sonobe T, Tanthapanichakoon W (2007) Pyrolysis behaviors of rice straw, rice husk, and corncob by TG-MS technique. J Anal Appl Pyrol 78:265–271
Zhou H, Wu C, Meng A et al (2014) Effect of interactions of biomass constituents on polycyclic aromatic hydrocarbons (PAH) formation during fast pyrolysis. J Anal Appl Pyrol 110:264–269
Zhou H, Long Y, Meng A et al (2015a) Interactions of three municipal solid waste components during co-pyrolysis. J Anal Appl Pyrol 111:265–271
Zhou H, Wu C, Onwudili JA et al (2015b) Effect of interactions of PVC and biomass components on the formation of polycyclic aromatic hydrocarbons (PAH) during fast co-pyrolysis. RSC Adv 5:11371–11377
Zuo Y, Zhu L, Wu Z (2004) 生活垃圾典型组分的热解特性研究 (Study on the pyrolysis characteristics of typical composition of municipal solid waste). Pollut Control 10:34–38

Chapter 6
Conclusions and Perspectives

Abstract Based on the investigation of combustible solid waste (CSW) components, this study selected nine kinds of CSW basic components. The thermochemical conversion kinetics, product distribution, gas production, and polycyclic aromatic hydrocarbons (PAHs) generation were investigated in thermogravimetric analyzer (TGA) and fixed bed reactor, and then the thermochemical reaction mechanisms of basic components were obtained. The influences of different factors (temperature, heating rate, atmosphere, and inorganics) on CSW basic components were investigated. In addition, the interacted effects of components on thermochemical reaction were investigated. In this chapter, the main conclusions are summarized. In addition, the innovative points of this thesis are proposed as follows. The inhibited effect on HCl formation from the interactions of polyvinyl chloride (PVC) and lignocellulosic basic components (LBCs) was obtained, and the mechanism was the catalytic effect of LBCs on the chain scission of PVC. The inhibition of air and CO_2 on PAHs formation from the thermochemical conversion processes of lignin and PVC was obtained, and the mechanisms were analyzed; the inhibition of NaCl, NaOH, and $CuCl_2$ on the PAHs formation from the pyrolysis of lignin and PVC was obtained. The tar amount from lignin slow pyrolysis was higher than that from fast pyrolysis, and the reason was that the secondary reactions were more significant in fast pyrolysis. A new peak analysis-least square method (PA-LSM) was developed to calculate the kinetics of thermochemical reactions, and the calculated results agreed well with the experimental results. Finally, the perspectives of this study are listed to provide some suggestions on the following research.

Keywords Combustible solid waste (CSW) · Basic component · Pyrolysis · Polycyclic aromatic hydrocarbons (PAHs)

H. Zhou, *Combustible Solid Waste Thermochemical Conversion*, Springer Theses,
DOI 10.1007/978-981-10-3827-3_6

6.1 Research Conclusions

Based on the investigation of combustible solid waste (CSW) components, this study selected nine kinds of CSW basic components. The thermochemical conversion kinetics, product distribution, gas production, and PAHs generation were investigated in thermogravimetric analyzer (TGA) and fixed bed reactor, and then the thermochemical reaction mechanisms of basic components were obtained. The influence of different factors (temperature, heating rate, atmosphere, and inorganics) on CSW basic components was investigated. In addition, the interacted effects of components on thermochemical reaction were investigated. The main conclusions were as follows:

1. Classification of CSW components and the selection of basic components based on thermochemical characteristics.
   Based on proximate analyses, ultimate analyses, and heating values, CSW typical components could be classified into 11 groups. TG curves could provide a kind of "fingerprint" property. Based on these, nine kinds of basic components were selected: hemicellulose, cellulose, lignin, pectin, starch, polyethylene (PE), polystyrene (PS), polyvinyl chloride (PVC), and polyethylene terephthalate (PET).
2. Thermochemical characteristics of CSW basic components.
   (1) The pyrolytic processes of basic components in TGA and Macro-TGA could be calculated by peak analysis-least square method (PA-LSM). Complicated pyrolytic reactions could be described by a series of paralleled reactions, and the calculated results agreed well with experimental results.
   (2) The derivative thermogravimetric (DTG) peak temperatures in Macro-TGA were higher than those in TGA, and this relation could be denoted by the equation $t_{\text{M-TGA}} = t_{\text{TGA}} + (54.7–0.033\ t_{\text{TGA}})$. With a higher temperature, the radiative heat transfer was stronger, and the temperature difference was smaller.
   (3) Among biomass basic components, cellulose and starch produced the most gas, and hemicellulose produced the most tar. Among plastic basic components, PE, PVC, and PET produced the most gas, and PS produced the most tar. PS and PVC generated the most polycyclic aromatic hydrocarbons (PAHs). Naphthalene was the most abundant PAH, and phenanthrene and fluorene were the most abundant 3-ring PAHs. For PS, PET, and lignin, PAHs could be formed directly from aromatic structures. PE could form PAHs through Diels–Alder reactions. For polysaccharides, PAHs could be formed from benzenes and cyclopentadiene (CPD) intermediates.
3. Influence of different factors on thermochemical conversion characteristics of CSW basic components.
   (1) Influence of temperature: For lignin and PVC, when temperature increased from 500 to 900 °C, the pyrolytic rate increased, the gas amount increased, solid amount decreased, and PAHs increased. Tar amount from lignin

pyrolysis decreased with the increase of temperature, and tar amount from PVC increased with the increase of temperature, while correspondingly, HCl amount decreased with the increase of temperature.

(2) Influence of heating rate: Compared to fast pyrolysis, slow pyrolysis of lignin and PVC generated less PAHs. For lignin, slow pyrolysis generated more tar; for PVC, slow pyrolysis generated more HCl and less tar.

(3) Influence of atmosphere: For lignin and PVC, the reactions in air or CO_2 generated less solid, more gas and tar compared to that in N_2. The total PAHs amount in air or CO_2 were lower than that in N_2.

(4) Influence of inorganics: For lignin, NaCl and NaOH had no significant influence on product distribution, while the solid amount decreased and tar amount increased with the addition of $CuCl_2$. NaCl, NaOH, and $CuCl_2$ had inhibited effects of different degrees on PAHs formation from the pyrolysis of lignin and PVC.

(5) Thermochemical conversion mechanisms: For lignin, pyrolysis generated monomers first, and then dehydroxylation and demethoxylation happened with the generation of benzene derivatives. With the increase of temperature, secondary reactions (demethoxylation, dehydroxylation, and demethylation) were promoted. For the slow pyrolysis of lignin, secondary reactions were unlikely to happen. Therefore, slow pyrolysis generated more tar, less gas, and less PAHs. For the gasification processes in air or CO_2, the intermediates of lignin pyrolysis might be oxidized, and thus, less PAHs were formed. PVC pyrolysis could be divided into two processes: dechlorination and chain scission. During slow pyrolysis, chlorination was slow, and thus, all the Cl would be present in the form of HCl. For fast pyrolysis, dechlorination and chain scission happened almost at the same time, and then the dechlorination was incomplete.

4. Influence of interactions on pyrolytic characteristics of basic components.

(1) Mixture of lignocellulosic basic components (LBCs): In TGA and fixed bed reactor, the co-pyrolysis of cellulose and lignin presented the strongest interaction effect. Gas and char amount decreased, and tar amount increased. The interactions had different effects on different kinds of PAHs.

(2) Mixture of PVC and LBCs: In TGA, the interaction of PVC and cellulose was strong, which promoted pyrolysis at first and inhibited pyrolysis later. In horizontal fixed bed reactor, the interacted effects of PVC and LBCs inhibited the generation of HCl and promoted the generation of tar, and the amounts of most PAHs decreased. LBCs could act as a catalyst promoting the chain scission process of PVC pyrolysis.

In conclusion, based on the selection of CSW basic components in China, the thermochemical reaction kinetics, product distribution, gas production, and PAHs formation characteristics were obtained. In addition, the influences of temperature, heating rate, atmosphere, and inorganics on thermochemical characteristics of basic components were further obtained. Finally, the interactions of CSW basic

components were explored. The results in this thesis could help to describe real CSW from basic components, understand the thermochemical conversion characteristics of CSW, and choose the optimal industrial reaction conditions. In addition, this thesis provided experimental evidence for further understanding of the thermochemical conversion mechanisms of solid materials, especially the formation mechanisms of PAHs.

6.2 Innovative Points

Based on the experimental study of thermochemical characteristics of CSW basic components, the influences of reaction conditions and interactions on thermochemical characteristics of basic components were obtained. The main innovative points are as follows:

(1) The inhibited effect on HCl formation from the interactions of PVC and LBCs was obtained, and the mechanism was the catalytic effect of LBCs on the chain scission of PVC.
(2) The inhibition of air and CO_2 on PAHs formation from the thermochemical conversion processes of lignin and PVC was obtained, and the mechanisms were analyzed; the inhibition of NaCl, NaOH, and $CuCl_2$ on the PAHs formation from the pyrolysis of lignin and PVC was obtained.
(3) The tar amount from lignin slow pyrolysis was higher than that from fast pyrolysis, and the reason was that the secondary reactions were more significant in fast pyrolysis.
(4) A new peak analysis-least square method (PA-LSM) was developed to calculate the kinetics of thermochemical reactions, and the calculated results agreed well with the experimental results.

6.3 Perspectives

(1) This thesis focuses on the study of basic components, while how to accurately describe the characteristics of real CSW from basic components needs further study. This is not an easy work, which needs a large amount of experimental data.
(2) This thesis investigated the interactions of LBCs during co-pyrolysis. However, LBCs are very complicated, and the interacted mechanisms are still unclear. Therefore, more advanced experimental technologies are needed to investigate the interacted mechanisms of LBCs.
(3) Limited by the number of experiments, many studies in this thesis adopt control variate method, i.e., investigate one factor while keeping other factors constant. In the following research, orthogonal experiments could be carried out to obtain the synergistic effects of different factors.